

A Proposal to NOAO for the Dark Energy Survey

July 15, 2004

Submitted by

Fermilab

J. Annis, S. Dodelson, B. Flaugher, J. Frieman, M. Gladders*, L. Hui, S. Kent, H. Lin,
P. Limon, J. Peoples, V. Scarpine, A. Stebbins, C. Stoughton, D. Tucker, W. Wester
* Carnegie Observatories

University of Illinois at Urbana-Champaign

R. Brunner, I. Karliner, J. Mohr, R. Plante, M. Selen, J. Thaler

University of Chicago

J. Carlstrom, S. Dodelson, J. Frieman, W. Hu, S. Kent, E. Sheldon, R. Wechsler

University of California Berkeley and Lawrence Berkeley National Laboratory

G. Aldering, N. Roe, C. Bebek, M. Levi, S. Perlmutter

In collaboration with:

Cerro Tololo Inter-American Observatory

T. Abbott, R. C. Smith, N. Suntzeff, A. Walker

Project Director: John Peoples, peop@fnal.gov, Fermilab, P.O. Box; MS 127, Batavia, IL
60510

TABLE OF CONTENTS

1.	Introduction and Summary	1
2.	The Science Program of the Dark Energy Survey.....	5
3.	Science Requirements	34
4.	Survey Planning	48
5.	The Survey Instrument	80
6.	Data Management	134
7.	Project Management	155
8.	The Relationship of DES to Other Astrophysics Projects	178
9.	Community Service	185
10.	Conclusions	187

Proposal to NOAO for the Dark Energy Survey

1. Introduction and Summary

The National Optical Astronomical Observatory (NOAO) issued an Announcement of Opportunity (AO) in December 2003 that requested proposals for the development of a major new instrument for the Blanco 4 meter telescope at Cerro Tololo Inter-American Observatory (CTIO) in partnership with NOAO. The AO encouraged the construction of an instrument that could exploit the wide field capability of the prime focus. We, a group of astrophysicists and physicists from Fermilab, the University of Illinois, the University of Chicago, the Lawrence Berkeley National Laboratory (LBNL), and CTIO formed the Dark Energy Survey Collaboration and are submitting this proposal to build a Survey Instrument consisting of a 520 megapixel CCD camera and wide field optical corrector for the prime focus. Our proposed instrument will have an effective field of view of about 3 square degrees and will have four filters that will enable observations in the g, r, i, and z bands. These features will give it greater survey power than any optical-near infrared camera currently in existence. We plan to use this instrument to carry out a deep imaging survey in these four bands over an area of approximately 5000 square degrees over the course of five years. Our collaboration will also develop the processing and archiving software for the data produced with our instrument and will provide the facilities and staff to process, archive, and distribute the processed data from our survey.

A number of national panel reports, including Connecting Quarks with the Cosmos (2003), the Physics of the Universe (2004), and the Quantum Universe (2004), have assigned high priority to answering the question: What is Dark Energy? Our collaboration proposes to determine the dark energy equation of state parameter, w , using four complementary techniques in a single survey: (i) the redshift distribution and clustering evolution of galaxy clusters, (ii) weak gravitational lensing on large scales, (iii) the evolution of galaxy clustering, and (iv) type Ia supernova distances. We selected 4000 square degrees of our proposed survey area to coincide with the area that the South Pole Telescope (SPT) collaboration plans to observe. The SPT project, which is already under construction, will detect and measure masses of galaxy clusters through the Sunyaev-Zeldovich effect. The DES will provide photometric redshifts for these clusters; in combination, the two projects will determine the redshift distribution and clustering evolution of the galaxy clusters. The two collaborations plan to carry out a joint analysis of the clusters in the overlap area. We expect that these four independent measurements of w when taken together will provide a measurement with a statistical precision of order 5%, substantially better than the present combined precision of $\sim 15\%$. Moreover, our use of multiple, complementary techniques allow us to probe for possible systematic errors and provide a far more robust constraint than any single technique can offer.

The Dark Energy Survey will catalog and provide photometric redshifts for roughly 300 million galaxies out to a redshift of order 1 (and a smaller number beyond that). Thus the DES will be substantially deeper and cover a larger volume than the Sloan Digital Sky Survey (SDSS): the DES galaxy catalog will contain nearly four times the number of galaxies contained in the SDSS catalog, the largest CCD imaging survey to date. Like the

SDSS, which has already had a deep impact on science, we expect that the public archive from our survey will yield rich scientific data and discoveries in a very wide range of topics of interest to astrophysicists, cosmologists, and particle physicists.

Fermilab will lead the effort to build the Survey Instrument, and it will take the responsibility for designing and building the camera, the prime focus cage, and the mechanical and electrical interfaces to the Blanco telescope. The University of Chicago plans to take the leadership role in designing, acquiring, and testing the optics, with assistance from Fermilab and CTIO. LBNL will manage the acquisition of the CCDs and deliver them to Fermilab. Fermilab will package, test, and grade the CCDs and then install them on the focal plane at its Silicon Detector Facility. The University of Illinois will design and build the data acquisition system, including the interfaces to the electronics in the prime focus cage. They will also provide all of the necessary software to operate the system in test environments at Fermilab and the operating environment at Cerro Tololo. CTIO will fabricate some of the mechanical components in its shops and provide the collaboration with the benefit of its experience in building and operating Mosaic II and the Blanco. CTIO will take the lead in defining the communications, electrical power, and cooling interfaces with the Blanco. The Survey Instrument team will integrate the camera, the data acquisition system, and the related mechanical and electrical components into a fully integrated, tested, and functioning unit at Fermilab prior to shipping the instrument to Cerro Tololo. CTIO will lead the instrument commissioning on the Blanco, with support from all of the participating institutions.

The University of Illinois Astronomy Department will lead the data management and archiving effort. Their efforts will be supported by the National Center for Supercomputing Applications (NCSA), the Fermilab Experimental Astrophysics Group, and the NOAO Data Products Program. This will allow the Collaboration to take advantage of the experience that NCSA and Fermilab have gained in processing, archiving, and distributing astronomical data. The University of Illinois will also distribute the Survey data and catalogs to the collaboration; after a period for validation of the archive, it will release the archive to the public in partnership with NOAO.

The Collaboration began work on the Reference Designs for the Survey Instrument and the Archive in November 2003. In March 2004 it submitted a proposal based on the Reference Designs to Fermilab, requesting support for the design and development of the Survey Instrument. The proposal was considered at the April meeting of the Fermilab Physics Advisory Committee (PAC) and, on the basis of the positive PAC recommendation, the Fermilab Director authorized the preparation of a more complete design and cost estimate. The Collaboration submitted the revised proposal, containing more detailed Reference Designs, preliminary cost estimates, and a funding model, to Fermilab on June 7. A special committee, appointed by the Director, reviewed the revised proposal, including the funding model, on June 7 and 8. The PAC considered the DES project for the second time during the week of June 21 and recommended stage 1 approval, which has since been given by the Director.

The estimated cost of the Survey Instrument is \$ 18.40 M. This estimate includes \$11.45 M for the cost of materials and services (M&S) and \$6.95 M for the engineering and technical

labor costs that will be incurred by Fermilab and the University of Illinois. Since the Collaboration has asked the participating institutions to make the cost of the overhead a contribution to the Survey Instrument, these figures do not include institutional overhead. Fermilab and the University of Illinois plan to contribute the scientific and technical labor for the Instrument. These cost figures have been escalated for inflation and are in as spent dollars.

The estimated cost of Data Management is \$1.8M, primarily for technical labor and computing professionals and a small amount for equipment. The University of Illinois administration and NCSA have already made a commitment to provide a significant fraction (\$0.6M) of the effort required for data processing and archiving as a contribution to the project. NCSA has also agreed to provide the computing and archiving equipment needed during the software development phase and later for base operations as well as the operations staff to operate it as a contribution to the project. An additional \$1.2 M is needed to cover the cost of the technical staff at U Illinois and NCSA for software development and hardware. The Collaboration plans to obtain the funds for these costs from the NSF.

On the basis of the current requests and commitments, the Collaboration needs to obtain an additional ~\$5 M of cash funds to fully fund the construction and commissioning phases of the Survey. The Collaboration plans to approach the NSF, the participating universities, and private foundations for the remaining funds. Faculty members from the University of Chicago and the University of Illinois have requested funds from their institutions to help pay the M&S costs for the Survey Instrument development phase that will begin this September 2004. At U. Illinois, the NCSA director and the Dean of the LAS college are enthusiastic about the Dark Energy Survey and have responded with pledges of institutional support. At U. Chicago, the Kavli Institute for Cosmological Physics has also responded favorably and will help support the project. Finally the Collaboration will seek additional partners that can contribute to the project in ways that will reduce the amount of funds that they plan to request from the DOE and NSF.

If funding can be obtained in accordance with the funding model, the Survey Instrument construction phase will begin in October 2005 and it will be completed at the end of 2008. After integration and acceptance testing at Fermilab, it will be shipped to CTIO in early 2009. In parallel with the instrument construction and commissioning, the data processing pipelines will be built, tested, and deployed with the Survey Instrument. Following a commissioning period of several months, the Survey Instrument at CTIO and the pipelines and computing systems at NCSA will be ready for survey operations. The first observations of the survey region near the south galactic cap could begin in September 2009. The survey will continue through five observing seasons (September-February), 2009-2013. Initial Dark Energy constraints could be completed in 2011, after the first two observing seasons, weather permitting. During the year prior to October 2005, the Collaboration will focus its efforts on the completion of the technology development of the CCDs, the creation of a CCD test facility at Fermilab, and the final design of the optical corrector, because the CCDs and the optical corrector present the greatest cost and schedule risks to the project.

We request that NOAO award the DES collaboration 30% of the observing time on the Blanco telescope over the five-year period beginning September 2009, in exchange for providing the new instrument and the software systems. Moreover, we request that CTIO upgrade the Blanco telescope controls and infrastructure to efficiently accommodate the new instrument prior to delivery of the instrument and software, as noted in the AO. In the event that this request is granted, the Collaboration will submit proposals to the Department of Energy Office of Science and the Astronomy Division of the National Science Foundation for funding.

The remainder of this proposal is organized in chapters as follows: Chapter 2 presents the compelling science that we expect to obtain with the DES, Chapter 3 contains the DES scientific requirements that flow from our science goals, and Chapter 4 describes the preliminary strategy that we propose for observations. The Reference Design of the Survey Instrument and the initial formulation of our Data Management Plan are contained in Chapters 5 and 6. Chapter 7 contains the project management plan and the relevant prior experience in instrumentation and large surveys. Chapter 8 describes the relationship of the Dark Energy Survey to other relevant astrophysical surveys in which the Dark Energy Collaboration members are engaged and the temporal relationship of our survey to other closely related astrophysics projects. Chapter 9 provides an outline of the science that could be done by general observers with the proposed instrument. Finally, Chapter 10 summarizes the observing time that the collaboration is requesting.

2. The Science Program of the Dark Energy Survey

What is the nature of the Dark Energy? To address this question, the dark energy must be probed by multiple, complementary methods with independent systematic errors and different cosmological parameter degeneracies. The Dark Energy Survey is designed to pursue several of the most promising of these methods in the context of a single experiment and thereby achieve a substantial advance in dark energy precision. In this chapter, we describe the science goals and drivers of the Dark Energy Survey. In the following chapters, these goals are translated into science requirements, hardware design, and survey strategy.

The Dark Energy Survey is designed to provide data that will yield accurate multi-band fluxes and shapes of galaxies to $i = 24$ over an area of 5000 square degrees (see chapters 3 and 4). The fluxes, and the resulting colors, will yield galaxy photometric redshift estimates (described in Section 2.7), a linchpin of several dark energy probes. The survey area is chosen to encompass the Sunyaev-Zel'dovich effect (SZE) cluster survey that will be carried out with the South Pole Telescope (SPT); the DES will obtain photometric redshifts for the vast majority of clusters detected by the SPT (all those out to $z=1.3$). Together, the SPT and DES data will enable measurement of the cluster redshift distribution and the cluster power spectrum, both powerful dark energy probes. In particular, the DES flux limit requirements are chosen so that we can optically identify and measure accurate photometric redshifts of *all* clusters and even some groups in the survey area to a redshift $z \sim 1.0$ and of a fraction of the clusters extending to $z \sim 1.5$. The DES will also measure the shapes of distant galaxies to infer the shear caused by weak gravitational lensing. The weak lensing measurements will independently calibrate the masses for massive clusters out to redshift $z \sim 0.7$, enabling a purely optical cluster abundance measurement of dark energy parameters in addition to that provided by the SZE. The survey depth and breadth, in combination with good atmospheric seeing, will also enable high signal-to-noise measurements of the weak lensing shear caused by large-scale structure and of the galaxy-shear cross-correlation, each of which provides new constraints on the dark energy. In addition, measurement of the evolution of the angular clustering of galaxies will provide an independent probe of dark energy, using features in the clustering power spectrum as standard rod distance estimators. Finally, through repeat scanning of selected areas of the survey, the DES will obtain densely sampled light-curves for ~ 1900 Type Ia supernovae and constrain the dark energy through the classical redshift-magnitude relation.

Together, these powerful, complementary techniques will probe the dark energy with unprecedented precision: individually they will probe the dark energy equation of state parameter w (see Sec. 2.1) at the 5-15% level; collectively they can in principle reach the few percent level. It is important to emphasize that these are estimates of statistical errors, assuming constant w , and do not yet include full accounting for systematic errors. Moreover, parameter constraint forecasts generally depend upon priors assumed for marginalized parameters as well as on assumptions about whether and how w evolves. As a result, extreme caution must be exercised in comparing the projected cosmological parameter sensitivity of different experiments and methods, and we will attempt to be explicit about the priors used in the projections below. In all cases, we assume massless neutrinos, no running of the primordial spectral index of the mass power spectrum, and a fiducial model with non-

evolving $w = -1$. More important than the expected statistical precision is the fact that the different methods the DES will use to probe dark energy are subject to *different* systematic errors and cosmological parameter degeneracies (see, e.g., Fig. 2.3-2), so their inter-comparison should provide a gauge of the systematic errors and a more robust final result.

As described in this chapter, these science goals can be achieved with a moderately deep ($\sim 24^{\text{th}}$ magnitude) survey in four optical passbands, g, r, i, and z. The following chapters show that such a survey can be completed using 30% of the telescope time over five years with a new 520 megapixel camera with a 3 deg^2 field of view on the existing Blanco 4-meter telescope at CTIO. To achieve the requisite depth in the redder passbands within the available survey time, we plan to use thick CCDs with much greater quantum efficiency at long wavelengths than conventional thinned devices.

In the following, we highlight the importance of dark energy for fundamental physics and briefly describe the current state of dark energy measurements. We then describe how each of the four methods—cluster surveys, weak lensing, galaxy clustering, and supernovae—will constrain the dark energy in the context of our survey. The last section of this chapter describes the expected accuracy of our photometric redshift measurements, a primary factor in determining the science reach of these dark energy methods. An Appendix describes the measurement of the cosmic shear sensitivity of the Survey.

2.1 Evidence for Dark Energy

In 1998, two research groups studying distant Type Ia supernovae independently found direct evidence that the expansion of the Universe is accelerating (Riess et al, 1998, Perlmutter et al 1999), arguably the most important discovery in cosmology since the serendipitous detection of the cosmic microwave background (CMB) radiation by Penzias & Wilson in 1965. According to General Relativity, if the Universe is filled with ordinary matter, the expansion should be slowing down due to gravity. Since the expansion is speeding up, we are faced with two logical possibilities, either of which would have profound implications for our understanding of the fundamental laws of physics: (i) the Universe is filled with a completely new kind of stress-energy with bizarre properties (in particular, negative effective pressure), or (ii) General Relativity breaks down on cosmological scales and must be replaced with a new theory, perhaps associated with extra dimensions. For simplicity, we will subsume both of these possibilities under the general rubric of ‘Dark Energy’, since in both cases the effects on the expansion of the Universe can generally be described by that of an effective fluid with equation of state parameter $w = p/\rho < -1/3$ (we use units in which the speed of light $c = 1$ throughout). For example, the dark energy could be the energy of the quantum vacuum, that is, Einstein’s cosmological constant (in which case, $w = -1$), or it could signal the existence of a new ultra-light particle with mass of order 10^{-33} GeV or less; in either case, particle physics currently provides no understanding of why the dark energy density should have the value that would explain the current acceleration of the Universe.

Since 1998, independent but indirect evidence for dark energy has come from several sources, most notably the combination of the CMB temperature anisotropy pattern—which points to a spatially flat Universe—and the evidence from large-scale structure and galaxy

clusters that the density of ordinary matter (mostly dark matter) is about 30% that of a flat Universe. These studies indicate that the dark energy comprises the remaining 70% of the energy density of the Universe, $\Omega_{\text{DE}} \approx 0.7$, and that its equation of state parameter $w < -0.75$ at 95% confidence (this upper bound comes from combining supernova, galaxy clustering, and CMB data, assumes w is constant, and depends upon priors on other cosmological parameters, cf. Fig.2.1-1). In order to pin down the nature of the dark energy and decide between the theoretical alternatives, we need to measure w with greater precision and determine whether and how it evolves with cosmic time. The Dark Energy Survey, in combination with the SPT Survey, is designed to determine w with a statistical (1σ) precision of order 5% (constant w) and the dark energy density Ω_{DE} to within ± 0.01 . In combination with CMB data, the DES should also provide interesting constraints on the evolution of the dark energy equation of state.

Figure 2.1-1 illustrates the complementarity of the current constraints on dark energy arising from the CMB (WMAP), large-scale structure (SDSS), and supernovae. While Figs. 2.1-1b and 2.3-2a show that the CMB anisotropy itself does not strongly probe the dark energy equation of state, it does accurately constrain the shape of the matter (mass) power spectrum, considerably strengthening the dark energy reach of galaxy clustering and weak lensing measurements. As Fig. 2.3-2a also shows, the CMB constraints on dark energy are nearly orthogonal to those from supernovae. The timing and scientific leverage of the Dark Energy Survey make it complementary to two next-generation CMB mapping experiments that will begin in 2007. The Planck Surveyor, a satellite that will measure the CMB temperature and polarization anisotropy, will provide constraints at the roughly 1% level on a range of cosmological parameters that determine the matter power spectrum. The South Pole Telescope, a ground-based, high angular resolution CMB mapping experiment, will carry out an SZE survey of galaxy clusters over 4000 square degrees. The combination of the Dark Energy Survey with these CMB experiments—especially the SPT—will provide even more precise information about the dark energy.

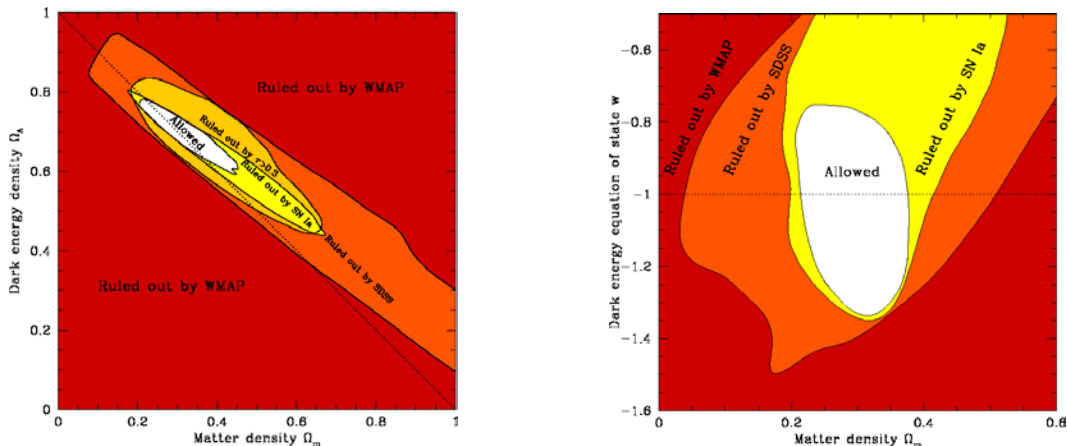


Figure 2.1-1 Current 95% CL constraints from joint analysis of WMAP, SDSS, and supernova surveys: (a) dark energy vs. dark matter density (assuming $w = -1$); (b) dark energy equation of state vs. dark matter density, assuming constant w and a flat Universe (Tegmark et al 2003).

2.2 New Probes of Dark Energy

Dark energy affects the history of the cosmic expansion rate, $H(z)$, over the last 10 billion years or so; this history determines the observables upon which all dark energy probes are based. While supernovae have provided the first direct evidence for dark energy (the observable is the peak apparent brightness as a function of redshift), in the last few years other techniques that complement the supernova method have been undergoing rapid development. The Dark Energy Survey is designed to exploit several of the most promising of these techniques, including supernovae.

The first new method involves measuring the redshift distribution and the evolution of clustering of massive clusters of galaxies. Galaxy clusters are the largest collapsed structures in the Universe, containing up to hundreds or thousands of individual galaxies. Because the expansion rate of the Universe determines the cosmic volume as a function of redshift as well as the growth rate of density perturbations, the redshift distribution of clusters and its cosmic evolution provide a sensitive probe of the dark energy equation of state. Realizing this technique is the primary science driver for the Dark Energy Survey.

A major project aimed at the cluster counting technique is now being planned for the South Pole. The South Pole Telescope (SPT, John Carlstrom, U. Chicago, PI), funded by the National Science Foundation, is an \$18 million project that will start survey operations in 2007. This project will use the SZE to detect galaxy clusters out to large distances. The SZE is caused by inverse Compton interactions of CMB photons and the hot gas (free electrons) that permeates clusters. These interactions introduce a spectral distortion into the perfect blackbody of the CMB. By precisely mapping the background radiation, the SPT will provide a census of tens of thousands of clusters over a 4000 square degree region south of declination $\delta = -30^\circ$. Because the SZE signal from a cluster is a measure of the vast thermal energy in the electron population, it is expected to be a robust indicator of cluster mass.

One advantage of the SZE is that it is a change in the spectral distribution of the CMB rather than a source of emission, so it is unaffected by the cosmological dimming that plagues studies of high-redshift objects. This makes it a cluster selection tool that works extremely well over a wide range of redshifts. However, once clusters are detected in the SZE, one needs another method to determine their redshifts, which are required to measure the redshift distribution and clustering evolution. The most efficient way to obtain cluster redshifts to the desired accuracy is by measuring the magnitudes and colors of the galaxies they contain: all clusters contain a population of luminous red galaxies, and the farther the cluster the redder the galaxies appear. Thus, the SPT survey must be combined, over the same area of sky, with an optical survey in several filters that can measure such color-derived photometric redshifts. Currently, no telescope in the Southern Hemisphere (which can survey the region of sky observable from the South Pole) has an instrument capable of carrying out such a photometric redshift survey with the requisite area and depth on a timescale of a few years.

In addition to providing redshift estimates for the SPT clusters, the Dark Energy Survey will provide an independent cluster counting probe of the dark energy. The cluster counting

method depends on having a good estimate of the mass of each cluster. The SZE technique provides one estimate of cluster mass, but optical observations of clusters provide others: the more massive a cluster, the more luminous galaxies it contains and the stronger its gravitational lensing effects on background galaxy images. Current observations indicate that gas-based probes of clusters (i.e., SZE or X-ray signatures) provide more accurate estimates of cluster masses than optical techniques alone. Projection effects are a major issue for lensing (e.g., White, et al 2002, Dodelson 2003) and, to a much lesser extent, for optical mass estimators (e.g., Lin et al 2003); projection is less problematic in SZE surveys. On the other hand, radio emission from the nuclei of galaxies can interfere with SZE cluster selection but does not affect optical cluster finding; moreover, optical and lensing mass estimates do not depend on assumptions about the state of the intracluster gas. Thus, SZE and optical cluster finding and mass estimation are complementary; by coordinating the Dark Energy Survey with the SPT survey, we can cross-check mass estimates and control systematic errors.

A second new technique for probing the dark energy involves weak gravitational lensing: by precisely measuring the shapes of distant galaxies, we can infer how those shapes have been distorted due to their light bending around foreground mass concentrations. The evolution of the statistical pattern of these distortions—for example, of its angular power spectrum—as well as of the cross-correlation between foreground lensing galaxies and background galaxy shear, is sensitive to the cosmic expansion history and thus to the dark energy (Hu 2002, Huterer 2002). Weak lensing studies of dark energy require surveys that cover a large area of sky from sites where atmospheric turbulence does not cause excessive blurring of the galaxy images. The site at CTIO is known to have excellent image quality.

The third technique exploits the dark energy leverage available in the power spectra of the spatial distribution of galaxies. The matter power spectrum as a function of wavenumber shows characteristic features, a broad peak as well as baryon wiggles arising from the same acoustic oscillations that give rise to the Doppler peaks in the CMB power spectrum. With the Dark Energy Survey, we will be able to explore the angular galaxy power spectrum in redshift shells out to $z \sim 1.1$. This approach will provide cosmological information from the shape of the power spectrum transfer function and physically calibrated distance measurements to each redshift shell (Eisenstein, Hu, & Tegmark 1998, Cooray et al 2001, Hu & Haiman 2003, Seo & Eisenstein 2003, Blake & Glazebrook 2003).

The fourth approach to dark energy will be to revisit 40 deg^2 of the sky every third night, enabling the discovery of and providing light-curves for a sample of approximately 1900 Type Ia supernovae at redshifts $0.3 < z < 0.8$. These SNe will provide relative distance estimates that can be used to constrain the properties of the dark energy—especially when combined with the other three approaches and the CMB.

These four techniques have very different sources of systematic error from one another. Because we do not yet know the fundamental limitations of these different techniques, and because the problems raised by dark energy are so profound, it is necessary to pursue all of the most promising probes. The Dark Energy Survey does so within a single project. Note that the three new techniques rely on an underlying paradigm for the formation of large-scale

structure, based on gravitational instability of cold dark matter in the Universe, although weak lensing measurements also yield a purely geometric dark energy test with reduced sensitivity (Jain & Taylor 2003, Zhang, Stebbins, & Hui 2003, Hu & Jain 2003). Despite the on-going theoretical challenges in fully understanding the formation and evolution of galaxies, recent CMB and large-scale structure data have repeatedly shown that this paradigm is robust, indicating that cosmological parameters can be confidently probed in these new ways.

Below we describe each science component of the Dark Energy Survey in greater detail.

2.3 Galaxy Cluster Studies of the Dark Energy

In recent years, it was recognized that large cluster surveys to redshifts $z \sim 1$ can be used to study the galaxy cluster abundance and its evolution and thereby deliver precise constraints on the amount and nature of the dark energy (Wang & Steinhardt 1999, Haiman et al 2001). A cluster survey carried out over large solid angle also constrains cosmology through the spatial clustering of the galaxy clusters. The correlated positions of galaxy clusters (encoded in the cluster power spectrum $P_{cl}(k, z)$) reflect the underlying correlations in the dark matter; these correlations contain a wealth of cosmological information, much like the information contained in the CMB anisotropy power spectrum. We plan to use the cluster redshift distribution and the cluster power spectrum as powerful cosmological probes to study the density and nature of the dark energy.

The observed cluster redshift distribution in a survey is the product of the comoving volume per unit redshift and solid angle, $d^2V/dzd\Omega$, and the comoving density of detected clusters n_{com} ,

$$\frac{d^2N}{dzd\Omega}(z) = \frac{d^2V}{dzd\Omega}(z)n_{com}(z) = \frac{c}{H(z)}D_A^2(1+z)^2 \int_0^\infty dM f(M, z) \frac{dn}{dM}(z) \quad (2.3:1)$$

where dn/dM is the cluster mass function, $H(z)$ is the Hubble parameter as a function of redshift, $D_A(z)$ is the angular diameter distance, and $f(M, z)$ is the redshift-dependent mass selection function of the survey. Figure 2.3-1 shows a characteristic redshift distribution for the SPT+DES cluster survey. The cosmological sensitivity comes from three basic elements:

- **Volume:** the volume per unit solid angle and redshift depends sensitively on cosmological parameters and has much in common with a simple distance measurement (such as that given by supernovae).
- **Abundance Evolution:** the evolution of the number density of clusters, $(dn/dM)(z)$, depends sensitively on the growth rate of density perturbations, which is determined by the expansion rate $H(z)$ and therefore highly sensitive to cosmological parameters. For example, the higher the matter density, the more rapidly perturbations grow at recent epochs, implying lower perturbation amplitude and therefore fewer clusters at high redshift. The number density also depends on the initial mass power spectrum.

- Mass selection function:** clusters are selected using some observable such as the integrated SZE flux (a measure of the thermal energy in the intracluster medium), galaxy number or light (a measure of the stellar mass in the cluster), or weak lensing shear (a measure of the projected mass density of the cluster). In general, all these observables are correlated with cluster mass. A flux-limited survey will pick out all clusters massive or luminous enough to lie just above the flux limit. Thus, the cluster selection function depends on the luminosity distance to that redshift, which depends on cosmology. The form of the selection function encodes the scatter about the characteristic mass—observable relation and at any redshift will vary from 0 for low-mass, undetectable clusters to 1 for very high-mass, easily detected systems.

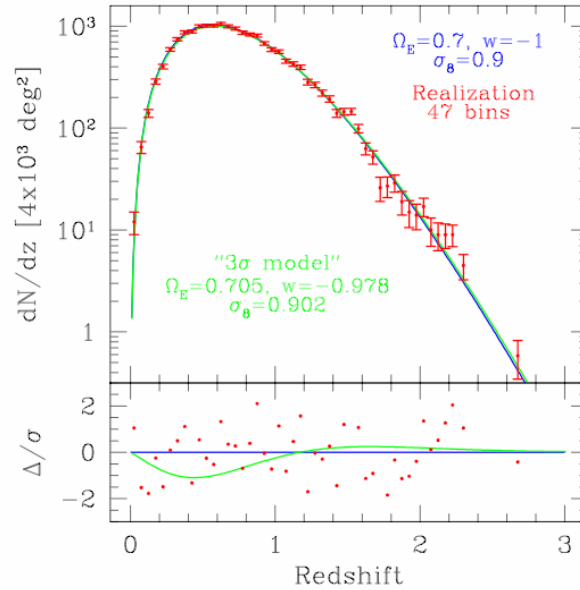


Figure 2.3-1 The redshift distribution (blue) for the SPT+DES cluster survey for a fiducial cosmological model with $\Omega_{DE} = 0.7$, $w = -1$, and power spectrum amplitude $\sigma_8 = 0.9$. A particular realization of the model appears with red points and error bars. The green model with slightly different cosmological parameters can be excluded with 3σ confidence using a likelihood analysis of this data. The lower panel shows the deviations between the 3σ model and the fiducial model as a function of redshift in units of $v = \Delta/\sigma$.

The cosmological sensitivity of the cluster power spectrum arises primarily because there are features—including a break—in the power spectrum that depend on the matter and baryon densities. These features provide a standard ruler, calibrated by the CMB power spectrum. By measuring the cluster angular power spectrum in a redshift bin, one measures the angular scale of these features. Comparing the angular and physical scale of these features provides direct angular diameter distance information to that redshift (Cooray et al 2001). The cosmological constraints from the cluster power spectrum are independent of those from the cluster redshift distribution; taken together, they constrain cosmology in a very robust manner (Majumdar & Mohr 2003b, Lima & Hu 2004).

Several crucial components make possible precision studies of dark energy using galaxy cluster surveys. First, the formation and evolution of dark matter halos must be precisely modeled; fortunately, this is well-understood theoretically and well-tested using N-body simulations of structure formation (Jenkins et al 2001, Hu & Kravtsov 2002, Linder & Jenkins 2003). Second, special-purpose surveys must be designed to cleanly select clusters over a large range of mass and redshift—survey completeness and contamination must be well understood when analyzing the cluster redshift distribution. Third, photometric redshift estimates must be available for large numbers of clusters—this drives the synergy between the SPT and DES surveys. Finally, a mass—observable relation must exist that can tie observable cluster properties (such as the SZE flux or the galaxy light) to the underlying halo mass. The combination of the DES and SPT surveys bring all these ingredients together, making it possible to deliver robust constraints on the dark energy from a sample of $\sim 20,000$ clusters.

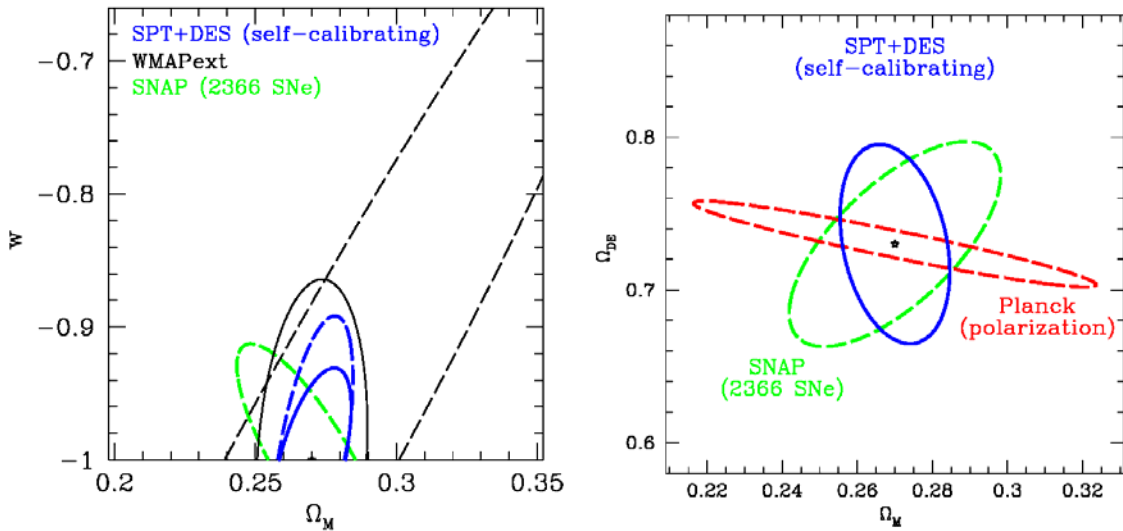


Figure 2.3-2 Forecast 68% CL constraints on the dark energy equation of state parameter w , the dark energy density parameter Ω_{DE} , and the matter density parameter Ω_m for the SPT+DES galaxy cluster survey (blue). For comparison, forecasts for SNAP supernovae (green; Perlmutter & Schmidt 2003), current constraints from WMAPext (black dashed; Spergel et al 2003), and forecasts for Planck polarization (red) are shown. The cluster constraints in the left panel either assume a flat universe (solid blue) or solve for geometry and w simultaneously (dashed blue); the solid black contour shows approximate constraints from two years of DES data, using photometric redshifts to $z = 0.8$. The constraints arise from the cluster power spectrum, the cluster redshift distribution (assumed distributed uniformly out to $z = 1$ for this figure), and 100 cluster mass measurements each accurate at the 30% level (1σ). Note that only the SNAP constraint includes a full estimate of systematic error.

Figure 2.3-2 shows forecasts for the dark energy constraints from the SPT+DES cluster survey, compared with projected SNAP supernovae and existing and projected CMB constraints, and assuming Gaussian initial density perturbations as expected from inflation.

The marginalized error on the dark energy equation of state from SPT+DES clusters is $\delta w \approx 0.05$ for a flat Universe. The complementary parameter degeneracies underscore the gains one can achieve by carrying out both cluster surveys and supernova distance measurements, as we plan to do in the Dark Energy Survey. The 30% cluster mass measurements will come from a combination of weak lensing constraints directly from the Dark Energy Survey, deep pointed X-ray observations with Chandra or XMM-Newton, and perhaps through dynamical mass estimates arising from spectroscopic studies of a subset of the clusters. We emphasize that these forecasts include survey self-calibration: the mass—observable relation and its evolution are extracted from the survey directly (Majumdar & Mohr 2003a,b; Hu 2003, Lima & Hu 2004). The precision of cosmological constraints suffers when one requires self-calibration, but the accuracy is improved by eliminating biases introduced by theoretically driven assumptions about the expected form and evolution of the mass—observable relations. Put another way, the constraints with self-calibration do incorporate an estimate of the effects of a major source of systematic error in the cluster measurements.

In calculating the forecasts shown above we have reserved considerable cosmological information for cross-checking our constraints. As shown in Equation 2.3:1, the redshift distribution involves an integral over the mass function. Using in addition the shape of the mass function directly would improve the cosmological constraints (Hu 2003), but with the approach outlined here we can, at the end of the analysis of the redshift distribution and cluster power spectrum, *predict* the cluster mass function as a function of redshift. A direct comparison of the theoretical mass functions for the best-fit cosmology and the observed mass functions derived from the survey (in essence, the observed luminosity functions, which can be converted to a mass function using the parameters of the mass—observable relation) will indicate the level of self-consistency—and effectively the level of accuracy—of our analysis. These multiple, independent sources of information from a cluster survey make it a particularly powerful probe of the dark energy.

Finally, we note that the constraints shown here and below (except as noted) assume that the dark energy equation of state parameter w is constant in time; if w evolves, then the corresponding constraints on its present value, w_0 , are generally less stringent. On the other hand, the SPT+DES cluster abundance, in conjunction with determination of the mass power spectrum normalization, can provide constraints on the evolution of w that complement those that will come from SNAP (Battye & Weller 2003, Hu 2004). We discuss constraints on the time evolution of w expected from the DES further below.

2.3.1 Optical Cluster Finding and Mass Estimates

The classical method of identifying clusters is to search for large aggregations of galaxies. Empirically, this method is justified by the strong observed correlation between the distribution of mass and the distribution of luminous galaxies on large scales. In the Dark Energy Survey, finding clusters optically and measuring the number of luminous galaxies they contain will provide estimates of the cluster abundance and cluster masses that are independent of those from the SZE.

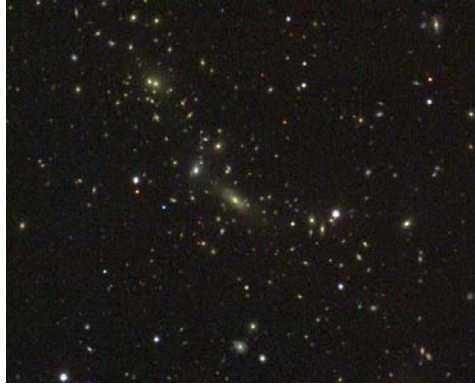


Figure 2.3-3: Optical image of a galaxy cluster at $z = 0.15$ (SDSS collaboration).

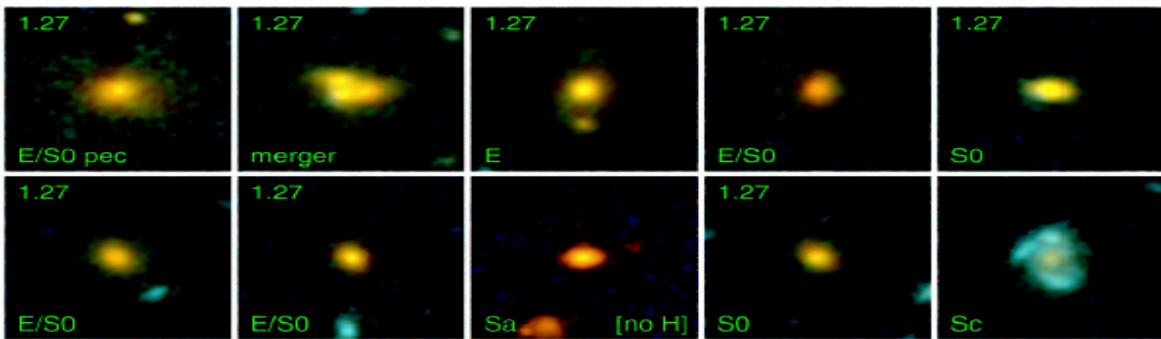


Figure 2.3-4 Galaxies in the red sequence from a cluster at $z = 1.27$ (van Dokkum et al 2001).

Clusters of galaxies can be identified optically by searching for concentrations of galaxies with the same color: clusters exhibit a population of red (elliptical or S0) galaxies that have remarkably uniform colors (Gladders and Yee 2000). With increasing redshift, cluster galaxies appear progressively redder, providing a basis for a color or photometric estimate of cluster redshifts. A version of this red-sequence technique for identifying clusters, called the maxBcg algorithm, has been used in the SDSS out to redshifts $z \sim 0.3-0.5$ (Annis et al 1999, Sheldon et al 2001, Bahcall et al 2003; see Fig.2.3-5). The maxBCG algorithm has been tested on N-body simulation-based mock catalogs, populated with realistic galaxy populations, out to these redshifts (Wechsler et al, in preparation). The use of a color-based selection technique reduces projection effects significantly: virtually all massive clusters are found with the method, and for $M > 10^{14} M_{sun}$, the scatter between mass and N_{red} is less than about 30%.

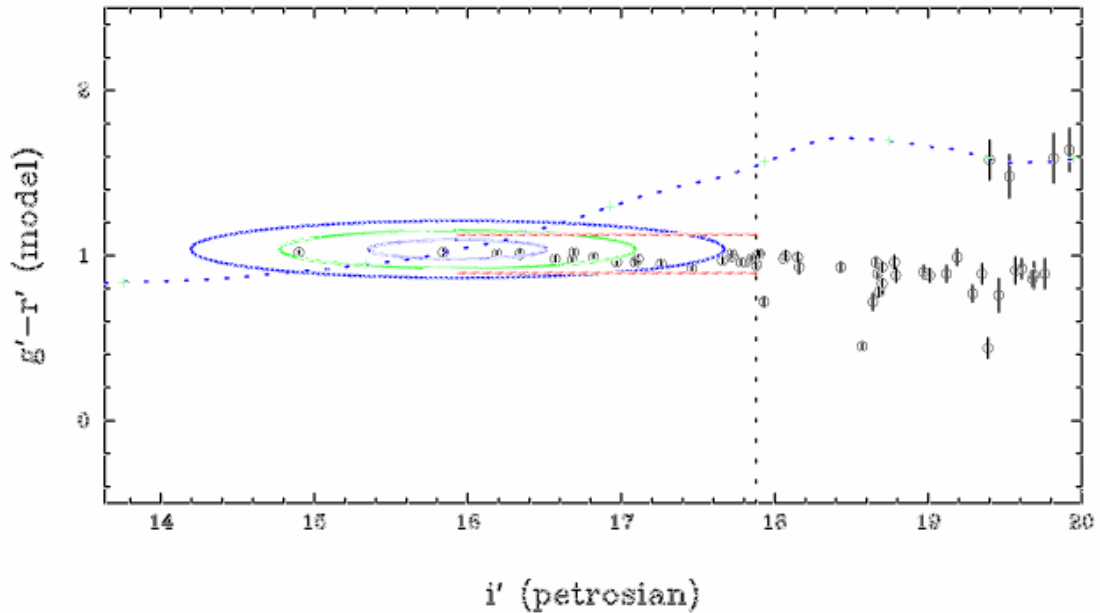


Figure 2.3-5 An example of the maxBcg algorithm used to identify clusters in SDSS imaging data. For galaxies in a small area of sky, $g-r$ color is plotted against apparent i -band magnitude. The dotted curve shows the expected locus of the most luminous galaxies found in clusters, with redshift increasing along the curve. This cluster is at $z=0.1$. Ellipses indicate the $1, 2, 3\sigma$ expectation values for the most luminous galaxy in a cluster at $z=0.11$, while the vertical dotted line shows the luminosity limit used for the count of red cluster galaxies, N_{red} .

We expect this method to work well out to higher redshift: cluster galaxies have been found to have homogeneous colors up to and beyond $z = 1$ (Ellis et al 1997, Stanford et al 1998; van Dokkum et al 2000, van Dokkum et al 2001; Lidman et al 2003), and the red-sequence technique has been applied to find clusters in this regime (Gladders et al 2003). A variety of observational studies of galaxy evolution indicate that the population of red galaxies as a whole, not just those in clusters, is quite stable out to redshifts of $z \sim 1$, indicating that this technique for cluster identification should be robust.

For the SPT survey, the observable used to statistically estimate cluster mass is the SZE flux. For optically selected clusters, one can use, e.g., total galaxy luminosity (e.g., Bahcall et al 2003, Lin et al 2004); for the remainder of this discussion, we will instead adopt the number of red galaxies above a limiting luminosity, N_{red} , as the optical mass estimator, since it is straightforward to measure with the maxBcg cluster finding technique (see Fig. 2.3-5).

Weak lensing measurements provide an additional method for calibrating the relation between N_{red} and cluster mass (see, e.g., Fig. 2.4-2). To obtain high signal to noise, one stacks many clusters of a given N_{red} and photometric redshift interval and determines the mean tangential shear profile, a technique used on a sample of early SDSS data by Sheldon et al (2001). The mass scalings derived from this method agree very well with those derived

from spectroscopic velocity dispersions (McKay et al 2004), an important cross-check on the method. The Dark Energy Survey will allow us to build weak lensing vs. N_{red} scaling relations out to $z = 0.7$. All three mass indicators derived from optically-selected clusters (optical luminosity or number of red galaxies, weak lensing mass, and cluster velocity dispersion) are being extensively tested and cross-checked with clusters identified with maxBCG in realistic simulation-based mock catalogs. This has allowed both tuning of the algorithm to get the most robust cluster selection and direct comparison to dark matter halo masses, which allows us to understand the systematic uncertainties inherent in each method.

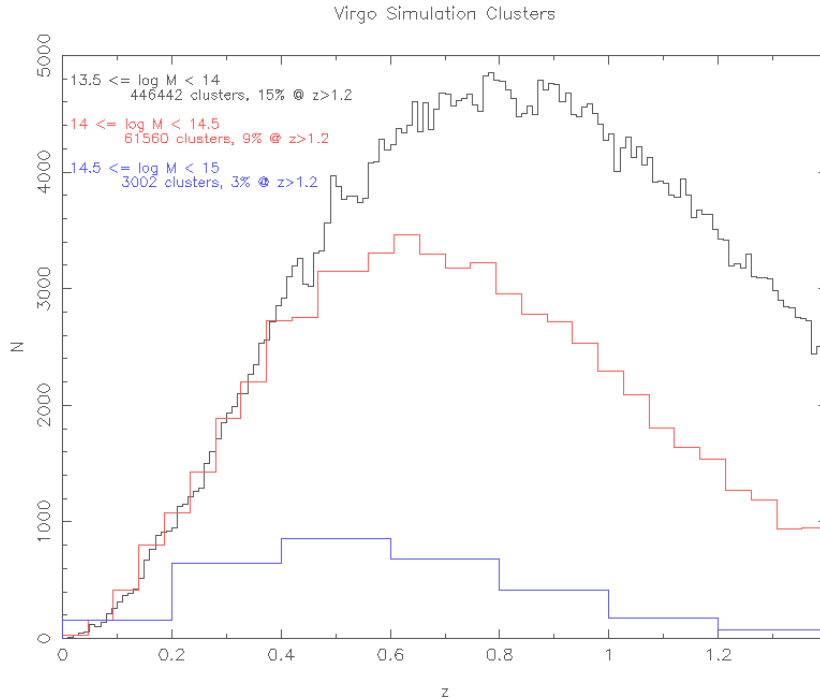


Figure 2.3-6 A realization of the DES cluster redshift distribution from the Hubble Volume N-body simulation. The three curves show the distribution for different mass bins, where M is the cluster mass in units of solar mass. The red curve corresponds roughly to the detection mass threshold for SPT clusters ($10^{14} M_{sun}$), while optical imaging can detect clusters down to lower masses, similar to that indicated by the black curve ($10^{13.5} M_{sun}$ or $N_{red} = 10$).

2.4 Weak Gravitational Lensing and Dark Energy

The bending of light by foreground mass concentrations shears the images of distant source galaxies. Dense mass concentrations such as galaxy clusters induce a coherent tangential shear pattern that can be used to reconstruct their surface mass densities. Larger scale structures with lower density contrast also generate correlated shear, but with lower amplitude—in this case one studies the shear pattern statistically, a method known as cosmic shear or shear-shear correlations. Since the foreground dark matter is associated to large degree with foreground galaxies, one can also measure the angular correlation between foreground galaxy positions and source galaxy shear, a technique known as galaxy-shear correlations or galaxy-galaxy lensing.

These weak lensing techniques provide powerful probes of the dark energy in the context of the Dark Energy Survey: the shear-shear and galaxy-shear correlations depend on and therefore constrain the dark energy density and equation of state. In addition, as noted above, lensing provides statistical cluster mass estimates that can cross-check SZE, X-ray, and galaxy-number-based mass estimators. Although shear-shear and galaxy-shear correlations were detected for the first time several years ago, the Dark Energy Survey, with its wide area coverage, depth, and photometric redshift information, will exploit the dark energy sensitivity of these techniques.

The shear-shear, galaxy-shear, and galaxy angular power spectra can be expressed as projections of the corresponding three-dimensional power spectra (e.g., Hu & Jain 2003),

$$C_\ell^{x_a x_b} = \int dz \frac{H(z)}{D_A^2(z)} W_a(z) W_b(z) P^{s_a s_b}(k = \ell / D_A; z) \quad (2.4:1)$$

where ℓ denotes the angular multipole, $a, b = (1, 2)$, x_1 and x_2 denote the two-dimensional angular galaxy (g) and shear (γ) fields, and s_1 and s_2 respectively denote the three-dimensional galaxy (g) and mass (m) density fluctuation fields at redshift z . The weight functions W_1 and W_2 encode information about the galaxy redshift distribution and about the efficiency with which foreground masses shear background galaxies as a function of their respective distances.

The dark energy density and equation of state affect these angular power spectra through the distance and weight factors and through the redshift- and scale-dependence of the three-dimensional power spectra P^{gg} , P^{mm} , and P^{gm} . For a given set of cosmological parameters, the mass power spectrum P^{mm} can be accurately predicted from N-body cosmological simulations; the shape (scale-dependence) of P^{mm} is also well constrained on large scales by WMAP data on the CMB anisotropy, and we include this as a prior in the forecasts shown below. In addition to cosmology, the power spectra involving galaxies, P^{gg} and P^{gm} , require a model for the *bias*, that is, for how luminous galaxies are distributed with respect to the dark matter. We describe the bias in terms of the ‘halo model’, with 5 parameters that determine how galaxies occupy dark matter halos; this model is physically motivated and accurately reproduces the results of N-body simulations that include gas dynamics.

To forecast constraints, we estimate the statistical errors on the angular power spectra; for illustration, we focus on the shear-shear spectrum, for which the uncertainty is (Kaiser 1992)

$$\Delta C_\ell^{\gamma\gamma} = \sqrt{\frac{2}{(2\ell+1)f_{sky}}} \left(C_\ell^{\gamma\gamma} + \frac{\sigma^2(\gamma_i)}{\bar{n}_A} \right) \quad (2.4:2)$$

where f_{sky} is the fraction of sky area covered by the survey, $\sigma^2(\gamma_i)$ is the variance in a single component of the (two-component) shear, and \bar{n}_A is the source galaxy angular number

density per sr. The first term in brackets comes from cosmic variance, and the second, shot-noise term results from both the variance in galaxy ellipticities (‘shape noise’) and random error in measuring galaxy shapes. Eqn.(2.4:2) assumes the shear field is Gaussian; although this assumption breaks down at large ℓ , the non-Gaussian variance is generally masked by the shape noise term. In what follows, we only use information from multipoles $\ell < 3000$.

Eqn. (2.4:2) indicates that weak lensing places a premium on maximizing the survey sky coverage and the surface density of source galaxies with measurable shapes. We choose to rewrite the shot-noise term in Eqn.(2.4:2) as $(0.32)^2/n_{eff}$, where the numerator is the empirical shape noise for large, well-measured galaxy images, and n_{eff} is the source galaxy density including noise weighting. In estimating the shear, the ellipticity measurement of each source galaxy is relatively weighted by the inverse noise, which has contributions from shape noise and shape measurement error. In addition, the ellipticity of each galaxy is corrected for PSF dilution by a factor that depends on the square of the ratio of the galaxy size to the PSF—for small galaxies the correction is large, and uncertainty in the correction factor means these galaxies are further downweighted in the shear estimate. These effects are incorporated into the noise-weighted galaxy density n_{eff} .

This effective or weighted number density is convenient because it can be used with power spectrum noise estimates that assume the usual shape noise amplitude.

To estimate n_{eff} for the DES, we studied a 900 sec CFH12K *I* band exposure taken in median seeing of 0.63" and artificially degraded the image to different seeing values. Note that this is the same exposure time to reach the DES *i* band survey requirement (chapter 3) and that the CFHT mirror aperture is close to that of the Blanco. We measured the ellipticities and sizes of the detected objects using an adaptive weighting scheme that is nearly optimal for lensing measurements (Bernstein and Jarvis 2002). . In the CFH12K image, the mean relative galaxy weight per magnitude bin is essentially unity out to $I_{AB} = 21.5$ and drops to about 0.5 at $I_{AB} = 24.1$, which is the nominal 10σ magnitude limit for galaxies. The effective source density for the DES *i* band images is shown in the bottom panel of Fig.2.7-1 as a function of seeing. An increase in seeing has two effects: (i) the PSF is a larger fraction of the size of the faint source galaxies, so they receive less weight due to the larger PSF dilution factor; (ii) the effective number of CCD pixels per object is larger, increasing the sky background per object and therefore the shape measurement error. Fig.2.7-1 shows that for 0.9" seeing, which is the assumed median for the DES, we expect an effective source galaxy density of $n_{eff} = 10$ arcmin⁻², and we have adopted this value in the analysis below. Note that this is smaller by about a factor of two than the actual source density above the 10σ detection limit of the Survey, because it includes weighting due to measurement error, PSF dilution, and shear polarizability. The upper panel of Fig.2.7-1 shows the shear sensitivity per component, which is just $\langle \gamma^2(\theta) \rangle_N^{1/2} / \sqrt{2}$ evaluated at $\theta = \sqrt{5000}$ degrees. In comparison to the CFHT Legacy Survey, which goes deeper over a smaller area of sky, the signal to noise on the shear variance for the Dark Energy Survey should be larger by a factor of three.

The survey depth also determines the redshift distribution of the source galaxies. In the estimates below, we used a distribution with median redshift $z_s=0.7$. This is consistent with the distribution inferred from redshift surveys to $I_{AB}=24$, the expected depth of the DES, and with models of galaxy counts. The actual source redshift distribution for lensing will differ from that for a survey with this flux limit because (a) we include source galaxies beyond the 10σ detection limit, and (b) fainter galaxies contribute less weight. These correction effects go in opposite directions, and we expect this adopted median source redshift to be reasonably accurate.

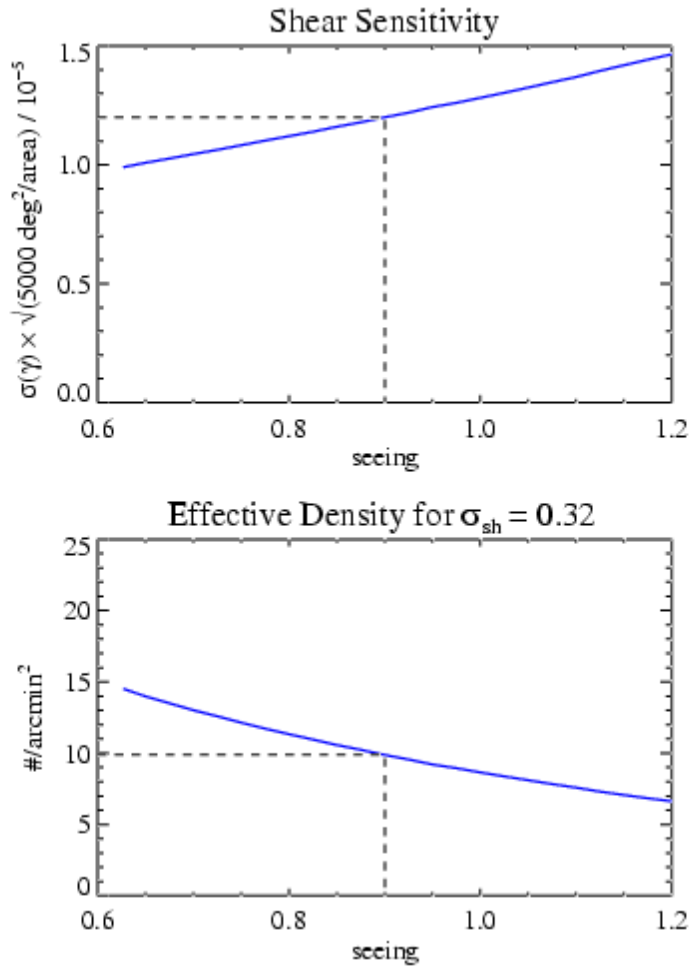


Figure 2.4-1 Upper panel: shear sensitivity for the Dark Energy Survey as a function of seeing, for 900 sec i band exposure. Lower panel: effective source galaxy density for lensing as function of seeing, for same exposure.

The three angular power spectra provide constraints on the multi-dimensional parameter space that includes the halo and cosmological parameters, and we forecast constraints on w and Ω_{DE} by marginalizing over the others, assuming spatial flatness. We include approximate

WMAP CMB priors, specifically, 10% errors on $\Omega_m h^2$, $\Omega_b h^2$, the primordial spectral index n , and the power spectrum amplitude $A^{1/2}$, but no CMB priors on any dark energy parameters. We assume the source galaxies can be separated into 4 photometric redshift bins of width $\Delta z = 0.28$ out to $z = 1.1$, plus a fifth bin for all higher-redshift galaxies. The lens galaxies are placed in bins of $\Delta z = 0.1$ out to $z = 1$ and are included if they reside in halos of mass greater than $10^{13.5} h^{-1} M_{sun}$. Although the shear-shear (cosmic shear) spectrum is proportional to P^{mm} and thus independent of the halo model parameters, it has the lowest signal to noise and is the most sensitive to systematic errors in measuring galaxy shapes. At the other extreme, the galaxy auto-power spectrum is most sensitive to uncertainties in the bias model, but it has the highest signal to noise. Fig. 2.4-2 shows the expected constraints from the Dark Energy Survey: all 3 power spectra jointly determine w with a statistical uncertainty of less than 4% and Ω_{DE} to better than 1%; more conservatively, cosmic shear alone yields a 1- σ error on (constant) w of 6%. These numbers will decrease with improved priors from Planck.

For comparison, Fig. 2.4-2 also shows approximate constraints expected after two years of DES data. Using the survey strategy described in chapter 4, the expected effective source galaxy density from two years of data is 6.6 per square arcmin (as opposed to 10 for five years of data). The noise in the shear measurements has been scaled up accordingly; in addition, the source galaxy redshift distribution after two years will be modestly shallower than for the full survey; this effect has not been incorporated in the figure, leading to a small underestimate of the two-year parameter errors.

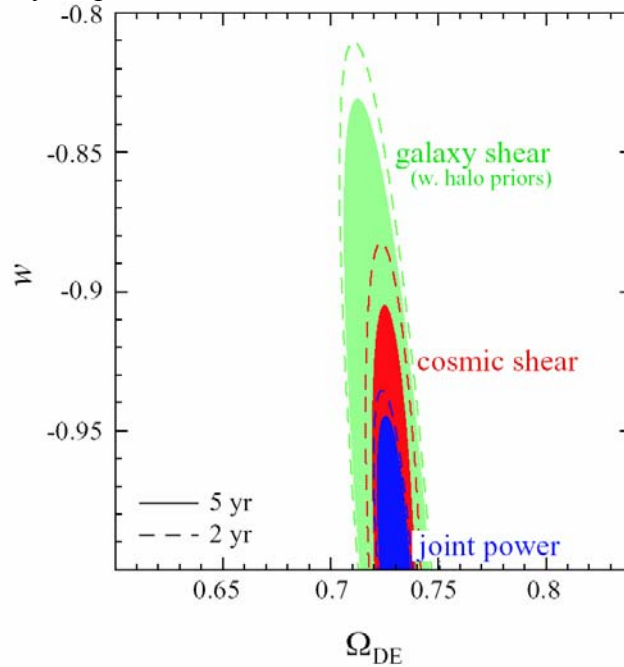


Figure 2.4-2 Forecast 68% CL constraints on w and Ω_{DE} from weak lensing in the DES. Red: shear-shear correlations; green: galaxy-shear correlations, with halo model parameters constrained by foreground galaxy auto-correlations; blue: joint constraints from all three power spectra. Dotted curves indicate approximate constraints expected after 2 years of data, according to the survey strategy described in Chapter 4.

The statistical accuracy of these parameter measurements, while impressive, can only be reached if systematic errors are kept under control. For shear measurements, the dominant systematic error comes from residuals in correcting galaxy shapes for the effects of an anisotropic point spread function (PSF), caused by optical and CCD distortions, tracking errors, wind shake, atmospheric refraction, etc. One uses the shapes of stars to measure, interpolate, and correct the PSF, but the finite angular density of well-measured stars yields a sparse sampling of the spatially and temporally varying PSF field. Our experience with weak lensing measurements using the wide-field Mosaic II camera on the Blanco 4-m telescope demonstrates that the PSF can be accurately mapped and corrected to be circular across the field to less than 0.5%. For the wider-field Dark Energy Camera and associated corrector, an optical design with low, stable, and smoothly varying distortion across the field of view is required. The galaxy-shear correlations are less sensitive to these systematics than shear-shear correlations, because PSF anisotropy tends to cancel out of the azimuthally averaged tangential shear field measured around foreground galaxies. Moreover, since the foreground galaxy auto-spectrum is independent of the shear measurements, it provides an independent cross-check on the shear systematics.

In addition to statistical measurements, weak lensing in the Dark Energy Survey will yield low-resolution projected mass maps and mass profiles for galaxy clusters, especially in the redshift range $z \sim 0.1-0.5$. In addition, the shear fields for clusters of given redshift and galaxy number or SZE flux can be ‘stacked’ to yield a mean mass profile, useful for calibrating cluster mass estimates based on optical galaxy counts or the SZE. An example of a low-redshift cluster mass reconstruction using the Blanco 4-m (with cumulative exposure time longer than for the DES) is shown in Fig. 2.4-3 (from Joffre et al. 1999); the shear in the inner regions, of order a few percent, is detected at 7σ .

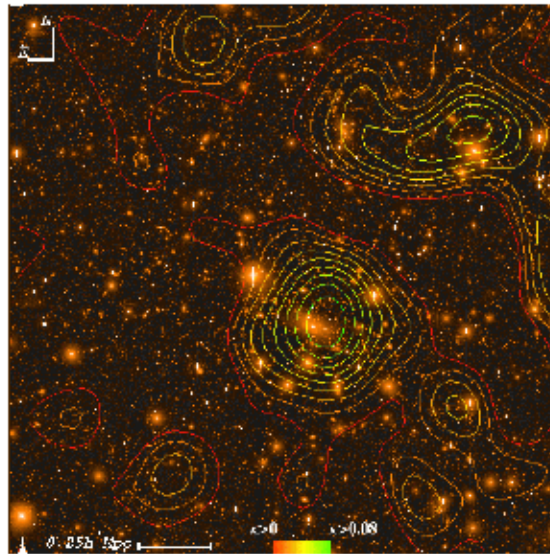


Figure 2.4-3 Reconstructed projected mass map for the $z = 0.05$ cluster Abell 3266 superposed on an R -band image with the BTC from the Blanco 4-m telescope. Contours are significance levels, and the image is 44 arcmin on a side; the galaxy source density used to reconstruct the mass map was 15 per arcmin².

2.4.1 Constraining Dark Energy Evolution with Clusters and Weak Lensing

The forecast constraints from the cluster survey and from weak lensing shown so far have assumed the dark energy equation of state w is constant in time. In fact, if $w \neq -1$, then it is likely to evolve as well; current constraints on the evolution of w are very weak, and determining it will be an important goal of future dark energy projects. It is convenient to parametrize the evolution by writing $w(a) = w_0 + (1-a)w_a$, where $w_a = -dw/da|_0$, subscript 0 denotes the present epoch, and the cosmic scale factor $a = 1/(1+z)$. Fig.2.4-3 shows forecast constraints on w_a vs. w_0 from weak lensing and from the cluster survey (Hu 2004). Note that, for illustrative purposes, the assumptions and priors used here differ somewhat from those used above. In particular, here the CMB priors on parameters (now including dark energy parameters) are more aggressive, coming from expected statistical errors from the Planck satellite. For cosmic shear, we use the same range of angular scales for the analysis as above; however, for the galaxy-shear measurement, here we include lens galaxies in halos down to $10^{12.5} h^{-1} M_{sun}$, i.e., we push the halo model down to lower masses, but we only include constraints from angular multipoles $\ell < 1000$, a more restrictive range than above. For the cluster redshift distribution and mass function, here we include all clusters more massive than $10^{14.2} h^{-1} M_{sun}$ in 10 redshift bins to $z = 1$. To show the effects of uncertainty in the mass-observable relation, we show constraints for (i) perfect calibration of the relation, (ii) allowance for uncalibrated power-law evolution of the relation with redshift, and (iii) inclusion of self-calibration using the cluster power spectrum (variance in counts in cells). For both weak lensing and the cluster survey, the forecast (purely statistical) constraint on the evolution of w is at the level of $\delta w_a \sim 0.5$.

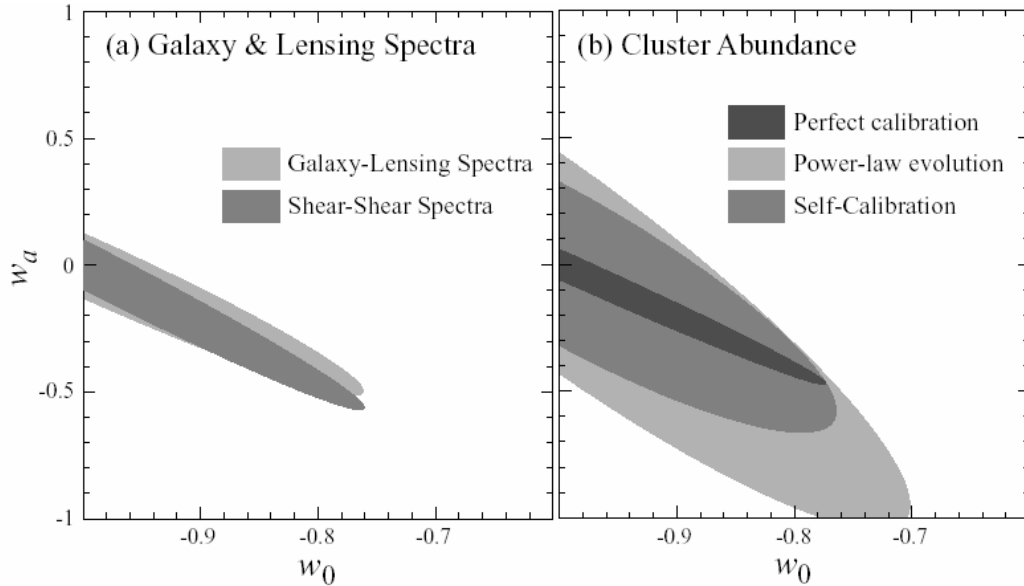


Figure 2.4-3 68% CL constraints on evolution of the dark energy equation of state w_a vs. w_0 for (a) cosmic shear ('shear-shear') and galaxy-shear ('galaxy-lensing') correlations and (b) the cluster abundance. In these plots we marginalize over dark energy density Ω_{DE} , assuming a flat Universe, and assume Planck CMB priors on cosmological parameters.

2.5 Galaxy Angular Clustering

The Dark Energy Survey (DES) will deliver a sample of over 300 million galaxies extending beyond a redshift of one. On large scales, galaxy clustering and its evolution should reflect the gravitational dynamics of the underlying dark matter distribution. The ratio of the galaxy and dark matter power spectra can be described by a redshift-dependent bias factor, $b^2(z)$, that is theoretically expected to be scale-independent on large scales, although its amplitude does depend on the type (e.g., luminosity, color) of galaxy being studied. In the linear regime, we can write the galaxy power spectrum as

$$P_{gal}(k) \propto k^n T^2(k, p_i) g^2(z, p_j) b^2(z), \quad (2.5:1)$$

where the initial dark matter power spectrum from the early Universe $\propto k^n$, $T(k)$ is the scale-dependent transfer function for dark matter perturbations, $g(z)$ is the scale-independent perturbation growth function, and the p_i remind us that these functions depend explicitly on cosmological parameters. In practice, we replace this simple bias model with the more physically motivated and numerically justified halo model mentioned above.

As with lensing, we will measure the galaxy angular power spectrum within photometric redshift bins to probe the dark energy. The angular power spectrum within a redshift shell can be written as

$$C_{gal}^i(l) = \int_0^\infty k^2 dk \frac{2}{\pi} f_i^2(l, k) P_{gal}(k), \quad (2.5:2)$$

where $f_i(l, k)$ is the Bessel transform of the radial selection function for redshift shell i (Tegmark et al. 2002, Dodelson et al. 2002).

The transfer function has a characteristic break on a physical scale corresponding to the horizon size at matter-radiation equality, determined by the mean dark matter density, as well as small wiggles associated with the effects of baryon acoustic oscillations on the dark matter distribution. Within each redshift shell, the angular power spectrum will reflect this characteristic break at some characteristic angle. Thus, the angular power spectrum constrains a redshift-dependent combination of the matter density and the angular diameter distance (Cooray et al 2001). An estimate of the resulting dark energy constraints, marginalized over the 5 halo parameters in each redshift shell, assuming spatial flatness, and restricting information to angular multipoles $50 < l < 300$ where the halo model of bias should be robust, is shown in Fig. 2.5-1. Here we have included statistical Planck CMB priors on the power spectrum, employed 10 photometric redshift shells to $z = 1$, and included galaxies in halos with mass greater than $10^{12.5} h^{-1} M_{sun}$.

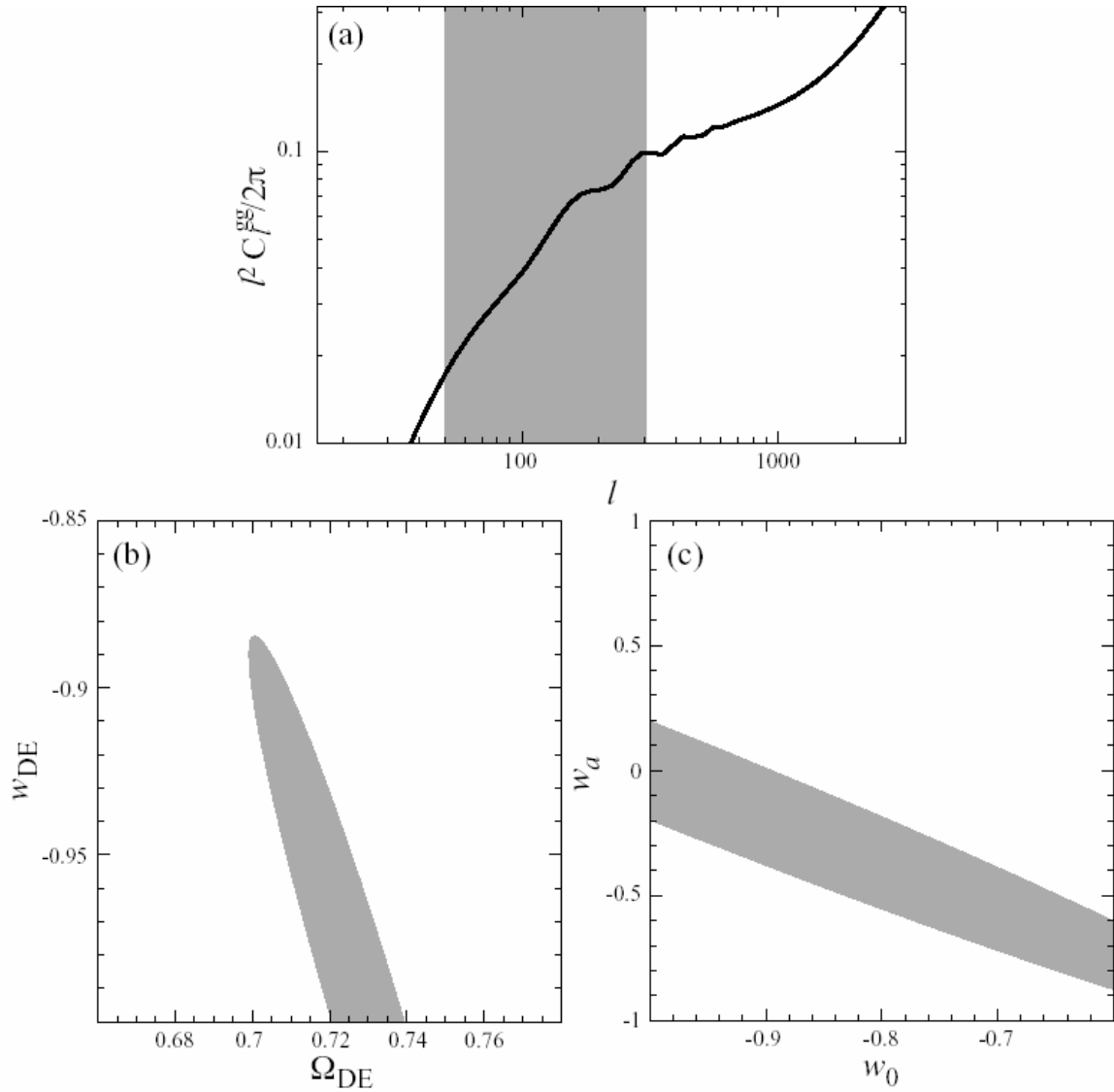


Figure 2.5-1 (a) Galaxy angular power spectrum at $z = 1$ in a bin of width $\Delta z = 0.1$; (b) 68% CL dark energy constraints for constant w , using the shaded band in (a) and 10 angular spectra; (c) constraints on dark energy evolution, marginalized over dark energy density Ω_{DE} . Here, Planck CMB priors on cosmological parameters are assumed.

2.6 Supernovae and Dark Energy

Using supernova (SN) light curves to measure the expansion history of the universe has rapidly become a foundational standard of cosmological studies. Studies of nearby SNe (*e.g.*, Hamuy et al. 1996a) provided the basis for the development of methods using Type Ia SNe as precision distance indicators (*e.g.*, Hamuy et al. 1996b, Riess, Press, & Kirshner 1996, Perlmutter et al. 1997), and the application of these methods to studies of high redshift SNe provided the first direct evidence for the accelerating expansion of the Universe (Riess et al. 1998, Perlmutter et al. 1999). Moreover, the dark energy constraints from supernovae

are complementary to those derived from the CMB, large-scale structure, and, in the future, from lensing and cluster surveys.

The methods used to extract information from SN light curves are now undergoing rapid refinement and improvement. The sources of systematic uncertainty are being addressed and either minimized or eliminated by new measurement capabilities and larger samples. As this control of systematic uncertainties improves, new supernova surveys successively take advantage of this knowledge by performing more detailed and controlled measurements on both the supernovae and the supernova samples, lowering the statistical uncertainty to the improved systematic limit.

With the Dark Energy Survey, we have the opportunity to make the next step forward in this progression. Compared to the current generation of supernova surveys (*e.g.*, ESSENCE on the Blanco telescope and the CFHT SN Legacy Survey), we will have new measurement capabilities and a wider field to collect larger numbers of supernovae over a wide range of redshifts. The proposed instrument design will allow much better control over the wavelength response of the entire photometric system. In addition, the proposed detectors will allow much better throughput in the redder wavelengths that are crucial both to measuring SNe at high redshift and to controlling and quantifying the systematics related to dust and intrinsic SN dispersion at lower redshifts.

Based on these new capabilities, we have designed a baseline supernova experiment which uses approximately 10% of the time dedicated to the Dark Energy Survey operations, assumed to be 30% of the telescope time over a five-year period. The requirements of this design include the production of a large number of well-sampled SN light curves in three bands in an observing strategy that fits within the 5000 deg² DES survey area and survey strategy. Balancing spatial coverage with depth to cover a wide range of redshifts ($0.25 < z < 0.75$), we have selected nominal exposure times of 200s in r , 400s in i , and 400s in z . These exposure times should give us reasonable signal to noise SN light curves in these bands out to $z \sim 0.75$. We would use roughly one hour per night over four months each year for five years. Each night we would cover roughly one third of our total survey area, returning to the same fields every third night. Each observation of a given field would be taken in r and alternately in i and z ; with this cadence, we would obtain r band SN light curves sampled every third night, with i and z band light curves sampled every sixth night. In total we would cover 13 Dark Energy Camera fields or 40 square degrees of sky, a much larger area than that covered by any current intermediate to high redshift SN survey.

With this baseline design, we have run Monte Carlo simulations of the SN survey, assuming that the Dark Energy Camera has roughly similar r and i band response to that of the existing CTIO Mosaic II camera (a conservative assumption) and with the improved z band response described in Chapter 5. Folding these sensitivities in with the historical weather, seeing, and other observational factors, we estimate that we will identify more than 1900 Type Ia SNe (along with many SNe of other types) over the course of the five-year program.

Using this large sample of well-characterized SNe, we can constrain dark energy parameters such as w . Figure 2.6-1 shows the results of propagating the simulated light curves through a

sample analysis to determine the resulting cosmological parameters. The panel shows the SN results alone and combined with the existing large-scale structure results of the 2dF survey. In combination with other DES dark energy probes, these constraints will be significantly tighter than those hoped for from the set of SN surveys currently underway.

These simulations have many assumptions folded in, most of them based on the experiences of past and current SN surveys, some of which may not be directly applicable to the DES SN survey. Most important among these is the implicit assumption that we will know the types and redshifts for all of the SNe in our sample through spectroscopic observations of the SNe and/or their host galaxies. We will discover more than 3000 SNe of all types in the planned DES SN survey, and *immediate* spectroscopic follow-up of *all* of these SNe is likely to be impossible. We can, however, rely on the host galaxy photometric redshifts generated by the Dark Energy Survey itself, as well as complementary photometric redshift measurements provided by other surveys which overlap the area covered in the DES SN survey, such as the SDSS, the VIMOS-VLT Deep Survey (VVDS), and the NOAO Deep Wide Field Survey (NDWFS). We estimate that we should have photometric redshift estimates for more than 80% of the host galaxies of the SNe we discover. In addition, host galaxy spectroscopic redshifts can be obtained over a longer timescale. Our preliminary studies indicate that the errors in photometric redshift are anti-correlated with both the K-correction errors and the uncertainties in the decline rate or width versus brightness relations. Based on these estimates, we predict that the rms of our SN distance determinations may increase from the ~ 0.15 magnitudes typical of well-studied samples with follow-up spectroscopy to ~ 0.25 magnitudes with photometric redshifts only.

We are nevertheless planning to propose for extensive spectroscopic follow-up with instruments on 4m to 10m telescopes worldwide; given the breadth of our collaboration, we will almost certainly be able to obtain spectra of a significant fraction ($>25\%$) of the SNe in our sample and a much higher fraction of host galaxy spectra. Existing spectroscopic measurements of host galaxies from SDSS, VVDS, and NDWFS will of course complement the spectroscopy we are able to obtain. This subsample of spectroscopically observed SNe will not only provide lower uncertainties for some fraction of our SN sample, it will also provide a control sample against which we can compare the results of our analysis of the SNe which lack spectroscopic observations. In particular, these studies will allow us to gauge the level of contamination of the color-selected Ia sample by other supernova types. Together, these efforts will decrease the uncertainties in our derivation of cosmological parameters from the “worst case” scenario relying on only the available photometric redshifts. In the simulations portrayed in Figure 2.6-1, we have used an rms value of 0.20 magnitudes to demonstrate the results which may be possible from detailed analysis of a sample of SNe with a mixture of photometric and spectroscopic redshifts.

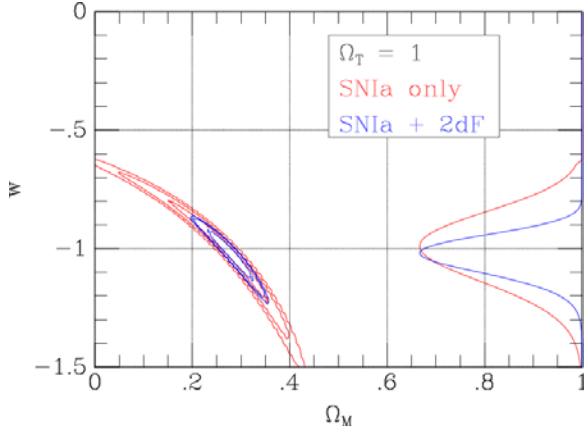


Figure 2.6-1. Projected constraints on Ω_M and w from the five-year DES SN survey. A flat cosmology has been assumed. Red: the SN survey alone; blue: joint constraints from SNe + 2dF ($\Omega_M = 0.278 \pm 0.042$). Contours represent 1, 2, and 3 σ confidence levels. The curves at right represent the constraints on w after marginalization over Ω_M .

It is important to note that our Survey Instrument would be one of the primary instruments in the world for this type of supernova survey during its years of operation. We expect that the current generation of surveys will yield suggestive results and puzzles that will be addressed by the DES SN work, so the baseline plan described above is very likely to be updated with a significantly more sophisticated plan that builds on what we know at the time we begin this effort. It is also significant that many of the challenges we face in the DES SN survey, such as the lack of spectroscopic information on the majority of SNe, are the same as those which will be faced in the following decade when we attempt to use the incredible samples of SNe which the LSST will identify continuously throughout its operational lifetime. Just as the results of the current generation of SN surveys will guide us in updating and refining the strategies we will employ for the DES SN survey, so will this survey provide crucial experience and guidance for deriving scientific results from the plethora of SNe discovered by LSST.

2.7 Photometric Redshifts

In order to achieve the dark energy scientific goals described above, the Dark Energy Survey will need to obtain accurate galaxy photometric redshifts to $z \sim 1$. This requirement is therefore a prime driver of the design and strategy of the Dark Energy Survey discussed in subsequent chapters. In the absence of spectroscopic data, redshifts of galaxies may be estimated using multi-band photometry, which may be thought of as very low-resolution spectroscopy. Though such photometric redshifts (or photo- z 's) are necessarily less accurate than true spectroscopic redshifts, they nonetheless are sufficient for the science applications we envision. Photo- z 's may be obtained less expensively and for much larger samples than is possible with spectroscopy.

There are two basic approaches to measuring galaxy photometric redshifts. The first relies on fitting model galaxy spectral energy distributions (SEDs) to the photometric data, where the models span a range of expected galaxy redshifts and spectral types (e.g., Sawicki et al. 1997). The second approach depends on using an existing spectroscopic redshift sample as a training set to derive an empirical photometric redshift fitting relation (Connolly et al. 1995). There are advantages and disadvantages to each approach, as well as a number of variants and hybrids of these basic techniques (e.g., Csabai 2003). However, photometric redshift methods ultimately rely on measuring the signal in the photometric data arising from

prominent “break” features present in galaxy spectra, e.g., the 4000Å break in red, early-type galaxies, or the Lyman break at 912Å in blue, star-forming galaxies. The key is to have photometric bands which cover such break features throughout the redshift range of interest, so that the primary redshift signal may be readily detected. Additional refinements in the photometric redshift measurement then come from the strength of the break features and the gross shape of the galaxy SED, as determined by the photometric data on either side of the spectral break.

2.7.1 Photometric Redshift Simulations for Cluster Galaxies

Cluster photometric redshift measurements are greatly facilitated by the strength of the 4000Å break feature prominently seen in the spectra of red cluster galaxies. This is illustrated in Figure 2.7-1, which shows a red, elliptical galaxy spectrum at redshifts 0, 0.5, and 1, superimposed on the *griz* filter bandpasses. The 4000Å break moves through the different filters as the galaxy redshift increases. Measurements of the relative galaxy fluxes through the different filters provide an estimate of the observed wavelength of the 4000Å break and hence of the galaxy redshift. This is demonstrated in Figure 2.7-2, where we compare photometric and spectroscopic redshifts for a sample of SDSS red galaxies, for which we are able to obtain photometric redshifts with a scatter $\sigma_z = 0.03$ out to redshifts $z \approx 0.6$. However, at higher redshifts we do not have such large samples of red galaxies available, and so we need to rely on Monte Carlo simulations to assess the quality of cluster galaxy photometric redshifts for the Dark Energy Survey.

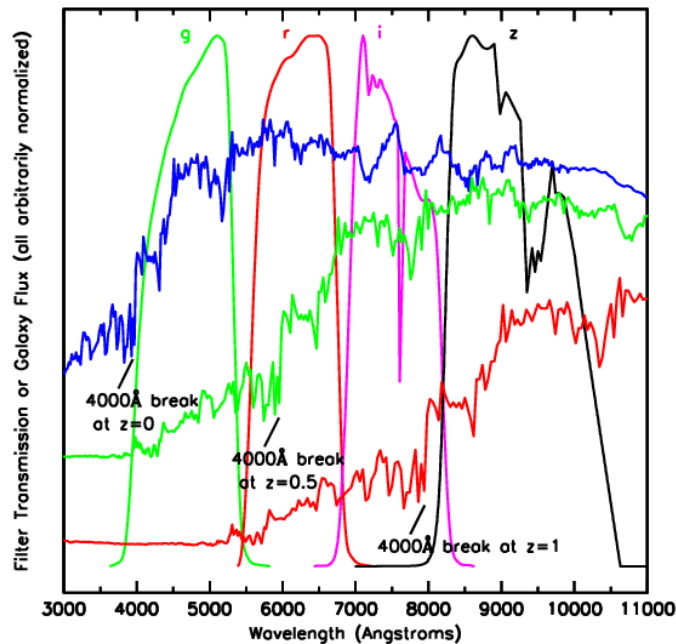


Figure 2.7-1 The spectrum of a red, elliptical galaxy is shown at redshifts $z = 0, 0.5,$ and 1, with the location of the prominent 4000Å break feature marked. The spectra have been vertically offset for clarity. Also shown are the *griz* filter bandpasses, arbitrarily normalized to the same peak value. Photometric redshift information for red galaxies comes primarily from changes in the relative galaxy fluxes in the different filters as the 4000Å break moves to longer observed wavelengths at higher redshift.

In our cluster Monte Carlo simulations, we adopt the local cluster luminosity function, and luminosity-mass and number-mass relations (within the virial region set by R_{200}), found by Lin, Mohr, & Stanford (2004). We take the cluster galaxies to evolve with redshift according to a passively evolving elliptical galaxy model from the Pegase-2 SED library (Fioc & Rocca-Volmerange 1997). The Pegase-2 model is designed to match the colors of SDSS red galaxies at low redshifts and is a 13 Gyr model that incorporates self-consistent star formation until the onset of galactic winds at $z=3$. A flat cosmology, with $\Omega_M=0.3$, $\Omega_\Lambda=0.7$, and $h=0.7$ is used. The cluster luminosity function faint-end slope is fixed at $\alpha=-1.1$, but we take the halo occupation number to evolve with redshift as $(1+z)^\gamma$, where $\gamma=1$ (Lin et al. 2004; Kravtsov et al. 2004). Using these assumptions, we can simulate the *griz* magnitudes of cluster galaxies as a function of redshift. Expected photometric errors are calculated by appropriately scaling the S/N relative to the 10σ magnitude limits *griz* = 24.6, 24.1, 24.0, 23.65, and by adding in quadrature a 2% error due to photometric calibration uncertainty (although these flux limits go beyond the survey requirements in *g* and *r* given in Chapter 3, the survey plan in Chapter 4 indicates they should be achievable; the enhanced depth in these bluer filters does not have a large effect on cluster galaxy photometric redshift errors). For the purposes of photometric redshift estimation for an entire cluster, it suffices to calculate the total light in each filter contributed by all cluster galaxies down to the 10σ limit in the *z* band, which maximizes the number of detected cluster galaxies. Here, we are considering the case in which we know a cluster exists along a particular line of sight based on the SZE detection from the SPT survey, so we are not concerned with the optical cluster detection significance, as we would be for a purely optical cluster finding technique. We will, however, scale our total light estimates by a conservative “loss” fraction of 0.5 to account for various effects, such as contaminating field galaxies, cluster blue fractions, and the like.

We use a simple least-squares template fitting method to determine photometric redshifts for clusters of mass 1.0×10^{14} and $2.5 \times 10^{14} M_{sun}$. For each case, 20,000 mock clusters are generated and distributed uniformly over the redshift range $z = 0-2$. Fig. 2.7-3 shows the results and demonstrates that the Dark Energy Survey should provide robust photometric redshifts for such clusters to $z \approx 1.3$. For these clusters, we find a small photo-*z* scatter (68% limit) $\sigma_z \leq 0.02$, with the tails of the photo-*z* error distribution extending no more than about 0.05 in redshift. At higher redshifts, $z > 1.3$, color degeneracies become important, and the tails of the error distribution become larger, though the 68% limit scatter is still typically $\sigma_z < 0.1$. Note also that removing our assumed halo occupation number evolution gives a change in photo-*z* quality comparable to that seen in reducing the cluster mass by the factor of 2.5 shown in Fig. 2.7-3. In practice, we will need to acquire a spectroscopic redshift training set (see below) in order to empirically measure the correct cluster galaxy SED to use for our final photo-*z* calibration, especially at redshifts $z > 0.7$ where existing galaxy cluster data are very sparse. However, our current simulation results do show that the expected Dark Energy Survey flux limits are sufficient to provide robust photometric redshifts for our cluster-based dark energy science goals.

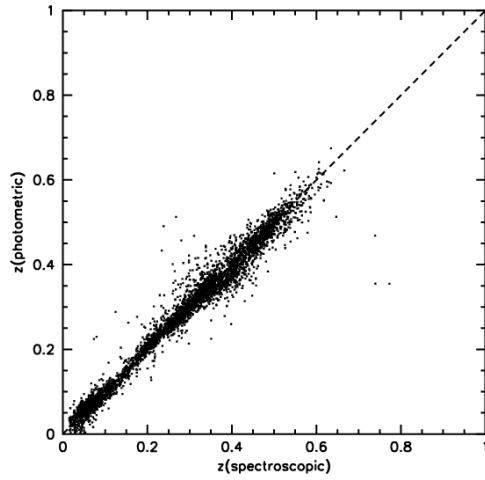


Figure 2.7-2 Photometric and spectroscopic redshifts are shown for a sample of SDSS red galaxies, for which a photometric redshift scatter $\sigma_z=0.03$ is obtained.

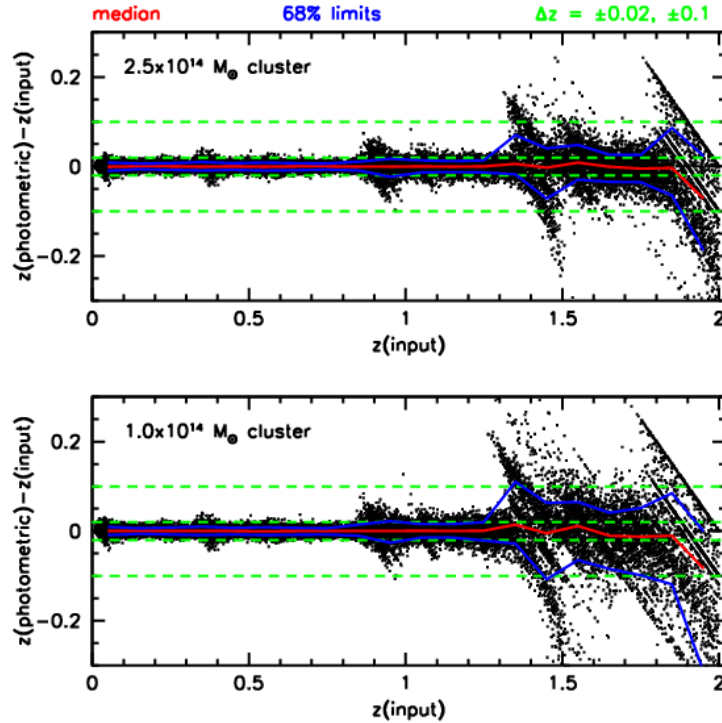


Figure 2.7-3 Photometric redshift results for the 1.0×10^{14} and $2.5 \times 10^{14} M_{sun}$ galaxy cluster Monte Carlo simulations; see text for the details. The red lines show the median difference between photometric and true redshift, the blue lines show the 1σ scatter (68% limits), and the green dashed lines are set at $\Delta z = \pm 0.02$ and ± 0.1 to guide the eye.

2.7.2 Photometric Redshifts for the General Galaxy Population

We also aim to obtain photometric redshifts for the general galaxy population, beyond red cluster galaxies, in particular to facilitate dark energy measurements using weak lensing,

galaxy clustering, and supernovae. Such photo- z 's are necessarily less accurate than those possible for cluster galaxies, as we must consider a much broader distribution of galaxy SEDs. Nonetheless, as we shall show, good photometric redshift measurements out to $z \approx 1.3$ can be achieved for the general galaxy population in the Dark Energy Survey.

We demonstrate this with a Monte Carlo simulation, using galaxy SEDs from the Coleman, Wu, & Weedman (CWW; Coleman et al. 1980) sample. We use 20,000 mock galaxies, uniformly distributed in redshift ($z = 0-1.5$), magnitude ($i = 23-24$), and SED type (E to Im), and noise is added as appropriate for the Dark Energy Survey *griz* flux limits given in Chapter 4. Note that this simulation is only intended to estimate the photo- z uncertainty (averaged over galaxy types) as a function of redshift, rather than to approximate a realistic galaxy redshift distribution. In particular, we apply a simple least-squares template fitting method that only uses color information; hence no flux-redshift correlations are used, as would be the case for polynomial photo- z fitting.

Our results are shown in Figure 2.7-4, where we find that the photometric redshift scatter (68% limits) is typically $\sigma_z = 0.1-0.2$ for these galaxies with $i = 23-24$ (note that $i = 24.0$ is the required survey 10σ limit). Though not shown in the figure, the photo- z scatter does of course improve at brighter magnitudes, where we find $\sigma_z \approx 0.05$ at $i = 22$. Note that the photo- z trends vs. spectroscopic redshift in Figure 2.7-4 are in general well behaved, except at the lowest redshifts, $z < 0.3$, where the photometric redshift is scattered systematically high. This is likely a consequence of the lack of a constraining filter blueward of the 4000Å break at these low redshifts.

We have also checked our photo- z results using an empirical, deep galaxy sample, the publicly available ground-based *VRIZ* photometric data obtained by Capak et al. (2004) in the GOODS/HDF-N area, combined with a training set of 1800 spectroscopic redshifts (down to the DES depths) from the compilations of Wirth et al. (2004) and Cowie et al. (2004). The *VRIZ* photometry serves as a best-effort approximation to *griz*, and we add noise to the original *VRIZ* photometry in order to match the Dark Energy Survey depths. We derive photo- z 's using polynomial fitting and find similar photo- z results as for our simulated galaxies. In general, it will be important to understand in detail the scatter and biases in our photometric redshifts by carefully measuring the photo- z error distribution using a large spectroscopic redshift training set. Two such large redshift surveys, the VIMOS VLT Deep Survey (VVDS; Le Fevre et al. 2003) and the Keck DEEP2 Survey (Davis et al. 2002), are both currently in progress. These surveys should provide spectroscopic redshifts sufficient to calibrate general galaxy population photo- z 's down to the Dark Energy Survey requirement limit of $i = 24$. In particular, the VVDS will obtain about 100,000 redshifts, and it is also being carried out from Chile. All the VVDS fields will be accessible to *griz* imaging using the Blanco 4-m, enabling us to derive detailed photometric redshift calibrations for the Dark Energy Survey.

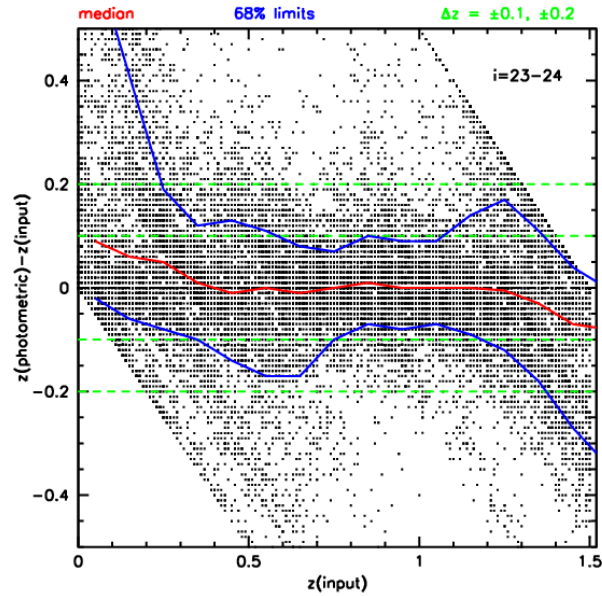


Figure 2.7-4 Photometric redshift results for the general galaxy population Monte Carlo simulations, for the magnitude range $i = 23-24$; see text for details. The red lines show the median difference between photometric and true redshift, the blue lines show the 1σ scatter (68% limits), and the green dashed lines are set at $\Delta z = \pm 0.1$ and ± 0.2 to guide the eye.

References

- Annis, J., et al. 1999, AAS, 195, 1202
Bahcall, N. A., et al. 2003, ApJS, 148, 243
Battye, R. & Weller, J. 2003, PRD, 68, 083506
Bernstein, G., & Jarvis, M. 2002, AJ, 123, 583
Blake, C., & Glazebrook, K. 2003, ApJ, 594, 665
Capak, P., et al. 2004, AJ, 127, 180
Coleman, G.D., Wu, C.-C., & Weedman, D.W. 1980, ApJS, 43, 393 (CWW)
Connolly, A.J., et al. 1995, AJ, 110, 2655
Cooray, A., et al. 2001, ApJ, 557, L7
Cowie, L.L., et al. 2004, AJ, submitted, astro-ph/0401354
Csabai, I., et al. 2003, AJ, 125, 580
Davis, M., et al. 2002, SPIE, astro-ph/0209419
Dodelson, S. 2003, astro-ph/0309277
Dodelson, S., et al. 2002, ApJ, 572, 140
Eisenstein, D., Hu, W., & Tegmark, M. 1998, ApJ, 504, L57
Ellis, R.S., et al. 1997, ApJ, 483, 582
Fioc, M., & Rocca-Volmerange, B. 1997, A&A, 326, 950
Gladders, M.D., et al. 2003, ApJ, 593, 48
Gladders, M.D., & Yee, H.K.C. 2000, AJ, 120, 2148

Haiman, Z. et al. 2001, ApJ, 553, 545
Hamuy, M., et al. 1996a, AJ, 112, 2408
Hamuy, M., et al. 1996b, AJ, 112, 2438
Hu, W. 2002, PRD, 66, 3515
Hu, W. 2003, PRD, 67, 1304
Hu, W. 2004, in Proceedings of the Tucson Dark Energy Conference
Hu, W., et al. 1999, PRD, 59, 3512
Hu, W., & Haiman, Z. 2003, PRD, 68, 3004
Hu, W. & Jain, B. 2003, astro-ph/0312395
Hu, W., & Kravtsov, A.V. 2003, ApJ, 584, 702
Huterer, D. 2002, PRD, 65, 3001
Jain, B., & Taylor, A. 2003, PRL, 91, 1302
Jenkins, A., et al. 2001, MNRAS, 321, 372
Joffre, M. et al. 1999, in “Gravitational Lensing: Recent progress and Future Goals”, eds. T. Brainerd and C. Kochanek, ASP Conf. Series (2000)
Kaiser, N. 1992, ApJ, 388, 272
Kravtsov, A.V., et al. 2004, ApJ, 609, 35
Le Fevre, O., et al. 2003, astro-ph/0311475
Lidman, C. et al. 2003, A&A, in press, astro-ph/0310516
Lima, M., & Hu, W. 2004, PRD, submitted, astro-ph/0401559
Lin, Y.-T., et al. 2003, ApJ, 591, 749
Lin, Y.-T., Mohr, J.J., & Stanford, S.A, ApJ, in press, astro-ph/0402308
Linder, E.V., & Jenkins, A. 2003, MNRAS, 346, 573
Majumdar, S., & Mohr, J.J. 2003a, ApJ, 585, 603
Majumdar, S., & Mohr, J.J. 2003b, ApJ, submitted, astro-ph/0305341
McKay, T.A., et al. 2004, in preparation
Perlmutter, S., et al. 1997, ApJ, 483, 565
Perlmutter, S., et al. 1999, ApJ, 517, 565
Perlmutter, S., & Schmidt, B.P. 2003, astro-ph/0303428
Riess, A., et al. 1998, AJ, 116, 1009
Riess, A. G., Press, W. H., & Kirshner, R. P. 1996, ApJ, 473, 88
Sawicki, M.J., Lin, H., & Yee, H.K.C 1997, AJ, 113, 1
Seo, H.J., & Eisenstein, D. J. 2003, ApJ, 598, 720
Sheldon, E.S., et al. 2001, ApJ, 554, 881
Spergel, D.N., et al. 2003, ApJS, 148, 195
Stanford, S.A., et al. 1998, ApJ, 492, 461
Tegmark, M., et al. 2002, ApJ, 571, 191
Tegmark, M., et al. 2003, PRD, in press, astro-ph/0310723
van Dokkum, P.G., et al. 2000, ApJ, 541, 95
van Dokkum, P.G., et al. 2001, ApJ, 552, L101
Wang, L., & Steinhardt, P.J. 1998, ApJ, 508, 483
White, M., van Waerbeke, L., & Mackey, J. 2002, ApJ, 575, 640
Wirth, G.D., et al. 2004, AJ, submitted, astro-ph/040135
Zhang, J., Stebbins, A., & Hui, L. 2003, astro-ph/0312348

3. From the Science Program to the Technical Requirements

Our science program was outlined in the previous Chapter and is summarized below. In this Chapter we show how the science program evolves into technical requirements for the Dark Energy Survey Instrument. The science requirements given below are unlikely to change; however, the technical requirements and the choices that we have made to reach them (e.g. number of filters) represent a reference design of the Dark Energy Survey Instrument. This is not a final design; further analysis may indicate better solutions are possible.

3.1 Science Goals

Our overarching science goal is to measure w , the dark energy equation of state, to a precision of order $\delta w \leq 5\%$ using four separate techniques:

1. **Cluster Survey:** In this method we measure the cluster redshift distribution and the cluster power spectrum. Cluster mass estimates come indirectly through the measured bias of the cluster power spectrum, and they also come directly from SZE, weak lensing, and cluster galaxy observables. To accomplish our goals, we must be able to locate and measure the redshifts of clusters of galaxies out to $z \geq 1$, because this is the expected extent of the coordinated South Pole Telescope SZE cluster survey. The cluster redshift distribution and power spectrum are sensitive to dark energy as probes of the volume and growth function. The survey must cover large solid angle to enable the cluster power spectrum measurement and to deliver large cluster samples. The survey must have multiple bandpasses for precision photometric redshifts, and faint limiting magnitudes to increase the number of galaxy photometric redshifts available for each cluster.
2. **Weak Lensing:** The weak lensing of background galaxies by foreground mass sheets, correlated with itself (shear-shear correlations) or with foreground galaxies (shear-galaxy correlations) is sensitive to dark energy as a standard ruler and growth function probes. The DES Instrument must be able to measure the weak lensing signal from large scale structure in several redshift bins with small and stable instrumental point spread functions. Large solid angle is required to probe the shear field over the largest possible range in physical scales.
3. **Galaxy Angular Power Spectra:** Measurement of the angular power spectra of galaxies in several redshift bins can also put constraints on w , because it is a standard ruler probe. To accomplish this measurement, we must have a stable photometric calibration, cover large solid angle to probe a wide range of physical scales, and have faint limiting magnitudes to increase our sample size and probe to redshifts beyond $z \sim 1$.
4. **Supernovae:** The apparent magnitude of Type Ia supernovae provides a standardizable candle luminosity distance measurement. The DES Instrument will be used to measure light curves of more than 1900 supernovae out to $z = 0.8$. The observations must cover a moderately large solid angle repeatedly to obtain lightcurves of the SNe. These SN observations must be taken in multiple (at least three) bandpasses to provide colors of the objects, both for reddening measurements and SN type discrimination based on colors. Excellent red response is necessary to obtain adequate signal for higher redshift

SN lightcurves. Detailed knowledge of the system passbands as a function of wavelength is required for accurate k correction calculations.

3.2 Science Requirements

The primary science requirement is to provide photometric redshifts for the galaxy clusters detected in the South Pole Telescope SZE survey. The data required to meet this primary requirement will facilitate coordinated studies of optically selected cluster samples, weak lensing, and the galaxy angular power spectrum. The observing efficiency and scientific return of an extensive photometric survey like the Dark Energy Survey benefits from the addition of the time domain SN Ia component, which will be pursued even during non-photometric time.

3.2.1 Filters

To meet the photometric redshift requirement we will bracket the 4000Å break signal in the elliptical galaxy spectrum typical of cluster galaxies. At $z=0$, the blue side limit is 400 nm. Redshift moves this restframe value redward. At $z=1$, the 4000Å break is at 800nm. Precision photometric redshifts require a filter redward of the observed break. We thus need bandpasses from 400nm to 1000nm. For our reference design, we adopt the SDSS filter set, g, r, i, z, with z as the fiducial bandpass. This choice allows us to leverage the existing body of work done with these filters to aid in analysis and calibration of DES data.

3.2.2 Limiting Magnitudes

Measuring accurate photometric redshifts of the clusters near the detection threshold in the SPT SZE survey at redshifts $z\sim 1$ drives us to faint magnitude limits. Reaching the cluster photometric redshift accuracy of $\delta z=0.02$ requires that we measure photometric redshifts of at least ten galaxies in clusters of mass $M=2\times 10^{14}M_{\odot}$ at $z=1$. A limiting absolute magnitude corresponding to a $0.5L^*$ galaxy suffices for photometric redshifts of this precision, and a side benefit is that photometry of cluster galaxies to this depth enables efficient optical cluster detection as well. The absolute magnitude of a $0.5L^*$ galaxy at $z=0$ is, in the i-band, $M_i = -21.0$ (Blanton et al 2003, redshift and evolution corrected). At $z=1$ such a galaxy would, if it followed the passively evolving old stellar population model appropriate for high luminosity cluster galaxies, have a z-band magnitude $z=23.3$. We require 10σ observations, for the photometric redshift techniques. Data from both the CTIO Blanco 4-m and the CFHT 3.6m show that 10σ is near where the differential number counts turn over, an indication that it is close to the completeness limit. We will go 0.3 mags deeper in the fiducial band in order to safely construct a flux-limited sample of galaxies. We therefore require a limiting magnitude of $z=23.6$.

The minimum apparent magnitudes in the remaining bandpasses follow by considering the redshifted, passively evolving spectrum of a cluster galaxy. The limiting magnitude required is that for a $0.5L^*$ galaxy at the redshift where the 4000Å break leaves the bluer filter and enters the redder filter. The 4000Å break leaves the g, r and i bandpasses at redshifts of 0.35, 0.65, and 1.0 respectively. The corresponding limiting magnitudes are shown in Table 3.1. We will see later that the requirements on the g and r limiting magnitudes are easy to meet.

Table 3.1 Limiting Magnitudes

Filter	g	r	i	z
Mag (10σ)	22.8	23.4	24.0	23.6

3.2.3 Photometric Calibrations

We plan to calibrate the final coadded map to 1%; however, meeting the science goals for the photometric redshifts only requires photometric calibrations accurate to the level of 2%. Our science goals also require that a calibrated spectrum, convolved with the DES system response, will predict the observed magnitude to 2%. We have no requirement on the calibration of single images, but we estimate that these can be calibrated to 10% using the USNO B2 star catalogue.

3.2.4 The Survey Area

The DES will cover a total of 5000 sq. degrees in the Southern Galactic Cap. Figure 3.1 and Table 3.2 show the specific areas. Below we describe the motivation for these choices.

Table 3.2 Dark Energy Survey areas

Overlap target	Right Ascension (deg)	Declination (deg)	Area (sq. deg.)
SPT	-60 to 105	-30 to -65	3988
	-75 to -60	-45 to -65	
SDSS Stripe 82	-50 to 50	-1.0 to 1.0	200
Connection region	20 to 50	-30 to -1.0	800

3.2.4.1 SPT overlap

The primary science requirement for the DES cluster survey measurement of w is to image an area overlapping that of the observations of the CMB by the South Pole Telescope (SPT). This will enable a combination of clean cluster selection from the SZE data from SPT and the photometric redshifts from the DES. The SPT collaboration will map the CMB in a 4000 sq-degree region observable from the South Pole. We plan to cover the same area in our survey. The largest area near the top in Figure 3.1 corresponds to the SPT overlap region.

3.2.4.2 Photometric Redshift Calibration Area

All of the science goals require precision photometric redshifts. To achieve the required limits on systematic uncertainties ($<2\%$), a calibration sample of roughly 1000 redshifts per 0.1 bin in redshift is needed in addition to the DES data. Our strategy is to make use of public spectroscopic datasets in areas of the sky that we can image. The largest and most diverse of these datasets is that of the SDSS Southern Survey which has 100,000 redshifts down to $i=20$ and out to $z=0.5$, in combination with the 2dF-SDSS survey, which has 10,000 redshifts of red galaxies out to $z=0.75$. This same area of sky also contains fields from both the VIRMOS-VLT Deep Survey (8 sq-deg with spectroscopic redshifts to magnitude $I_{AB} = 22.5$, and 2 sq-deg with redshifts to $I_{AB} = 24$) and the Keck Deep2 Survey (2 sq-deg with spectroscopic redshifts to $R_{AB}=24$). These surveys will deliver tens of thousands of spectroscopic redshifts extending over our redshift range of interest. The Southern Survey area is the narrow region at the bottom of Figure 3.1.

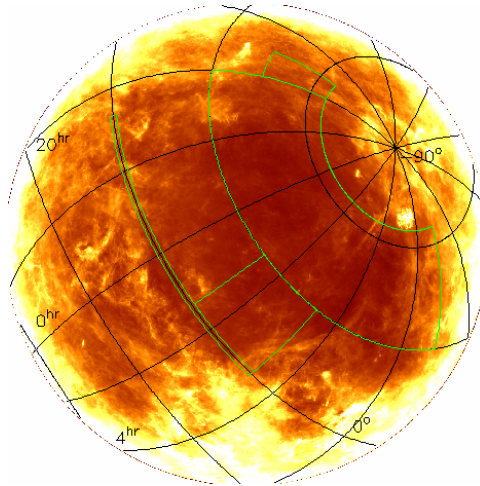


Figure 3.1 Map of the galactic dust in the South Galactic Cap. The South celestial pole is at top. Our reference design survey footprint is inside the green line. The Large Magellanic Cloud is visible in the upper right corner of the survey area.

3.2.4.3 Connection Area

Precise photometric redshift determination also requires the same photometry in the spectroscopic calibration areas as in the main survey areas. To address this we plan to image a contiguous 800 square degree area between the SPT area and the SDSS Southern Survey area. This area is optimally placed for providing targets and optical follow up for the optical and radio telescopes in Chile, including the ACT SZE survey, and the observations of the ALMA array.

3.2.5 The Point Spread Function

The weak lensing science goal drives the requirements on the point spread function (PSF). Measurement of the effects of large scale structure on the shapes of galaxies requires shear measurements at the 1% level. As discussed in the appendix to Chapter 2, the density of galaxies useful for weak lensing measurements is a strong function of PSF size. To achieve our goals we need median seeing to be $0.9''$ FWHM. Using the current prime focus imaging instrumentation the Blanco 4-m delivers typical seeing between $0.8''$ and $1.1''$. The best seeing in our survey will be determined by a combination of site and dome conditions as well as the optics of the corrector. We will impose an upper limit of $\sim 1.1''$ such that only data with seeing better than $1.1''$ will be included in the survey coadded images.

Stars in the science images are used to measure the PSF. In a single 100 second exposure we can reach magnitude 21 at $S/N=100$. At this magnitude there are about 2000 stars per sq-degree. Based on experience with SDSS, roughly a quarter of these 2000 stars will be away from frame edges, cosmic rays, and other stars and galaxies. Using the plate scale of the Blanco 4-m (55 microns/arcsec) this corresponds to a little more than 1 useful star per sq-cm (≈ 9 sq-arcmin). With this information, a map of the PSF and possible variations over the focal plane will be generated. One can sample the PSF on scales smaller than 1 sq-cm by averaging over several images but only if the instrumental PSF is constant against, for example, gravity induced flexure changes or thermal effects.

To measure the weak lensing distortions at 1%, we require less than 0.1% change in PSF over 1 sq-cm areas delivered at the focal plane, and that the flatness variations in a CCD over 1 sq-cm areas produce changes in the size of the PSF due to focus effects of less than 0.1%. These goals are aimed not at keeping the mean value the same, but at keeping changes smoothly varying and only on scales larger than 1 sq-cm.

3.2.6 Science Requirements Summary

The science goals discussed in Chapter 2 results in the following list of requirements:

1. 5000 sq-degrees in the South Galactic Cap
 - a. 4000 sq-degrees to overlap the SPT survey area
 - b. 200 sq-degrees to overlap redshift surveys for photo-z training samples
 - c. 800 sq-degrees connection region optimal for CTIO and Atacama telescopes
2. Photometric redshifts for clusters to $z=1.0$ with $\delta z \leq 0.02$
 - a. SDSS g,r,i,z are sufficient
 - b. $g=22.8, r=23.4, i=24.0, z=23.6$
 - c. Photometric calibration to 2%, enhanced goal to 1%
3. A stable and small PSF
 - a. Seeing $< 1.1''$ FWHM with median $\leq 0.9''$ FWHM
 - b. PSF stable to 0.1% over a 1 sq-cm (9 sq-arcmin) area of focal plane

3.3 Technical Specifications

To meet the science requirements listed above we must make choices that strike a balance between the science requirements and what is technically feasible. Below we present our reference design for the CCDs, the integration time of the images, readout time and read noise, the pixel size, image quality required for the optics, and the size of the field of view of the corrector and camera. These lead to a set of technical requirements which are used to guide the design of the DES corrector and camera.

3.3.1 CCDs

For the purposes of developing a reference design for the DES Instrument, we have chosen the LBNL CCDs. The technical specifications are described in more detail in Chapter 5. The critical features for this discussion are that they are 2k x 4k 4-side buttable devices with 15 micron pixels and a $QE > 50\%$ in the z band. They have been clocked at 250 kpix/sec with $7e^-$ read noise. If the corrector optics preserve the plate scale of the Blanco 4-m prime focus at 55 microns/arcsec, then each CCD has an active area of 170 sq-arcminutes and each 15 micron pixel covers $0.272''$. We note that the thick LBNL CCDs will also eliminate fringing effects, thus simplifying data reduction and improving signal-to-noise for the z and i band.

3.3.2 Integration Times

To achieve our science goals we require a signal-to-noise of 10 at the limiting magnitudes. The integration time is the total of all individual exposures. The calculation of the exposure time depends on the mirror area, the throughput of the system, the read noise of the instrument, the pixel size, the sky background, and the area over which the object is spread. Table 3.3 and the discussion below describe our calculation of the integration times needed to meet our science goals.

The Blanco 4-m telescope has an effective light collecting area of 10.3 sq-meter. We will use the SDSS filters, but our reference design for the corrector has two more optical elements than the SDSS design. In Table 3.1 we give CCD quantum efficiencies (QE) and the transmission of the optics and filters ($T d\lambda / \lambda$) using those from the SDSS, except that we assume (1) 5 times better QE in z as we are using the LBNL CCDs, (2) a wider z filter, and (3) an additional overall transmission factor of 0.9, allowing for the losses in transmission due to the extra two optical elements. We assume the camera has a read noise of $10e^-$, and that the pixel size is $0.27''/\text{pixel}$.

The SDSS has measured the sky brightness in each of the filters, albeit at a site distant from CTIO (but consistent with measurements made there), and we tabulate it in Table 3.1. The sky brightness varies in time and a half magnitude increase in the sky brightness results in a quarter magnitude decrease in the limiting magnitude. The solar cycle causes sky brightness variations on the order of 0.5 magnitudes, and the next solar maximum is roughly 2012. We note that the sky brightnesses in Table 3.3 are from SDSS data taken in the years near the last solar maximum. Table 3.3 also shows the effect of observing in “gray time” using data from the SDSS Photometric Telescope. This is time within 45 degrees of a moon at a phase fuller than half. The table shows that we can image through the i and z filters in such conditions. Note that we are in the process of compiling griz sky brightness data for CTIO from the southern standard stars NOAO survey program of Smith and Tucker. A small initial data set from that program indicates that the CTIO sky values are consistent with the much more extensive SDSS sky data measured at APO; we will have more thorough CTIO data available shortly.

The sky brightness contributes to the noise in galaxy magnitudes and colors in proportion to the area of the aperture one uses to measure the magnitudes. We assume the seeing at the Blanco 4-m is $1.0''$, and use an aperture of $1.7''$ diameter, as is appropriate for the measurement of the colors and magnitudes of faint galaxies. The resulting minimum integration times are listed in Table 3.3.

Table 3.3 Limiting Magnitudes to Integration Times

Filter	g	r	i	z
Limiting magnitude (10σ)	22.8	23.4	24.0	23.6
CCD QE	0.65	0.85	0.65	0.5
Filter and optics $T d\lambda / \lambda$	0.18	0.14	0.13	0.18
Sky brightness (mag/sq-arcsec)	21.7	20.7	20.0	18.7
Sky Brightness 45° from moon	19.7	19.7	19.25	18.5
Minimum integration times (sec)	27	130	900	1600
Adopted integration times (sec)	400	400	1200	2000

The last row gives our adopted integration times for the reference survey strategy; please see Chapter 4 for a detailed discussion. The increased exposure times in the g and r filters reflect our photometric calibration strategy which will use multiple survey tilings and a minimum exposure time of 100 sec.

We demonstrate next that our reference design choice of LBNL CCDs, with their high z-band QE, is primarily motivated by our science requirement to obtain a complete sample of cluster galaxies at redshift one. Recall from Section 3.2.2 that our z-band depth was chosen to safely construct a complete, flux-limited sample down to $z=23.3$, the z-band magnitude for a $0.5L^*$ passively-evolving cluster galaxy at redshift one. In particular, we compare the z-band depth for LBNL CCDs against that of a commercially available e2v deep depletion device (CCD42-90), which has a factor of 2 less QE integrated over the z-band, and hence a 0.38 magnitude shallower z-band depth for the same exposure time. Specifically, we use the deep z-band image (3.9 hr total exposure on the Subaru 8.2m) of the Hawaii HDF-North (Capak et al. 2004, AJ, 127, 180), and add Poisson noise to simulate images taken using an LBNL CCD and an e2v CCD, for the same adopted integration time from Table 3.3. We then run SExtractor photometry on the original and noise-added images, and compare the source number counts in the noise-added images against those in the original image. Figure 3.2 shows the resulting plot of completeness vs. z-band magnitude for the LBNL and e2v cases. We see that the source counts start to become incomplete immediately faintwards of the indicated 10σ limits, and that the completeness has dropped to about 0.75 by 0.4 magnitude beyond the 10σ limits. We further see that the e2v case barely meets the completeness requirement for a $0.5L^*$, redshift one cluster galaxy, while the LBNL case safely meets the requirement with about a 0.4 magnitude margin. Note that such a margin will be needed for any survey areas observed with worse than median seeing (i.e., $> 0.9''$ FWHM) or with fewer than the full number of tilings (see Chapter 4).

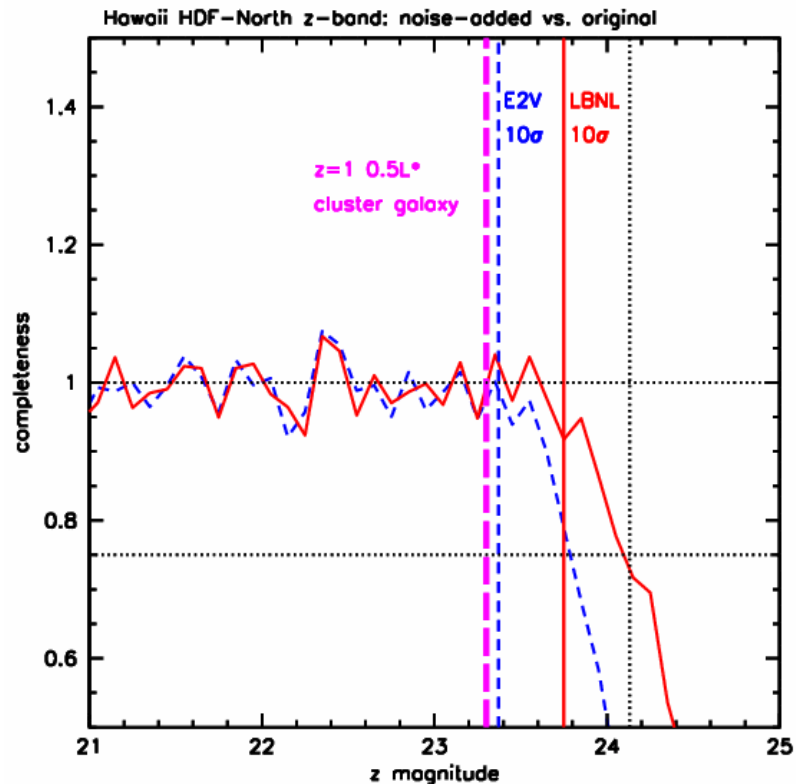


Figure 3.2. Comparison of source count completeness vs. z magnitude for the cases of an LBNL CCD (red-solid) and an e2v CCD (blue-dashed), both for the same total survey z-band exposure time. The vertical magenta (long dash) line shows the z magnitude of a redshift one, $0.5L^*$ cluster galaxy.

3.3.3 Read Noise

One of the components of the exposure time calculation is the read noise of the devices. Because the collecting area of the Blanco 4-m is large, the time required to reach the regime where sky noise dominates over read noise is quite short. Read and sky noise add in quadrature. To meet our science goals we require that the read noise be a factor of 2 smaller than the sky noise so that in the quadrature sum, the effect of read noise is less than a 10% increase above pure sky noise. The g band has the darkest sky (thus smallest sky noise), and with our 100 sec exposures, a read noise of 15 e- will meet this requirement. The CCDs we have chosen for our reference design have been clocked at 250 kpix/sec with a corresponding read noise of 7 e-. An additional contribution from the front end electronics (system noise) will add in quadrature to this. State of the art instrumentation can achieve < 5 e- read noise from the front end electronics. We choose 10 e- as our technical goal for the total read noise. In practice, following modern design techniques, the system noise will most likely be low enough to allow a slower scan readout generating images limited by the lowest readout noise attainable with these CCDs of 2-3 e-/pixel.

3.3.4 Point Spread Function

Our science goals encourage us to obtain the smallest possible PSF. The delivered PSF is a combination of atmospheric and dome-induced seeing, the optical design, mechanical alignment and stability, as well as the telescope tracking (guiding and focus). The seeing at the Blanco 4-m with the existing Mosaic II imager and its corrector is typically between 0.8" and 1.1", and the instrument on the best nights can deliver seeing as small as 0.6" FWHM; the site delivers considerably better than this. We set as a technical goal that the combination of factors within our control should not contribute more than 20% to the PSF width in ideal seeing of 0.6" (so that the effective seeing is 0.72"), and 10% to the PSF in typical seeing of 0.9". This translates into a requirement on the delivered PSF from the combination of these effects of ≤ 0.4 " FWHM everywhere on the focal plane, for bandpasses of i and z which will be used for weak lensing. Note also that pixels < 0.288 " will then satisfy 2.5-pixel Nyquist sampling in ideal conditions, when the effective seeing is 0.72".

As the technical design of the DES instrument progresses we will perform detailed finite element analyses of the various instrument components and of the entire telescope structure. We will use these analyses to help us minimize the various contributions to the PSF due to mechanical alignment and stability issues, including static optical alignment errors, construction errors in the lenses and the mirror, quasi-static errors (such as uncorrected mechanical deflection of the prime focus cage and imperfect focus), and possibly others.

3.3.4.1 Telescope tracking and focus

The delivered PSF can be strongly affected by the telescope tracking and focus. The TCS incorporates an interpolated lookup table model (pointing model) to compensate for flexure and irregularities in open-loop telescope tracking. Guide cameras follow stars near the object being observed, sending tracking corrections to the TCS every second and closing the tracking servo loop thus guaranteeing good quality images for exposures of up to 1800 seconds in most observing programs. Focus changes at the Blanco telescope resulting from changes in ambient temperature are corrected manually by the observer.

As noted before, the existing prime focus camera delivers seeing typically between 0.8" and 1.1". Unguided focus sequences, which are designed to locate current best focus, show a median seeing of 0.7" to 0.8". It is tempting to conclude that the telescope performs well on the 10 second timescale of a focus exposure sequence, but less well in the several hundred second exposures of a typical observing run. This would probably be erroneous as many observers will happily and appropriately refocus the telescope should the seeing improve, but not when it degrades when it would be a waste of observing time. The existing tracking and guiding algorithms are not perfect and effort will be put into refining them where possible.

As described in Chapter 5, for our reference design we have chosen to devote space on the focal plane to both guide and focus CCDs. We will read out the focus CCDs with each science exposure, while the guide CCDs will be read out on a 1 sec time scale. This has the advantage that the guiding and focus measurements are made by CCDs that are rigidly attached to the focal plane and improves on the current imager by allowing for continual monitoring of telescope focus.

As discussed above (Section 3.2.5), we expect ~25 well measured stars ($S/N = 100$) per science CCD in a 100 sec. science exposure. If the focus chips were 10 times smaller than the science CCDs (i.e., focus chip area = 17 sq-arcmin), 2 stars per CCD would be expected and we believe this to be sufficient. For our reference design we assume the guide exposures will be 1 second. One can measure sufficiently accurate centroids to guide from a star of $S/N=20$. If we take the sky noise to be $16e^-$ and the read noise over the star image to be $20e^-$, then we need a star producing 1000 e^- in 1 second. This is magnitude 19 for the r or i bandpasses, which have surface densities of $\Sigma=0.2$ per sq-arcmin (5×10^{-5} per sq-degree) near the galactic pole. Assuming the stars are randomly distributed on the sky, then the probability of finding no useable guide stars within a guide camera of solid angle Ω is $P(0)=e^{-\Omega\Sigma}$. There are about 2000 fields in our survey. We choose a target probability of e^{-10} , where there would be about a 10% chance of having one field without a guide star. This suggests that we need 25-50 sq-arcmin of guider to be assured of at least one guide star in each field.

3.3.5 Field Size

The size of the field necessary to meet the science goals depends on many aspects of the survey. The primary constraint is to cover the 5000 sq-deg DES area in the time available for the DES during the 5 year period. However, consideration must also be given to factors of weather, survey strategy, and operational efficiency, among others. Research into the technical feasibility of obtaining optical components has resulted in few hard limits, for example, the availability of blanks for elements up to 1.2 m in diameter.

An order of magnitude calculation shows the essentials. We are proposing to use 30% of the Blanco 4-m time over 5 years, resulting in a survey of 525 nights. Our supernova program will take 10% of the time, leaving 473 nights for the imaging survey of 5000 sq-degrees. This requires an acquisition rate of 10.6 sq-degrees per night. The nights in the Southern summer will be around 8 hours long, giving a 10.6 sq-degree/8 hour rate. Assuming half the nights will be unusable due to weather then gives 10.6-sq-degrees/4 hours. Our total exposure time on a given field will be of order an hour, so the camera must cover 2.7 sq-degrees.

A careful analysis (see Chapter 4), incorporating overheads, a four-bandpass calibration strategy, and a sophisticated weather model, calculates a need for a camera whose single image tiles cover an area of 3.0 sq-degrees. This is realized in our optical design which has a 2.2 deg. diameter field of view.

3.3.6 Requirements for the DES corrector

Here we summarize how the science requirements and technical choices listed above drive the design of the corrector for the DES. The resulting corrector design is presented in Chapter 5. We recognize that the camera will be used for a variety of purposes by the general astronomical community and the corrector has been designed with this in mind. Any changes in requirements beyond those required for DES that have a significant cost impact will require that those costs be borne by an organization other than the DES Collaboration.

1. The full wavelength range will be 390 to 1100 nm. The design shall be optimized for performance within individual passbands of 390-540, 560-680, 690-820, and 820-1100 nm. It is allowed that the focus and/or scale may change among passbands.

Basis: These are the passbands needed for measuring the photometric redshifts of elliptical galaxies from $z=0$ to 1. The passbands match the SDSS except that the longest wavelength has been extended. The overall passband matches the optimal response of the LBNL CCDs.

2. The pixel scale shall be 17.7 - 19 arcsec/mm (average over focal plane if distortion is present). The field of view shall be no smaller than 2.2 degrees.

Basis: The pixels will be 15 microns. The scale corresponds to 0.265 - 0.29 arcsec/pixel (the same as the existing Blanco). The larger value is the scale at the prime focus before any correction. It gives a resolution of 2.5 pixels for an image size of 0.72 arcsec (the target minimum PSF). Coarser scale impacts the ability to do weak lensing science. The angular field size is the minimum needed to complete the SZE and supernova surveys within the allotted time [30% of nights for 5 years.] At the smallest pixel scale, the size of the field is 447 mm.

3. The images shall have a polychromatic $D80 < 0.64$ arcsec, for a merit function that averages over all wavelengths in a rectangular bandpass, for the bandpasses specified in requirement 1 at all locations on the focal plane. It is also a goal that the monochromatic $D80$ be achieved for all wavelengths 390-1100nm everywhere in the focal plane.

Basis: This value of $D80$ corresponds to a FWHM of 0.4 arcsec. From raytrace spot diagrams, we find roughly that $D80 = 1.59 * \text{FWHM}$ where FWHM is 1-D. For a Gaussian, $D80 = 1.53 * \text{FWHM}$, $D80 = 3.59 * \text{sigma}$, and $\text{FWHM} = 2.35 * \text{sigma}$. A FWHM of 0.4" is the target contribution to the final image PSF from all non-atmospheric causes.

4. No atmospheric dispersion correction (ADC) shall be incorporated.

Basis: The need for an ADC is not compelling. The maximum allowed differential refraction is 0.8 arcsec peak-peak across the bandpass of a filter. This corresponds to a $D80$ of 0.64 arcsec (actually a little less); for an azimuthally-averaged PSF, the

equivalent 1-D sigma is 0.17 and the 1-D FWHM is 0.40 arcsec. The driving filter is SDSS g. The maximum airmass is 1.49. The declination for such an object on the meridian is -78 deg. This is more than required to image the South Pole Telescope survey area (declination > -75 deg). The longest exposure time in the g band will be 100 sec. The longer-wavelength filters are much less affected.

The following requirements are driven by technical needs.

5. The focal plane shall be flat.

Basis: It is easier to design and construct a mosaic array with a flat vs. curved focal plane. Reference design studies show that no significant gains are to be had by allowing the focal plane to be curved.

6. The operating temperature shall be -5 C to +27 C

Basis: Numbers taken from CTIO website.

7. The maximum diameter of any optical element shall be less than 1300 mm. The leading optical element shall be no more than 2300 mm in front of the focal plane.

Basis: These are the mechanical constraints placed by the available space in the current design for the prime focus assembly. Smaller elements are desirable, if possible, for cost reasons. It is not thought that a diameter of 1300 mm provides any serious procurement problem.

8. The preferred glass type for all elements is fused silica.

Basis: The glass type(s) should be chosen subject to the constraints of:

- a) lens blanks can be procured of the diameter and thickness required by the optical design
- b) the glass type meets the performance requirements of the design
- c) durability and manufacturability
- d) low coefficient of thermal expansion
- e) low radioactivity
- f) short procurement time
- g) fused silica seems to meet most if not all of these requirements.

9. Transmission shall be uniform in wavelength (10% peak-peak variation) over the full wavelength range specified in requirement 1.

Basis: We do not want to compromise performance due to the choice of a glass that has reduced transmission at either extreme of wavelength, particularly at the blue end. The number 10% is a soft target. It is thought that "optical quality" fused silica would meet this requirement handily.

10. A 15 mm thickness filter shall be accommodated in the design. It is desired that it be located in a region of the corrector that has a minimum airspace whose size is the diameter of the filter plus 51 mm, but otherwise be as close to the focal plane as possible. Within that airspace, the filter shall be placed 10 mm away from the optical element closest to the focal plane. The filter will be made of fused silica.

Basis: The filter must be thick enough to be mechanically sturdy. Sag due to gravity is thought to be immaterial on the optical design for this thickness. It is expected that filters will be mounted vertically in the prime focus cage and will be rotated 90 degrees and translated to insert them into the optical path. The airspace is needed to accommodate the rotation of the filters. There is no requirement to accommodate filters of different thicknesses.

11. A 25 mm minimum thickness glass window that is integrated with the vacuum dewar of the camera shall be included in the design. The glass type may be specified as part of the design. The window shall be located 40 mm in front of the focal plane. The window may have power. The material shall be chosen for low radioactivity. Fused silica meets this requirement.

Basis: The thickness is the minimum needed to support the window against the air-vacuum pressure interface. A 25 mm thick flat plate has a safety factor of 4.3 (at sea-level). Radioactivity generates spurious charge events in the CCD and must be minimized. If the window has power, the thickness of the window at its thinnest point shall be 25 mm. The distance from the focal plane is determined by requiring that the diameter of a ghost image of a star from the focal plane formed by the nearest optical element be sufficiently large that the surface brightness is a small fraction of that of the night sky.

The curvature of the window induced by the air-vacuum pressure differential must be computed and its impact on the optical design assessed. It is thought that the sag could be of order 60 microns, which would require such an assessment.

12. Space for a shutter mechanism shall be provided with thickness 51 mm. The location is not critical but should be as close to the focal plane as feasible.

Basis: Closer to the focal plane means a smaller beam size. Space for the shutter is constrained in the prime focus cage.

13. Ghosting images shall be computed assuming a reflectivity for the CCDs in the focal plane of 15%, a reflectivity from the back of the dewar window and the front surface of the first element of the corrector of 2%, and all other surfaces of 0.8%. The variation in intensity of the exit pupil ghost image reflected back to the focal plane shall be no more than 2.5%.

Basis: Ghosting impairs one's ability to do flatfielding and creates artifacts that must be modeled and subtracted from data as part of routine data processing. The figure of 2.5% is not a hard one, but it is known that ghosting properties can vary significantly for minor changes in other figures of merit for a particular design. Ghosting is minimized by minimizing the curvatures of those surfaces close to and concave to the focal plane. The reflectivities are nominal values expected for the LBNL CCDs, MgF2 coatings for two surfaces that must be hard to withstand environmental conditions, and Sol-Gel coatings on all other surfaces.

14. Within the constraints of the above requirements on performance, the optical design shall minimize the total cost of construction.

Basis: Costs are driven by the glass type, spherical vs. aspherical surfaces, details of lens shape (e.g. thickness), the total number of elements (both w.r.t. procurement and to mounting complexity), the delivery schedule, and the availability of qualified vendors.

3.3.7 Science and Technical Requirements Summary

Below we summarize the science requirements and the corresponding list of technical requirements we have chosen for the DES instrument.

Science Requirement: Image 5000 sq-deg in the South Galactic Cap in 30% of 5 years

Technical requirement: 3 sq-degree camera with ≥ 2.2 deg FOV

Science Requirement: Measure galaxy cluster photometric redshifts to $z=1.0$ with $\delta z \leq 0.02$.

Technical requirements:

- a. SDSS g,r,i,z filters covering 400nm to 1100nm
- b. Limiting magnitudes $g=22.8$, $r=23.4$, $i=24.0$, $z=23.6$
- c. QE > 50% in the z band
- d. Photometric calibration to 2%, enhanced goal to 1%
- e. Read noise <10 e-

Science Requirement: A small and stable PSF

- a. Seeing < 1.1" FWHM with median ≤ 0.9 " FWHM
- b. PSF stable to 0.1% over a 1 sq-cm (9 sq-arcmin) area

Technical requirement:

- a. Pixel size and optical plate scale which give <0.3"/pixel
- b. Optical, mechanical and telescope tracking which contribute < 0.4" FWHM across focal plane in the i and z bands
- c. Focus chip area > 17 sq-arcminutes
- d. Guide chip area > 25-50 sq-arcminutes, 1 Hz readout rate

Technical Requirements on the DES Corrector

Considerations of the conditions at the site and technical feasibility, combined with the science and technical requirements listed above, result in the following specifications for the DES Corrector:

1. The full wavelength range will be 390 to 1100 nm.
2. The pixel scale shall be 17.7 - 19 arcsec/mm (average over focal plane if distortion is present). The field of view shall be no smaller than 2.2 degrees.
3. The images shall have a polychromatic D80 < 0.64 arcsec (corresponding to a FWHM < 0.4") averaged over all wavelengths listed in requirement 1 at all locations on the focal plane. It is a goal that the monochromatic D80 should be achieved for all wavelengths 390-1100nm everywhere in the focal plane.
4. No atmospheric dispersion correction shall be incorporated.
5. The focal plane shall be flat.
6. The operating temperature shall be -5 C to +27 C
7. The maximum diameter of any optical element shall be less than 1300 mm. The leading optical element shall be no more than 2300 mm in front of the focal plane.
8. The preferred glass type for all elements is fused silica.
9. Transmission shall be uniform in wavelength (10% peak-peak variation) over the full wavelength range specified in requirement 1.

10. A 15 mm thickness filter and space for changing filters shall be accommodated in the design.
11. A 25 mm minimum thick glass window that is integrated with the vacuum dewar of the camera shall be included in the design. The window shall be located 40 mm in front of the focal plane. The window may have power. The material shall be chosen for low radioactivity.
12. Space for a shutter mechanism shall be provided with thickness 51 mm.
13. Ghosting images shall be computed. The variation in intensity of the exit pupil ghost image reflected back to the focal plane shall be no more than 2.5%.
14. Within the constraints of the above requirements on performance, the optical design shall minimize the total cost of construction.

4. Survey Strategy (WBS 1.3)

This section describes the elements of the Reference Design for the Dark Energy Survey. It includes the survey observing strategy, the photometric, astrometric, and photo-z calibration strategies, the survey data simulations, and testing strategies for the data production system and the data analysis system. The reference design is not intended to be the final design, as we are still evaluating a number of technical choices, but it serves as a vehicle to illustrate where we are in our thinking and as a working model to guide our evaluations. Section 4.1 presents the observing strategy, section 4.2 presents the plans for calibrating the data, and sections 4.3-4.5 present the plans for the simulations that we will use to test the data management systems and tune the science analysis software.

4.1.1 Survey Strategy Work Breakdown Structure

There are six level three WBS elements in survey strategy, shown in Figure 4.1. The first is the confusingly named survey strategy, which covers two lower level elements: 1) the survey science requirements and technical consequences, and 2) the survey observing strategy. Chapter 3 described the survey science requirements and the derived technical requirements. The survey strategy WBS element concerns itself with the creation and the maintenance of these documents. Chapter 4 describes the survey observing strategy, and the WBS element concerns the creation and implementation of this observing program.

The second level three element is survey calibrations. This covers three lower level elements: 1) photometric calibration, 2) astrometric calibration, and 3) photometric redshift calibration. All three are necessary for the attainment of our science goals.

The third level three element is survey data simulations. We intend to simulate a large fraction of the survey data. We intend to do this because it will help us understand our instrument, help us understand the universe we are observing, and help us understand the analyses we will undertake.

The fourth level three element is the mock data reduction challenge, which is aimed at taking the simulations of the survey that we produce sending them through the data management system. This tests both the data management system and our ability to deal with its output.

The fifth level three element is the mock data analysis challenge, which is aimed at taking the output of the mock data reduction challenge and sending it through our science analysis codes. This is, in some sense, the core deliverable of the science working groups: analysis codes that are ready and waiting for the data as they roll in. Our window of opportunity is quite long, but there is no reason we cannot be ready to spend our first summer working the science and not the analysis codes. This WBS is thus a way to organize the activities of the collaboration scientists interested in analysis towards a deadline.

The sixth level three element is survey operations, which is aimed at carrying out the photometric calibration activities, the quality assurance activities, and the survey tracking activities. We will develop this plan in the future, but here we are focused on construction and commissioning activities and will not describe this element further.

Dark Energy Instrument Work Breakdown Structure

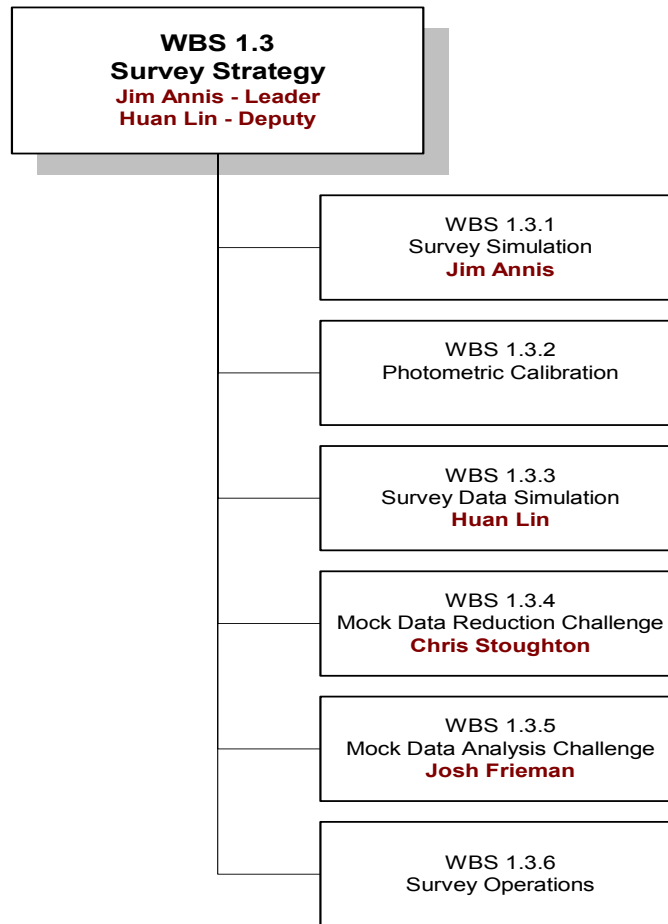


Figure 4.1 Organization of the Dark Energy Survey Planning Project

4.2 Survey Observing Strategy (WBS 1.3.1)

Large scale astronomical surveys aim to produce large sets of homogeneous data that enable high precision statistical astronomy. Homogeneity of data is the core strength of these surveys, but it does not come easily nor freely; it must be planned for and thought must go into the strategy for acquisition of the data.

4.2.1 Overview of Survey Strategy

The observing strategy design goals are to

- Efficiently attain the required depth
- Minimize the photometric calibration errors, and
- Obtain scientifically powerful data at natural points in the survey
 - Year 2, at the time of the co-added data release
 - Year 5, at the end of the survey

We will present two strategies that span the space of reasonable strategies satisfying the design goals, evaluate them, and derive a reference strategy from them. We focus on reasonable strategies, but it is easy to imagine strategies that meet some design goals at the expense of others. The maximally efficient survey strategy would be to point to a given piece of sky, image it once in a given bandpass, and continue on until all 4 filters are done. This strategy, unfortunately, leads to deeply imaged islands, with little overlap and tends to maximize the photometric calibration error across the survey array as well as maximum cosmic rays in the data. A strategy better thought through but only somewhat less unfortunate aims at complete photometric depth through multiple tilings at the expense of area. This strategy leads in year 2 to a survey of 2000 sq-degrees, but the realities of observing large areas of sky lead either to disjoint regions or in a long thin rectangle. Unfortunate strategies are common, but the space of reasonable strategies, strategies that meet survey goals with reasonable certainty, is relatively compact.

The science case clearly makes the argument that area of the sky is of primary importance. It is useful to recall that the time to reach a given signal to noise¹ goes from linear in time for source noise dominated objects to square root in time for sky background noise dominated objects. Essentially all of the objects of interest in our science case are faint. A few tens of seconds exposure is sufficient to reach high signal on the sky, and thus to reach the magnitude characteristic of the transition from quick increase in depth in the linear regime to slow increase in depth in the square root regime. For a 4 meter class telescope this characteristic magnitude is $\sim 22^{\text{nd}}$ magnitude and is cosmologically interesting. Even short exposures over the entire survey area would allow us to embark on our science program.

We are thus led to our first design decision, that area is more important than depth². We will aim to image the entire survey area in each bandpass in the first year. This guides the survey strategies towards those strategies that cover the entire area once or more per year.

Our second design decision flows from considering the photometric calibration: we adopt tilings of the survey area as the core means of obtaining the required photometric calibration. Large overlaps between neighboring images allow the reduction of systematic errors by comparing the same source observed in the different images. Images taken on different nights allow the reduction of absolute calibration error through root N averaging. Taken together, we are led to the idea of tilings of the sky obtained on different nights and different years, with half camera scale offsets between the tilings.

These two design decisions enable us to make substantial progress in the survey design. Much of the rest of the constraints, as the landscape and the surroundings constrain the architecture of a building, come from considering the geometry of the survey area as seen from South America and from the statistics of the weather at the Cerro Tololo site in Central Chile. First though, we will consider the tilings of the survey.

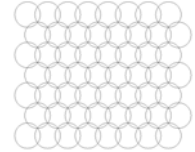
¹ The exact statement is more complicated. The transition between the linear regime and the square root regime is determined by the telescope aperture, instrument throughput, point spread function, and the sky background level.

² Area is more important than depth, given that one is starting with a 4m telescope and a high efficiency instrument.

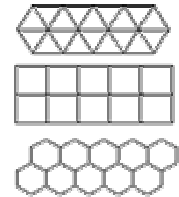
4.2.2 Tiles and Tilings

The survey area will be imaged multiple times and how the images fit together determines what use we can make of them. In the interest of obtaining high quality calibrations we plan to fit the images together as tiles in a tiling. A tiling is the unique covering of the plane, or an area on a plane, using shapes that can fit together without overlap. These shapes can be irregular or the tiling can use more than one shape, but for the purposes of mapping the sky a tiling that uses one shape, a shape that approximates a regular shape, is most useful. The fact that the sky is seen as a sphere makes the tiling an interesting problem.

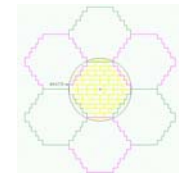
Tilings: Telescope fields of view are circular and the diameter of the circle the Dark Energy Camera (DECam) corrector provides is 2.2 degrees. Circles cannot tile the plane, as they either leave gaps or overlaps, though the overlapped circles form a “tessellation” which does cover the plane. If the goal is to make a homogeneous map of the sky, we see that the overlaps do not contribute to the covering, so they are irrelevant other than to the cost of the instrumentation.



The three regular shapes that do tile the plane are the triangle, the square, and the hexagon, and all of these obey the rule that the angles at any vertex add to 360 degrees, the key to the proof that there are only three. Hexagons are special in another way: any partition of the plane into regions of equal area has a perimeter at least that of the regular hexagonal honeycomb tiling³. The perimeter of the CCDs on the focal plane of the DECam approximates a hexagon by design. There exist tilings of the sphere using hexagons with a handful of pentagons: the climate modeling community (e.g., Randall et al 2003) has developed algorithms and software that use these tilings.



In detail, the actual DECam CCD layout forms a non-regular tile, though one which still tiles the plane. There are some overlaps as half of few CCDs project past the perimeter of the tiling area and these overlaps do not contribute to the tiling. The tiling is slightly larger than the inscribed hexagon, but its most salient difference from a hexagon is that it is not a filled tile. The tiles will tile the plane, but the CCDs, because of dead zones around them, do not fully fill the array, thus leading to interesting effects.



The focal plane array consists of closely packed CCDs abutting on four sides, yet because of the 1 mm guard ring around the edge of each LBNL CCD, the tile of an individual image is sparse at the 10% level. The implication of a sparse array is that a complete tiling has an uncovered fraction that equals the inactive area of the tile. A second tiling will cover this area usefully, but its own inactive area leaves a different area without new coverage. The process is shown in Figure 4.2.

The area not covered is always the dead area fraction, 10%. The area of sky with less than the full number of exposures accumulates at a rate of N times the inactive area. Thus at 5

³ This is the Honeycomb Conjecture proved by Hales in 1999 after a mathematical history of 2500 years.

tilings half the area has the targeted 5 tilings, while half the area has 4 tiling coverage. At 10 tilings, the entire area is covered by 9 tilings. As N becomes large, the difference in exposure between areas covered N times and the area covered $N-1$ times becomes small. The statistics of the coverage distribution, shown in Figure 4.3, is slightly more complicated because of the small areas of overlap between adjacent pointings in a single tiling.

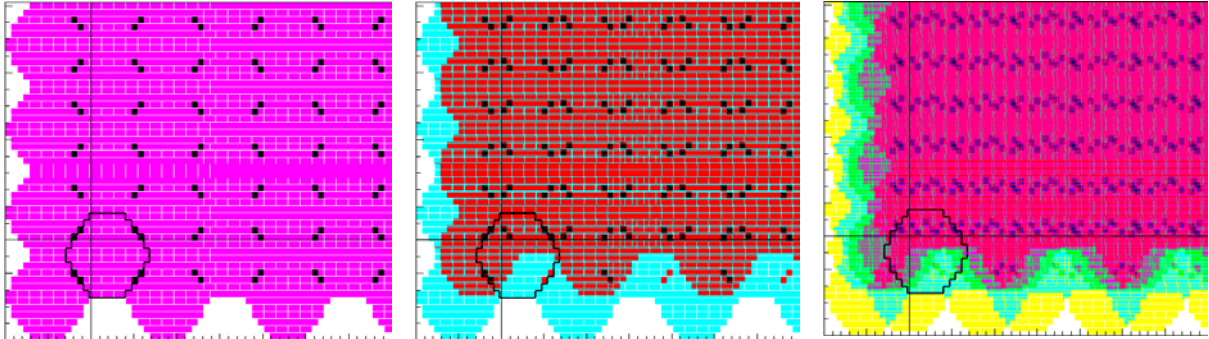


Figure 4.2 The effect of a sparse tile on the sky coverage. The figure on the left shows a single tiling. Pink is the area imaged, black is area covered more than once by CCD area extending beyond the tile figure, and white shows area uncovered by an image. The tile pattern is the reference design focal plane array layout. The figure in the middle shows the effect of a second tiling. Here blue is covered once, and red is covered twice. Blue peeks out between the CCDs. On the right is the effect of three tilings, with 1 tile coverage in yellow, two tile coverage in green, and three tile coverage in red⁴. The distribution of coverage is textured.

The number of tilings has an effect on three areas, most obviously exposure time. It also affects the image processing⁵ where voting techniques allow robust rejection of artifacts on a pixel by pixel basis, as long as there are 3 or more images that can vote, and the lack of 3 images forces algorithms to consider neighboring pixels. This is an example of where it is possible to keep complexity out of software by survey design. The other area for which the number of tilings comes into place is in calibrations.

Many or most of the systematics in photometric calibration are dependent on the location in the camera. Multiple tilings provide leverage in removing systematics by providing multiple exposures of the same piece of sky through different parts of the camera. Tiling patterns that allow for maximal overlap between adjacent tiles in different tilings provide much more leverage than tiling patterns that, say, overlap the outer 5% of the camera. And if the goal is to maximize unique overlaps, there exists optimal mapping strategies. Arbitrarily take the first tiling as the reference tiling (Figure 4.4a). The second and third tilings have hex centers placed on the vertices of the reference tiling such that the three centers form one of the 6 triangles that make up a hexagon (Figure 4.4b). They provide 33% overlaps with 3 hexagons from the reference tiling. The 4th through 6th tilings have hex centers placed on the centers of the edges of the reference tiling (Figure 4.4c). These provide 42% overlaps with 2 reference tiling hexes, and 8% overlaps with two others. This set of 6 tilings provides the maximally

⁴ The color scheme seems to be: N tilings is red, $N-1$ tilings is blue, $N-2$ tilings is yellow, and if there is only one tile, it is pink.

⁵ The number of tilings also directly affects the data volume, as each tiling when reduced takes roughly 2 Terabytes of disk space.

unique interlocking pattern. The section on photometric calibration will consider these effects further.

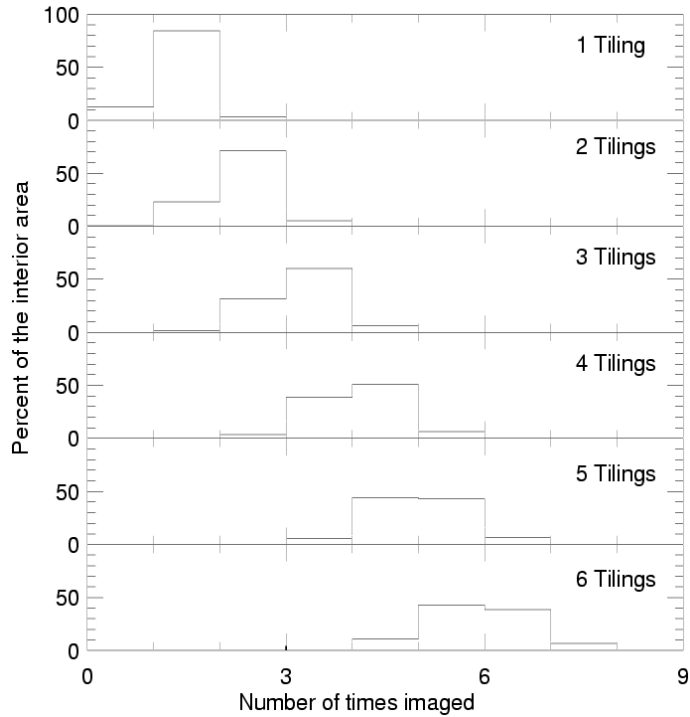


Figure 4.3 The statistics of the tiling coverage for the DES tile pattern. The fraction of area covered $N-1$ times equals the fraction of area covered N times for 5 tilings. For 3 tilings, 30% of the area is covered only twice. As there are significant image processing simplifications and algorithm improvements⁶ possible for three images, the statistics of the coverage suggest 4 as the minimum number of tilings.

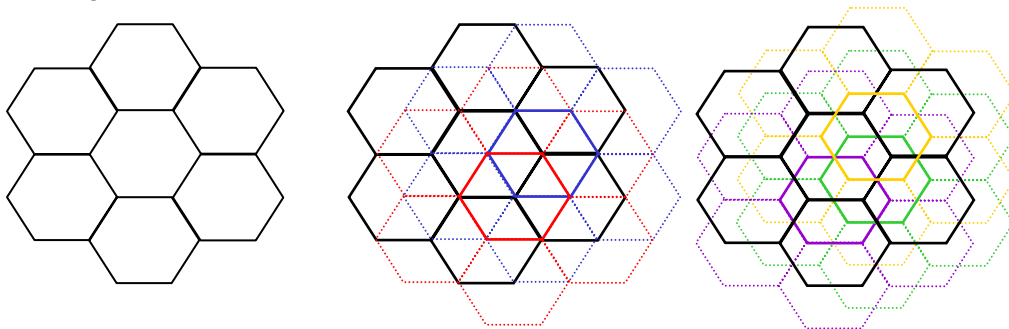


Figure 4.4 a) The left panel shows the reference tiling in black. b) The middle panel shows the reference tiling and the two 33% overlap tilings in red and blue. c) The right panel shows the reference tiling and the three 42% overlap tilings in purple, green, and gold. These six tilings provide a maximally unique interlocking tiling pattern.

⁶ The algorithm improvements are all based on the idea that if there are three or more images, it is possible to vote on the truth on a pixel by pixel basis, whereas if there is one or two images, one must examine surrounding pixels.

4.2.3 Survey Geometry and the Weather at Cerro Tololo

The survey area is easiest to observe in Austral Spring. The season matters because of the length of night and because of the weather. This can be seen in Figure 4.4, where the longer nights of early spring are balanced, on average, by the poorer spring weather, so that the actual number of useful hours per night is the same in early spring (day ~225) and early summer (day ~325).

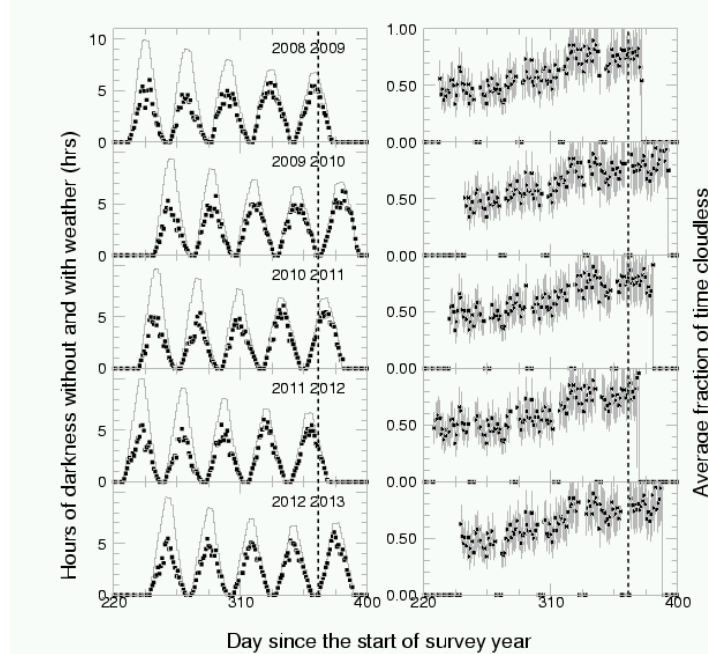


Figure 4.5 Lunar cycles around the time of the survey. Plotted on the left are the hours per night of dark time (thin curve) and photometric dark hours per night (heavy squares). On the right are the average fraction of cloudless time based on 30 years of weather data from CTIO; the same data are in each of the right hand panels, modulated by full moons and end of seasons. In the left hand panels, it is clear that the length of nights may be longer in the early Austral Spring, but the weather is better later in the early Austral Summer.

The calculation of the averages is possible because CTIO has kept useful weather data over a 30 year span. The weather data statistics are summarized in Figure 4.5, and both seasonal variations and the poor conditions of the El Nino years can be seen. There is little that can be done about the El Nino years: in any given El Nino year, one must endure as little as half the photometric weather of a normal year, and reasonable survey strategies must be robust against such a setback. On the other hand, the seasonal patterns can be planned for. The high summer days (numbers 0-70) have very good weather, the fall days (70-135) exhibit rapidly decaying weather, and during winter and spring days (135-365) the weather slowly gets better.

Combined, these data make the time span from September to January the optimal time to pursue the observing of the survey area, as shown in Figure 4.6. The footprint of our survey sets Austral Spring as the time the survey is easiest to observe, but the Chilean weather patterns set late spring and early summer as the times we are most likely to observe the survey area successfully.

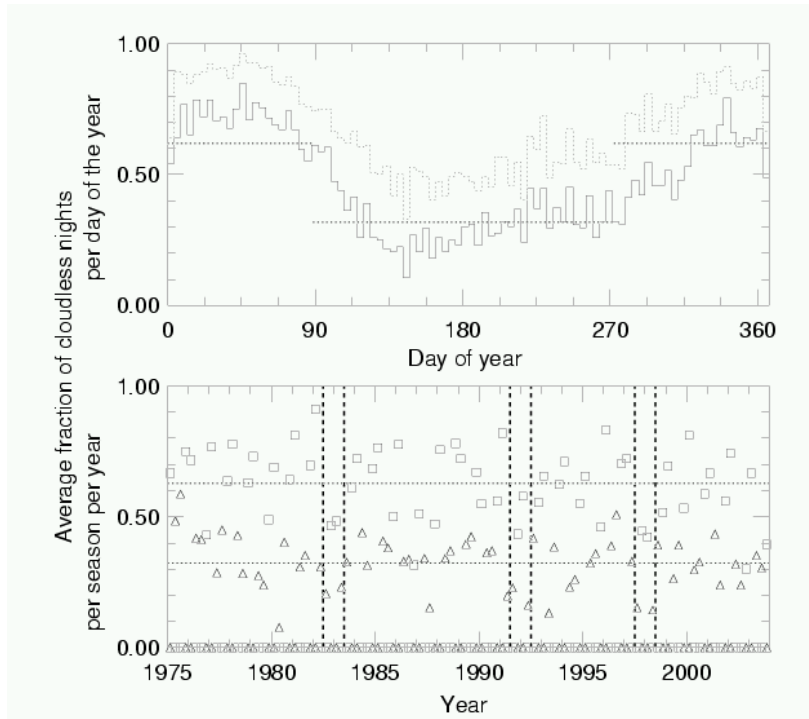


Figure 4.6 Thirty years of CTIO weather data summarized as the average fraction of cloudless nights, plotted against day of the year (top) and as a seasonal average/year (bottom). In the top panel, the dotted line includes nights partly clear and partly cloudy whereas the solid line is purely clear nights. In the bottom panel, the triangles correspond to purely clear nights and the squares to the dotted line in the top panel. Also in the bottom panel, the heavy dotted lines show that these El Niño years have significantly lower fractions of clear time. If a given year turns out to be El Niño, one might endure a year with half the photometric time of a normal year. (Note that the horizontal dashed lines in the top panel do not correspond to the parameterizations in the text.)

This bodes well for the weak lensing component of our science goals, as the seeing at the Blanco 4m gets better as spring moves into summer. The site itself shows 0.85'' seeing in October, 0.65'' in November and December, and 0.60'' in January. Time in January is, for weak lensing purposes, more valuable than time in August.

An Analytic Calculation of the Time Available for the Survey: Issues of survey geometry and weather have been explored, but the question of how much time is available for the survey remains, and so we turn to the detailed analytic analysis presented in Wester (2004). The calculation invokes specific criteria to address the issues of the spherical astronomy of the survey area and the weather of the site.

The dark time is taken as the hours between the evening and morning astronomical twilight, defined as the sun 18-degrees below the horizon, during periods when no moon is above the horizon⁷. Gray time is defined similarly but allows for the presence of the moon and includes 18- to 12-degree twilight. We analyze the 5 contiguous lunar cycles that end in January (143

⁷ The moon actually does not enter the SPT survey area: the moon remains within 6 degrees of the ecliptic plane, and the ecliptic plane is at its closest 67 degrees away from the South Galactic Pole. We can image in z-band in the SPT area for any moon position.

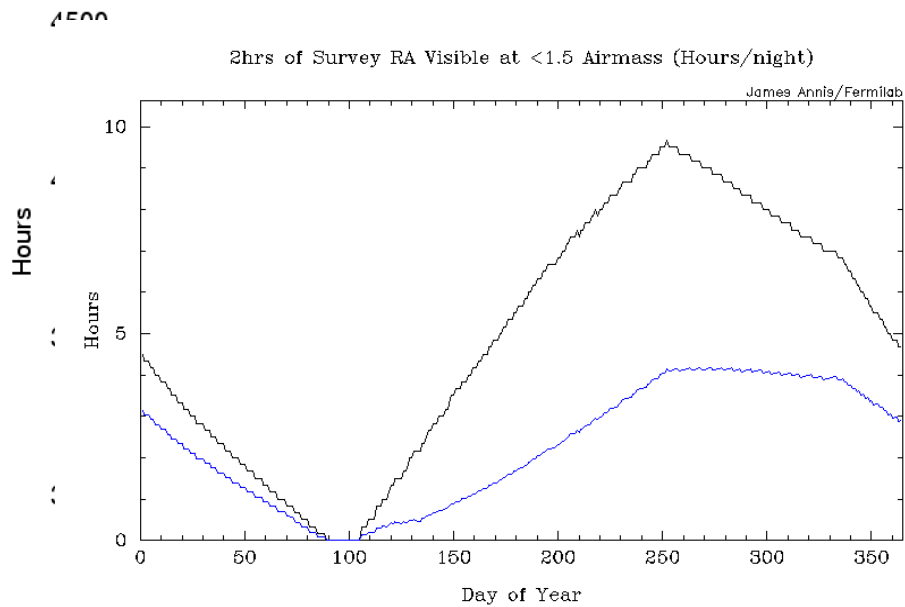


Figure 4.7 The black line shows the number of hours per night that 2hr-stretches of survey RA are visible (airmass < 1.5) as a function of the day of the year. Important factors in the shape of the black line are the RA range of the survey and the seasonal lengthening and shortening of nights. The blue line shows the number of hours multiplied by the fraction of clear nights using the seasonal parameterizations given above. Obviously the 100 day stretch from September through November where the average number of useful hours is flat and independent of the length of the night.

nights). The survey starts on different dates in different survey years in 2008-2012 due to the lunar cycle, which impacts the available time since the time between astronomical twilight varies over the course of a year.

To estimate the impact of weather, we analyze the 30 year CTIO weather record, which quantifies the measured cloud cover during four quarters of each night from 1975-2003. We count only photometric time, defined to be when there is no cloud cover. While we have calculated the average fraction of cloudless nights as a function of day of the year, we instead use an analysis that better includes the effects of the El Nino induced extreme conditions. This more sophisticated analysis maps the historical weather statistics in all five-year periods from 1975-2003 onto our planned observing time in 2008-2012. This analysis is shown in Figure 4.8.

We find average values of 1749 dark and 2142 gray hours over 5 years. The five years cover 143 days, more than the 105 we will use for the survey. We scale down to our expected survey usage by multiplying by 73%, resulting in

- 1300 hours of useful dark time and
- 1600 hours of useful gray time and
- an estimate of 2900 hours of total photometric time over the survey.

When a significantly illuminated moon is above the horizon, it is bright time, but the light has the yellow spectrum of the sun and affects the g and r bandpasses much more than the redder i and z bandpasses. How much less affected is seen in Figure 4.8, which shows the distribution of sky brightnesses of 1000 sq-degrees of SDSS imaging data, taken in dark time, and of the effect of moon light on the sky brightnesses of SDSS Photometric Telescope data as a function of separation from the moon. We can work in any moonlight with the z-filter, and during most moon conditions with the i-filter.

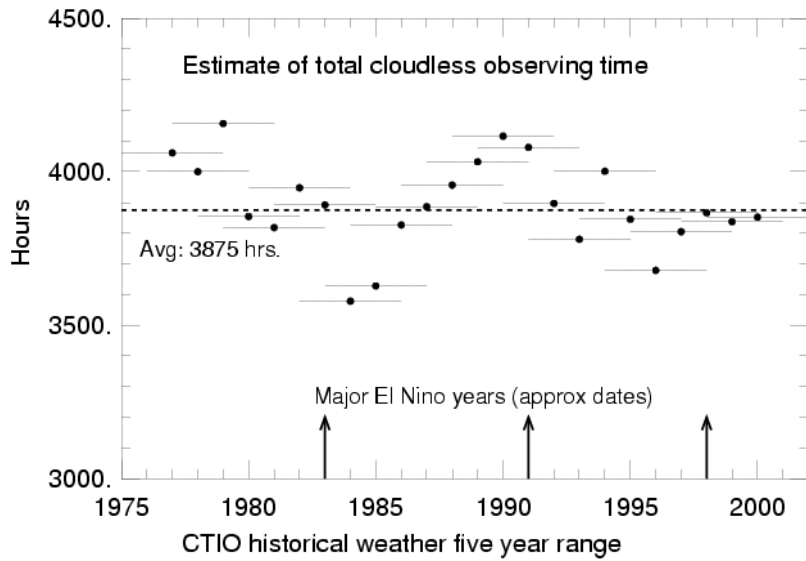


Figure 4.8 The total cloudless time over a 5-lunation period ending in January, over the last 30 years. The methodology is to calculate the time available in 5 year moving windows. The data points are therefore correlated, but then, so is the weather.

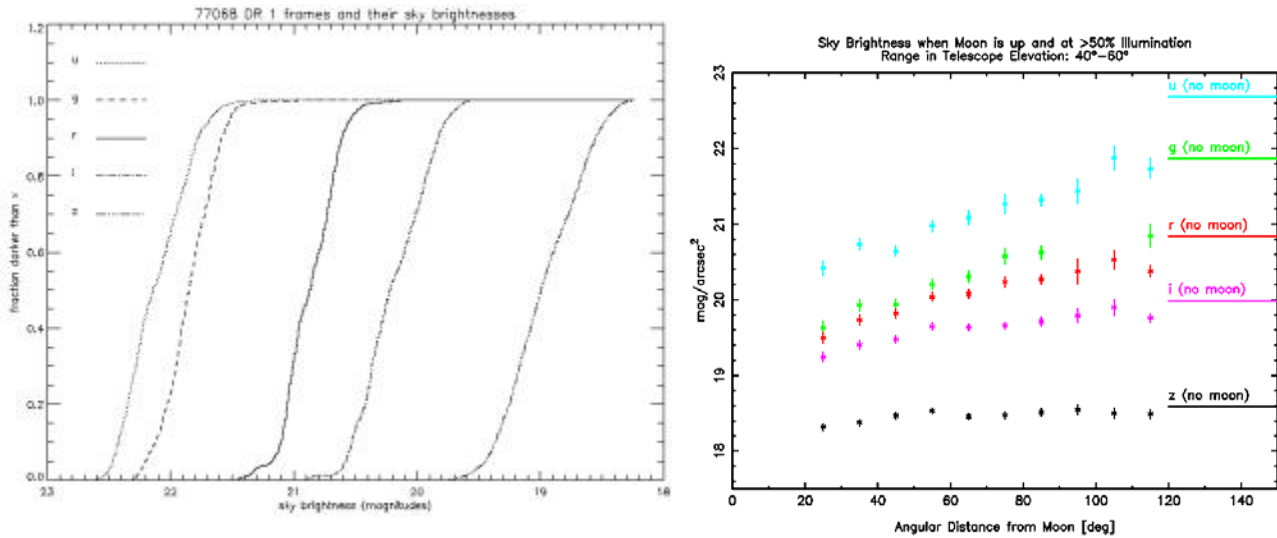


Figure 4.9 The plots of sky brightness. The left panel shows the distribution of sky brightnesses for the 77,000 images in the SDSS Data Release 1. The panel on the right shows the sky brightness as a function of moon separation for images taken when the moon is at 50% illumination or greater. These show that we can work in the i and z filters in full moon conditions, in the z-band during any time, and the i-band when the moon is 50 degrees or farther away.

There are also nights that are photometric but have poor seeing. If the seeing is beyond the $< 1''.1$ window, set in the science requirements, then the data we acquire will not be part of the survey coadd and we are free to use it for other purposes. The CTIO weather records on seeing are not as extensive as for clouds, but early estimates suggest 10% of the observing time in the Austral Spring is worse than $1''.1$. Cloudy and bad seeing data are not useful to

us in the main though the criteria in the supernova survey for useful data are less stringent, and we will explore using the time for that. During periods of good seeing, time neither photometric nor totally overcast, we will acquire data in our normal fashion, but assign that data to a non-photometric tiling that we can add into the survey coadd, but not use for survey calibration. As there is less time in the non-photometric category, it is exceedingly unlikely we would complete one non-photometric tile per year. Periods of photometric and good seeing are prime survey time for i and z, and if it is dark time, for g and r as well.

The photometric poor seeing time allows for an interesting use: calibration of star fields in the survey area from standard stars. If we devote this time to the transfer of the absolute calibration, we would have roughly 300 hours to use for this purpose, as seen in Table 4.1, of which approximately 130 hours are dark time. The ~1700 tiles in our area would, if one out of 7 were used as a calibration field, require on the order of 250 fields. Our rate of transfer star field acquisition would have to be better than 2/hour, not a demanding rate. This idea is developed further in the section on photometric calibration.

Table 4.1 Breakdown of Time over the 525 Nights of the Survey

Hours	Total Hours	Good Seeing ($\leq 1.1''$)	Bad Seeing ($> 1.1''$)
Photometric	2900	2600	300
Non-Photometric	950	850	100
Nights	Total Nights	Good Seeing	Bad Seeing
Photometric	396	355	41
Non-Photometric	129	116	13

4.2.4 Observing Strategies

The time to complete a tiling depends on observing strategy design choices centering around exposure time and photometric calibration strategy. The two design decisions we have made push us in a particular way: that area is more important than depth drives imaging the entire survey area at least once per year; and that the use of multiple tilings enables precision photometric calibrations. The boundaries on the range of reasonable strategies are not overly broad. We can examine the implications of the remaining choices available by exploring two strategies.

Strategy A: We divide the needed integration time into 100 second exposures for the first five tilings, and 200 second exposures for any remaining tilings. This choice leads to 5 tilings for g and r, 7 for i and 13 for z. Five is chosen as the minimum number of tilings as a means of reaching 1% relative photometry. At a given sky position images in two filters (g,r in dark time, i,z in bright) are acquired before the telescope slews to the next position. Positions are chosen along constant airmass tracks in order to simplify the photometric calibration

equation, eliminating airmass as a term⁸. This strategy aims at the highest precision relative photometry.

Strategy B: We aim at one tiling per year per filter, and to take three years to do g,r and five years to do i,z. This leads to 166 second exposures for g and r, 180 second exposures for i and 420 second exposures for z. The data are acquired in a pattern consisting of a main hex and its 6 neighboring hexes (Figure 4.9). Each set of 7 hexes is taken preferably on the same night and airmass. At each position, an image is taken through each of a pair of filters: g,r if dark time, i,z if bright. Each main hex is the subject of a transfer calibration from standard stars. The aim of this strategy is minimal observing overhead combined with a more traditional photometric calibration.

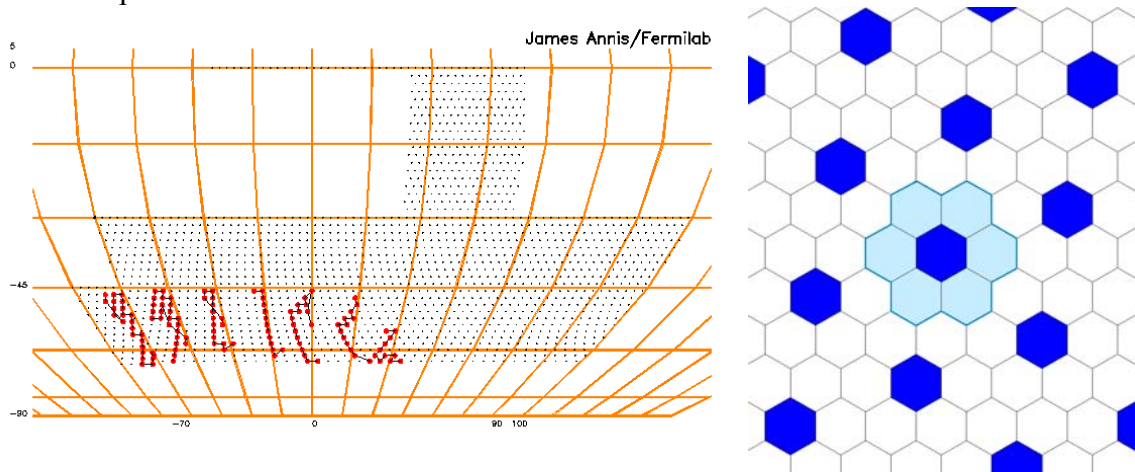


Figure 4.10 The spatial layout of the two strategies. Strategy A aims at constant airmass stripes, which are shown in the left panel as connected red lines for a series of constant airmass observations taken in October. Strategy B aims at central hexes (dark blue) and their zones of control, the 6 hexes immediately surrounding the central hex and shaded light blue in the right panel. Each strategy assumes that a single calibration along the stripe or in the central hex will calibrate all of the connected hexes.

Table 4.2 Characteristics of Strategy A and Strategy B

	g tilings	r tilings	i tilings	z tilings
Strategy A	5x 100 sec	5x 100 sec	7 (5x100, 2x200)	13 (5x100, 8x200)
Strategy B	3x 166 sec	3x 166 sec	5x 180 sec	5x 420 sec
Number of tilings	Strategy A		Strategy B	
Year 1	g,r,iz = 2,2,2,2		g,r,iz = 1,1,1,1	
Year 2	g,r,iz = 4,4,4,4		g,r,iz = 2,2,2,2	
Year 3	g,r,iz = 5,5,6,6		g,r,iz = 3,3,3,3	
Year 4	g,r,iz = 5,5,7,9		g,r,iz = 3,3,4,4	
Year 5	g,r,iz = 5,5,7,13		g,r,iz = 3,3,5,5	

⁸ The actual spatial pattern is constrained by 1) constant airmass, 2) select low RA first, then low Dec, and 3) preferentially stay inside the current sector, a 15 by 15 degree box. The latter two constraints are needed to work on the parts of the sky best visible early in the season rather than late in the season.

Each strategy employs a telescope camera system that is capable of 35 second slews, 15 second readouts, and 10 second filter changes, any of which can be simultaneous.

The survey observing time is divided into another two categories: the main imaging time and the supernova survey. Ten percent of the available time is devoted to the supernova time domain survey. Further, perhaps five percent of the time the system will be down for repair or upgrade.

Doing the arithmetic, one finds that strategy B obtains 1 tiling per year and per filter⁹ and that strategy A obtains 2.2 tilings per year per filter. Given the 35 second slew time, aiming at significantly more than 8 tilings per year total would be inefficient and would have to be driven by some compelling need. Some characteristics of the tilings obtained as a function of time are shown in Table 4.2. There is one number that makes it easier to do quick calculations: 800 seconds/year. It is possible to cover the full 5000 sq-degrees with a 3 sq-degree camera in 30% of a year with 800 seconds of exposure: 8 tilings of 100 seconds exposures or 1 tiling of 800 second, the difference in overhead is about 20%, so for quick calculations can be neglected.

Well planned large homogeneous surveys can obtain all of their data at low airmass: both strategies place a limit on observations of aimasses ≤ 1.5 . There is some room to make this airmass limit smaller.

In both strategies, the spatial layout of observations is driven by plans for photometric calibration. The connected observations allow one to transfer sparse photometric calibration images onto a larger number of images, 7 for strategy B and roughly 13 for strategy A. The spatial patterns are shown in Figure 4.10.

Table 4.3 Characteristics of Strategy A and Strategy B

	g tilings	r tilings	i tilings	z tilings
Strategy A	5x 100 sec	5x 100 sec	7 (5x100, 2x200)	13 (5x100, 8x200)
Strategy B	3x 166 sec	3x 166 sec	5x 180 sec	5x 420 sec

Number of tilings	Strategy A	Strategy B
Year 1	g,r,iz = 2,2,2,2	g,r,iz = 1,1,1,1
Year 2	g,r,iz = 4,4,4,4	g,r,iz = 2,2,2,2
Year 3	g,r,iz = 5,5,6,6	g,r,iz = 3,3,3,3
Year 4	g,r,iz = 5,5,7,9	g,r,iz = 3,3,4,4
Year 5	g,r,iz = 5,5,7,13	g,r,iz = 3,3,5,5

4.2.5 Simulating the Observing

The survey observing strategies can be tested against simulations of the survey progress if the simulations incorporate the major elements of survey observing, such as the survey geometry and the weather. In the pursuit of an optimal survey observing strategy we have constructed such an observing simulator.

⁹ This was unsurprising because the exposure time was chosen to obtain 1 tiling per year, and we adjust it accordingly.

For our simulator, we took the night as the base element and incremented time from sunset astronomical twilight to sunrise astronomical twilight. The night was noted as “moony” if the moon was at 50% illumination or greater. The nights allocated to NOAO community observing were assigned the earliest possible dates in the month. The weather was checked, and the night declared photometric or cloudy. If non-NOAO, dark time, and clear, the observing commences at astronomical twilight with an observation (two, actually, as two filters are observed at the same position) and a slew. Time is incremented, and data obtained until the sunrise astronomical twilight. The observations are selected by looking at the pool of unobserved tiles in a tiling at less than 1.5 airmasses, and then picking the most interesting tile in ways idiosyncratic to the particular observing strategy.

This structure allows the major elements of the survey to be assigned models:

- A NOAO time allocation model, in which NOAO reserves
 - September: 4 bright /4 dark nights
 - October: 4 bright /5 dark nights
 - November: 4 bright /4 dark nights
 - December: 4 bright /4 dark nights, with the telescope shut down Dec 25 and Dec 31.
 - January: 4 bright /5 dark nights, 2nd half of remaining nights
 - February: 3 bright /3 dark nights, 2nd half of remaining nights
 - The remainder of the time in September through February devoted to the Dark Energy Survey, a total of 108 nights/year.
- A weather model:
 - Based on the 30 year CTIO weather data
 - The percentage of clear nights (F) given a day number (d):

$F = 70 + 0.00*d$	$0 < d < 70$	Austral Summer
$F = 124 + -0.77*d$	$70 \leq d < 135$	Austral Fall
$F = 0 + 0.17*d$	$135 \leq d \leq 365$	Austral Winter/Spring
- The footprint of the survey:
 - SPT
 - -60 to 105 degrees RA, -30 to -65 Dec
 - -75 to -60 degrees RA, -45 to -65 Dec
 - SDSS Stripe 82
 - -50 to 50 degrees RA, -1.0 to 1.0 Dec
 - Connecting region
 - 20 to 50 degrees RA, -30 to -1.0 Dec

Strategy Evaluations: Our metrics are driven by the science, and are:

- Efficiently attain required depth
- Minimize photometric calibration errors
- Obtain scientifically interesting data at natural points in the survey
 - Year 2, at the time of the coadded data release
 - Year 5, at the end of the survey

For our purposes here we will simplify the footprint to the rectangular region that can be seen in Figure 4.10. The simulation was run here for 2008. Strategy B was simplified from zone of

control around a central master hex to a line of 6 hexes around the central master hex, a simplification which will have no effect on our comparison. Strategy A nearly completed the tiling for both tiles; recall that Strategy A aims at two tilings per filter in the first year. Strategy B appears to not have completed its single tile, but this is an artifact of the strategy model. Strategy A attempts to start at the farthest west, lowest declination unobserved hex, whereas Strategy B attempts to start at the farthest west unobserved master hex. That master hex starting point is significant: if the 7 hex line is not completely observed, the implemented model has no means of finishing off the observations. Time to do so was available, however, so we assume that Strategy B would be able to finish the tiling with point and shoots.

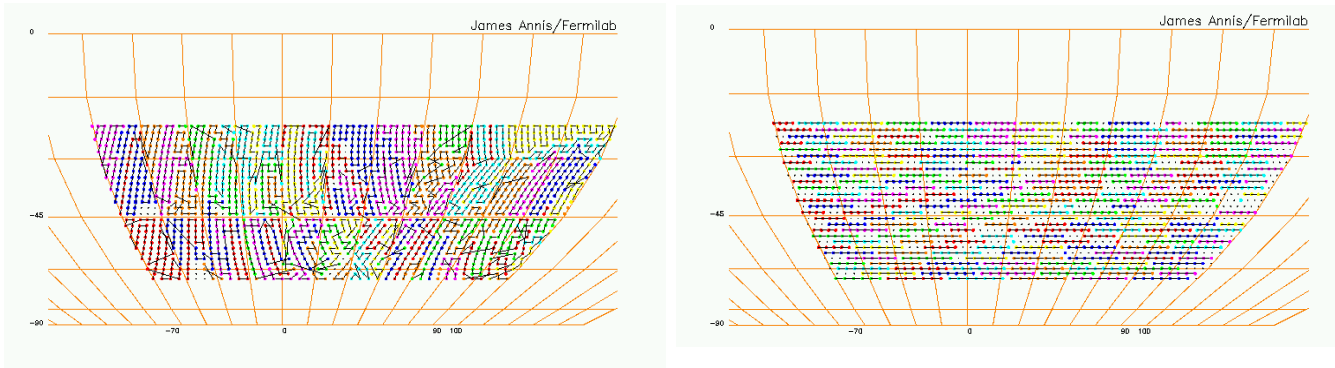


Figure 4.11 Sample tiles from Strategy A, on the left, and Strategy B, on the right. The strategy for B was simplified to be 7 hex long lines centered on the master hexes, a simplification that will not affect our comparisons. The unobserved tiles are shown as black dots. In Strategy A these were legitimately missed, whereas in Strategy B they resulted from a strategy model that did not allow for the finishing of the 7 hex strings when airmass or dawn interfered. There was plenty of time left in Strategy B to pick these up; we assume that it completed the tiling, and added them in to the statistics where appropriate.

Efficiently attain required depth: The distributions of image airmasses is shown in Figure 4.11. In both cases the majority of the observations are at airmass < 1.25 . Strategy B has a noticeably larger tail of high airmass observations, and it is likely that the inclusion of the fill in hexes will increase this. The statistics however, are very similar: mean airmass = 1.20, and median airmass = 1.17.

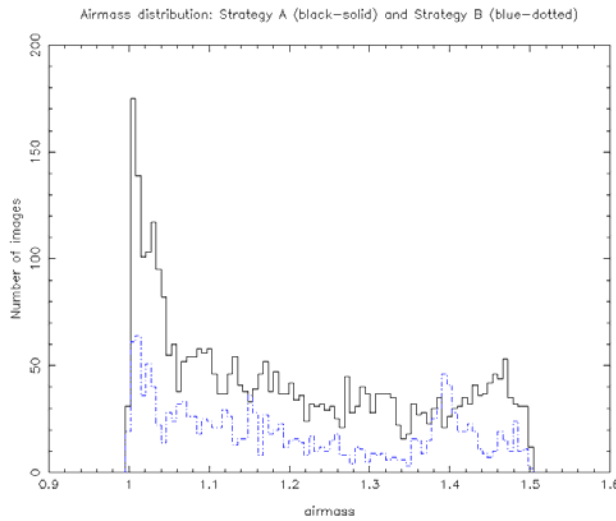


Figure 4.12 The distribution of airmasses. All observations are at airmass < 1.5, and the majority of both strategies are at airmass < 1.25. Strategy A is the solid line, and Strategy B is the dotted line.

The distribution of slew lengths shows some differences. The mode of the slew distribution for Strategy A is 1.6 degrees, and the mode for Strategy B is 2.0 degrees. The mean, median, rms lengths of the constant airmass stripes in Strategy A are: 17, 13, 16, whereas the mean, median, rms lengths of the zone of control stripes in Strategy B are: 6, 7, 1.5. The lengths are noticeably smaller in Strategy B, and this is before the 14% of all tiles in the “broken hexes” that must be slewed to be included. Likewise, the 75% quartile of the Strategy A slew distribution is 2 degrees, where in Strategy B, again without the broken hexes, is 5 degrees. The telescope does, in fact, handle these 5 degree slews with the same level of efficiency as it does for 2 degree slews. Data on slew times from the CTIO 4m can be described by the following model:

Slew (degrees)	Time (seconds)
≤ 3	34
$3 < \text{slew} < 20$	$2 * \text{slew} + 27$
≥ 20	75

The distribution of slews (with Strategy B’s broken hexes assigned a 10 degree slew) along with the model of the slew times and our expected readout time of 17 seconds allows the calculation of an overall efficiency. We calculate the inefficiency over all 4 filters and all five years. For Strategy B it is 14%, and for Strategy A, 20%.

It is worth calculating what improvements in the telescope slew performance and camera readout times would gain us. If the telescope control system could be improved to give 17 second slews for 1 degree or less slews, with the slew time rising smoothly to 34 seconds for 3 degree slews, the inefficiency of Strategy B improves to 13% and Strategy A to 14%.

The increase in efficiency would translate directly into longer exposure times and deeper overall data set. It should be pointed out that this is true for Strategy B in comparison to Strategy A as well.

Minimize photometric calibration errors: The biggest difference between Strategy A and Strategy B is in the number of tilings obtained per year, and the resultant photometric calibration accuracies. The calibration accuracies depend on the number of tilings N as \sqrt{N} for the absolute calibration¹⁰, essentially from calibrating the same piece of sky every year. For relative calibrations, the accuracy increases better than \sqrt{N} , but not as well as N . It is clear that having more tilings will produce better photometric calibrations. Whether 3,4, or 5 tilings is sufficient to reach the survey goals depends in large part on the (as yet unknown) level of systematic errors in the Dark Energy Survey instrument.

Table 4.5 The expected calibration accuracy

	Absolute: B/A	Relative: B/A
Year 2	$g,r,i,z = \sqrt{2}$	$g,r,i,z = 1.5$
Year 5	$g,r,i,z = \sqrt{5/3}, \sqrt{5/3}, \sqrt{7/5}, \sqrt{13/5}$	$g,r,i,z = 1.5, 1.5, \sim 1, \sim 1.5$

Obtain scientifically interesting data at natural points in the survey: The interesting points in the survey are at 2 years and 5 years; the interesting metric is the quality of the data set at these times. We are to explore the time progression of the survey.

For this, we will use the full footprint, which is shown in Figure 4.13. This footprint has been changed to make the observing easier. The changes: the lower border of the area is -65 degrees declination: lower declinations are hard to observe and include the LMC. It was replaced with the area in the west. The connecting region was thinned to 30 degrees width, and moved as far to the east as possible before the galactic dust distribution contributes substantial extinction.

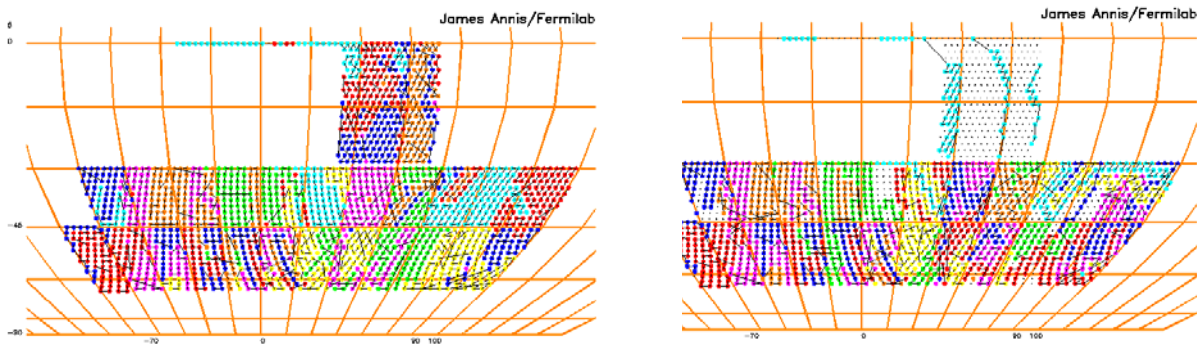


Figure 4.13 Simulations of the progression of observing in 2009. On the left is a great year, on the right is a year whose weather is worse than normal.

The plots in Figure 4.13 show the effects of weather, especially in the patterns of untiled sky on the right panel. The distribution of number of tiles observed versus hours of clear weather is interesting. As can be seen in Figure 4.14, we image the entire survey area in about $1/3^{\text{rd}}$ of the simulations, even if we have an optimal hex selection algorithm. There remains a 10% discrepancy between the analytic model of the weather and the simulation

¹⁰ The difference between relative and absolute calibrations is developed in section 4.2.1.

which we have not tracked down; the analytic model predicts 10% more time. The figure also shows that bad years are bad years; there will be years in which the weather is poor, and we will achieve less than full coverage on the tilings.

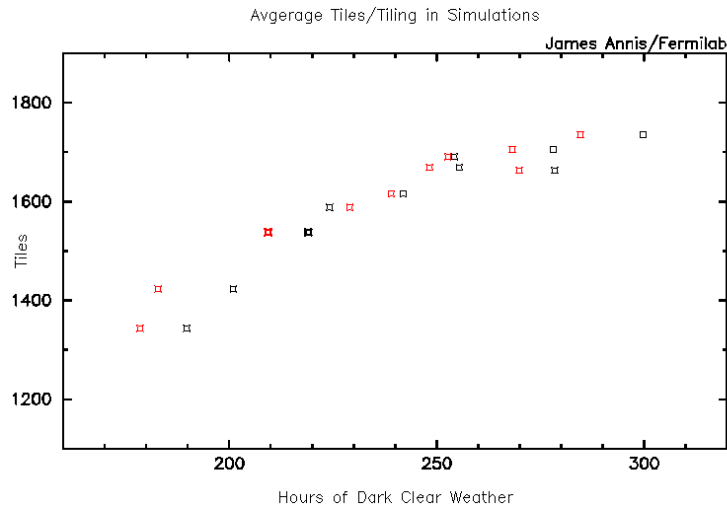


Figure 4.14 The distribution of tiles observed versus hours of dark clear nights. The footprint has 1750 tiles¹¹. All of these simulations were for 2009. The red symbols shows a variation on the time distribution in which survey nights in late February are traded for nights in December. The curve is essentially linear to about 250 hours, and then flattens out. The flattening is due to time available that cannot be used in the tiling; in other words the hex selection algorithm can be improved. Two thirds of the simulations are in the linear regime: 2/3rds of the time we will observe 1667 tiles. The change in time distribution did little.

The distribution of time allocated to the survey may be used to shape which part of the survey is most likely to be missed due to weather in a given year. We ran simulations that allocated time from the half nights in the 2nd half of February to full nights in December. Once the simulations are averaged, the probability map may be examined. Two of these are shown in Figure 4.14. Similar in success rate, the diagrams are dissimilar in spatial patterns. Given less time in December and more in February, the standard time distribution is less able to fill in the connecting region between the SPT and the SDSS Stripe 82 area, but more able to complete the SPT area in the far east. Both suffer from a lack of time in October.

The spatial probability pattern of the standard time allocation is favorable¹² to the science priority of the three regions. The SPT area is of prime importance, the SDSS Stripe 82 is of great interest for calibration of photometric redshifts, and the connecting area's strategic

¹¹ Our survey area has 5000 sq-degrees, the DECam has a tiling area of 3.0 sq-degrees, and there are thus 1667 tiles in the survey area. When we lay down a hexagonal grid on the celestial sphere in the simulation, we find we need 1775 tiles. We ascribe the difference to a declination dependant tiling area. The mapping of a hexagonal grid on the sphere is an interesting problem, one that has been explored by the climate modeling community (Randall et al. 2003), and we are examining their solutions while continuing our own exploration of the topic.

¹² It works well, assuming that the problems in October can be resolved by working the hex selection algorithm. This is likely as the current algorithm weights equally objects in the east and in the west, whereas hexes in the west are more valuable, as they sink with season as well as with the passing hours.

usefulness rests on its direct connection of the photometric redshift training ground to the main survey area. The three pillars in the submarine conning tower of the left panel of Figure 4.14 provide the minimum necessary to do this, though the hex selection algorithm would have to be guided to their importance.

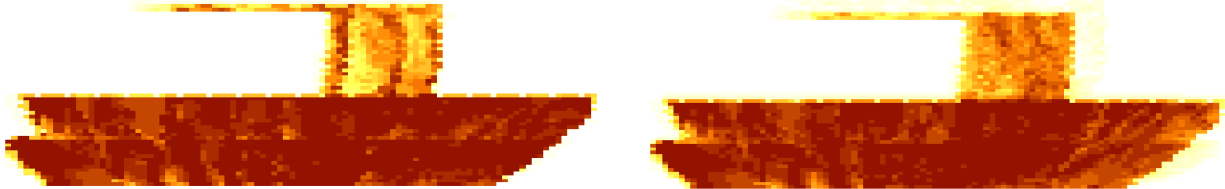


Figure 4.15 Probability maps of the survey area. Dark corresponds to the highest density of observations of a hex, light to the lowest. The panel on the left shows the reference distribution of survey time. The panel on the right shows what happens if the time in the second half of February is instead given to December. The probability map is more uniform, but the coverage of the main SPT area is lower. The reference distribution shows a fairly uniform distribution in the SPT area (modulo problems on the left, a lack of time in October), with the connecting area not as well imaged.

The simulation is lacking several features, of which photometric nights with poor seeing and the supernova field observations are both 5-10% effects, that perhaps balance the difference in time that is clear in the simulations versus the analytic calculations.

4.2.6 Reference Strategy

We will take the lessons learned from the simulation and develop the reference design survey strategy.

First, the sparse tile pushes us to four or five tilings in order to have three or more observations everywhere. Our goal of science quality data at the end of the second year then demands multiple tilings per year per filter. Second, the overhead of thirty five seconds per slew pushes us towards longer exposures, ideally 350 seconds (or lowering the slew time to 15 seconds). This pushes us back away towards as few tilings as possible, down to two per year. Third, the realities of weather can cut the clear observing time in half. A strategy aimed at two tilings per year can still complete a tiling in the face of bad weather.

A good reference strategy is to steer the middle course between strategy A and strategy B, aiming to get two tilings per year per bandpass. We would obtain g and r data for the first two years, i data for the first 4 years, and z data for all five years. Details of the reference strategy are shown in Table 4.6. Increasing the exposure time above 100 seconds decreases the overhead and thus there is more time available for on-target integration, but we have not included this in the total integration times. In year 5, for example, effectively another tiling of 200 seconds should be possible.

Table 4.6 Reference Survey Strategy

Year	filter	Area	Total Tilings	Int.	Total Int.	Magnitude	Photometric Calibration		Cluster z and weak lensing n_g (galaxies/arcmin ²)
		sq-deg.		seconds	seconds	10σ	Relative %	Absolute %	
1	g	5000	2	100	200	24.2	1.8	3.5	$n_g \sim 8$ $z = 0.7$
	r	5000	2	100	200	23.7	1.8	3.5	
	i	5000	2	100	200	23.3	1.8	3.5	
	z	5000	2	100	200	22.6	1.8	3.5	
2	g	5000	4	100	400	24.6	1.2	2.5	$n_g \sim 12$
	r	5000	4	100	400	24.1	1.2	2.5	
	i	5000	4	100	400	23.6	1.2	2.5	
	z	5000	4	100	400	23.0	1.2	2.5	
3	g	5000	4		400	24.6	1.2	2.5	$n_g \sim 16$ $z = 1.0$
	r	5000	4		400	24.1	1.2	2.5	
	i	5000	6	200	800	24.0	≤ 1	≤ 2	
	z	5000	6	200	800	23.4	≤ 1	≤ 2	
4	g	5000	4		400	24.6	1.2	2.5	$n_g \sim 20$
	r	5000	4		400	24.1	1.2	2.5	
	i	5000	8	200	1200	24.3	≤ 1	≤ 2	
	z	5000	8	200	1200	23.6	≤ 1	≤ 2	
5	g	5000	4		400	24.6	1.2	2.5	$n_g \sim 28$ $z = 1.3$
	r	5000	4		400	24.1	1.2	2.5	
	i	5000	8		1200	24.3	≤ 1	≤ 2	
	z	5000	10	400	2000	23.9	≤ 1	≤ 2	

The reference design presented here will obtain 4 tilings of data at the end of year two (3 if there is a year of bad weather), sufficient to have 3 exposures per point for over 90% of the survey area. It will produce a dataset capable of being calibrated to $< 2\%$ relative and $< 3\%$ absolute accuracy. The reference design is flexible enough to deal with an El Nino year at any point. The price will be less depth in the z band. In fact, a careful examination of the science requirements versus the reference design expectations will note that we meet theour requirements at the end of year 4. We take the year 5 data in z in order to increase the depth and therefore the weak lensing grasp, but weather is a problem. In a five year period we should expect an El Nino so the conservative survey designer will also take the year 5 times as a buffer and contingency to ensure meeting the requirements.

In this conservative view, in the unlikely event that we experience 5 good years of observing, without an El Nino event, the resulting excess contingency time can effectively be used in a number of ways. It could be used to acquire more z band data, as envisioned in the reference

design, to increase the weak lensing grasp. It could be used in part to target the SPT “blank fields”, those SPT sources without DES counterparts, in J and H using NEWFIRM as a means to collect the small percentage of SPT clusters at $z > 1.5$. We will continue to develop ideas for the good luck case while we continue to retain the fifth year contingency in our design.

4.3 Calibration Strategy (WBS 1.3.2)

There are three components covered in calibration: photometric calibration, astrometric calibration, and photometric redshift calibration.

4.3.1 Photometric Calibration

We are proposing a large area, multicolor, imaging survey requiring precision photometry. Traditional photometric reductions which place observations onto a standard system are inappropriate here. It is much more important for extremely large sets of homogeneous photometric data produced using a single instrument to be internally consistent than it is for them to be on previously established photometric systems. For such surveys, the aim of calibration is to produce data sets for which:

- The magnitudes may be calculated by convolving a spectrum with good spectrophotometry with the system bandpasses, and
- The magnitudes vary only by $2.5\log_{10}(f_2/f_1)$, where f_2/f_1 is the ratio of the photon fluxes, independent of position.
- The magnitudes have a well-defined absolute zeropoint.

The first goal puts a premium on knowing the system response curve with precision. The second goal demands knowing the atmospheric effects, but also puts a premium on understanding flat fielding and scattered light effects. The third is a question of standard star observations. We will discuss these three requirements in the next three sections.

A multiply imaged survey demands a calibration strategy that differs from both a single pass survey and a deep pencil beam survey. The pencil beam surveys proceed by observing a set of standard stars at a variety of airmasses in order to calculate the parameters of an atmosphere model, from which one can calibrate data taken anywhere in the sky. This form of precision calibrations demands a concordant amount of the telescope time be devoted to the standard stars. Single pass surveys cannot afford the devoted time, so they employ a dedicated small telescope to monitor extinction during a night and to transfer a star network down to fainter magnitudes to calibrate the main survey. In a multiply imaged survey one should take advantage of the multiple images by acquiring them on different nights and thus averaging down the absolute calibration error. One should also acquire the images on offset pointings of the scale of the camera to average down the relative calibration errors.

Determining the System Response: The observed magnitudes must be predicted within 2% by convolving calibrated spectra with the system response curves. *We must measure the system response as a function of wavelength.* Understanding the system response curves is critical to using photometric redshifts, and is in fact fundamental to understanding the photometric data.

System response curves are relative efficiency curves over the entire wavelength coverage of

the instrument. The measurement of system response curves requires shining calibrated monochromatic light through the corrector, filters, and onto the CCDs. The light must be sent at the correct f-ratio, because the angle the light beam makes to the surface changes the wavelength response of interference coatings. The response curves must be measured using on the order of 100 resolution elements across each bandpass, which for our 150nm wide filters is 1.5 nm resolution.

We plan on doing this at the telescope with a system that will perhaps be more capable than what we describe here, depending on the outcome of a research program CTIO is pursuing. Regardless, we plan on measuring the response curves before we deliver the camera, during the full up testing of the camera at Fermilab. The system will require creating test beam optics that create a f/3 beam to be sent to the focal plane array, though we plan on illuminating only one CCD at a time.

This system will also be able to test the other components of an astronomical photometric instrument: flat fields and read noise being the two most important. Testing of the entire Dark Energy Camera system, from focal plane to corrector to data acquisition to observing programs, is of course a very important task. It should be done before we ship the system to CTIO.

Relative Photometry: Relative calibration is the step of placing all of the instrumental magnitudes, onto a magnitude system corrected for instrumental effects and the atmosphere, but without regard to the magnitude zeropoint.

Overlapping tilings can make this a powerful technique, and we will use them to perform high precision relative photometry. The essential step is to use ratios of the counts of the same stars observed on two different images to tie the photometry together. Large scale overlaps provide 10^3 - 10^4 stars appearing in two different images providing numerical precision on the ratios better than 1%, much better than one can know the zeropoints of the images. The limiting factor in this approach is systematic errors, primarily flat fielding and scattered light. Both of these tend to be more problematic at the edges of the field of view. The overlapping hex tilings allow one to average these out. The relative photometry strategy produces a very flat map, optimal for relative photometry.

Given these overlapping tilings, the optimal way to think about relative photometry is to ask for the best mapping of the underlying star field given the observations of the star field. The techniques developed for CMB mapping strategies (Wright 1996, Tegmark 1997) can be applied to this problem. The mapping strategies are in essence least squares solutions to the problem of estimating the underlying map given many noisy observations. One forms linear equations of the form $\mathbf{y}=\mathbf{A}\mathbf{x}+\mathbf{n}$, where \mathbf{y} is the data, \mathbf{n} the noise, \mathbf{A} is the known observation matrix and \mathbf{x} is the underlying map one is solving for. One solves for the map $\mathbf{x}=\mathbf{W}\mathbf{y}$, by constructing \mathbf{W} via $\mathbf{W}_{coadd}=[\mathbf{A}^t\mathbf{A}]^{-1}\mathbf{A}^t$. This method is fast, simple, and minimizes the error map variance in the case of white noise.

We have explored this technique using a model for the systematics of the camera.

- A multiplicative flat field gradient of amplitude 3% from east to west.
- A multiplicative 3% rms flat field error per CCD

- An additive scattered light pattern with a $1/r^2$ amplitude from the optical axis, 3% at the edge of the camera
- An additive 3% rms scattered light per CCD

The amplitude of these effects are probably slightly worse than the DECam will exhibit, and work towards understanding the actual levels is ongoing. We also incorporate an atmospheric model for wavelength dependent fluctuations in the extinction at the level we expect at CTIO, with the additional feature of a 10% gradient in the extinction value during a night, which would induce large scale RA dependent zeropoint variations. We simulate the progress of the survey with the survey simulation program mentioned briefly last section, and the relative mapmaking algorithm. The decrease in the systematic error floor level is faster than \sqrt{N} but slower than linear in N , the number of tilings. A table showing the improvement is below, and a realization of a resulting map is given Figure 4.15. This process gives a very flat map, receptive to an absolute calibration.

Relative Calibration	
Tiling	σ
1	0.035
2	0.018
5	0.010

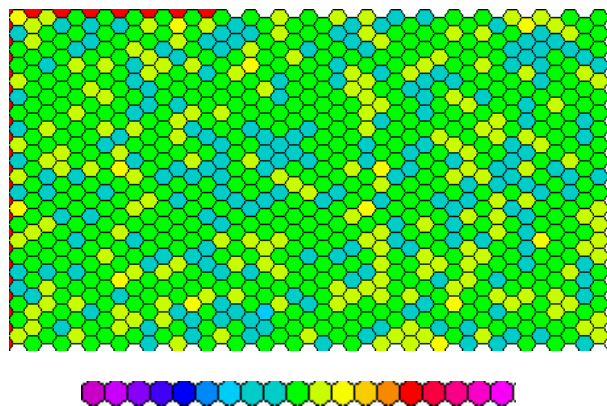


Figure 4.16 This figure shows a map of the photometric calibration error using relative photometry. The full scale of the scaling bar is -0.20 mags to $+0.20$ mags. The map is that resulting after 3 tilings and has a rms scatter of $\sigma=0.013$, starting from 10% photometry and a variety of flatfield and scattered light systematics imbedded at the $\sigma=0.03$ level.

Absolute Calibration: Absolute calibration is the process of transferring the calibration from known standard stars onto unknown stars. The calibration of standard stars includes an energy flux calibration, and the process of absolute calibration determines the ratios of the energy flux between the unknowns and the standards.

There are choices to be made here in the pattern of observations. We consider two scenarios. The first is motivated by a desire to convert into a far simpler form the standard equation of photometry, $m = -2.5 \log C - a - k(t)X - c\Delta M\Delta X$ where m is the magnitude of an object, C is the measured counts, a is the measured zeropoint, $k(t)$ is the time dependent extinction coefficient, X is the airmass, c is the second-order extinction coefficient. The last term reflects the varying extinction across the broad filters typical of large area surveys.

First, one notes that wide area surveys have a limit on the maximum airmass they will accept: airmass 1.5 is a pragmatic choice. This eliminates the c term, as the values of c are of order 0.03 and thus the second-order extinction term is of order 0.005. Ignoring it places a photometry calibration error floor somewhat below 1%. Second, one notes that the zeropoint a changes night to night, while the extinction coefficient $k(t)$ changes both night to night and drifts during a night. If one were to arrange to observe only at one airmass during the night, the equation would become $m = -2.5 \log C - a(t)$. We thus aim for long strips of hexes all observed at the same airmass. Later a hex along the constant airmass strip is absolutely calibrated, and the rest of the hex assumed to be on the same calibration.

The second scenario aims at providing absolute calibrations to compact areas. The observation progression is to observe a hex and then its “zone of control”, the 6 surrounding hexes, before moving on to a new central hex. Later the central hex is absolutely calibrated and the zone of control hexes is assumed tied to it.

An absolute calibration, albeit to low accuracy, is possible as soon as the standard stars are taken. For one tiling, the experience is that absolute calibration is possible to 3-4% with the roughly ten standard star observations that current survey techniques use.

After multiple tilings are in hand, one can improve the accuracy of the absolute calibration by using the fact that we observe the same fields on different nights, using different observations of the standard stars. We use the same atmospheric model that we described above but here taken to have 5% uncertainty, the constant airmass observation progression, and neglected systematic errors. We solved for the zeropoint map using the coadd technique described above. We find that one determines the zeropoint of the coadded images with s/\sqrt{N} precision, where N is the number of tilings in that filter. Starting at 5% rms zeropoint error, one reaches 2% after 5 years by leveraging the many observations of standards that are taken. This 2% is the RMS constraint on any gradients or small scale features in the map. We show a map of photometry errors resulting from this approach in Figure 4.17.

In both scenarios, we plan to use the photometric time with seeing quality not acceptable for the imaging survey to transfer the calibration from standard stars to ~ 10 to 20% of the hexes. These exposures would be shorter than an imaging survey exposure because of brightness at the standards, so they should fit in an available poor seeing time.

There are two calibration programs ongoing that will be helpful to the DES calibration effort. The NOAO Surveys Project of Smith, Tucker and collaborators is constructing a Southern u',g',r',i',z' standard star grid. They use the CTIO 0.9m telescope to observe stars between $8 < r' < 18$ magnitude in fields spaced every hour in RA at Declination -30 , every two hours at Declination -60 , every four hours at -75 , and in several special fields. The program is fairly far along and will be completed by the time of the DES.

These stars are very good standards for the DES, as can be seen in Figure 4.18. Recall that we will not be aiming to place our observation directly on the u',g',r',i',z' system (the SDSS is not, for example), but onto the natural instrumental system of the DECam.

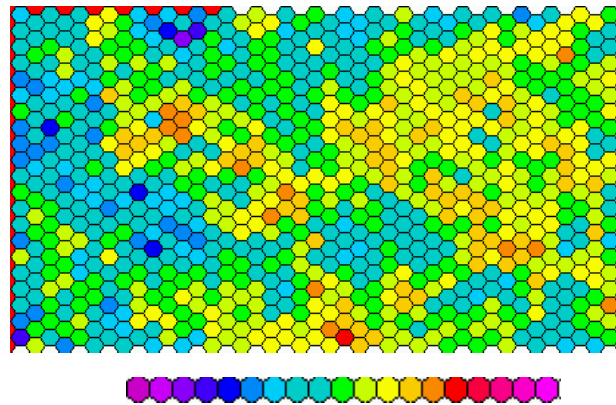


Figure 4.17 This figure shows a map of the absolute photometric calibration error using map making techniques. The full scale of the scaling bar is -0.20 mags to $+0.20$ mags. The map is that resulting after 3 tilings and has a rms scatter of $\sigma=0.037$, starting from 10% photometry. The level scales with initial photometry level and with \sqrt{N} of the number of tilings: for 5% photometry and three tilings the rms scatter would be $\sigma=0.022$.

The second program is the Stromlo Southern Sky Survey (SSSS), a project led by Dr. Brian Schmidt of the Australian National University. This five year project will provide a precision calibration of the whole southern sky in the photometric bands `ugriz+stromgren_v` to depths 0.4 magnitudes deeper than the SDSS. For our purposes, this data set would at least replace the USNO-B catalog as a source of per image calibrations, and has the potential to be the “standard star network” of choice.

Lastly, we expect that community users will observe standards especially for non-standard filters such as DDO51 and the narrow band interference filters. Although not specifically useful for the survey calibration, this could be helpful for other users of the DECam.

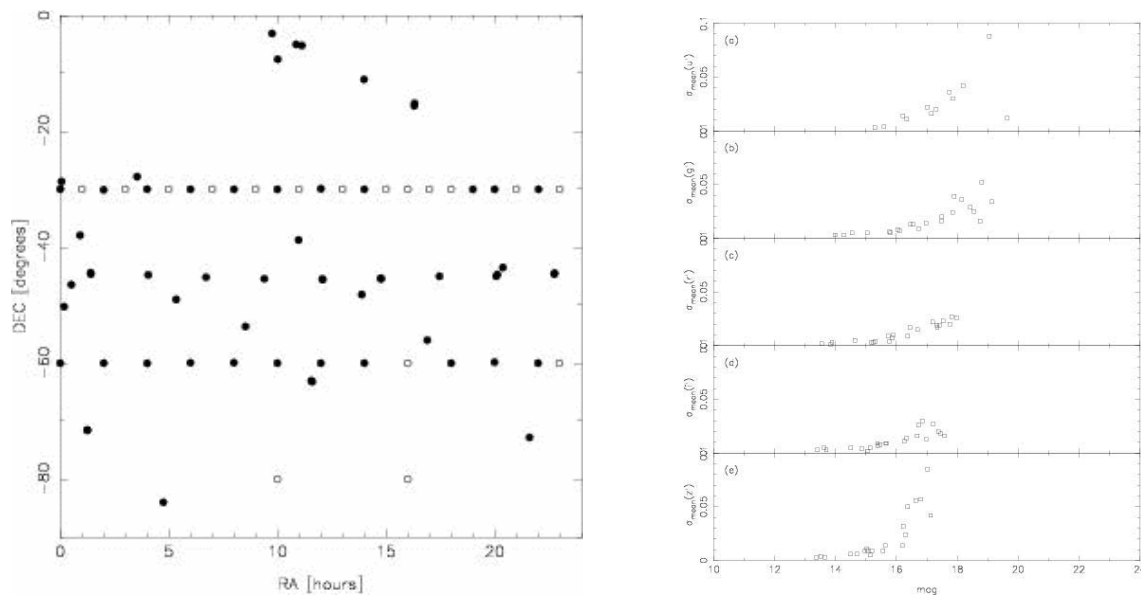


Figure 4.18 Standard Stars from the SDSS Southern Standards Program. On the left is the spatial distribution of standard stars in the program. On the right is a plot of the error distribution versus magnitudes of the standard stars in one of the standard fields, which serves to show us the magnitude range of the standards.

Checks on the Photometry: We must be able to check the accuracy and precision of our calibration.

The mapping strategies we have explored aim to measure magnitudes, and make no use of colors. This allows us to use known astrophysics to check our photometry. The stellar locus in color-color space has extremely well defined principal axes. The SDSS has shown that in the twin color spaces of g-r, r-i and r-i, i-z one knows the location and direction of the principal axes to a precision of

$$s=s_0 \sqrt{(4000/N_{stars})} \sqrt{(N_{bins}/64)}$$

where s_0 is of order 0.003 magnitudes. In single exposures of 100s, the DEC reaches about 21 mag at a S/N=100. This implies about 2000 stars/sq-degree. The SDSS experience is that only about 1/4 of these are clean, in the sense of being located away from image edges and not blended with other objects. We will have about 500/sq-degree of useful stars, which corresponds to roughly 20/CCD. This means we can use the stellar locus in three ways to check our calibrations:

- CCD calibration on full sensor scales: Three adjacent hexes provide enough stars to check the calibration on each CCD to 0.003. Recall that the equation above scales to 64 bins, and our current designs have about 60 CCDs.
- CCD calibration in 100x100 pixel scales: A complete tiling of 2000 hexes provides enough stars that when one selects all the stars observed by a given CCD one has enough statistics to explore the calibration in 100x100 pixel sub-regions.
- CCD calibration on 300x300 pixel scales: Breaking the complete tiling up into 10 blocks of 200 hexes each, one can do the same on 300x300 pixel sub-regions and check for variations with, say, right ascension.

It is worth pointing out how powerful this check is. We are calibrating the magnitudes independently of the colors, and checking the resulting colors, which are magnitude differences, using a precise test.

4.3.2 Astrometric Calibration

The requirement on astrometric calibration is $< 0.1''$ absolute. The design of the corrector optics provides for low, but non-zero, distortion. It may be necessary to include terms beyond the standard linear (affine) terms in the World Coordinate System convention. IPAC has put forward an extension to account for the distortion in the Spitzer Telescope IRAC instrument, and we will adopt this convention.

Astrometric calibration of images from DECam is straight forward and will be implemented using a variant of the astrometric pipeline developed for the Red-Sequence Cluster Survey (RCS). This method has been demonstrated to work well on similar mosaic data from the CFH12K (on the CFHT), Mosaic-II (on the CTIO 4m) and the currently largest operating imaging mosaic, MegaCam on the CFHT. Astrometric calibration will be done in a two-stage process. First, an astrometric reference frame of a sufficiently densely populated field will be used to define a relative solution between all chips in the camera. Each chip is treated by a low order polynomial (typically 2nd-3rd order) which maps pixel x and y in relative RA and DEC about some fiducial camera center. The reference field will be chosen to provide a density of 500+ objects per chip to make this mapping precise and robust. This reference field can be a moderate galactic latitude field with existing USNO-B astrometry, or more preferably one of the equatorial fields with precision astrometry

developed as reference fields for the Sloan Survey. Snapshot reference fields can be acquired in twilight on a regular basis (typically a few times a run) to monitor the camera's astrometric stability. The full image for all chips in DECam for a given science pointing is then mapped onto the sky as defined by the USNO-B catalog using a second polynomial which spans all chips. Over the area of DECam there will typically be 1000's of objects to match to, which is more than sufficient to ensure a good solution. Application of this algorithm produces astrometry which is accurate to about 0.1" in each coordinate, as is shown in Figure 4.35 for existing RCS mosaic data.

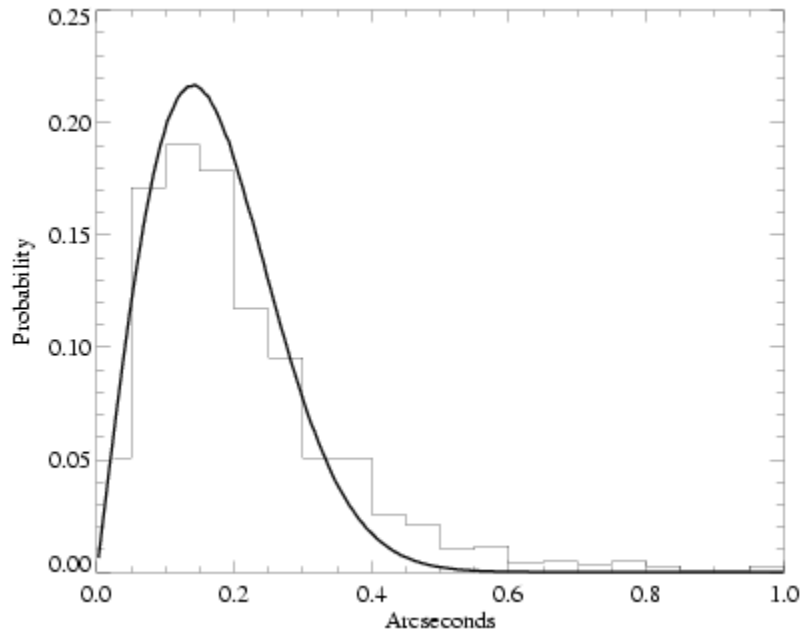


Figure 4.19 The histogram shows the distribution of residuals (both coordinates summed in quadrature) between RCS and SDSS positions for moderately-bright point sources in the overlapping fields. This comparison independently shows that the typical residual, per coordinate, is about 140 milliarcseconds between the SDSS and RCS. The uncertainty, per coordinate, for the SDSS is 50-100 milliarcseconds, suggesting that the RCS (and by extension, the DECam data) can be astrometrically calibrated to a similar accuracy.

4.3.3 Photometric Redshift Calibration

At the core of all of the science goals is accurate photometric redshifts. Our plan is to observe the areas of several ongoing redshift surveys. We expect to require roughly 1000 redshifts per 0.1 bin in redshift from $0.1 \leq z \leq 1.5$. This requirement becomes progressively more difficult as the redshift is increased. We plan to overlap several surveys. These include the 200 sq-degree SDSS Southern Survey, which has 100,000 redshifts down to $i=20$ and out to $z=0.5$, in combination with the 2df-SDSS survey, which has 10,000 redshifts of red galaxies out to $z=0.75$. In addition, two other large but deeper redshift surveys, the VIMOS VLT Deep Survey and the Keck DEEP2 Survey, are both currently in progress and will overlap the DES on or near the equator. These surveys will provide of order 100,000 redshifts, out to $z=1.5$ and above, useful for photometric redshift calibration of the DES.

In Section 2.7, we described our initial simulations of photometric redshifts for red cluster galaxies as well as for the general galaxy population. Our current plans for improving our

understanding of photometric redshift calibrations will focus on a detailed characterization of the photo- z error distribution (i.e., mean, variance, skewness, catastrophic error rate) for galaxies down to the DES depth ($i = 24$). This will be done as a function of the most relevant galaxy parameters, in particular magnitude, redshift, and SED type or color. For this purpose, we are using mainly data from the GOODS HDF-N and CDF-S fields, which contain spectroscopic galaxy redshifts to the relevant DES depths, along with available multicolor imaging. We will use the GOODS data sets, as well as simulated Monte Carlo galaxy catalogs generated from them, to characterize the photo- z errors expected for the DES observational parameters. In addition, we will supplement the GOODS sample with CNOC2 and SDSS data, which do not reach the DES imaging depth, but will provide, at brighter magnitudes, much larger spectroscopic redshift samples than are possible from the smaller GOODS fields

4.4 Survey Data Simulation (WBS 1.3.3)

The survey has precision measurements of dark energy as its highest goal. To extract our science, we must understand both the cosmological physics we are using in the measurements and the impact of the instrumental signatures on those measurements. To design our survey, we must understand what we would expect to observe under various scenarios, be it the question of simplicity of selection function with redshift for clusters given a range of i or z limiting magnitudes, or the effect on weak lensing moment measurement efficiency of decreasing the point spread function by 0.1". *We must produce a scientifically reasonable simulation of the survey.*

We envision using a combination of analytic methods, catalog-level simulations and image-level simulations for the Dark Energy Survey. Analytic models and methods (e.g. Fisher analysis) provide us with a quick means of estimating measurement and parameter uncertainties. Catalog-level simulations provide the next step of complexity, and allow us to incorporate more detailed and realistic models of statistical and systematic errors (on e.g., photometry, shear, photo- z 's), and also allow us to test and optimize the science analysis pipelines using large mock data sets. Finally, full image simulations provide a means of characterizing instrumental or observational systematic effects which are otherwise difficult to model analytically ab initio. An example would be measuring flatfielding or scattered light photometric residuals, as the images are propagated through the many steps of the coaddition and data reduction pipelines. Such image simulations then provide the data needed to analytically model the systematic effects and to subsequently feed them back into the catalog simulations in a simple manner.

One aim is to build up simple fitting functions and approximations from the simulations that can be applied in the analytical techniques.

4.4.1 Catalog Level Simulations

The start for this effort is in simulations of the dark matter distribution either from N-body simulations or from analytical approximations. Work will be needed here, probably from outside the collaboration, to extend these simulations to a grid in W_L and w . Collaborator Albert Stebbins (Fermilab) is exploring a fast analytic technique using mult-gaussians to approximate the dark matter distribution.

Next, galaxies must be placed on the dark matter distribution. The spectral energy

distributions (SEDs) of the galaxies must be assigned, and apparent magnitudes calculated. The output of this is a catalog containing ra, dec, z, mag, SED for the galaxies in the survey area, along with catalogs of the dark matter clusters and the expected shears. The current simulations that do this do not deal with size, shape or morphology, and they will have to be extended to incorporate these, likewise for the effects of galactic dust. Further, the galaxies that are put in usually are limited to brighter galaxies due to the resolution of the N-body simulation, and an analytical model is needed to put in the lower luminosity galaxies. The output of this work is a galaxy catalog. Collaborator Risa Wechsler is working on accurate methods of placing the observed galaxy distributions onto N-body simulations. We are also pursuing analytical expressions for observed galaxy property distribution functions and photometric redshift error distributions, using relevant imaging and redshift data available from the GOODS, HDF, CNOC2, SDSS and other samples.

Next is the addition of the stars. Here we should take advantage of the existing star maps, from the Hipparchos Tycho (10^8 stars) or USNO-B1.0 (10^9 stars) catalogs. The USNO-B1.0 catalog reaches to $V=21$ in two bandpasses. Fainter than this, we will adopt a galaxy structure model such as Bahcall-Soniera to predict the statistical distribution of stars. The output of this is the star catalog.

Shear induced by intervening mass concentrations must be applied. Collaborator Erin Sheldon is exploring shear measurement sensitivity and systematics as a function of PSF and galaxy property.

Lastly, a model for the Galactic dust must be used to apply extinction and reddening. This can be done using the Schlegel, Finkbeiner, and Davis dust maps. The galaxy and star catalogs will be combined, and the galactic dust model applied.

As an aside, cluster catalogs can be constructed from the galaxy catalog, the shear maps, and the dark matter catalogs. One should also extend this to SZE cluster samples.

Instrument Model: The survey simulation will break these galaxy+star catalogs up into telescope pointing and time series information.

Once assigned a pointing, the stars and galaxies may be assigned to a given CCD. This brings us to the instrument model. The instrument model will be taken to start at the atmosphere and end at data reduction. It will consist of :

- The weather model: correlations between time of year and the atmosphere model
- The atmosphere model: sky brightness, seeing, zeropoints, extinction, differential extinction
- The optics model: distortion due to the optics design, optics induced PSF variations, temperature dependent filter effects
- The sensor model: QE, gain, read noise, bad columns, cosmic rays, cross talk.

The output of this is a modified star/galaxy catalog containing the instrumental effects as well as the cosmological objects.

Notable among the existing elements of the model is Steve Kent's optics program, which can predict the PSF at any position in the focal plane for the DES optics. Much of the sensor model work consists of working with the CCD testing team and the photometric calibration team to extract the necessary information. These include such straightforward

items as read noise and bad column maps to more complicated issues such as system throughput.

4.4.2 Image Level Simulations

For many purposes the catalog level simulation will suffice. For the full mock data challenge, we will need to take the next step to full image simulations. Given the catalog of objects, one places them into artificial images. If one takes as a given that the catalogs contain -all- of the information necessary to produce the images, then this step contains much interpolation on the natural grid of galaxies. The alternative is to use CCD level information packaged in a different way, as will probably be most efficient for the spatially varying PSF that can be predicted from the optics model.

We have begun exploring four well known packages available for simulating optical/NIR astronomical images. These are the Shapelets package written by Richard Massey, the ARTDATA package in IRAF, the Terapix Skymaker package written by Emmanuel Bertin, and the SDSS simSurvey package. In all four of these packages, simulated images are generated using object lists of stars and galaxies. These lists can either be supplied by the user or generated directly from the software package. The relevant features of these codes:

Shapelets: The Shapelets code (Massey et al 2004) aims at producing the most realistic galaxy morphologies, by decomposing the objects detected in the Hubble Deep Field into their shapelet parameterizations and then resampling the shapelet coefficients to build up realistic simulated galaxies. The Shapelets code is in the IDL framework.

ARTDATA: ARTDATA is part of the IRAF astronomical image processing package, and has been robustly tested by the astronomical community. It can generate stellar images using moffat or gaussian profiles; in addition, user-supplied profiles or images can be used to generate stellar images. Galaxy images are simulated using either de Vaucouleurs or exponential disk profiles; as with stellar images, user-supplied profiles or images can also be used to generate galaxy images. ARTDATA does not generate diffraction spikes, saturated objects, or bleeding along columns, although cosmic rays can be simulated.

Skymaker: The Terapix Skymaker package generates the most realistic instrumental effects. Skymaker includes the effects of tracking errors, atmospheric seeing, diffraction spikes, and low-order aberrations into its PSFs. Skymaker can also simulate saturation and charge bleeding along columns. Galaxies are modeled using de Vaucouleurs profile bulges and exponential disks. Skymaker is written in standard C, and the source code is available for modification. Skymaker unfortunately has little documentation, but descriptions of it can be found in Erben et al. (2001) and Blaizot et al. (2003).

simSurvey: The SDSS simSurvey package was written to generate simulated data to test the SDSS imaging pipelines. Stars and other point sources (like asteroids) are simulated by delta functions which are then convolved with instrumental and atmospheric PSFs. Galaxies are simulated using de Vaucouleurs bulges and exponential disks. Power law wings can be added to the image profiles. It is written in the SDSS ASTROTOOLS/DERVISH software environment, which is based upon ANSI C and Tcl/Tk. As a Fermilab in-house product, it would be easy to modify, though major modifications may be required to use simSurvey for the Dark Energy Survey simulations.

We will likely select the best components of each package. For example, Steve Kent's

program cray will generate PSFs from the DECam optical model, be fed through Skymaker code to modify the PSF for a variety of instrumental and atmospheric effects, and sent on to the Shapelets code to generate the galaxies and stars. Our aim is not to produce another simulation package, but rather to generate useful simulation data sets.

4.4.3 Image Simulation Production

We are discussing a very large simulation, requiring much computation and storage to create. We will take advantage of the GRID3 architecture that Fermilab and the US DOE/NSF grid community is creating. This features a shared security architecture that allows virtual organizations, say the Dark Energy Survey Simulation Team, to access all of the computing and storage of a distributed grid of compute clusters.

We will use a workflow management system, Chimera, that allows us to both manage the production side of running the jobs on the compute farms and to track the provenance of the data we create. We will use the Storage Resource Management (SRM) tools to shepherd the data during the simulation construction and during the transfer of the data to NCSA for data reduction. The aim here is to use the standards of the Virtual Data Toolkit, including Globus, as a means of leveraging the large amounts of work the core experiments of the Grid Physics Network (GriPhyN), the International Virtual Data Grid Laboratory (iVDGL), and the Particle Physics Data Grid (PPDG) (CMS, LIGO, SDSS, ATLAS, and others) have contributed. This is a data intensive science application and we propose joining the Grid3/Open Science Grid effort.

4.5 The Mock Data Reduction Challenge (WBS 1.3.4)

A mock data challenge is a tool for testing the accuracy and robustness of a data management system. This project component (WBS 1.3.4) is led by Chris Stoughton and will produce the mock data needed for these challenges, coordinate with the data management team (WBS 2.6) to carry out the reduction of these data, and then analyze the results. The results provide feedback that the data management team will use to improve the system.

Three milestones drive the development of the mock data and the pace of the data processing system development. All of the data produced at the milestones will be processed through the data production system as it exists at the milestone.

The three milestones:

- One tile: multiple exposures in four filters to completely cover one tile at a time. This exercises data formats that define the detectors in the focal plane, readout system, telescope, image data and log files. At this first milestone, values for these configurations, as well as the read noise and sky level, are in place. The goal is to provide baseline versions of all of these files and sample data to baseline code development.
- One night: several complete tilings, and some incomplete tilings. This tests the functionality of the databases to associate objects within single tiles and in areas overlapped by more than one tile. For completed tiles, run processing to produce the complete catalog. Exercise algorithms to plan future observing, especially in light of bad or incomplete data. Measure performance of all systems to scale to full system.
- One month: a full stress test of the data systems demonstrates that we can process data at the rate they are collected, and provide realistic benchmarks for data access methods for catalogs and files.

4.6 The Mock Data Analysis Challenge (WBS 1.3.5)

Once catalogs are produced, the science must be extracted. Surveys allow a broad range of science to be done, but here we focus on the 4 key projects of the Dark Energy Survey. We can test the analysis pipelines using the simulations and the results of the mock data reduction challenge. We will test the analysis pipelines on a years worth of simulated data before the survey begins. This is a commissioning task, to be done in 2007-2008.

The 4 key projects are:(1) The evolution of the population of clusters of galaxies out to $z > 1$ (2) Weak lensing power spectra and cross-correlation cosmography (3) Galaxy angular power spectra (4) Supernovae out to $z=0.8$. All four projects depend on the existence of good photometric redshifts. At the heart of photometric redshifts there are two generic techniques. The first is polynomial fitting of observed colors to redshifts. The second uses templates to predict the observed colors. Both are being explored. The cluster counting projects and weak lensing projects both require optimal shape measurement codes and shear analysis packages. The cluster counting projects, the weak lensing projects, and the galaxy angular power spectra projects all require angular power spectra measurement techniques, often based on fast correlation function calculations. There are analysis packages specific to the individual key projects. For example, in optical cluster finding there are two generic techniques to find optical clusters, using the E/S0 ridgeline of red galaxies to locate clusters or to use a matched spatial/luminosity filter on photometric redshift shells. There is also the problem of computing the selection function, which occurs both using the simulations and by putting fake galaxies into the data stream and reanalyzing the data.

The whole collaboration is tasked with developing the analysis codes under the lead of the data management group. What we outline here is the organizing of all of the packages to accept the catalogs from the data reduction and produce the cosmological constraints we are interested in.

4.7 Summary

We have described a reference design for the Dark Energy Survey Strategy that meets our survey science goals and requirements. The reference design represents our current thinking and choices for the survey strategy. Further analysis may show that better options are available. The design of the Dark Energy Survey Instrument will be discussed in Chapter 5.

References

- 1 Wester, W. (2004), DECam note, "Useful Observation Time at CTIO for the Dark Energy Camera Survey"
- 2 Randall, D. (2003) "Climate Modeling with Spherical Geodesic Grids", Computing in Science and Engineering
- 3 Wright, E.L. (1996), astro-ph/9612006
- 4 Tegmark, M. (1997), ApJ, 480, L87
- 5 Massey et al (2004), MNRAS 348, 214
- 6 Erben et al (2001), A&A 366, 717
- 7 Blaizot et al (2003), astro-ph/0309305

5. The Dark Energy Survey Instrument

5.1 The Reference Design

This section describes the essential elements of the Reference Design for the Dark Energy Survey Instrument. It includes the camera, cooling, wide-field optical system, the data acquisition system (DAQ), and the mechanical and electrical interfaces to the V. M. Blanco Telescope and its infrastructure. The Reference Design is not intended to be the final design, since we are still evaluating a number of technical choices. Nevertheless, it has allowed us to develop a reasonably complete enumeration of the tasks that must be executed in order to build the Dark Energy Survey Instrument. In Section 5.2, we describe the present configuration of the Blanco and in sections 5.3-5.17, we describe the choices we made in the Reference Design and the issues that we must resolve before proceeding to a final design. With the Reference Design in mind, we have developed a Reference Work Breakdown Structure (WBS) and identified the critical items that will require development before production can start. We have made a preliminary estimate of the schedule and the resources that will be needed for the construction of the instrument and its interfaces to the Blanco as well as the commissioning of the instrument in Cerro Tololo. This is provided in Chapter 6. These initial estimates suggest that we should be able to deliver a fully tested instrument with a fully integrated and tested DAQ to CTIO in Jan. 2008.

5.2 The Blanco Telescope

The Blanco is an equatorial mount telescope with a flip cage at the prime focus. A photograph of the Mayall telescope at Kitt Peak, which is a near twin of the Blanco, is shown in Figure 5.1 and a drawing of the layout of the optical components in the Blanco cage is shown in Figure 5.2. Together, they provide a perspective of the layout of components at the Blanco prime focus.

In the present configuration on the Blanco, the light from the primary mirror is focused onto Mosaic II, the existing wide-field imaging camera, when the cage is in the position shown in Figures 5.1 and 5.2. Mosaic II consists of eight $2k \times 4k$ CCDs. An optical system corrects the field of view over an angular diameter of 0.85 degrees. It consists of 4 lenses and an atmospheric dispersion corrector. The optical system, filters, camera and the $f/8$ secondary mirror are all mounted on the cage that is attached by the spider to a ring. When the cage is flipped through an angle of 180 degrees into the other position, the $f/8$ secondary mirror reflects the primary beam on to the Cassegrain focus. The prime focus plate scale at the Blanco is $55 \mu\text{m}/\text{arcsec}$ (1 meter/5 degrees). Table 5.1 provides a further enumeration of some of the essential parameters of the Blanco telescope.

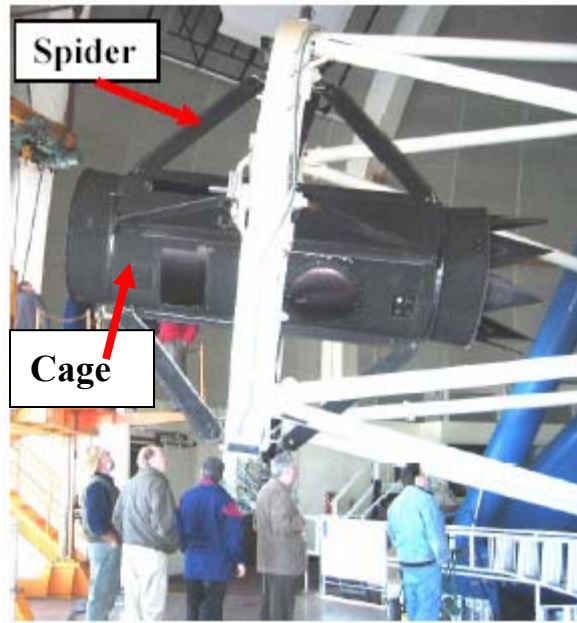


Figure 5.1 Side view of the cage on the Mayall telescope. The Mosaic camera and corrector are mounted inside the cage. The spider attaches the barrel to a ring that is in turn attached to the main truss (white) of the telescope. The ring can flip the orientation of the cage such that the other end points toward the primary.

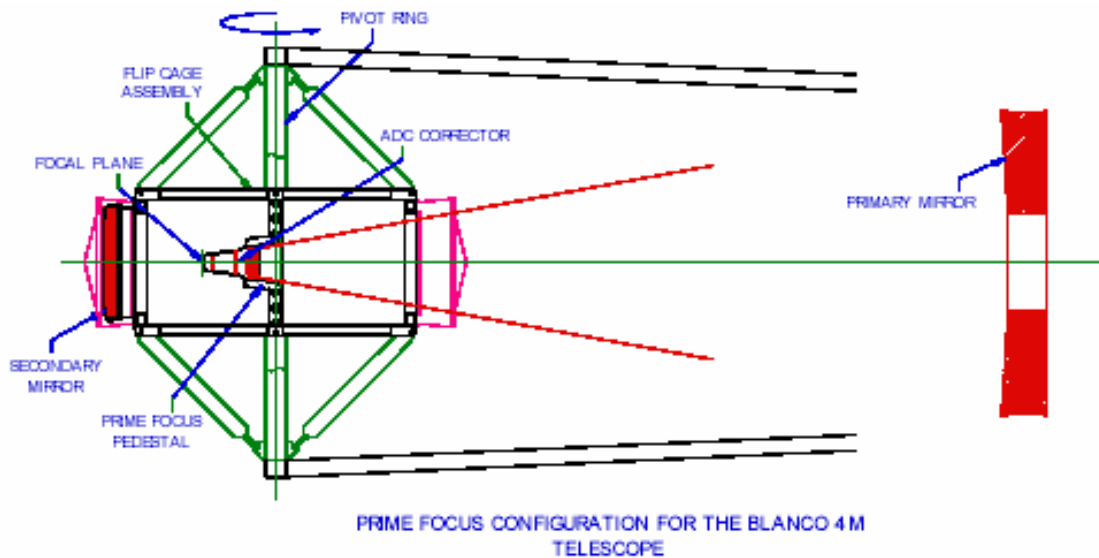


Figure 5.2 The cage and optical components of the Blanco 4m telescope. The corrector lenses are contained in a barrel, which is supported by a pedestal bolted to the centerpiece of the cage. The secondary mirror is located on the far left.

Table 5.1 Parameters of the Blanco Telescope and Facilities at the Site

Blanco location	Lat. 30° 10' S, Long. 70° 49' W Altitude 2200 m (7200 ft)
Primary Mirror	4m dia., 50cm thick, 15 ton
Telescope Mount	Equatorial
Prime Focus	f/2.87
Plate scale	55 $\mu\text{m}/\text{arcsec}$
Typical V-Band seeing FWHM	0.8 to 1.1 arcsec
Outside Temp. Range	-10 to +25 deg. C
Slew time	35 sec. for 1 or 2 deg. slews
Guider Update Rate	2 sec.
Adj. Range needed for focus	~2 cm
N2 plant on mountain top	9 lts/hr capacity, 50,000 lts annual consumption Cost ~ \$1/lit
Power	120V, 60hz in dome and cage

We propose to replace the cage and everything inside it except for the atmospheric dispersion corrector which is not needed for our survey due to the proposed short exposure times and because the Dark Energy Survey does not propose to observe at airmass greater than 1.5. We also propose to replace the mechanical, electrical, and communication interfaces between the cage and telescope. This project incorporates handling of the f/8 secondary mirror in order to avoid compromising other functionality of the telescope. To provide room for the camera vessel and services, we may need to remove the f/8 secondary mirror from the cage. In this case we will develop a repeatable precision mounting system that will allow the mirror to be reinstalled during the day to the required alignment tolerances and with minimal risk to the f/8 secondary.

The Mosaic II has two guide cameras in addition to the eight image CCDs. The guide cameras provide small corrections for the telescope tracking system so that a star image will stay in precisely the same location during an exposure. In our Reference Design we have CCDs on the focal plane devoted to guiding, along with additional CCDs devoted to a new semi-automatic focusing system.

5.3 Technical Specifications

Our science program was presented in Chapter 2 and Chapter 3 showed how those science goals translated into technical specifications. Chapter 4 outlined how the survey would be performed with an instrument that met the technical requirements of Chapter 3. A brief summary of the science goals and technical specifications is given below:

Science Requirement: Cover 5000 sq-degrees in the South Galactic Cap in 5 years (≤ 550 nights)

Technical requirement: 3 sq-degree camera (2.2 deg FOV)

Science Requirement: Measure galaxy cluster photometric redshifts to $z=1.0$ and $0.5L^*$ with $\delta z \leq 0.02$

Technical requirements:

- a. SDSS g, r, i, z filters covering 400nm to 1100nm
- b. Limiting magnitudes $g=22.8$, $r=23.4$, $i=24.0$ $z=23.6$
- c. QE > 50% in the z band
- d. Photometric calibration to 2%, enhanced goal to 1%
- e. Read noise <10 e-

Science Requirement: A small and stable PSF

- a. Seeing < 1.1" FWHM with median ≤ 0.9 " FWHM
- b. PSF stable to 0.1% over a 1 sq-cm (9 sq-arcmin) area

Technical requirement:

- a. Pixel size and optical plate scale which give <0.3"/pixel
- c. Optical, mechanical and telescope tracking which contribute < 0.4" FWHM across focal plane in the i and z bands
- d. Focus chip area > 17 sq-arcminutes
- e. Guide chip area > 25-50 sq-arcminutes, 1 Hz readout rate

5.4 Overview of Dark Energy Survey Instrument Project

5.4.1 Introduction

As mentioned earlier, we plan to replace the prime focus cage and everything inside it. Figure 5.3 shows a solid model of the Reference Design of the new cage, corrector and camera. The camera vacuum vessel contains the CCD focal plane, the liquid nitrogen cooling system, and all power and signal feedthroughs. Cables will be routed to two crates containing the front end electronics. In our current design, all the cryogenic and cable connections are made through the sides of the cryostat. This facilitates the camera assembly process and does not interfere with the existing f/8 secondary mirror mounting system. If it is necessary to provide more space for the camera and associated services, we propose to remove the f/8 secondary mirror from the back of the cage and make a repeatable mount system for it on the front of the cage. Further design of the electronics, the camera vessel, and the layout in the cage will show if this is necessary.

The optical configuration consists of five active lens elements and four interchangeable filters. The corrector components are shown in Fig. 5.3 along with a filter storage and changing system. The filters are stored outside the optical path, but within the corrector support barrel. The camera vessel is aligned to and supported by the corrector barrel. A shutter is located directly in front of the camera window.

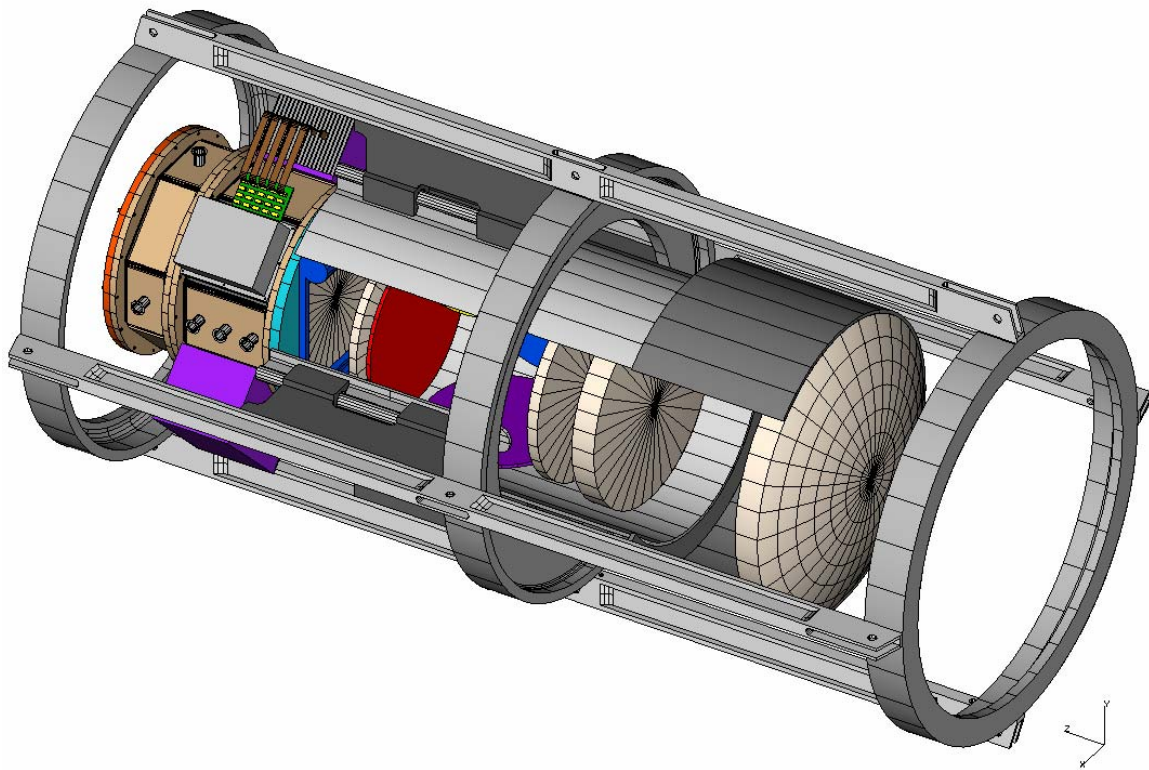


Figure 5.3 Proposed layout of the prime focus cage with the 2.1 degree corrector (lenses are white), filters (red is in the optical path, blue and yellow are shown in their storage locations), shutter (blue), camera vessel (grey) and 2 crates (purple) for data acquisition electronics (may not be needed).

5.4.2 Organization (Level 2)

The Dark Energy Survey Instrument Project has been divided into seven distinct Level 2 subprojects. Figure 5.4 shows the organizational structure of the project at Level 2.

Instrument Management, WBS 1.1, is where all the management costs associated with the instrument project are accumulated, including the Management Committee costs relevant to the instrument. This also covers costs associated with the preparation of schedule and costs, management and specification of technical requirements, active tracking of progress of the project (periodic reports) and reviews. WBS 1.2, Instrument Construction, covers the design and construction of the camera, cage, corrector and all associated equipment. Most of the remainder of this chapter is devoted to describing this element and what we call our Reference Design for the instrument. Survey Strategy, WBS 1.3, covers the strategy for collection of the images and was described in detail in Chapter 4.

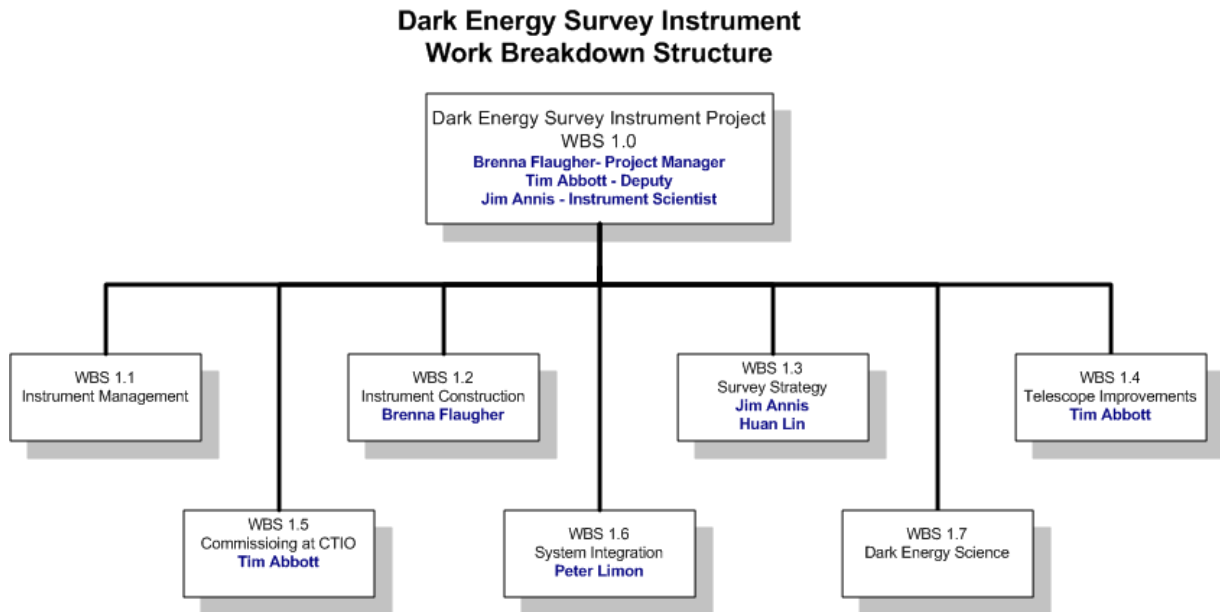


Figure 5.4 Work Breakdown Structure of the Dark Energy Survey Instrument Project

Telescope Improvements, WBS 1.4, and Commissioning at CTIO, WBS 1.5, represent activities at the Blanco site and are presented near the end of this Chapter. System Integration, WBS 1.6, covers development and implementation of interface control documentation for Level 2 systems 1.2 - 1.5 and the Level 3 subsystems within them. This also covers review of the testing plans to make sure they are consistent with specifications. Dark Energy Science, WBS 1.7, covers the support needed for doing science and writing papers with the data.

5.4.3 Organization for WBS 1.2, Dark Energy Survey Instrument Construction

The Instrument construction project, WBS 1.2, is divided into eleven Level 3 sub-projects. These are:

- 1.2.1 CCD procurement
- 1.2.2 CCD packaging
- 1.2.3 Front end electronics
- 1.2.4 CCD testing and grading
- 1.2.5 Data acquisition
- 1.2.6 Focal plane, camera vessel
- 1.2.7 Cooling
- 1.2.8 Optics (corrector and filters)
- 1.2.9 Prime focus cage and integration with all cryogenic, electrical, and mechanical systems
- 1.2.10 Auxiliary components
- 1.2.11 Assembly and testing

The corresponding organization chart is shown in Figure 5.5. The next sections describe these subprojects and the choices we have made for the Reference Design.

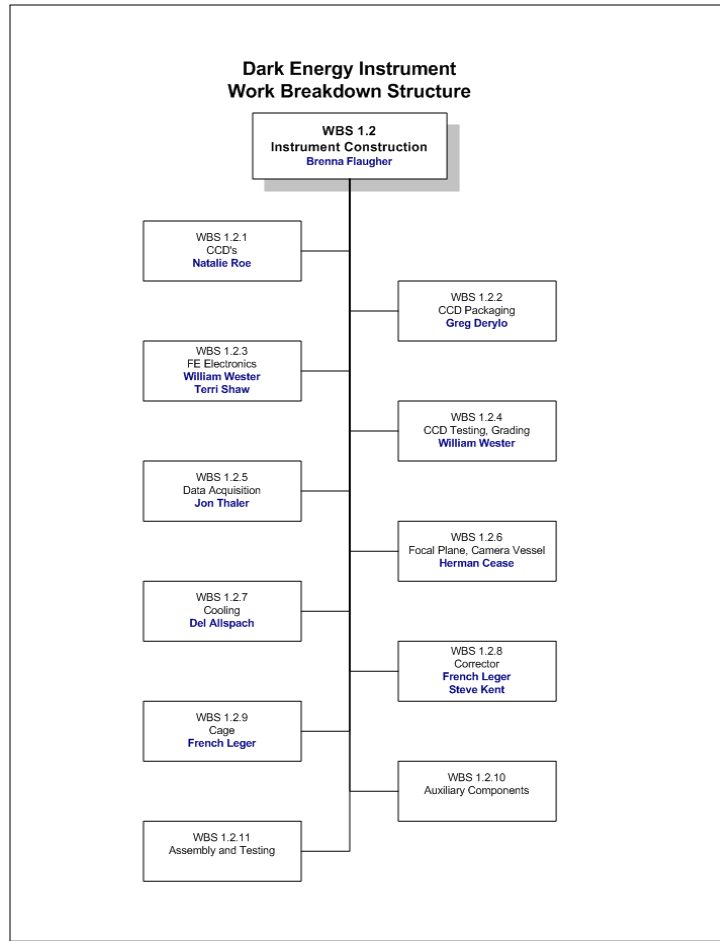


Figure 5.5. Organization of the Dark Energy Instrument Construction Project

5.5 CCDs Properties and CCD Procurement Plans (WBS 1.2.1)

5.5.1 CCD Technical Specifications

Our survey goals require that we have high quantum efficiency (QE) at the near infrared wavelength of ~ 1000 nm. The standard astronomical CCDs typically have a QE at this wavelength of 5-10% because the charge collection region is 10-20 μm thick and the total device thickness is often less than 50 μm . The absorption length in silicon is 205 μm at a wavelength of 1000 nm and thus thick sensors are required for a better QE at that wavelength. Photons at near infrared wavelengths will simply pass through 50 μm of silicon. LBNL has already developed thick, fully depleted, back illuminated CCDs 200-300 μm thick¹. For our Reference Design we use 250 μm thick LBNL CCDs. The QE of the LBNL CCDs is shown in Figure 5.6 and compared to a standard thinned astronomical CCD and a deep-depleted CCD².

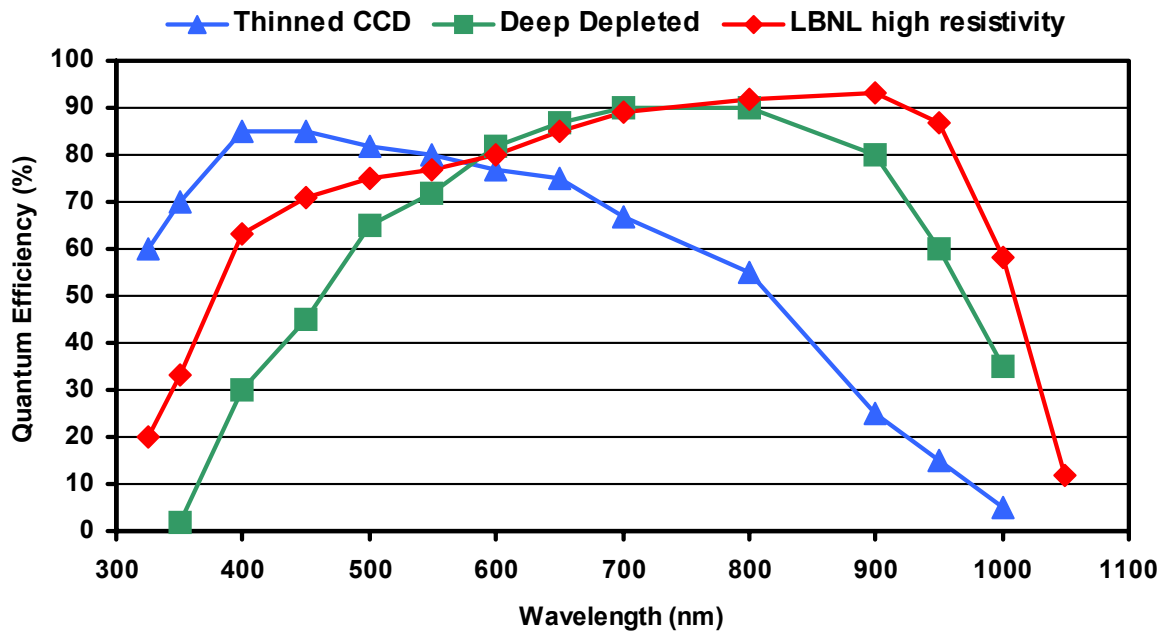


Figure 5.6. QE curves from different types of CCDs.

LBNL has produced a variety of CCDs for different projects and several devices have already been deployed for astronomical use. Figure 5.7 shows a 6" diameter wafer with LBNL CCDs. For our Reference Design we choose the 4-side buttable 2048 × 4096 CCD. These are the two largest devices shown on the wafer. The development of this CCD is complete. This CCD has 15 μm pixels, 2 readout channels and meets all of our specifications as shown in Table 5.2. These devices have been clocked at 250 kpixel/s with a readout noise of 7 e⁻ and 4 e⁻ at a rate of 100 kpixel/s. At this rate the readout will take 17.5 sec which is well within the 35sec slew time of the Blanco.

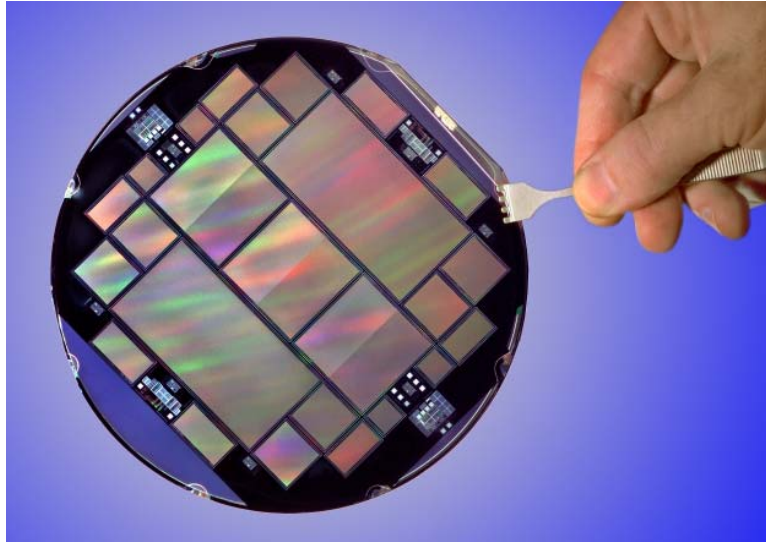


Figure 5.7. LBNL CCDs on a 6” wafer

Although we have not ruled out using commercially available CCDs, the approach in our reference design is to assume we will use the LBNL fully depleted, thick CCDs. We believe this maximizes the science possible with the instrument while minimizing the R&D needed for this project by using CCD designs that have already been proven. As discussed in Chapter 3, deep depleted CCDs are commercially available, but their QE in the near-infrared region is about half that of the thick fully depleted LBNL CCDs. They could be used for our survey, but the completeness of our galaxy redshift catalogue would suffer.

Figure 5.8 shows our Reference Design for the focal plane layout with the $2k \times 4k$ 4-side buttable LBNL CCDs. It contains 62 CCDs and a total tile active area of 3.0 deg^2 . This satisfies the requirements described in Chapter 3 for the camera size.

Table 5.2. CCD Specifications

	LBNL CCD performance	DECam requirements/ Reference Design
Pixel array	2048×4096 pixels	2048×4096 pixels
Pixel size	$15 \mu\text{m} \times 15 \mu\text{m}$	$15 \mu\text{m} \times 15 \mu\text{m}$ (nominal)
<QE (400-700 nm)>	~70%	>60%
<QE (700-900 nm)>	~90%	>80%
<QE (900-1000 nm)>	~60%	>50% at 1000 nm
Full well capacity	$170,000 e^-$	$>130,000 e^-$
Dark current	$2 e^-/\text{hr}/\text{pixel}$ at -150°C	$<\sim 25 e^-/\text{hr}/\text{pixel}$
Persistence	Erase mechanism	Erase mechanism
Read noise	$7 e^-$ @ 250 kpixel/s	$< 10 e^-$
Charge Transfer Inefficiency	$< 10^{-6}$	$< 10^{-5}$
Charge diffusion	$8 \mu\text{m}$	$< 10 \mu\text{m}$
Linearity	Better than 1%	1%

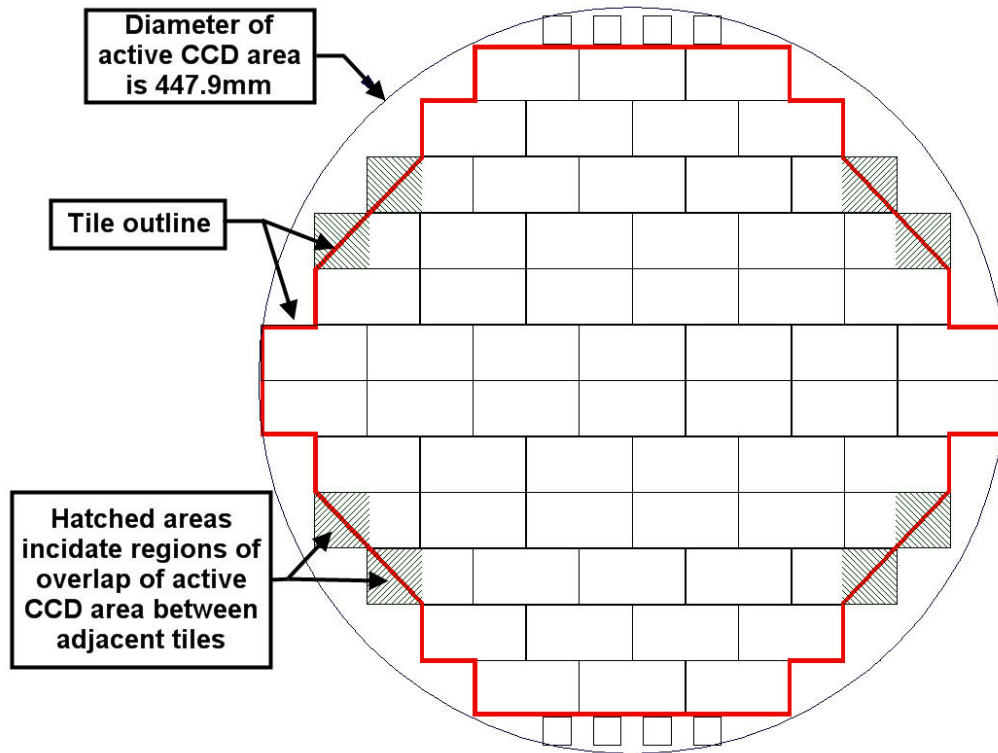


Figure 5.8. Focal plane layout using 62 $2k \times 4k$ LBNL CCDs and 8 additional small CCDs for guiding and focus. The dark (red) line shows the outline of the tile area.

5.5.2 Guide and Focus CCDs

LBNL has developed a variety of small CCDs. For our Reference Design we have selected a 982×935 pixel device with $15 \mu\text{m}$ pixels. These are shown along the top and bottom of the focal plane layout in Figure 5.8. At the nominal rate of 250 kpixel/s these can read out in 2 sec. For guiding however, we expect to be able to tolerate higher noise and will operate at a higher readout rate. Once the guide stars are identified, it is also typical to read out only a small number of the surrounding pixels, further reducing the readout time.

For focus our Reference Design has two sets of these chips installed $\sim 200 \mu\text{m}$ above and below the mosaic focal plane. As the telescope drifts out of focus for the image CCDs, the focus in one or the other set of chips will get better. The focus chips will be read out with the image CCDs. The focus is thus monitored with every image and can be adjusted as necessary.

These CCDs can easily be incorporated into the new mask needed for the $2k \times 4k$ devices by using the leftover space on the 6" wafer.

5.5.3 CCD Acquisition Plan

LBNL has produced and packaged the $2k \times 4k$ devices we have chosen in small quantities⁴ and these devices are in use in telescopes at UCO/Lick Mount Hamilton and Kitt Peak National Observatory with great success. A production model for CCD fabrication has been established in which the silicon wafers are manufactured by a commercial vendor and delivered to LBNL for final processing. The steps performed by LBNL include thinning to $250 \mu\text{m}$ from the $650 \mu\text{m}$ thick wafers supplied by the vendor, application of the backside

layers and antireflective coatings, and finally etching and application of the Al for the front-side electrodes and bond pads. Through discussions with our collaborators at LBNL we have developed a conservative CCD procurement and delivery cost and schedule. In our model, LBNL oversees the production process at the foundry, receives the wafers, performs the final processing and tests the wafers on a cold probe station. These tests are performed at $-40\text{ }^{\circ}\text{C}$ and test for shorts, opens, broken readout amplifiers and warm or hot columns. LBNL is responsible for dicing the wafers into the individual devices and shipping all the unpackaged devices to Fermilab along with the testing results. Fermilab will perform the packaging and subsequent testing.

We have avoided extensive development on the CCDs by basing our plans on the existing $2\text{k} \times 4\text{k}$ design. However, the CCDs have a lead time of approximately 10 months for delivery of processed, unpackaged CCDs and the yield is as yet unknown. At the time of writing, experience is limited to a few devices; out of a total of 10 devices which were packaged in a picture frame but not thinned or backside coated, 6 have been determined to be good quality. For our purposes we will assume a yield of 25% and develop a CCD acquisition plan based on this number. In the plan outlined below we determine the yield before committing to the majority of the CCD processing costs and thus significant cost and schedule saving will be possible if the yield is higher. Contingency plans have been developed to cover the additional cost and schedule issues if the yield is lower than 25% and this is discussed in Chapter 6.

Discussion with LBNL and our experience with the construction of silicon vertex detectors leads us to believe that it will require a dedicated effort to develop CCD packaging skills and techniques at Fermilab and to develop an efficient CCD packaging production line. We will begin this process as soon as possible to reduce the possible risks later in the project.

Our CCD acquisition strategy proceeds in 4 phases:

- Phase A: Sept. 04, order mechanical parts for packaging studies, and 4 unpackaged engineering grade electrically functional CCDs, ~ 3 month delivery time
- Phase B: Sept. 04 design new mask with four instead of two $2\text{k} \times 4\text{k}$ CCDs/wafer, plus as many $1\text{k} \times 1\text{k}$ devices that fit. Order preproduction parts and process ~ 2 wafers, est. 10 month delivery = July 2005
- Phase C: Aug. 05, process the remaining wafers, ~ 3 month delivery, establish yield
- Phase D: Aug. 05, place production order, ~ 8 month delivery

Phase A is the purchase of a large number of mechanical CCDs (blank silicon with the top layer of metal for wirebonding studies), as well as four unpackaged devices. These will be used to develop our packaging techniques, tooling and procedures, assess adhesives, and study thermal behavior and mechanical warping during cooling down.

The initiation of Phase B (preproduction) is on the critical path for the project and is a key step towards reducing both cost and schedule risk. In Phase B we ask LBNL to generate the preproduction masks for our project and place an initial minimum order for 24 wafers. The existing masks for the $2\text{k} \times 4\text{k}$ CCDs have only two of these devices per wafer. The new mask would use the same, proven, $2\text{k} \times 4\text{k}$ CCD design and would have four devices per wafer as well as $1\text{k} \times 1\text{k}$ devices that fit in the empty spaces. The delivery schedule is ~ 10 months after the masks have been approved by the foundry. These 10 months consists of 7

months at the foundry and 3 months for processing at LBNL. On receipt of the wafers at LBNL (~May 2005) only ~2 wafers will be processed for use in our initial CCD acceptance and packaging studies. The remainder of the wafers will be set aside for phase C. Delivery of phase B CCDs to Fermilab is anticipated in August 2005. These will be packaged, evaluated and tested with the goal of proceeding with Phase C and the production order (Phase D) before the end of August 2005.

In Phase C, we will authorize LBNL to process the wafers that were set aside in Phase B. Based on LBNL experience we assume that out of the initial 24 wafers, 2 will be lost due to breakage and 2 more will be used by the foundry for processing tests. Phase B processing used 2 wafers, leaving 18 wafers for processing in phase C. The wafers would already be at LBNL and thus delivery of these devices would begin 3 months ARO. LBNL is estimating that they can process and test 5 wafers/month, thus delivering 20 tested devices/month to Fermilab. This represents roughly one quarter of the processing capacity of the LBNL Micron Systems Lab. These CCDs would start to arrive at FNAL in ~November 2005 and finish in February 2006. They would be used to start the ramp up to full production packaging and to determine the yield. The testing information provided by LBNL will be used to determine the order in which the CCDs are packaged. Initially in Phase C we will package the lower quality parts and reserve the high quality parts for after the packaging process is perfected. With these assumptions and 25% yield, we will have 54 low quality parts for packaging development and 18 high quality parts that could be used in the focal plane.

The final phase, D, is the production run of 3 lots of 24 wafers each. Unless significant problems were found from the preproduction run and analysis of the packaged Phase B parts, phase D would use the preproduction wafer mask. For our initial planning purposes we assume that 20 out of each 24 wafer/lot will be available to us for a total of 60 wafers. With the assumption of 25% yield we will need to process all 60 wafers. We thus anticipate delivery of 240 CCDs to Fermilab. The LBNL delivery rate will be 20 tested devices per month for a total delivery time of 12 months. As in Phase C, we will use the testing results provided by LBNL to determine the order in which CCDs will be packaged. The Phase D wafer order would be placed in August 2005 with the delivery of fully processed tested parts to Fermilab expected 8 months later (April 2006) continuing to April 2007.

Processing and packaging of the Phase C parts will indicate if our assumptions of the yield are correct. If the actual yield is higher than 25% we can reduce the total cost by limiting the number of Phase D wafers to be processed at LBNL. This would also accelerate the schedule. If the actual yield is less than 25% we have sufficient cost contingency to cover an additional 24 wafer lot order. This order would be placed after analysis of Phase C was completed (~March 2006).

One way to advance the schedule beyond what is presented above is to increase the Phase B order to 2 lots (48 wafers) and to proceed with continuous processing as soon as they arrive at LBNL. This could potentially gain 5-6 months in the schedule. The cost and risks associated with this approach will be discussed in Chapter 6.

5.6 CCD Packaging (WBS 1.2.2)

CCD sensors are packaged into modules that provide an electrical interface and mounting features. The CCD package consists of a sensor, a readout hybrid, and a mounting foot. Our Reference Design for the CCD package is based on the package developed at LBNL⁴. The readout hybrid is glued to the front (non-optical) surface of the sensor and has a pad layout designed to allow wirebonding connections to pads on the CCD that extend out beyond the edges of the hybrid, as shown in Figure 5.9. The board is also equipped with an electrical connector. A few small surface mount components, such as a temperature sensor, will be added very near the connector location. Aluminum nitride ceramic is to be used for the hybrid substrate since its thermal expansion characteristics are similar to that of silicon.

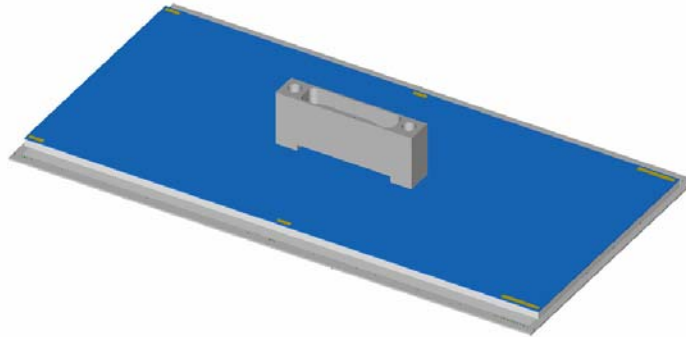


Figure 5.9. A readout hybrid board packaged with a 2k × 4k CCD

A mounting foot is also glued to this assembly, as shown in Figure 5.10, in order to provide structural support and precision mounting engagement to the focal plane support plate. It is constructed of Invar to provide a stiff, thermally-stable framework for the module. A clearance hole permits access to the connector on the hybrid. Mounting pins engage locating holes in the focal plane support plate and set the module position. One pin is designed with a diamond-shaped cross-section to permit ease of installation for small variations in machining tolerances. Pin lengths are longer than the overall thickness of the foot / readout hybrid / sensor package in order to guide the module accurately past its neighbors during installation. Threaded holes in the foot permit attachment with screws from the back side of the focal plane support plate. The pin and threaded hole volume are vented in order to eliminate trapped volumes that can act as virtual leaks inside the evacuated camera environment.

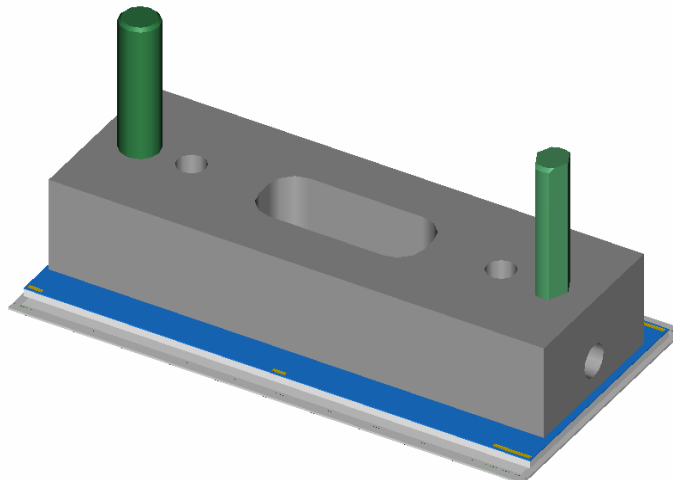


Figure 5.10. A fully packaged 2k x 4k CCD module

CCDs are typically operated at temperatures of -90 to -120 °C, however, they must be glued to the support and readout hybrid at approximately room temperature. This wide temperature difference requires careful consideration of the thermal expansion properties of all the materials involved, as flatness of the focal plane is important for the camera to achieve a good focus. As described in Reference 4, LBNL has demonstrated packaging of $2k \times 4k$ CCDs.

For construction of our camera, we need to develop packaging techniques and establish a production model at Fermilab that can handle a large number of CCDs. The Silicon Detector Facility at Fermilab already has significant expertise in bonding and gluing ceramic parts to silicon sensors as a result of the construction of the numerous silicon vertex detectors for the Fermilab Tevatron collider program. We believe that CCD packaging will be a natural extension of that experience.

Each CCD module will be constructed in several steps. The first is to assemble the components and connector onto the readout hybrid. Second, the readout hybrid is epoxied to the front (non-optical) surface of the CCD sensor. Fixturing that holds the parts with vacuum is used to control the flatness and relative positioning of the two pieces based on their physical edges. Spacers that are part of this tooling set the thickness of the epoxy joint. After curing, the electrical connections between the readout hybrid and the CCD are wirebonded. A test is then performed to verify the basic functionality of the module. Fixturing is then used to attach the foot assembly to the readout hybrid with an epoxy joint. This tooling is used to precisely control the overall package height in order to maintain uniformity of the focal plane planarity. It also accurately locates the foot mounting pins relative to the physical edges of the CCD sensor in order to ensure that the edges of the assembled module do not violate the clearance gap between adjacent modules. After epoxy curing, the CCD package is complete. Due to the height of the foot assembly, wirebonding repair is not possible on a completed package.

During production, a delivery rate of 20 CCDs per month translates into an average throughput of one module per day. The assembly steps discussed above are each anticipated to require only a few hours of technician time, but they typically require a one-day curing time for the epoxy to reach satisfactory handling strength. Therefore, it is possible to construct modules with a one-per-day throughput with a single set of fixtures. However, two sets will be needed to ensure that this average capacity could be sustained over an extended period.

5.6.1 Guide and Focus CCDs

As discussed in Chapter 3, an area of ~ 40 sq. arcmin would typically have \sim three bright stars which are useable for guiding and/or focusing. LBNL has developed a variety of small CCD options. For our Reference Design we have selected a 982×935 device with $15 \mu\text{m}$ pixels. Each CCD covers 18.6 sq. arcmin and has two readout channels. Four of these CCDs would be used for each of the focusing and guide systems.

The packaging of these units is anticipated to be similar to the $2k \times 4k$ CCD modules, with its own aluminum-nitride readout hybrid board and mounting foot design. These devices will not be 4-side buttable as the connector covers a significant fraction of the CCD itself. Both thicker and thinner mounting feet will be fabricated for the focus CCDs. With adjustable assembly fixturing these modules can then be constructed with the desired total heights.

5.7 Front-end Electronics (WBS 1.2.3)

The front-end (FE) electronics provides the interface between the CCD sensors and the Monsoon data acquisition system (DAQ) (WBS 1.2.5). Figure 5.11 shows a block diagram of the reference design for the FE electronics. The proposed scheme provides for electrically isolated optical signal transmission between the FE electronics attached to the camera cryostat and the DAQ system located off the telescope. Within the cryostat, the FE electronics will include the design of the circuitry on the aluminum nitride (AlN) hybrid used to back each CCD sensor. A flex cable circuit will connect the hybrid to a printed circuit board that also forms the vacuum seal (vacuum seal board). The flex cable will carry active components that switch clock lines and that preamplify the CCD analog outputs.

The vacuum seal board will receive flex cables from each device and route signals from inside to outside of the vacuum. Cables will provide connection to modules that reside in compact-PCI crates attached to the cryostat. These modules will function to provide the correlated double sampling of the analog signals, analog to digital conversion, distribution of clock signals and control lines, and power distribution. The temperature of the FE electronics will be controlled so that thermal air currents from the electronics will not impact the seeing. The compact-PCI crate will also provide the optical drivers to send signals to the Monsoon DAQ that is located off of the telescope.

An alternative implementation would be to locate the full Monsoon DAQ crates on the cryostat and interface directly with the vacuum seal board. In this implementation, Monsoon detector head electronics (DHE) modules process and digitize the analog signal. It is thought that this alternative implementation requires enclosed crates and more stringent thermal management than the current reference design. A decision between the alternatives will be made after experience is obtained operating LBNL CCDs and the Monsoon DAQ electronics.

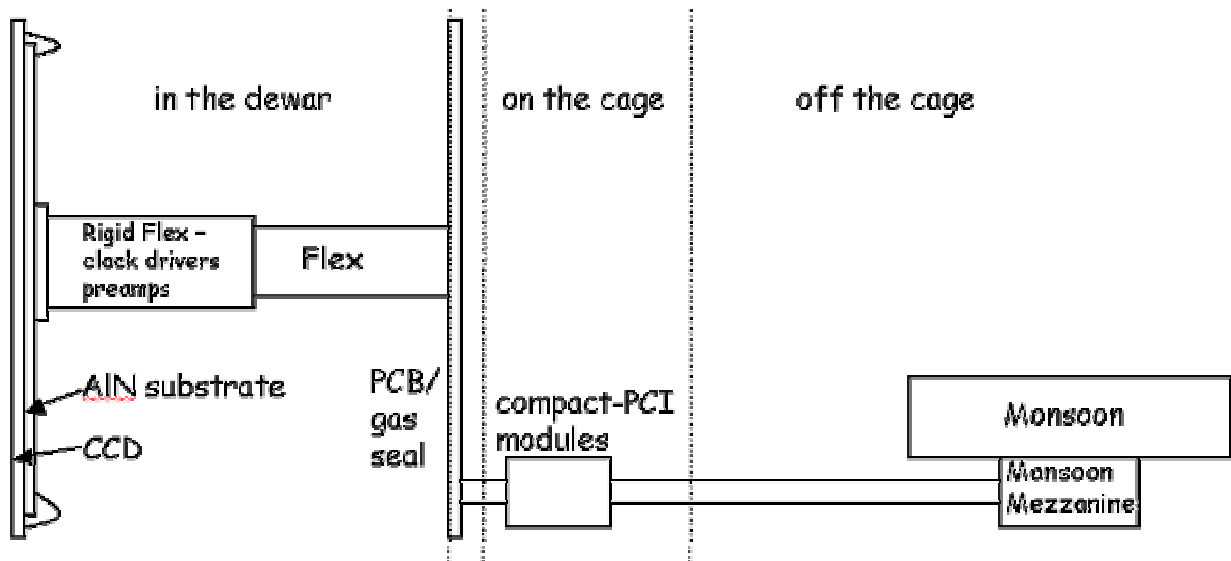


Figure 5.11. Schematic drawing of the FE electronics reference design.

5.7.1 Requirements for the Front-end Electronics

The requirements for the FE electronics are briefly described. For the Dark Energy Survey, the requirements are relatively loose compared with other CCD systems. The FE electronics must accommodate the characteristics of the LBNL CCDs. The output signal from the CCD has an expected level between 0-1V corresponding to the expected well depth of 170K electrons. The requirement on the FE electronics system noise is to be less than $5e^-$ so as not to dominate the noise from the CCD devices at 250 kpixel/s. The electronics system must maintain linearity over the dynamic range at a level of 0.25% so as not to dominate the total system linearity limit of $\sim 0.5\%$, which is required for precise photometry. The electronics needs to be compatible with a readout rate of 250 kpixel/s over the entire CCD array so that a focal plane image can be read out faster than 20 sec, less than the time required for slewing the telescope. These requirements have been achieved on other CCD systems. A key challenge for the FE electronics is to meet or exceed these requirements with such a large CCD focal plane array. The enhanced design goal of the front-end electronics is to exceed these rather loose requirements so that the instrument has the widest possible use.

5.7.2 Aluminum Nitride Hybrid

The aluminum nitride (AlN) hybrid functions to bring the required pads of the CCD device to a connector. The hybrid is part of the four-side buttable packaging effort (WBS 1.2.2) to manufacture CCD modules. We describe the aspects of this board that are relevant to the front-end electronics. Pads on the CCD sensor are connected to traces on the hybrid through wirebonds. In addition to traces, the hybrid will have a good reference ground plane that should benefit the LBNL CCDs. Other large-scale CCD systems have had performance compromised through the effect of “substrate bounce” that would be less likely to occur in the presence of a good ground plane. As for the electrical traces, the AlN circuit will route the various lines from the CCD device to the connector on the AlN board. Two trace layers are required in order to tie various clock lines together to minimize pin count. Each hybrid will have space for a temperature sensor to be mounted but only a fraction of the devices on the final focal plane will be required to have a temperature read out.

5.7.3 Flexible Cable

The flexible cable interfaces between the connector on the back of each CCD module’s AlN board and the vacuum seal printed circuit board. The design of the flexible cable will emphasize several features that are directed towards the requirements of the FE electronics. The flex cable will carry the reference ground in a separate conducting plane. Trace widths will be determined on the basis of proper impedance for signal propagation and for voltage levels including the bias. The cable will allow for passive components to perform necessary bypassing and filtering.

The reference design of the flex cable includes a section that will be stiffened to allow for the mounting of active components. We are especially concerned with driving the clock lines (with high switching currents) over a long cable. Putting solid-state switches on this stiffened section so that the clocks going to the device can be generated and driven locally mitigates this concern. Another concern is the low-noise transport of the analog output and the protection of the output transistor. Putting preamplifiers on the flexible cable would mitigate both of these concerns.

Any component mounted on the flexible cable will be considered for use in the cryogenic environment. Of particular concern is use of components at extreme temperatures. While a thermal model for the temperature on the cable hasn’t been performed, we have begun an

investigation as to the suitability of different components at extreme temperatures. In this investigation, we have found information used by the space community that lists known problem components as well as successes at low temperatures. We plan to limit parts inside the cryostat to those with well understood outgassing and hygroscopic properties, with the goal of avoiding the deposition of water or other foreign material on the CCDs.

Finally, we recognize that any electronics inside the cryostat must be robust against failure since it will be difficult to service the inside of the cryostat once the camera is commissioned. The Reference Design reflects the concerns that have been mentioned. Testing of individual and multiple devices will be done to determine the need for active components inside the cryostat. If these active components are not required for the FE electronics to meet the requirements, then the flexible cable will not carry them and other functions such as protection will move to the vacuum seal board.

5.7.4 Vacuum Seal Board

The vacuum seal board is a printed circuit board and provides connectors that accept the flexible cables inside the cryostat. As shown in Figure 5.12, the board is mounted into a metal frame by sliding through a slot in the frame on one edge. It is potted (glued) to the frame, and then vacuum-side connectors are assembled onto the board. The board's frame is then installed on a flange on the cryostat and covered with an o-ring sealed cap. The board thus has regions both inside and outside the cryostat and conducting traces on the board function as the feedthroughs of the cryostat wall, as shown in Figure 5.12. These traces will be appropriately multiplexed and will terminate into connectors that will be used to bring signals to electronics that sit in compact-PCI crates. The vacuum seal board will be designed based upon experience at Fermilab in the design of a similar board for the BTeV project.

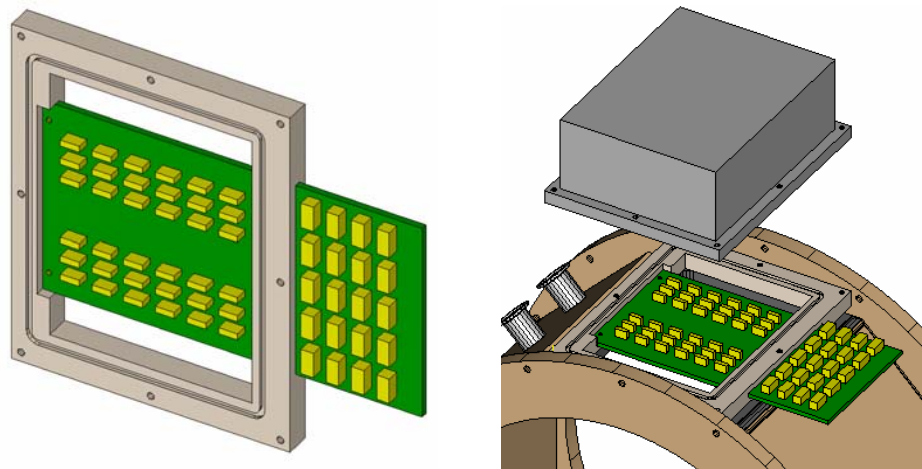


Figure 5.12 Electronics feed-through using the Vacuum Seal Board

5.7.5 Camera Vessel Crate Electronics

Cables from the vacuum seal board will carry signals to printed circuit boards that will reside in compact-PCI crates mounted on the cryostat. These crate electronics include boards that perform a variety of functions for the FE electronics. The analog signal lines from each CCD will undergo correlated double sampling (CDS) in order to reduce noise from the reset amplifier. In this sampling scheme, a charge sensitive amplifier will sense the analog line both during an integration window during which a signal may be present and during an

equivalent time window when no signal is present. An electrical subtraction removes correlated noise that is generated when the reset switch of the output transistor is turned on and off. The subtracted signal will then be converted to a 16-bit digital signal using a commercial low noise analog-to-digital converter (ADC) chip. The digitized data will be serialized and sent over a high-speed serial optical link to the interface to the Monsoon DAQ system. The control of the CDS and digitization and data formatting will be accomplished by suitably sized field programmable gate arrays (FPGAs). The data stream will include digitized levels from temperature sensors and other similar monitors.

Clock signals and control lines will also be distributed by the crate electronics. The generation of these signals (the sequencing) will be handled by the DAQ. The generated clock signals will be converted by the crate electronics into the logic levels that are sent into the cryostat to control the solid-state switches that generate the actual clocks that go to the CCDs.

The crate electronics will include circuitry that distributes all the required voltages for the CCDs. These voltages will be derived from a voltage source that is the output of an isolation transformer. The transformer will isolate a voltage source that comes up the telescope in order to separate the electronics in the cage from other electrical circuits that may be susceptible to undesired transients or subject to fluctuations due to nearby lightning strikes.

5.7.6 Interface to the Monsoon Data Acquisition

The interface to the Monsoon data acquisition consists of circuitry that makes all the signals compatible with the Monsoon system. In particular, this board will send and receive optical transmission to the FE electronics. This interface board is likely to be connected to the backplane of the Monsoon crates. This board is at the border between FE electronics and DAQ. Depending on the complexity of this board in its final design and whether the final implementation is chosen to have Monsoon crates on or off the telescope will determine whether this interface printed circuit board remains under FE electronics or whether it becomes a DAQ task.

5.8 CCD Testing and Grading (WBS 1.2.4)

Testing and grading CCD activities include an initial phase where CCDs are exercised and characterized and a production phase where these activities are used to classify the production devices to determine the best ones that should populate the focal plane. The initial phase is important to develop the infrastructure and experience so that the production phase may begin when production devices first become available. The production phase will be designed to test up to 20 devices per month, with some capacity to absorb bursts of higher delivery rates.

In the initial phase, a CCD test stand will be developed that incorporates the Monsoon data acquisition system. Various optical devices and test and measurement equipment for CCD characterization will be added and incorporated into the testing lab. As the test stand develops, it will also be used for evaluating FE electronic design options. After the testing program is developed, a production testing procedure will be documented and devices will be tested and graded with proper bookkeeping, travelers, and a database of test results. These results will form the basis of an initial calibration of each sensor.

The testing and grading task is required to make a comparison of the test results against the device requirements to insure that each CCD device that is installed meets the minimum requirements for use in the DES. The task is also required to assign a grade so that devices with the highest grades above the minimum requirements will be used.

5.8.1 Test Stand Overview

Figure 5.13 shows a block diagram of the test stand that will be commissioned. The various optical and DAQ components will be used to perform a sequence of measurements on the CCD device under test. The test stand provides a variety of measurement conditions. Dark images can be obtained by reading out the CCD when the shutter is closed. Uniform illuminated images can be obtained by reading out the CCD when the shutter is open and broadband light from the integrating sphere is shown on the device. A calibrated photo-diode will provide an absolute intensity measurement of the light. Exposure of the CCD to Fe^{55} also can be used for charge transfer efficiency measurements. The monochromator and filters can be used to select a narrow band of wavelength for illumination onto the device for quantum efficiency measurements.

For production testing, two additional test stands will be commissioned to increase the testing throughput. Ideally, all three test stands will be configured equally in order to benefit from test stand software development. After visual inspection, the production testing is estimated to take two full days per device. The device is first carefully loaded into the test cryostat and cooled down. The first day of testing will record image data under various conditions. On the second day, scans to measure the quantum efficiency will be made. Since the QE depends on temperature especially at the longer wavelengths, the QE vs temperature will be measured. Each device will be thermally cycled and checked to better insure robustness against thermal cycling. Finally, the device will be warmed up, removed from the test dewar, and testing data will be checked.

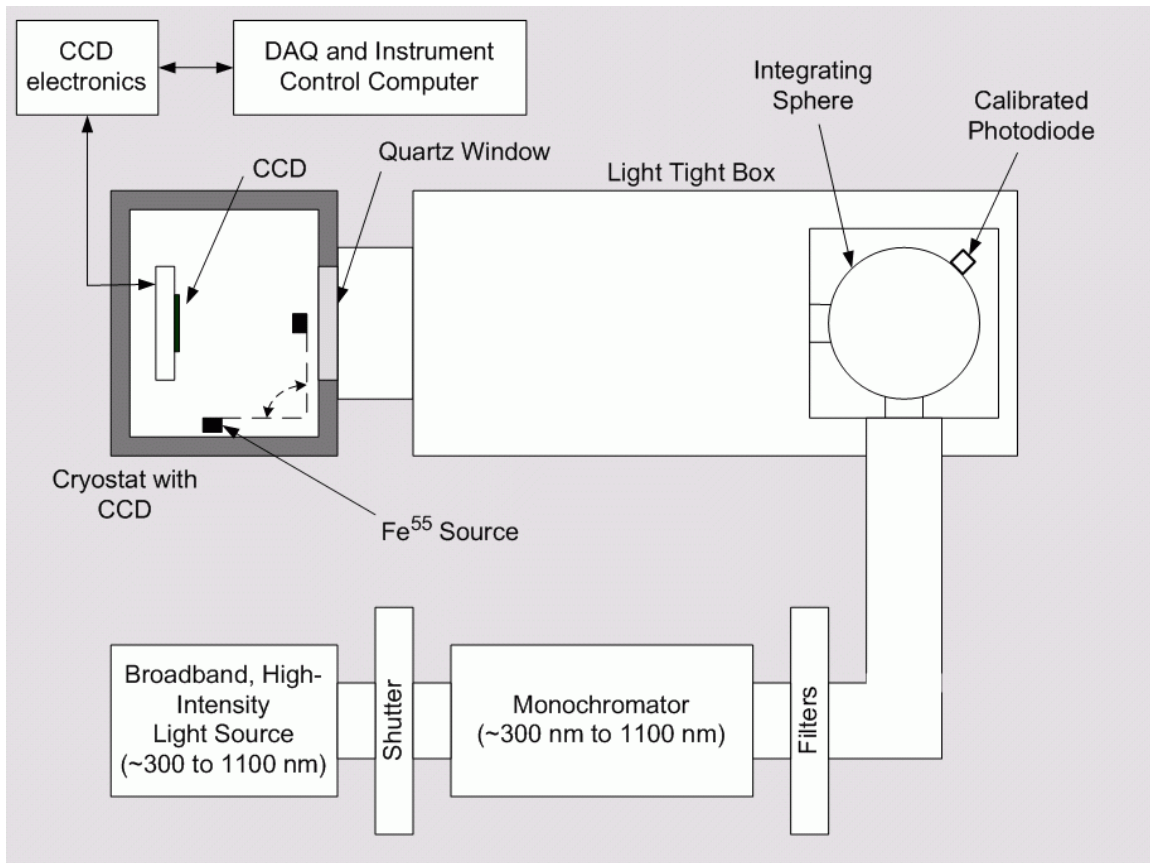


Figure 5.13 Diagram of the test stand.

5.8.2 Test Dewar

The test cryostat or dewar, seen in Fig. 5.14, is designed to cool down and warm up rapidly for fast turn-around of the CCD tests. This dewar is patterned off of a similar dewar in use at LBNL in the CCD evaluation lab. The dewar consists of a copper thermal shield in a vacuum box that is in contact with a boiler column cooled by liquid nitrogen. The level of liquid nitrogen in the boiler is self-regulating due to gas pressure built up in the vertical column. A fused silica window allows light on the CCD when a door is open.

Fast cooldown is initiated by opening an exhaust valve, allowing liquid nitrogen to directly cool a cold mass and the CCD bolted to it. After a few minutes, when the CCD is cold, the valve is shut, and the cold mass and CCD come to equilibrium at a temperature established by the balance between a thermally conducting foil connecting the cold mass to the boiler and the various heat sources. This foil is sized to establish the equilibrium temperature slightly below the desired operating point. A small electrical heater embedded in the cold mass maintains the test temperature.

Illumination enters the end of a light-tight cylinder that surrounds the window. There is also an Fe-55 X-ray source for independent calibration of the CCD. After the tests are complete, warm up is accomplished by evacuating the liquid nitrogen from the boiler and heating the shield and CCD with electrical heaters until they are safely above the dew point.

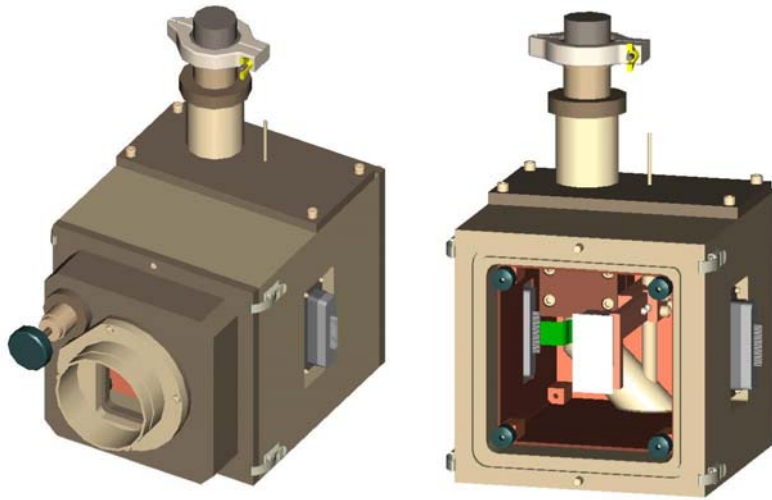


Figure 5.14 3D model of the test cryostat. A light tight cylinder surrounds a fused silica vacuum window (left). On the right, the front cover is removed to show the cold plate on which CCD devices can be mounted.

5.8.3 Testing Procedure

The exact testing procedure and acceptance criteria will be specified after experience is obtained using the test stand to operate and characterize LBNL CCDs. Listed below are a variety of tests that can be performed using the test stand described above. For the Dark Energy Survey, the strategy of recording multiple images over the survey area relaxes the need for perfect devices. A study has been performed that introduces approximately 100 consecutive bad columns randomly for each of 62 devices – thought to represent a worse case. The net result after five tilings is that only about 1.5% of the survey area is imaged less than three times, which is acceptable. The enhanced goal of the testing is to select devices that exceed the minimal CCD requirements. As a guide, we will strive to select devices that fall into the top grades defined by the number of bad columns assuming the devices are otherwise fully functional and that other defects affect fewer pixels than a column (4096). The grading scheme motivated by another large focal plane (Megacam) specified acceptable devices as:

- Science Grade 1: Fewer than 6 bad columns
- Science Grade 2: Fewer than 12 bad columns
- Science Grade 3: Fewer than 20 bad columns
- Engineering Grade: functional, non-science grade device
- Mechanical Grade: non-functional

Visual Inspection

Each bare CCD needs to be visually inspected for gross flaws and particle contamination before it is mounted and tested. This will be done with a low power inspection microscope. Devices that show gross defects will be classified as non-science grade.

Pixel, Column, Row Defects

Pixel defects are defined as any CCD pixel that has a response outside of a predefined range for a given input light intensity. Pixel defects can take the form of a dead pixel (no or little response) or a hot pixel (large response for little input). Defective pixels can also be defined as a pixel with a response that is far from the average pixel response of a good CCD pixel.

Column and row defects are defined as any column or row that has a response outside of a predefined range. Pixel defects can be found by taking many CCD flat field images at a constant low light level then finding the mean and sigma of each pixel over all the images. Bad pixels have a large sigma or a mean outside the average.

Linearity

CCD pixel response over a range of illumination intensities allows one to measure the linearity of the response of the CCD. Multiple images are taken at a number of different illumination levels over the full dynamic range of the CCD, using constant integration times (or a constant illumination level and a range of exposure times). Illumination intensity is measured with the integrating sphere photodiode and is plotted versus average pixel response over a stable CCD region. A linear fit is applied and the maximum deviation from the fit defines the CCD linearity.

Pixel Full Well, Serial Register, Parallel Registers Full Well Capacities

The full well capacity can be measured by either spatially varying the illumination intensity across the CCD or by illuminating the CCD during readout. Since this is just a check of available dynamic range, the measurement need not be very precise. With all of these measurements, care must be taken not to saturate the pixel, serial register and amplifier before saturating the acquisition ADC. This can be done by limiting the gain from CCD to ADC.

Pixel Full Well Capacity

Flat field illuminate the entire CCD at the beginning of readout such that the CCD will saturate by the end of the readout cycle. Pixels across columns will have a response proportional to their order in readout. A profile of the number of electrons per pixel versus column will show a plateau which is the pixel full well capacity.

Serial Register Capacity

Similar to pixel full well capacity measurements except that one bins rows together. This allows the serial register response to increase with readout time up to saturation.

Output Amplifier Capacity

Similar to pixel full well capacity measurements except that one bins rows together along with pixels along row to form an N x M region of pixels input to the output amplifiers.

Charge Transfer Efficiency

Charge transfer efficiency (CTE) is a measure of how efficiently a CCD moves charge from pixel to serial register to output amplifier. High-quality imaging requires that large CCDs have a very high CTE. An accurate method for measuring CTE is to use a Fe⁵⁵ source that produces a precise number of electrons in a pixel.

The CCD under test is exposed to an Fe⁵⁵ source with an activity level that produces a few 10's of X-rays per second per cm². Many images are acquired of these X-ray exposures. Since each X-ray produces either 1616 electrons (5.9 keV X-ray) or 1778 electrons (6.2 keV X-ray), a known quantity of electrons is produced per pixel. Pixel CTE can be measured by comparing the response of pixels near the serial register to pixels far from the serial register. Serial register CTE can be measured in a similar way by comparing signals near the output amplifier to those far from the output amplifier.

In addition, Fe^{55} measurements give a value of the conversion factor of pixel electrons to ADC counts. This conversion factor can be found from the mean of the Fe^{55} signal histogram of pixels near the output amplifier.

Quantum Efficiency

This is normally a difficult and time consuming measurement requiring measurement of absolute pixel response over several narrow optical bandpasses at, possibly, several temperatures. The measurement proceeds by passing the broadband optical source of the test stand through a narrow band monochromator to select a measurement frequency. The CCD is then illuminated by this source and the CCD and integrating sphere calibrated photodiode responses are acquired. In general, the calibrated photodiode response gives a measure of photons per second per cm^2 at the CCD surface. The quantum efficiency, as a function of wavelength, can then be recorded as the ratio of the number of electrons measured to the number of incident photons.

However, there is a quartz optical window between the integrating sphere and the CCD which must be accounted for. This is done by placing a second calibrated photodiode inside the cryostat in place of the CCD and measuring its response compared to the integrating sphere photodiode response for each measurement wavelength. This gives a response measurement of the quartz window which can be used to determine the photons per second per cm^2 on the CCD surface.

Dark Current

Dark current is a measure of the random thermal signal produced in each pixel. At operating temperatures and exposure times selected for the Dark Energy Camera, these signals are very small and therefore difficult to measure. Also, cosmic rays must be removed and stray light contamination must be eliminated. Small dark current signals can be measured by binning several pixels into one pseudo-pixel before being read out. Dark current can then be measured by taking the pseudo-pixel signal difference between a short (1 second) and long dark exposure (few hours) and dividing by the number of binned pixels and the number of seconds in the long exposure minus the short exposure.

Read Noise

Read noise is a combination of noise of the external electronics and noise of the CCD output amplifier. Read noise can be determined from several zero integration time, dark field images. The zero integration time eliminates dark current effects while the dark field eliminates light induced signals.

Thermal Cycling

During the testing process, each CCD module will be thermal cycled between ambient and operating temperatures several times to identify any weaknesses in the fabrication process.

5.8.4 Database Software and Travelers

The test results will be recorded into a web-based database and information of each device tested will be recorded on a traveler document that stays with each device. Similar tracking tools for production testing have been developed at Fermilab for other projects. We plan on adapting these tools for the use of CCD testing.

Each CCD will be assigned a grade that indicates its potential end use. Devices that are functional but have too many defects or other problems will be classified as engineering grade. Devices that meet the scientific requirements will be classified as science grade devices. Testing data will be further analyzed so that best science grade devices are the ones that are used on the focal plane.

5.9 Data Acquisition (WBS 1.2.5)

The data acquisition (DAQ) serves two functions. One is to convey data from the sensors to permanent storage for subsequent (off-line) analysis. The other is to monitor and control the telescope and environmental parameters that determine image quality. The DAQ contains both hardware and software components. It must be able to respond to commands issued by the personnel operating the telescope. It must also be able to operate autonomously, maintaining optimal telescope behavior during routine operations and responding appropriately to abnormal conditions.

The data acquisition will be a collaborative endeavor led by the University of Illinois and involving Fermilab, LBNL, and NOAO. NOAO has developed a data acquisition framework, called Monsoon, which we propose to adapt to this project. This approach carries two advantages over an entirely new design. It reduces the cost and time to completion of the project by taking advantage of previous work. It also maintains and extends a standard for astronomical data acquisition, reducing the costs of future projects. We will use the data acquisition during instrument fabrication and assembly as well as during survey operations. The former use, in “test stands,” not only will permit testing of the data acquisition, but also will provide a test facility for the CCDs and focal plane. Test stand operation requires that the DAQ be operational well before the instrument as a whole. We will begin by using an unmodified Monsoon system, replacing components with their production versions as they become available.

In the existing Monsoon system, CCD digitization is performed in detector head electronics (DHE) crates by acquisition (ACQ) cards, which must reside within about a meter of the CCDs in order to minimize noise. Each DHE crate also contains a clock/control board (CCB) that sends clock signals and bias voltages to the CCDs and a master control board (MCB) that communicates with the outside world and controls the ACQs and CCBs.

In the production DAQ that we plan to build, the analog functionality will be separated from the digital, allowing us to move much of the electronics off the telescope. Figure 5.15 shows block diagrams of the two architectures. Image sensors include both the main image CCDs and the focus CCDs, which are read out together. Guide CCDs are read out separately. The left diagram shows the existing Monsoon architecture. The right diagram shows our modified architecture. The DHE is a crate with a cPCI backplane. The PANs (pixel acquisition nodes) and supervisor are processes running on PCs.

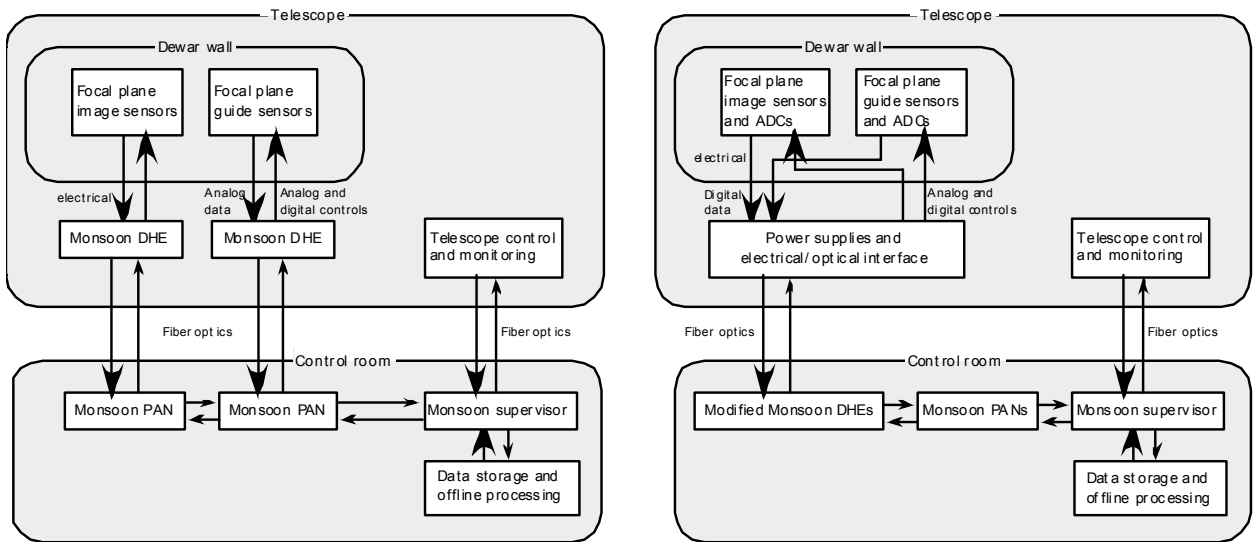


Figure 5.15 Block diagrams of data and control signal flow.

5.9.1 Data Acquisition Test Stands (WBS 1.2.5.1)

The first use of data acquisition will be in test stands that will be used to verify the functionality and measure the performance of CCDs as they are produced by LBNL and packaged by Fermilab. The test stands will also be used in DAQ software and hardware development.

To match the CCD development schedule, these test stands must be functioning by October 2004. In order to meet this schedule, they will consist of unmodified Monsoon DAQ systems. We already have the NOAO software in hand, and two sets of hardware (sufficient to read 8 CCDs each) have been ordered by UIUC for delivery in September 2004. The time before hardware delivery is being used to evaluate the capabilities of the system, to ensure that all required diagnostic capabilities exist. In particular, to simplify the data analysis, the test conditions must be included as metadata in the FITS files that Monsoon produces. FITS (Flexible Image Transport System) is an astronomy standard, and much existing analysis software can read data that is in this format.

As the new electronics becomes ready, we will verify its performance by using it in the test stands. This means that testing of the focal plane during assembly (starting in mid-2006) will use the production DAQ. Test stand use drives the DAQ schedule. See the Management chapter for schedule details. As well as being the initial test stand implementation, the unmodified architecture also serves as a fallback design, in case the new front-end electronics is not ready on schedule. While less optimal (more expensive, and more space and power on the telescope), the fallback would allow the DES instrument to operate.

Table 5.3 Data Acquisition parameters. The front end to DAQ data rate is the highest (burst) rate in the system. The data rate to storage is significantly lower (*e.g.*, 9.7 MB/s for 100 sec image exposures).

Image CCD Array (+focus CCDs)	
Number of CCDs	62 (+4)
Pixels per CCD	2048×4096 (1024×1024)
Amplifiers per CCD	2
Pixel digitization rate	250 kHz
Digitization time	17 sec
Bytes per image	971 MB
Data rate (FE→DAQ)	57 MB/s
Guide CCD array	
Number of CCDs	4
Pixels per CCD	1024×1024
Amplifiers per CCD	2
Pixel digitization rate	1 MHz
Digitization time	0.5 sec
Bytes per guide	8 MB
Data rate (FE→DAQ)	16 MB/s

5.9.2 Telescope Data Acquisition (WBS 1.2.5.2)

The important DAQ parameters are listed in Table 5.3. The focal plane contains 62 image CCDs and four focus CCDs (placed slightly out of the focal plane). These 66 CCDs are read out together. The focal plane also contains four guide CCDs that are read out during the exposure in order to maintain telescope pointing accuracy.

The highest data rate, 57 MBps between the front end ADCs and the DHE ACQ buffers, occurs during the 17 s required to digitize the 971 MB of CCD information. This is high by astronomy standards, but is not beyond what particle physics experiments routinely achieve. The data rate is determined by the 250 kHz CCD digitization rate. Because the data is carried on 140 optical fibers, data flow is not a significant technical issue. The DAQ could easily handle a 2 MHz digitization rate. The data rate to permanent storage is much lower (9.7 MBps for 100 s image exposures).

In the proposed architecture, CCD digitization is performed by custom front end electronics to be developed at Fermilab. Digital data will flow off the telescope on 140 optical fibers (one per ADC) to modified ACQ cards in the DHE crates. The modified DHEs have no analog functionality and do not directly control the readout. Readout control is performed on the telescope in response to digital signals from the DHE. This allows us to move all of the DAQ, except for ADCs, DACs, and electrical/optical interfaces, off the telescope. Separating analog and digital functionality retains the ability to minimize noise by keeping the ADCs near the focal plane, while reducing the heat and space budget by moving most electronics off the telescope. Because the current Monsoon implementation performs both the analog and digital operations in detector head electronics (DHE) crates, some electronics must be redesigned, as described below.

The DAQ will accept the digitized CCD pixel information and deliver it to permanent storage for further processing. The guide CCDs will be read out once per second during image exposure, and real time processing will include using guide stars to control the telescope pointing. Thus, there will be two readout sequences, one for the image CCDs and one for the guide CCDs. For organizational purposes, electronics on the telescope is considered to be part of the front-end subsystem. The DAQ includes hardware and software that resides off-telescope.

5.9.2.1 DAQ Work Packages

Although Monsoon is a working data acquisition framework and implementation, we must make significant changes to accommodate our hardware configuration:

- Signal digitization will be performed outside the DHE crates, by the front end electronics.
- The CCDs will be read out at two different rates, one for telescope guiding, and one for image acquisition.

Monsoon work must be closely coordinated with the design of the front end electronics (WBS 1.2.3). This coordination will be one of the principal responsibilities of the Data Acquisition Working Group (DAWG).

5.9.2.2 DAQ Hardware (see the Management chapter for a cost itemization)

Much of the hardware will be a replication of the existing Monsoon configuration. This includes two DHE crates, each with a Master Control Board, a Clock/Bias Board, and several Acquisition boards. The system also requires a Pixel Acquisition Node (PAN) PC and a Supervisor PC. We have not yet determined how much of this functionality can reside on one computer and one electronics crate.

Some hardware must be modified or newly designed:

- The use of the front end ADCs obviates digitization in the Monsoon detector head electronics (DHE). As a consequence, the DHE Acquisition cards will be redesigned and greatly simplified. They will become digital buffers.
- The Clock/Bias Boards generate the digital control signals and analog voltages for the CCD focal plane array. We must redesign them to accommodate the LBNL CCDs. The functionality will be split in two: a card in the DHE crate will generate digital control signals that electronics on the telescope (part of the front-end) will turn into the analog signals needed for the CCD readout.
- The on-cage interface converts the electrical data signals to optical for transmission off the telescope. It also receives (isolated) AC power from off-telescope and generates the appropriate DC voltages.

5.9.2.3 DAQ Software

The existing Monsoon software is functional, but we must adapt it to the needs of our project. For example, the DAQ will actively control telescope pointing (on a one second time scale) during exposure. The real-time software must measure the point-spread functions of stars imaged by the guide CCDs and send commands to the telescope controls. Also, CCD diagnostics must be developed for the test stand application. These diagnostics will then be modified for use as focal plane monitors on the telescope. We

will also develop graphical interfaces, both for the description of the readout sequences and for the operational displays.

5.9.2.4 Fallback scenario

As was mentioned above, in case the front end digitization development does not proceed quickly enough to be useable on our timescale, the fallback DAQ scenario is to use the existing Monsoon system with minor modifications. This fallback will be more expensive, will dissipate more power in the telescope cage (251W vs. about 60W), and will require more space in the cage (two cPCI crates). These parameters are not ideal, but would not fatally compromise DES performance. In this scenario, the main hardware design work would be of a 16 (or higher) channel ACQ board, to minimize space requirements. NOAO engineers have already begun such a redesign, and we will assist them if it becomes necessary.

5.10 Camera Cryostat Vessel and Focal Plane (WBS 1.2.6)

This section describes the vacuum vessel that houses the CCD focal plane and all the associated cooling and mechanical components.

5.10.1 Camera Vessel

The Camera Vessel (cryostat), shown in Figure 5.16, consists of a front plate, a forward spool piece that houses the supporting electronics, a rear spool piece that contains the cooling package. The front plate of the cryostat, which mounts to the corrector optics housing assembly, contains the housing and vacuum seal for the C5 optical lens and supports the focal plane plate with its CCD modules. The front plate of the cryostat is attached to the forward spool piece, shown in Figure 5.17, which supports the cables, the cable vacuum feed-through board and outer crates for the Front End Electronics (FE). The two FE crates are mounted on opposite sides of the camera vessel. The two electronic feed-through board enclosures are located between the crates. A vacuum port and a port for a vacuum gauge are also mounted to the forward spool piece.

The rear spool piece supports a liquid nitrogen dewar, as shown in Figure 5.18. The dewar is thermally coupled to the focal plane via copper braids. The dewar is cylindrical and the outer diameter is small enough to leave access between the dewar and the cryostat wall for attachment of the copper braids. Mounted to the back surface of the dewar is a cell of Zeolite to help maintain good vacuum even with some out-gassing from the cables and PC boards inside the cryostat. Ports are attached to the spool piece for utilities such as liquid nitrogen dewar supply and return lines, a vacuum port and a port to mount a vacuum gage. The back of the rear spool piece is used for access during final assembly and maintenance. The back plate used to close this opening has no connection ports. The heat load to the dewar is reduced by polishing or gold/nickel plating all of the internal metal surfaces and additional internal radiation heat shields are not required. With two separate spool piece modules, the camera portion of the cryostat can be preassembled at the same time the cooling package is assembled and integration of the two systems is simplified. The cryostat dimensions are shown in Table 5.4.

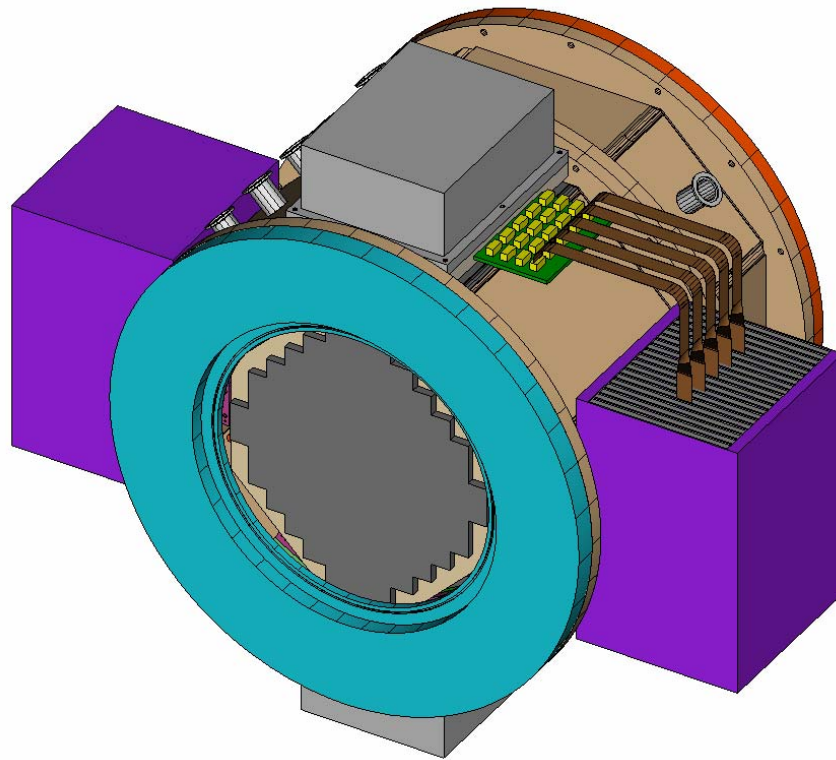


Figure 5.16 Camera vessel assembly with vacuum seal boards for signal feed-through and crates for electronics

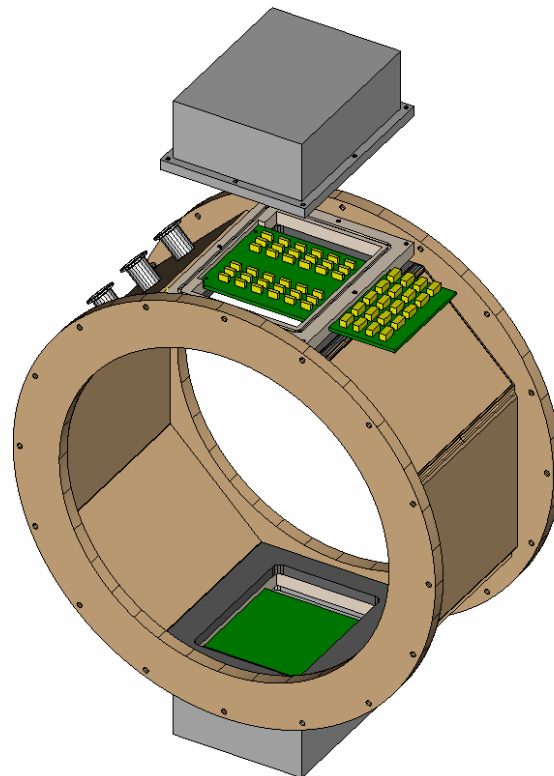


Figure 5.17 Camera vessel forward spool piece with vacuum seal boards.

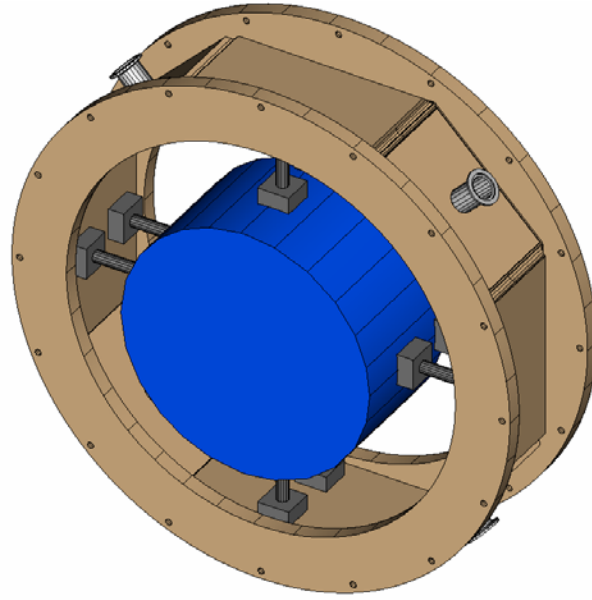


Figure 5.18 Camera vessel rear spool piece with liquid nitrogen dewar.

Table 5.4 Cryostat Dimensions

Feature	Dimension	
	Inch	mm
cryostat overall length	30.0	762
cryostat flange outer diameter (OD)	32.0	813
crates, between outside walls	49.5	1257
crates, OD of a wrapping cylinder	52.4	1331
boards, with cover, OD of a wrapping cylinder	41.2	1047
Inner diameter of prime focus cage	62.0	1575
CCD mounting plate, between long flats	19.5	495
CCD mounting plate, between short flats	20.6	523
dewar total height	8.0	203
dewar OD	16.0	406
minimum distance between dewar and CCD support plate	5.0	127

5.10.2 Focal Plane

The CCDs will be precisely located and attached to a large metal plate called the focal plate. This plate defines the interface between the CCDs and the camera vessel. The positions of the CCDs are set by engagement of locating pins in the CCD module support feet with precision holes machined into the focal plane support plate. Additional holes are provided to permit a screwed connection from the rear of the plate to fix the CCDs into place and to provide access for the readout cable connection. The focal plane support plate will be several centimeters thick in order to provide a stable support and limit the effect of gravitational sag to a few μm .

In order to maximize the active area density within an image, it is desirable to minimize the gaps between adjacent CCD modules. The closeness which can be achieved depends on the accuracy to which the mounted module profile is known. A study of anticipated tolerances

on the modules, focal plane plate, and assembly jig concepts has been performed assuming the following tolerances:

Sensor size	~15 μm
Machined feature locations	~13 μm
Machined hole diameters	~13 μm
Minimum pin / hole radial clearance:	~2 μm

The sequential stack-up of the various factors involved in the CCD module assembly and mounting into the focal array found that the location of an edge could vary by 124 μm when the individual factors were added linearly and 42 μm when added in quadrature. For our Reference Design we assume a gap of 250 μm is needed between modules to accommodate these tolerances and allow for removal and or installation of a CCD after the focal plane is completed.

To achieve the low noise necessary for astronomical applications, the CCDs are typically cooled to -90 to -120 °C. For our Reference Design we assume they need to be cooled to -100 °C, although we will investigate running them at warmer temperatures. The focal plate will be thermally coupled through copper braids to a cold mass that is directly cooled by a liquid nitrogen volume inside the vacuum vessel. Small heating elements will be used to actively regulate the temperature of the focal plate. The focal plane support will be designed to keep temperatures uniform to within a few degrees and to minimize distortions resulting from temperature changes during cool down and from temperature variations within the plate. This can be achieved by designing the plate's mounting system to accommodate its contraction as it cools and by designing the plate to have small thermal variations and stable mechanical characteristics.

During assembly onto the focal plate, handling rods inserted into the backs of the CCD modules aid in handling and installation by providing a convenient handhold away from the sensitive electronics and by providing guidance into the focal plate before the module alignment pins are engaged. Once the module is in place, these installation rods are replaced one-by-one with fasteners to fix the module in place. The flexible module cables can be installed onto each module from the rear. This cable will be clamped to the back surface of the focal plate in order to provide strain relief and a thermal intercept for any heat conducted along the length of the cable. The populated focal plate is then assembled into the front half of the cryostat vessel, which contains the C5 optics window and the vacuum feed-through boards. The cables are connected to the feedthroughs and dressed in place, and then the cooling module of the cryostat vessel is installed and connected to the focal plate via copper braids. Finally, the back cover of the cryostat is installed.

Once integrated into the completed camera vessel assembly, replacement of individual CCD modules can be achieved with the camera cryostat assembly removed from the telescope and placed in a clean work environment. The rear spool vessel module of the cryostat and the C5 optical window package are then removed. With some CCD cables disconnected for access, a CCD can be re-equipped with installation rods and then extracted through the C5 window opening. The module can then be replaced and recabled and the camera vessel reassembled.

5.11 Cooling & Vacuum Systems (WBS 1.2.7)

This section describes the systems that provide cooling to the CCD focal plane and vacuum inside the camera cryostat vessel.

5.11.1 Cooling System

Figure 5.19 shows a sketch of the cooling system components located within the camera vacuum vessel. These components include the focal plate (CCD's mounted on the cold plate), a liquid nitrogen reservoir, copper braids used to thermally connect the liquid nitrogen reservoir to the cold plate, and zeolite to assist in maintaining a low vacuum level in the vessel.

5.11.1.1 Camera Heat Load

The camera heat load is due primarily to the radiative heat load through the window (~50 Watts), the CCD's (~20 Watts) and associated electronics. The mechanical support of the focal plate will be from the window end of the vacuum vessel and will be minimized by fabricating the supports using a low conductivity material. The load due to the focal plate supports is estimated at 10 Watts. The wiring and cables contribute about 25 Watts. The radiative heat load other than that realized through the window is another 20 Watts. The total of these estimated heat loads is 125 Watts. Since detailed information about the heat load from the electronics is not known and in the interest of including a safety factor, a total heat load of 200 Watts in the camera vessel is presumed at this time.

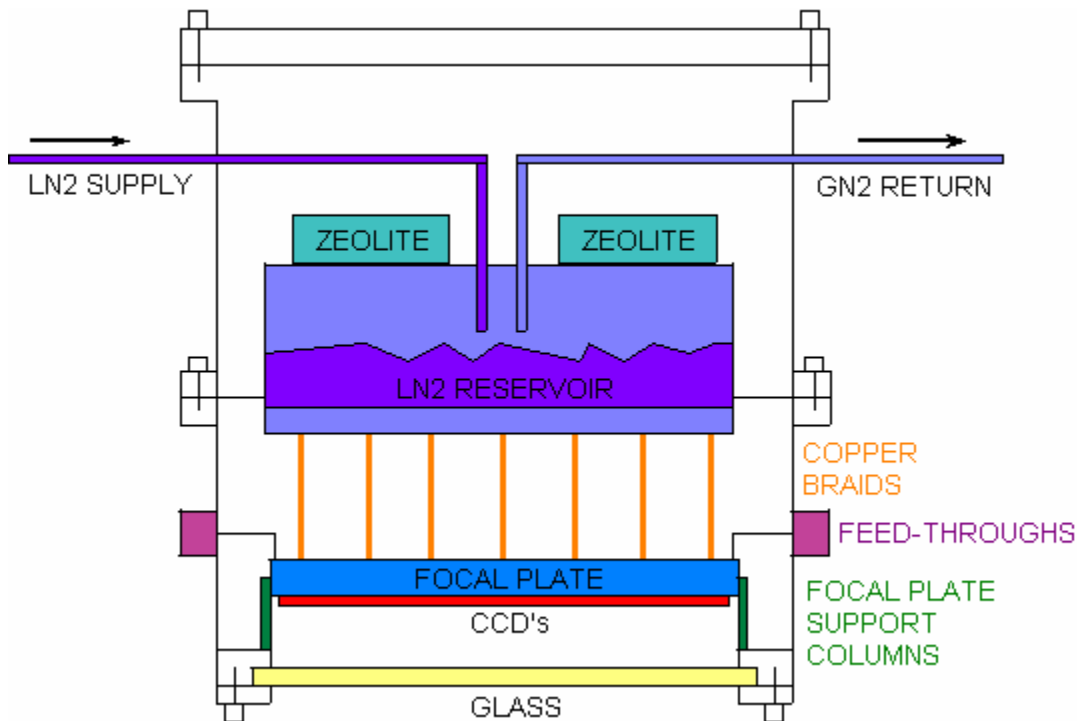


Figure 5.19 Schematic of the Dark Energy Camera Using Liquid Nitrogen Cooling.

5.11.1.2 Liquid Nitrogen Cooling System

It is assumed in this discussion that the camera will be cooled with liquid nitrogen. In order to avoid manually filling the liquid nitrogen reservoir, an automatic filling system is planned. This system includes a refrigeration system to cool and condense the nitrogen, a

dewar to store the liquid nitrogen, a liquid nitrogen pump, and transfer lines. The supply and return transfer lines between the camera and the liquid nitrogen storage dewar require a length of about 150 feet each. The total heat load of the transfer lines is estimated at 140 Watts. The liquid head of the supply line will range from 70 to 100 feet depending on the camera position.

The heat load of the storage dewar must also be considered and is estimated at 60 Watts. The total system heat load is thus estimated at 400 Watts. One appropriate refrigeration system for this heat load is the Stirling refrigeration cycle. A system is available which produces 10 to 14 liters of liquid nitrogen per hour depending on the supply pressure chosen.

Based on these estimates, a liquid nitrogen supply rate averaging seven liters per hour will be required. The camera will use roughly five liters per hour while the supply line will require two liters per hour to remain cold. Taking into account some vaporization of the liquid through the supply transfer line, the pump should be able to deliver to the camera vessel at a rate of 1.4 liters per minute. If fill periods of 30 seconds each are used, 10 fills per hour are required. This implies one fill every six minutes. This will maintain the camera liquid at a fairly constant level, varying by only 0.5 liter.

The camera liquid nitrogen reservoir size is currently designed at 22 liters. By maintaining the liquid level in the reservoir at 10 liters, a two hour reserve of liquid nitrogen is available at any given time. It is possible to design a larger reservoir in order to provide a longer reserve if deemed necessary. A cooling reserve is intended to provide time to switch to a backup dewar of liquid nitrogen if maintenance on the refrigeration system is required. Using a portable 160 liter backup dewar would provide close to one full day of cooling.

The camera will be positioned in any of several angles during fills. By positioning the supply and return points very near the center point of the liquid nitrogen reservoir coupled with maintaining the maximum liquid level slightly lower than one-half full (10 liters), flow of nitrogen to and from the reservoir will not be impeded and liquid will not drain into the nitrogen return line. The liquid will be pumped from the storage dewar to the camera liquid nitrogen reservoir via a submersible pump located inside the storage dewar. The pressure at the pump outlet will be on the order of three atmospheres absolute while the storage dewar will be maintained only slightly above one atmosphere. The camera liquid nitrogen reservoir will also be only slightly higher than atmospheric pressure.

The components of the refrigeration system are such that they are separable and may be located apart from one another. The nitrogen condenser and storage dewar must be located together, however, the refrigeration system compressor may be located some distance away from the condenser/dewar. The compressor is where heat is rejected from the refrigeration system. Liquid coolant, already available at CTIO, is required at the compressor in order to accept this heat and carry it some distance away from the telescope before rejecting it to the atmosphere.

5.11.1.3 Consideration of a Cryo-Cooler Cooling System

As an alternative to liquid nitrogen cooling, the possibility of using cryo-coolers is being considered. Those types being examined include the Gifford-McMahon, Pulse Tube, and Joule-Thomson type refrigeration systems. Use of cryo-coolers to cool the camera brings the advantage of lower power consumption, however, one must address the issues of cooling capacity, vibration, maintenance, and space.

The Gifford-McMahon type offers a high cooling capacity independent of its orientation but produces significant vibration. Units with a cooling capacity of 300 Watts at 80K are available. The possibility of dampening the vibration will be studied. The Pulse Tube type offers a good cooling capacity (60 Watts at 80K) but multiple units would be required to cool the camera. The Pulse Tube type has a relatively low vibration level but is sensitive to orientation requiring its cold end to be pointed down. Its sensitivity to position makes it an unlikely choice as the camera must operate cold at many angles. The Joule-Thomson type cooler has the lowest capacity (about 24 Watts at 120K) of these three types and would require multiple units to keep the camera cooled. Even with multiple units, we would be required to operate the coldest mass in the camera at around 120 K. Its vibration is the lowest of all and its capacity is independent of orientation.

With any type of cryo-cooler, actual maintenance on a unit will require some camera downtime. Spare units may be installed for use in the case that an operating unit fails but it would contribute to the camera heat load when not in use. Swapping out units likely means another camera vacuum pump-out period which could keep the camera out of service for days.

Use of cryo-coolers requires that space is available inside and outside of the camera vessel to install the quantity of units needed. Also, a *cold mass* is required to provide a cooling reserve in place of the liquid nitrogen reservoir. To provide an adequate cooling reserve, the *cold mass* weight may necessitate a support system other than the cryo-coolers. A support system will add to the camera heat load. These issues will be addressed in our consideration of cryo-cooler use for this camera.

5.11.2 Vacuum System

The vacuum system provides a vacuum better than 10^{-6} Torr in the camera vessel. A roughing pump is used to achieve a vacuum of 10^{-4} Torr, then a turbo pump is used to achieve an initial vacuum better than 10^{-6} Torr. During camera operation, the cold mass inside the camera vessel cryopumps water vapor and maintains the vessel vacuum without the need of being connected to a mechanical pump. A vacuum valve on the camera vessel allows isolation from the mechanical vacuum pump when the telescope is operating. Opposite from the vacuum pump port on the camera vessel is another port that supports a vacuum gage for continuous monitoring of the vacuum.

5.11.2.1. Outgassing

The camera vessel contains PCB boards and cables that will outgas. The outgassing rate is estimated in Table 5.5. The pumping speed required to maintain 10^{-7} Torr is equal to 17,611 liters/sec. The water pumping rate is $1.40 \times 10^{+5}$ liters/sec/m² at 77 K. The surface area required is then 0.125 m² LN2. The surface area of the liquid nitrogen dewar is 0.5 m² which is four times larger than the required surface area to maintain 10^{-7} Torr.

Table 5.5. Gas Loading

	Area	Quantity	Rate	Total Load	Data
Item	(cm²)		Torr-l/s	Torr-l/s	Source
Flex Cables (Kapton)	375	62	7.5×10^{-8}	1.74×10^{-3}	LHCb
Silicon (CCDs)	21	62	4×10^{-9}	5.31×10^{-6}	Pyrex value
Stiffened Flex Cable	6.3	62	1×10^{-8}	3.91×10^{-6}	BTeV note 2578 *
Aluminum Focal Plane	1734	1	1×10^{-10}	1.73×10^{-7}	A. Roth
Feed Thru boards	37	2	2×10^{-9}	1.48×10^{-7}	BTeV note 2578 *
C5 Optic Window	1963	1	4×10^{-9}	7.85×10^{-6}	Pyrex value
			Total Load	1.76×10^{-3} Torr-l/sec	

* Outgassing rates are after 150 hours of pumping.

5.11.2.2 Warming

During either an intentional warm-up of the camera such as for a scheduled maintenance or in the case of an unintended warm-up such as the result of a power failure, the CCD surfaces must be maintained at a temperature higher than the cold surfaces that act to cryo-pump the vessel's vacuum environment. This minimizes the possibility of condensing any material onto the CCD faces as the cold surfaces in the camera warm up. The highest heat load to the camera is the radiative load on the CCD array and focal plane, thus these surfaces remain warmer than the hardware associated with the liquid nitrogen reservoir. The heaters on the focal plate may be used to provide additional heat to the focal plane and thus the CCD's. Use of these heaters during a power failure requires an independent, backup power supply for the heaters and temperature monitoring.

5.12 Optical System (WBS 1.2.8)

5.12.1 Introduction and Requirements

An optical corrector is needed to achieve good image quality over the 2.2 degree diameter field of view of the camera. Such a corrector will require the use of large, custom-made glass lenses that have a long lead time to acquire. Correctors of sizes approaching this size have been built at the AAT, CFHT and Subaru telescopes. A number of design studies also exist, including for LSST, with even larger optics than those proposed here. We have adopted a baseline design that meets the requirements for the Dark Energy Survey and otherwise minimizes the technology and schedule risks associated with the procurement and fabrication of the lenses.

The requirements for the corrector are listed in Chapter 3. The basic requirements are that it has a 2.2° diameter field of view, a wavelength range of 0.39 to $1.1\ \mu\text{m}$, an image size (full width half maximum) of less than $0.4''$, and a plate scale such that $15\ \mu\text{m}$ pixels correspond to $< 0.3''$. Additionally, space must be available for a shutter and for insertion of large glass filters.

5.12.2 Design

The adopted corrector design is shown in Figure 5.20. The design prescription is listed in Table 5.6. It has five lenses, of which one also serves as the window for the camera dewar, plus a glass filter. All lenses are made of fused silica. One surface has a mild aspheric shape; the other surfaces are all either flat or spherical. This design blends together elements from two concept designs commissioned by CTIO, one from PRIME Optics, the other from V. Terebizh, but is actually more similar to two designs that have been proposed for the Lowell 4 meter telescope (Epps and diVittoria 2003; Blanco et al. 2003).

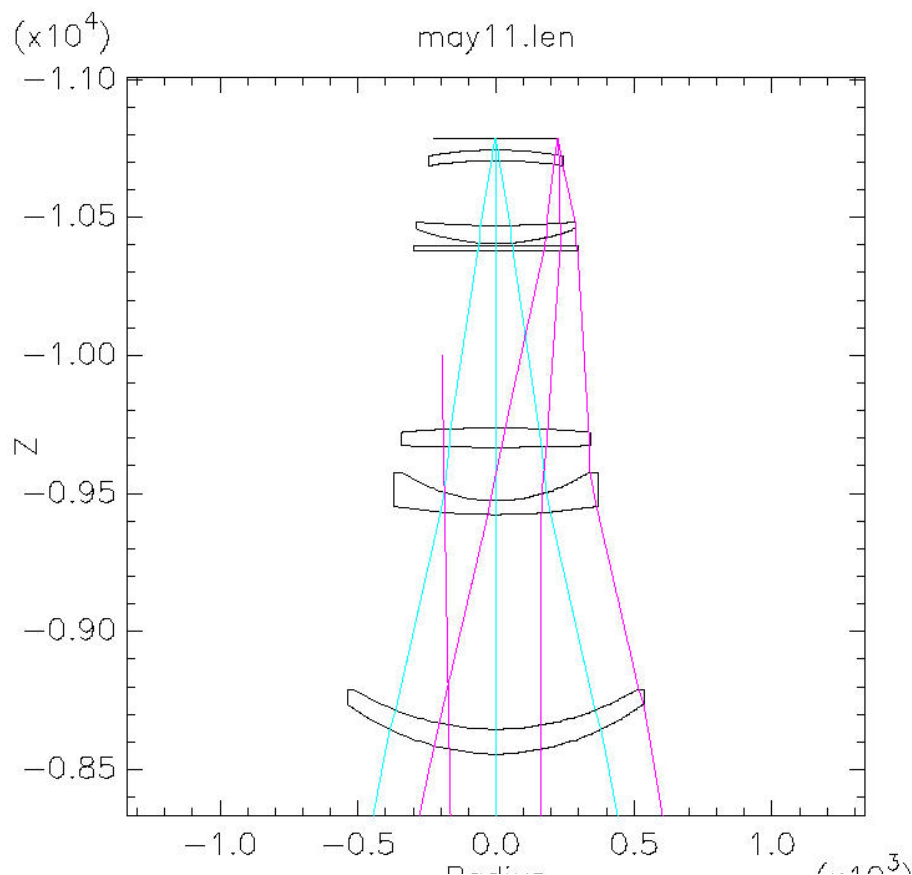


Figure 5.20. Corrector Design

Several factors were involved in the process of developing the design. These include:

- a. Few glass types are available at the sizes needed. Fused silica blanks of the required size can be manufactured and delivered by Corning on a firm schedule. The largest lens (C1) is thick enough that the blank will need to be slumped first.
- b. Aspheric surfaces are more difficult and hence take longer and are more expensive to figure than spherical surfaces.

c. The accuracy with which the curvature radii can be measured is limited by vendor's testing equipment; for example, Optical Sciences Center switches from a high accuracy to a lower accuracy method once the radii exceed 40 inches.

d. Ghosting characteristics are often ignored by designers but can have an impact on data quality. Small changes in design can amplify or mitigate the impact of ghosting.

Table 5.6. DES 2.2° Corrector Design

Surface	Radius (mm)	Thickness (mm)	Glass
1	-21312 ccon = -1.1	-8556	reflect Primary
2	-888	-90	Fused Silica C1
3	-1003	-778	Air
4	-2360	-50	Fused Silica C2
5	-622	-194	Air
6	-10031	-70	Fused Silica C3
7	3731	-643	Air
8	0	-15	Fused Silica Filter
9	0	-10	Air
10	-869 a4 = -3.15e-10 a6 = -9.48e-16 a8 = -4.83e-21	-65	Fused Silica C4
11	-3382	-235	Air
12	1551	-39	Fused Silica C5 (Window)
13	1293	-40	Air
14	0	0	Focal Plane

5.12.3 Performance and Characteristics

Table 5.7 gives the image sizes averaged across the SDSS filter bandpasses. The worst-case value of D80 is .59", which exceeds the requirement of .64". In the r and i bands, where the best image quality is sought for the weak lensing measurements, the equivalent FWHM is $D80/1.53 = .27''$ worst-case. This is the size of 1 pixel.

Table 5.7 D80 (arcsec) for images in the 4 SDSS Filters (as a function of focal plane radius)

Radius	g	r	i	z
0	0.32	0.11	0.17	0.31
45	0.35	0.19	0.21	0.34
90	0.39	0.14	0.22	0.33
135	0.40	0.21	0.25	0.33
180	0.50	0.32	0.36	0.42
226	0.59	0.37	0.41	0.47

The lens sizes are given in Table 5.8. The clear aperture includes an overfill of 1-2 mm. The outer diameter includes a 20 mm edge to be used for mounting and support.

Table 5.8 Lens Sizes for the DES Corrector

Lens	Clear aperture (mm)	Thickness (mm)	Thinness (mm)	Outer Diameter (mm)
C1	1072.3	234.1	54.0	1112.3
C2	736.7	153.1	50.0	776.7
C3	683.4	70.0	48.6	723.4
Filter	591.4	15.0	15.0	631.4
C4	581.7	77.2	24.0	621.7
C5 (Window)	486.2	57.9	35.2	526.2

5.12.4 Finite Element Analyses

A handful of analyses have been done to identify any possible critical problems in the design due to the size and weight of the lenses. So far, none have been found. The design is tolerant of a wide range of thicknesses for each lens, so any problems encountered in the future (but before procurement of the blanks) could likely be corrected without a major redesign.

The change in shape of each lens due to gravitational loading was calculated and found to have negligible impact on the design. The most critical lens is the one forming the dewar window, since it must support the differential between sea-level atmospheric pressure and vacuum. The current thickness in the design is 38.7 mm. A finite element model was constructed with the IDEAS program to study the deflection of the window (Derylo May, 2004). The result is shown in Figure 5.21. The midpoint deflection is 55 μm which is marginally important for the design. The maximum stress is 4.4 MPa, which yields a factor-of-safety over 11 for the flexura strength value of 50 MPa reported for fused quartz material.

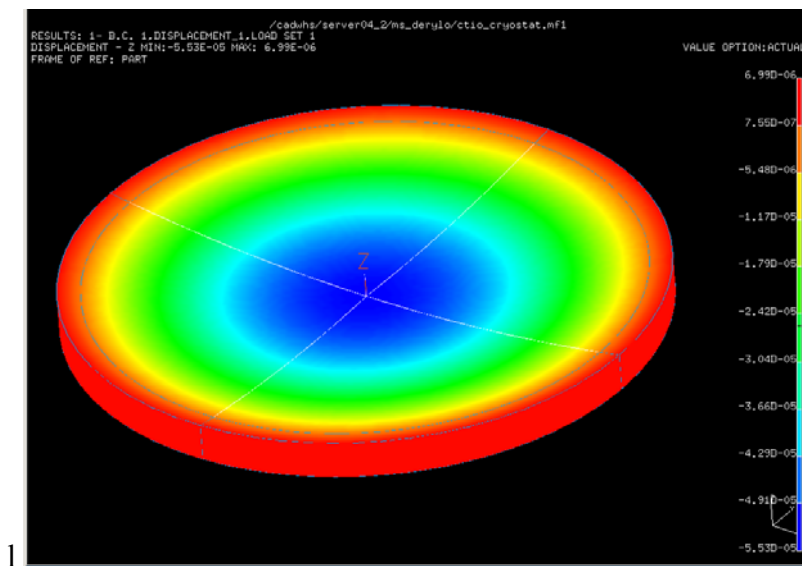


Figure 5.21 Expected Deflection of C5 optic based on and FEA analysis

5.12.5 Tolerancing and Assembly

The design is robust against small inaccuracies in the lens curvatures, thicknesses, and refractive indices provided that these quantities are measured accurately after fabrication and compensated by adjusting the positions of the lenses during assembly.

A preliminary tolerance analysis has been done to identify possible problem areas in fabrication or assembly. The figure of merit used for the analysis was a weighted average of r.m.s. spot size across the focal plane as measured in the four SDSS filter bandpasses. Factors that were investigated included positioning errors (translation and tilt), curvature errors including both fabrication and measurement, refractive index errors, inhomogeneities in the glass, and primary mirror alignment errors. A sensitivity analysis was run in which an allowed degradation of performance was assigned to each variable, and the maximum permissible error of that variable determined. These values were compared against numbers taken from standard practice or specification sheets. For one corrector element, C1, the radius of curvature of one surface was reduced slightly so it could be tested more accurately. Otherwise it was found that standard practice would always do as well as or better than required. The overall contribution to image degradation is estimated to be .24" worst-case in D80 (which is added in quadrature to all other contributions).

5.12.6 Coatings

Coatings for the optics are necessary in order to reduce reflection losses at air-glass interfaces. In the Reference Design using fused silica, each uncoated surface produces a loss of ~3.5%. Without coatings, the total loss through the 5-element corrector would be about 30%. A nominal goal is coatings on all surfaces which reduce reflection losses to 1% or better, per surface, yielding an acceptable total loss of about 10%.

A second reason for minimizing reflection losses is the impact on ghosting. The obvious effect is to reduce the intensity of all ghosts, but it secondarily allows for greater flexibility in the optical design since less of the total "optimization budget" must be spent on minimizing ghosts optically if the coatings are good.

There are two basic options often used in astronomical applications for coating optics this large. The preferred method for the first 4 elements (C1-C4) of the corrector is some form of Sol-Gel coating. This is a semi-hard coating with excellent performance which is relatively easy to deposit on optics this large, and has the advantage that it can be cleaned off and reapplied if it gets damaged. The other option is a hard dielectric coating. The simplest would be a 1/4 wave of MgF₂, with better-performing multi-layer coatings being a possible option on all but the largest element (C1). The dewar window (C5) must have some form of hard dielectric coating to ensure no outgassing into the vacuum dewar. A final possible option for coating most of the optics is a hybrid solgel coating. This recently developed coating technology combines an undercoat of MgF₂ with a tuned Sol-Gel overcoat and provides spectacular performance (losses less than 0.5% over the optical waveband). These coatings are currently significantly more expensive, and can only be sourced from one supplier, but we may reasonably expect prices and availability to improve in the coming few years. Also, CTIO has developed a facility for Sol-Gel coating and has recently put Sol-Gel on MgF₂ for the elements

of the SOAR Optical Imager, with excellent results. Study on scaling up this facility to the larger DES optics is under way. A final decision on coatings will require a detailed analysis of the costs and benefits regarding both ghosting and throughput.

5.12.7 Ghosting

The high reflectivity of CCDs combined with the large number of surfaces in the design mean that ghost images of single stars and the diffuse night sky from the focal plane deserve attention. It is assumed that the LBL CCDs reflect 15% of the incident light, the Sol-Gel coatings reflect 0.8%, and MgF_2 coatings reflect 1.5%.

Ghost images of stars create an annular halo of light around but not centered on each star image. The best strategy for minimizing their impact depends somewhat on one's science program. For studying large, extended objects, one might want to minimize the size of the halo so that the sky background over large areas is kept uniform. For studying small sources, one might want to maximize the size of the halo (but reduce its surface brightness) so one can measure accurate local sky backgrounds. The latter strategy is chosen here. To achieve this, the dewar window is located 40 mm from the focal plane. This diffuses the ghost image of a point source to a diameter of 27 mm (480 arcsec). A 1st magnitude star produces a ghost that has a surface brightness of 21 mag/sq-arcsec, about as much as the night sky.

The ghost image of the exit pupil is formed by reflections of the night sky between the CCDs and the ensemble of all surfaces in the corrector. If one is careless in the design, it is possible to create an in-focus image of the exit pupil that requires extra software in data processing to remove (which happened with the Mayall 4 m prime focus corrector). A composite ghost image was computed and is shown in Figure 5.22. The dominant contribution comes from the leading surface of lens C4, which acts to focus reflected light back onto the focal plane. The peak intensity is about 6% of the incident light in the center of the field, falling to less than 1% at the edges.

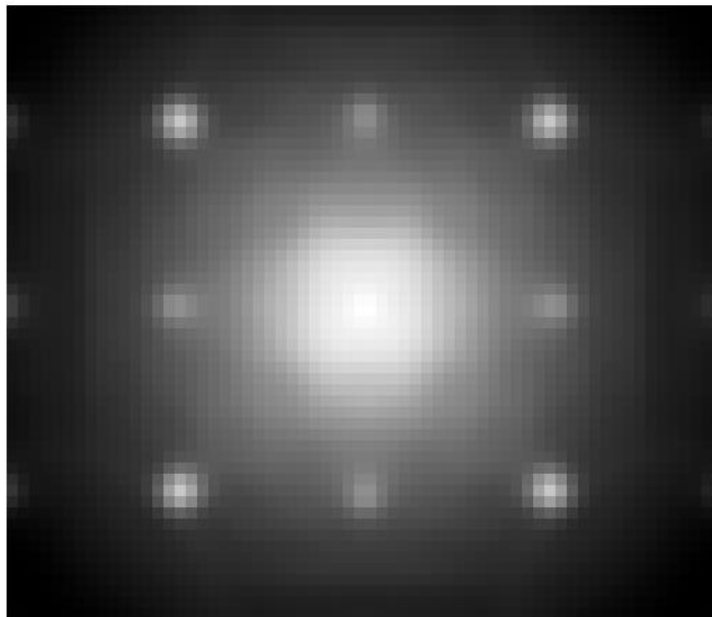


Figure 5.22 Computed ghost image in the Dark Energy Camera. The square grid of smaller images is a computational artifact and should be ignored.

5.12.8 Filter Characteristics

We adopted the SDSS g, r and i filters for our Reference Design since they will provide the required accuracy in the determination of the photometric redshifts of our target galaxies. As noted earlier, our z band red cutoff differs slightly from the SDSS z band. While both are effectively defined by the red cutoff of the silicon, the thick, high resistivity silicon CCDs that we plan to use have a much higher QE in the z band than the SDSS CCDs. The filter characteristics were selected to bracket the Calcium H and K break at 394 nm in the spectrum of red galaxies, which is typical of galaxies in clusters. At 0.05 redshift the H and K break is at 410 nm, just blue-ward of blue cutoff (50%) of the g band filter. At a redshift of 1.1 the break is at 830nm, just red-ward of the red edge (50%) of the i filter. Note that we want filters to bracket both sides of the H and K break in order to derive good photometric redshifts; in particular the z filter is necessary at redshifts near one in order to provide coverage red-ward of the H and K break. The proposed characteristics of the filters are shown in Table 5.9.

Table 5.9. The Proposed Wavelength Characteristics of the Filters

Name	Center (nm)	FWHM (nm)	Trans. (%)
g	480	140	0.91
r	625	140	0.97
i	770	150	0.98
z	950	240	0.98

5.13 Prime Focus Cage and Corrector Housing (WBS 1.2.9)

5.13.1 Prime Focus Cage

Figure 5.23 shows a detailed view of the cage. The corners of the cage represent the interface to the existing spider. This joint marks the outer mechanical boundary of what we plan to replace. The internal layout of the cage has been designed with ease of servicing in mind. The corrector is supported from the center of the cage. A focusing mechanism is part of the interface between the cage and the corrector. The linear bearings internal to the cage allow the corrector to be separated from the camera and moved towards the primary. This will allow access to the shutter on the camera face and to the filter changing mechanism. Cables and cooling tubes from the floor of the telescope will follow the trusses and spider to the left end of the cage. Development of a clear understanding of the cable and cooling tube routes, and how to deal with the cage rotation, is a critical aspect of the integration of our proposed design with the existing infrastructure at the Blanco. Our Reference Design has the cooling tubes and the CCD cable connections on the sides of the vessel.

A major advantage of replacing the entire cage and all of its service functions is that it minimizes the complexity of the interfaces with the Blanco telescope. In addition, it allows us to assemble the entire camera and all of its services in a self-contained module that can be completely tested before shipment and installation at Cerro Tololo. This means that the integration effort is localized and is a far simpler task than if the new camera were installed piece by piece into the existing cage. We have a Level 2 sub project devoted to integration and are in close contact with our NOAO representative (T. Abbott) for discussions of integration

issues. As the Reference Design progresses, an integration and configuration control committee will be established to provide the organizational structure necessary for successful integration of the Dark Energy Survey Instrument with the infrastructure at the Blanco.

5.13.2 Corrector Barrel

The corrector barrel is a series of cylinders, one per lens, four in number; lens C5 is mounted in the camera dewar. These cylinders will be made of either forged steel, aluminum or Carbon fiber. Forgings eliminate many internal stresses that can be developed during welding processes, thereby minimizing warping during machining. Finished components fabricated from forgings tend to be stronger and more dimensionally stable than welded components. Use of carbon fiber in the long cylinders could reduce the effects of temperature changes on the corrector focus. Fermilab has experience with and equipment for fabrication of this sort of carbon fiber structure. The cost difference between components fabricated of either forgings or weldments is minor. In some cases, due to shape complexity, forgings offer a considerable cost benefit. The material choice will be determined by the effect of the thermal expansion on the relative positions of the lenses and on a cost benefit analysis. The system is designed to allow assembly in either a vertical or horizontal orientation within the cage assembly. Once mounted to the telescope, assembly and disassembly can be accomplished with the aid of fixtures mounted to one of the prime focus cage end-rings.

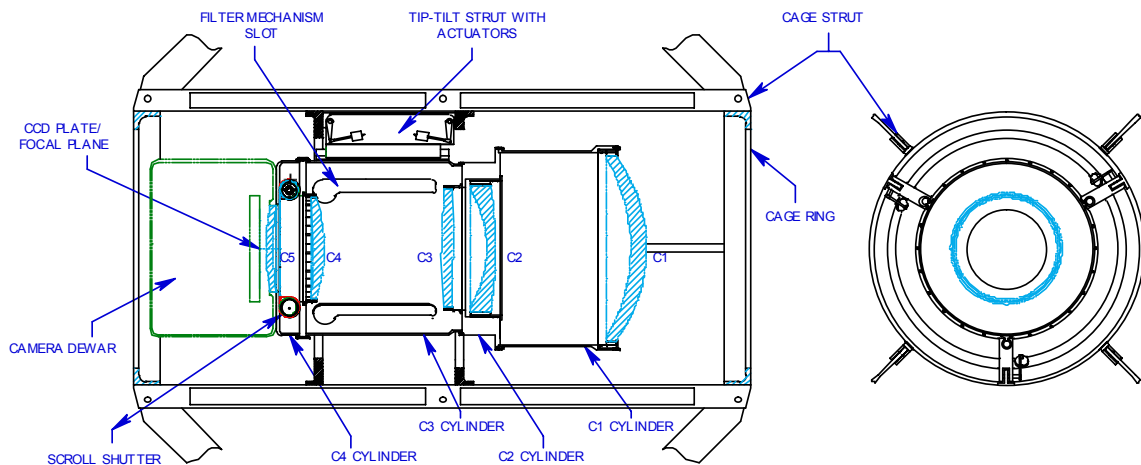


Figure 5.23 Corrector barrel in the prime focus cage

Interior and exterior finish is to be bead-blasted and painted flat black for steel, and bead-blasted and anodized for aluminum.

Weight comparison for aluminum or steel construction:

Camera with both corrector and cage fabricated of steel: 11625 lbs. = 5275 kg

Camera with both corrector and cage fabricated of aluminum: 5643 lbs. = 2560 kg

The entire corrector will be continuously purged with dry nitrogen to provide a stable and dry atmosphere for corrector elements and coatings. In particular, the C5 lens will be cooled via radiative heat transfer from the CCD focal array and will experience condensation if the purge is not maintained. Heaters may also be installed around the edges of this lens if further analysis shows that this is necessary to eliminate condensation.

5.13.3 Lens Mounting System

Lenses will be “potted” around their circumferences into Invar-36 rings (figure 5.24). These have CTE very close to that of fused silica and will offer a mounting platform for the lens flexure ring. These flexure rings will ensure that the lenses remain within centering tolerances while compensating for differential expansion between barrel and lens.

The potting material will be some form of Silicone product and will be specified as we approach the lens mounting in the production schedule.

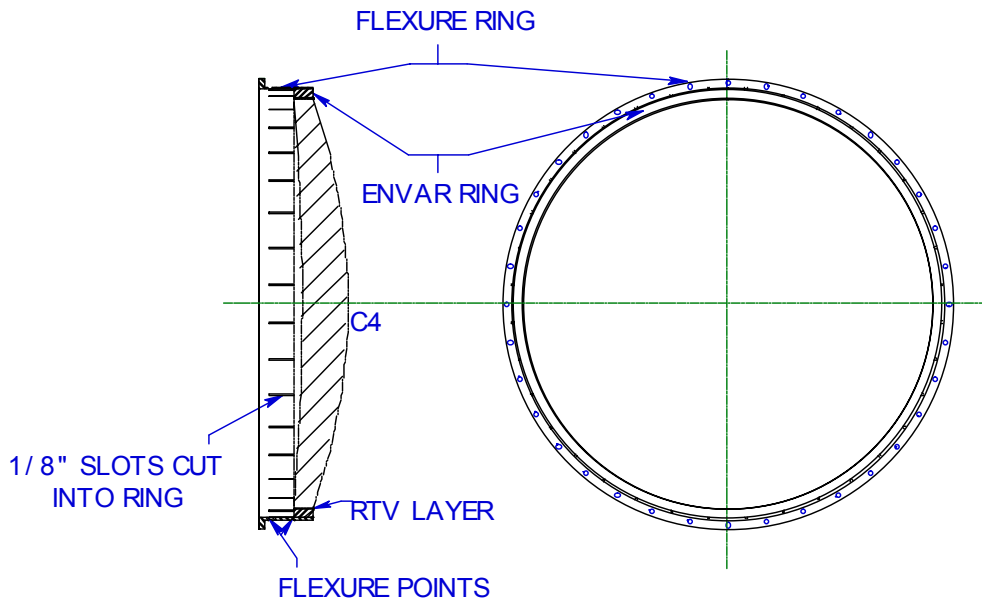


Figure 5.24 Lens mounting ring detail.

The Invar rings will incorporate a set of safety rims to ensure lens capture, should the Silicone bond fail.

This design, as mentioned above, will maintain the lenses on the optical center but will move with the barrel material parallel to the optical axis. This mounting system can be dimensionally altered to accommodate the final lens configuration after lens fabrication is completed.

5.13.4 Filter Changing Mechanism

Typically there will be multiple filter changes per night. For example, when the moon rises, the i and z band observing are not affected, while g and r are significantly degraded. This will motivate a filter change. We are designing a filter changing system which will make it possible to change the filters quickly and reliably. The time estimated for a filter change is ≤ 5 sec. and it will be possible to perform a filter change during slewing. The large space between element C4 and C3 is the optimum location for the filters and the filter changing mechanism. The implications of this choice are 1) these filters are quite large, $\sim 560\text{mm}$ ($\sim 22''$) diameter and 2) the guide and focus CCDs, which are located on the focal plane with the image CCDs, will see filtered light and thus must also be sensitive in the z band.

A modular approach is used for the filter changing mechanism. Cutting a set of four slots into the C4 barrel cylinder and mounting a guide rail inside this cylinder will allow easy installation and removal of each filter mechanism (Figure 5.25). These filter housings will be attached with a plate, employing threaded fasteners, to the slot side the corrector barrel. The opposite end of the filter housing will anchor to a receiving plate mounted to the opposite side of the barrel from the entry slot.

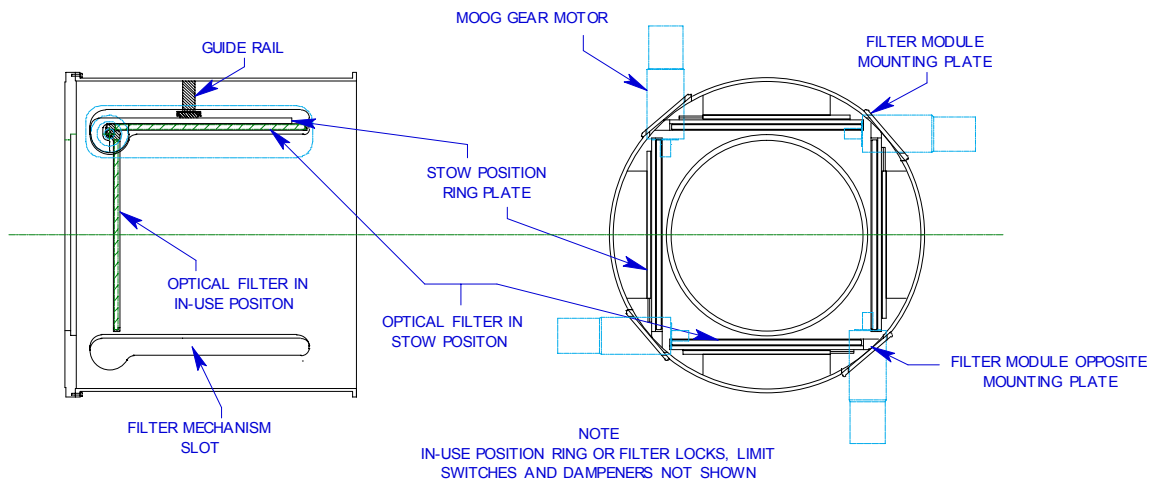


Figure 5.25 Filter changing mechanism

The filter housing will provide mounting surfaces for the filter locking pins, stop switches and motion dampeners. The drive actuators will be Moog gear head DC brushless motors with sufficient torque and speed to move the filters through their arc within 5 seconds.

We have incorporated a series of safety interlocks into the filter design. Encoders mounted on the motors will determine filter position and will be monitored by a controller. This controller will allow only one filter to move at a time. A torque limiting coupling, located between the actuator output shaft and filter mounting ring pivot shaft will prevent damage in case of collision with either another filter or its own storage ring. The receiving rings for both in-use and stowed filter positions will have limit switches wired in series to stop motor rotation. Two acceleration dampeners per filter per direction will be installed to prevent excessive contact

forces between the filter mounting rings and their receiving rings in both the in-use and stowed positions. Locking mechanisms will be employed on the receiving rings to ensure that the filter positions remain stable when in-use or in the stowed position while the telescope is in motion. This will also allow the actuator motors to be de-energized, minimizing heat-loading around the cage and corrector environment. The modular design will allow the filters to be removed and new filters installed in approximately an hour.

5.13.5 Focusing Mechanism

The focusing ring will be mounted to the same struts that comprise the tip-tilt adjustment system described below. This is done to ensure that the focusing ring rotational axis remains parallel to the corrector's optical axis when tip-tilt adjustments are made (Figure 5.26).

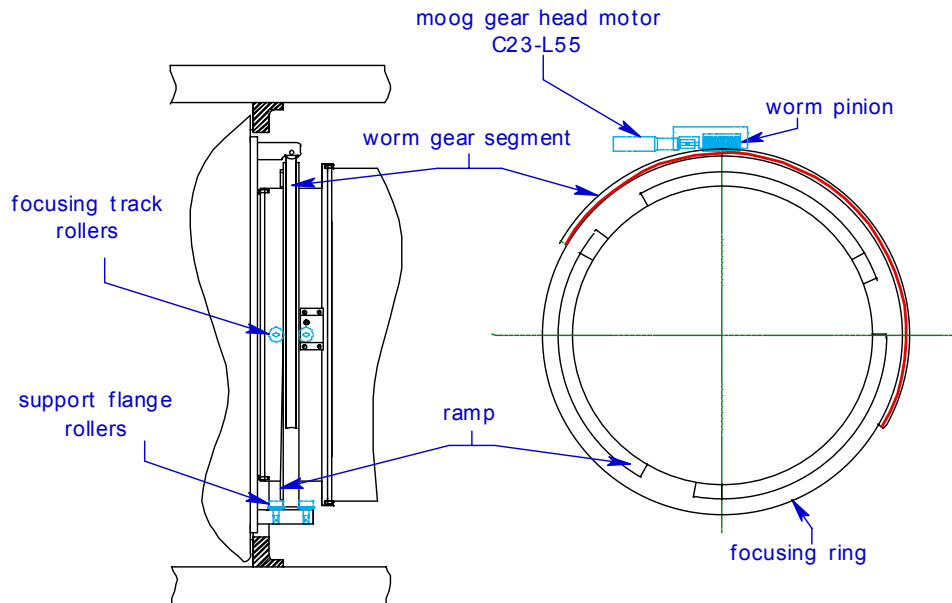


Figure 5.26 Focusing mechanism

An anti-backlash pinion for a worm gear segment mounted to the outside circumference of the ring and actuated by a small Moog gearhead motor will drive the ring. The ring will be supported through three sets of two flanged track rollers preloaded against each other on the outer rim of the ring and mounted to the adjustment struts through a strut-connecting ring. Axis motion parallel to the optical axis will be generated by a set of three ramps machined into the focus ring at 120° spacing and consuming a 90° arc on the surface of the ring. The ramps will rise 1/2" from the neutral surface of the focus ring. These ramps will be the guide surfaces for three sets of two preloaded crowned track rollers acting against each other through ramp surfaces. These track rollers will be mounted to the outside circumference of lens cylinder C2

and also spaced 120 deg apart. This system will allow extremely accurate and smooth movement of the focusing ring and will not require the gear motor to remain energized to hold position regardless of telescope motion.

5.13.6 Lateral and/or Tip-tilt Adjustment Mechanism

At this time, we do not know whether it will be necessary to adjust the transverse and tip-tilt for the focal plane actively (while the telescope is in motion). For our Reference Design we have a system that can be set up to do manual adjustments or, by incorporating a set of actuators, can be used to do active adjustments while slewing to a sky position. The tip-tilt is adjusted through the use of cams mounted on each end of the tip-tilt support struts (figure 5.27). There will be three of these strut units mounted between the cage and the corrector barrel, separated by 120° spacing. One end of the strut will be attached to the corrector through a set of bars housing linear bearings sliding on a shaft mounted to the outer circumference of lens cylinder C3. These linear bearings and shaft are part of the focusing mechanism.

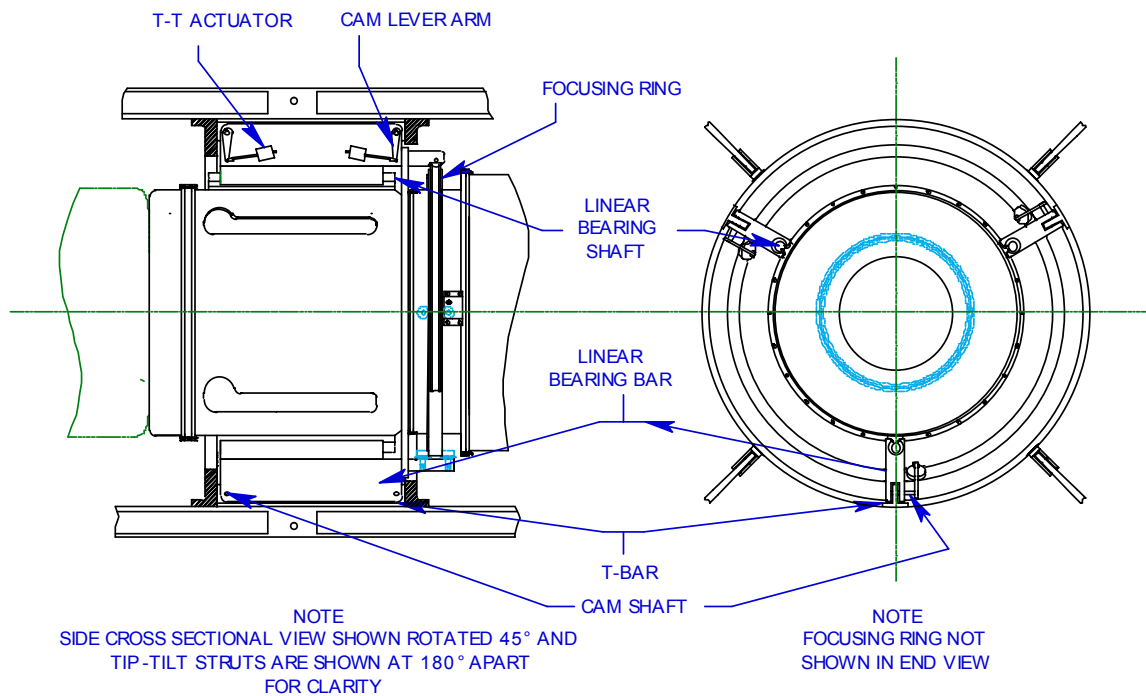


Figure 5.27 Lateral adjustment system

The opposite end of the strut unit will consist of a T-shaped bar mounted to cage rings. This T-bar will extend into an oversized slot, machined into the linear bearing bar. Two shafts, with cams machined onto them, will pass through the T-bar at opposite ends and be mounted into a spherical bearing that will allow shaft movement off the perpendicular axis to the T-bar surface. These same camshafts will extend through journals in the two tangs of the oversized slot in the bearing bar. A lever arm attached to one end of the camshafts can effect lateral movement between the two strut bars.

If used manually, the level arms are adjusted and the struts locked into position. If active adjustment is required, an actuator can be incorporated to move the lever arms. Should we need only lateral motion - movement perpendicular to the optical axis - a single actuator operating a strut's two lever arms would accomplish the task. If both tip-tilt and lateral motion become necessary, then using an actuator per lever arm will meet the need. This system can also be used to preload the linear bearings, thereby removing any unwanted compliance in the focusing system.

5.13.7 Scroll Shutter

The shutter employed for the Reference Design is a scroll shutter. The shutter will be driven in both directions and has been designed for 0.5 second maximum open or closing times (figure 5.28).

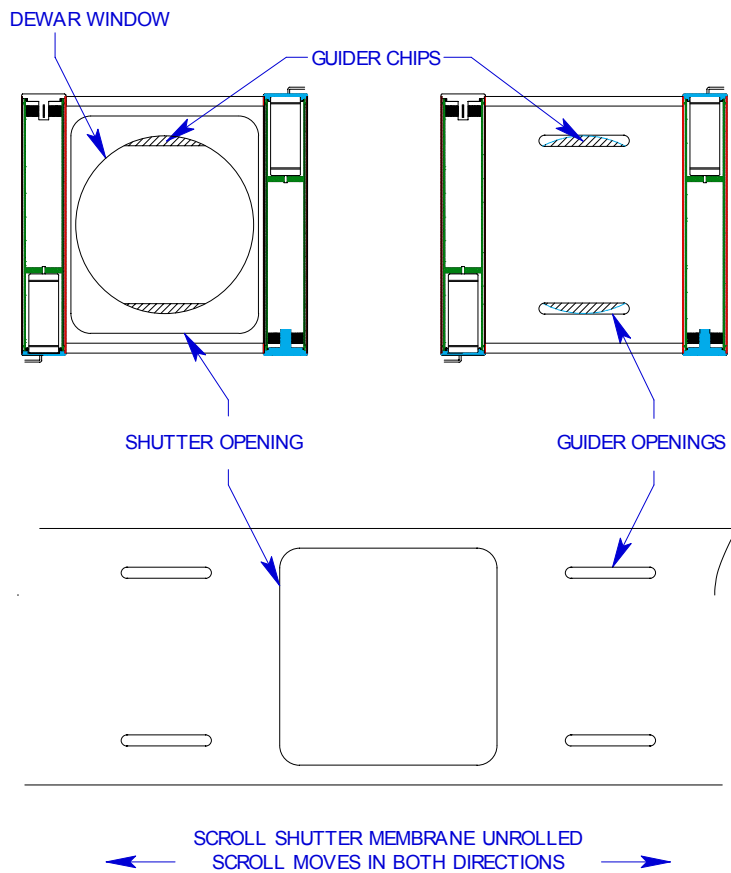


Figure 5.28 Scroll shutter design

The shutter has been designed as a stand-alone package that will provide for modular installation and removal from the corrector body. The spools will be driven by a set of Moog gear-head DC brushless motors with encoders for position monitoring. To ensure position and exposure time repeatability, sensors will also be mounted along the scroll track.

5.14 Auxiliary Systems

5.14.1 Guiding

The Mosaic II has two guide cameras in addition to the main image CCDs. The guide cameras provide small corrections for the telescope tracking system such that a star image will stay in precisely the same location during an exposure. The Blanco accepts these signals every 2 sec. We are currently investigating the options for guide systems. In our Reference Design we have CCDs on the focal plane devoted to guiding along the top and bottom of the focal plane. Corresponding slits in the shutter allow exposure of the guide CCDs prior to exposure of the image. Figure 5.29 shows the guide CCDs in the partially vignetted region of the focal plane. The MegaCam MMT project has a similar arrangement. Alternatively, we are also investigating the benefits of a separate guide camera. This type of camera could be constructed by our collaboration or purchased elsewhere. A pickoff mirror could be installed just in front of the shutter, outside the main image light path as shown in Figure 5.30.

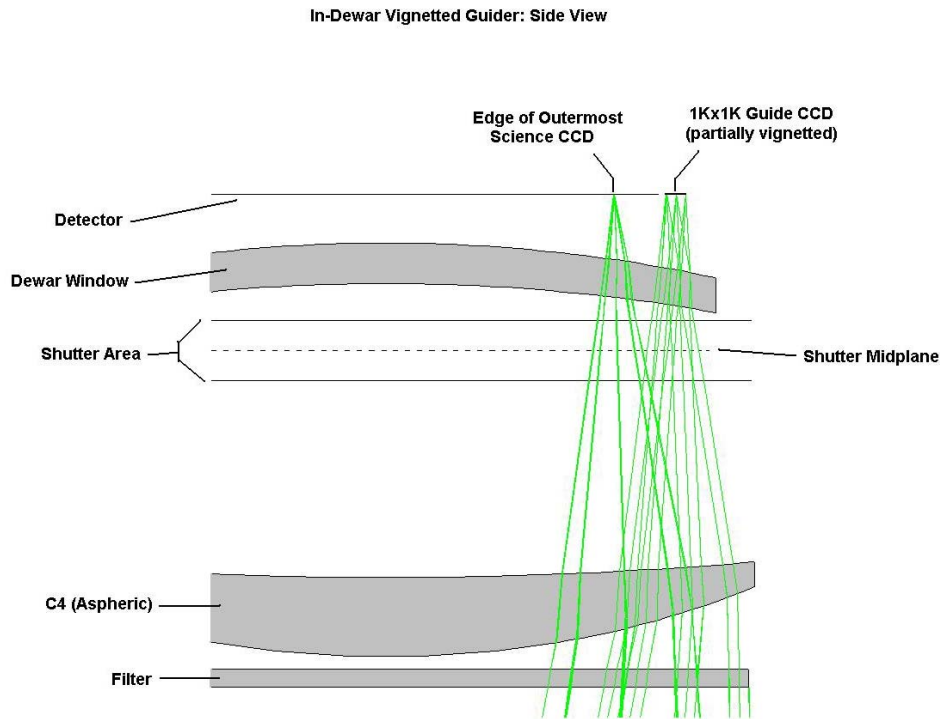
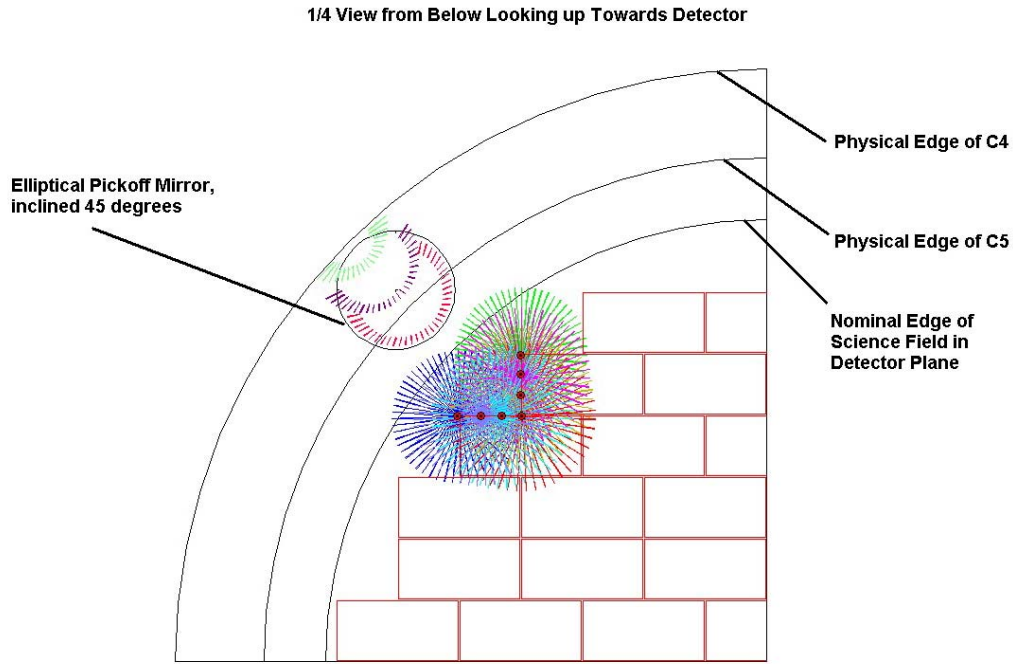


Figure 5.29 Schematic of guide system layout with CCDs on edge of focal plane.



Rays shown for points ● at edge of science field, as well as far-field rays incident onto the pickoff mirror.

Note that the ray bundles at the pickoff mirror are partially vignetted.

Note that rays are drawn from a plane level with the edge of the pickoff mirror furthest from the detector.

Figure 5.30 Schematic of guide system with a pick off mirror and separate guide camera

Guide camera CCDs have two requirements in addition to those listed in Table 5.2. These are a fast readout rate ($< \sim 1$ sec) and the possibility to operate in frame-store mode. The fast readout rate is needed so that corrections to the telescope position can be generated on a time scale that matches the 2 sec. update rate accepted by the Blanco control system. This faster rate also implies a separate DAQ path for the guide CCDs and this is discussed in section 5.11.

Frame-store mode is a technique for collecting clean images without the use of a shutter. This is accomplished by coating one half of the CCD with an opaque layer and collecting the image only in the other half. At the end of an exposure, the charge image is transferred very quickly (~ 1 ms) from the imaging side to the storage side. Once the image is on the storage side of the CCD, it is decoupled from the imaging side and a new exposure is initiated while the previous image is read out of the storage area of the CCD.

The $1k \times 1k$ LBNL CCDs described above are a good match for our guiding requirements. To cover the desired area we would need 4 of these CCDs (note only half of each CCD is used to collect the images). A readout rate of 240 kpixel/sec results in a readout time of ~ 0.9 sec. Reading out only a small area surrounding the guide star(s), once identified, would greatly reduce the readout time. Figure 5.8 shows 4 guide and 4 focus CCDs along the top and bottom of the focal plane layout. There is room for additional guide/focus CCDs if they are needed.

5.14.2 Cloud Camera

For accurate photometry a precise measurement of the atmospheric conditions is needed. We will use already existing infrastructure at Cerro Tololo (TASCA all-sky camera, Differential Image Motion Monitor (DIMM), Multi-Aperture Scintillation Sensor (MASS), and the Weather Station) to monitor conditions. Direct photometric monitoring using an already-existing CTIO small telescope as an auxiliary program is a possibility we will investigate. We may construct a cloud camera to further monitor the sky conditions. For our reference concept we follow the design of the cloud camera used by SDSS as shown in Figure 5.31. It consists of an IR camera from Raytheon, a hyperbolic mirror, a control communication system along with associated display and control software.

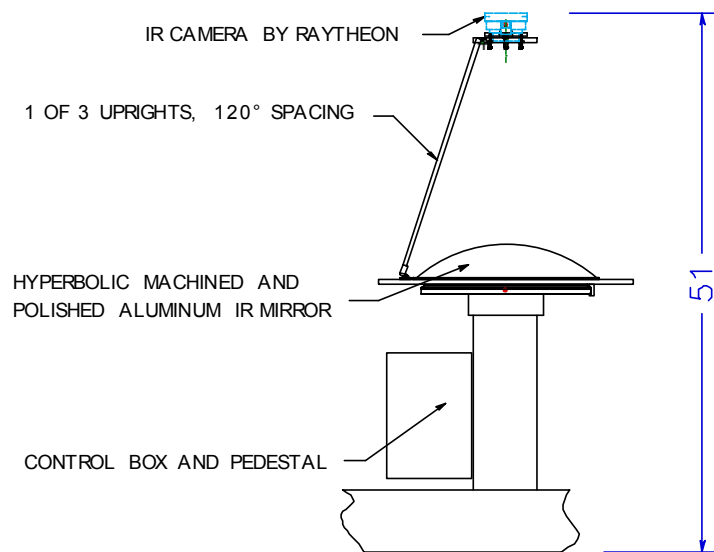


Figure 5.31 SDSS Cloud Camera

5.14.3 Full Camera Calibration System

We are considering development of a system to calibrate the instrument by measuring the response of the entire corrector and focal plane array package with monochromatic light, CCD by CCD. This would involve setting up a test beam that simulates the beam expected from the CTIO 4m primary, a $f/3$ beam, illuminated by an Optronic Laboratories OL-426 (TBD) integrating sphere calibration standard. The beam will illuminate a CCD with a calibrated surface brightness (radiance) at a given wavelength with a small spread in wavelength. We note that the test beam optics can be no closer than 1.5 meters from the focal plane, which gives as a minimum size for the test beam optics of 0.5 meters. The test beam will be able to illuminate any point on the focal plane array by being moved by a x,y translation stage.

The integrating sphere calibration source provides a calibrated surface brightness at the exit pupil of the sphere. This is converted to a collimated beam using an off-axis parabolic telescope. The collimated beam is converted to an $f/3$ beam by the test beam optics. This process will produce a light on the focal plane array that is stable and whose relative

wavelength characteristics are well known, but is no longer absolutely calibrated. If we need the absolute calibration we will require a calibrated photodiode on the DEC focal plane edge.

The output of this test beam will be system response curves as a function of wavelength for all the CCDs that make up the DEC focal plane array. Given this test capability, we will also be able to measure read noise, gain, and bad columns, and will be able to explore flat fields. If we develop the ability to mask the sphere's exit pupil to project a small Gaussian onto the focal plane array, we will be able to test the optics collimation.

These tests will be of the entire Dark Energy Instrument, from focal plane to corrector to data acquisition to observing programs. They do not replace the test stand testing of individual CCDs.

5.15 Activities at CTIO

5.15.1 Telescope Improvements (WBS 1.4)

There are two areas in which the Blanco telescope may be usefully improved to better support the Dark Energy Survey Project:

5.15.1.1 The telescope control system (TCS).

The TCS connects the operator's console in the control room to the array of remotely operable systems within the telescope building. It is normal that the TCS be upgraded from time to time and the Blanco's current system is now a few years old and several subsystems are becoming obsolete, overloaded or mildly unreliable. Whether or not the DES instrument is deployed at the Blanco, the TCS will be upgraded, but the arrival of the DES instrument will condition the direction taken by this upgrade.

The general scheme of the upgraded system will follow that of the existing system, but our intention is to migrate as close as possible to the system used to run the new telescope SOAR which is also run by CTIO (the TCS is LabView based). Our immediate intention is to upgrade the SunOS Linux computer, which hosts the operator interface, and the VME computer at the center of the system. As we progress, some of the various subsystems of the TCS may be replaced. The upgrade will seek maximum efficiency for the Dark Energy Survey's scheme of integration times of 100 sec with slews of a few degrees between each.

5.15.1.2 Image quality

The Blanco telescope and building has, over the years, undergone a number of modifications with the aim of reducing local atmospheric turbulence responsible for degrading image quality (or "seeing"). Essentially, such turbulence degrades the image as though by convolution with a Gaussian-like kernel of FWHM of order 1" and variable on all relevant timescales. This can be caused in part by poor temperature equilibrium between the telescope and its environment. Past improvements have involved removal of excess heat sources, relocating the control room to the ground floor, removal of all nonessential facilities from the telescope building, refrigeration of the dome floor, forced air cooling of the primary mirror in daytime, and the installation of doors in the sides of the dome to improve nighttime ventilation.

A range of possibilities remain to be explored, although it is difficult to identify precisely what may have the greatest effect. DECam itself is expected to improve over current prime focus image quality through the inclusion of an active cooling system to ensure its equilibration with ambient temperatures. We also continue to monitor and make occasional checks of the telescope environment with a thermal infrared camera to protect against the inadvertent introduction of new heat sources. Further improvements are under discussion, including increasing ventilation via additional dome doors or fans and the removal of further unnecessary parts of the telescope environment (including, possibly, the wholesale removal of nonessential walls). Nevertheless, it must be remembered that we are ultimately limited by the heavy steel and concrete construction of the telescope and building.

Image quality is also affected by the optical quality of the telescope. The Blanco does incorporate active support of the primary, although it is only possible to apply small correction of low order aberrations in a 50 cm thick Cervit mirror. This active control system is tuned up occasionally and future in-depth tests specific to the prime focus are planned. Again, DECam itself is expected to improve the quality of Blanco observations via a better corrector than that which is currently installed.

5.15.2 Commissioning at CTIO (WBS 1.5)

Here we summarize the plans for commissioning of the Dark Survey instrument at CTIO. On delivery to CTIO, we anticipate a period of commissioning before the instrument is ready to reliably produce scientific data. The stages of this process and estimates of the time investment required are as follows:

- Delivery.
- Unpacking (1d).

- Assembly of dewar (2d).
- Vacuum integrity verification (without mosaic installed) (3d).
- Assembly of mosaic and dewar (2d).
- Pump assembled dewar until specified vacuum quality achieved (5d).
- Mosaic brought to operating temperature (2d).

- Assembly of controller (1d).
- Verification of controller integrity (2d).
- Controller and mosaic connected (1d).
- Mosaic read out and verified (3d).

- Assembly of corrector (2d).
- Assembly and test of filter, focus, shutter and f/8 mechanisms (4d).
- Assembly of prime focus cage (1d).
- Integration of corrector, dewar, filter mechanism, focus mechanism, shutter mechanism, controller and prime focus cage (5d).
- Test of integrated prime focus assembly mechanisms (3d).
- Reference optical alignment of prime focus assembly (3d).

Some of these items can proceed in parallel. We estimate that it will take a total of 6 weeks to complete the reassembly and testing of all the components in the prime focus cage. We would then proceed with the operations that will impact telescope operations:

- f/8 mirror installed (1d).
- Telescope taken off line.
- Old prime focus assembly removed (1d).
- New prime focus assembly installed (1d).
- Balance the telescope (1d).

- Integration of DECam with Blanco TCS (3d).
- *In situ* verification of prime focus assembly mechanisms (2d).
- Reference, coarse alignment of prime focus cage (2d).
- Fine alignment of prime focus corrector and mosaic (2d).
- Fine alignment of f/8 secondary (1d).

- *In situ* characterization of DECam CCDs (3d).
- First light.
- Hartmann testing of DECam (1d).
- Shack-Hartmann testing of f/8 (1d).
- Fine tuning of optical system (1d).
- Photometric characterization of DECam on standard stars (4d).
- Astrometric characterization of DECam (4d).

At this point (12 weeks after delivery to CTIO) we are ready to take images and begin to commission the operation of the Dark Energy Survey Instrument. All software associated with instrument control, readout, and data handling will be fully tested and debugged before delivery. We estimate that this commissioning period will take 4 weeks.

5.16 System Integration (WBS 1.6)

The system integration task is largely one of document generation, maintenance and distribution, and control functions to verify compliance. The goal is to assure that the pieces that comprise the Dark Energy project fit together properly and work in harmony.

5.16.1 System Integration Organization

The integration of the DES instrument falls into two major categories: 1. the integration of the physical elements that are assembled into the cage, and 2. the integration of the cage and its internal elements with the telescope. The intention is to assemble the cage and test it at Fermilab, and ship it either as one piece or in a few large pieces to Cerro-Tololo for final assembly on the telescope. Each of the major subsystems that comprise the cage has its own engineer, who may have a particular specialty and multiple responsibilities. Out of this group, we will construct an Integration Committee that will advise the System Integration Leader and the Project Manager. After the project is baselined, changes required for integration issues will be passed up through the change control mechanism.

1. Project Manager ----- Change Control

1.6 System Integration

Integration Committee

Document control

Document distribution

1.6.1 Cage Integration

1.6.1.1 Mechanical

1.6.1.2 Electrical

1.6.1.3 Cooling

1.6.1.4 Optical

1.6.1.5 Controls

1.6.2 Telescope Integration

1.6.2.1 Mechanical

1.6.2.2 Electrical

1.6.2.3 Cryogenic & cooling systems

1.6.2.4 Telescope improvements

1.6.2.5 Telescope environment, power,
etc.

This particular organization covers the major functions that have to be integrated as we see the task now. It will evolve as we gain experience.

5.17 Summary

We have described a Reference Design for the Dark Energy Survey Instrument that meets our technical specifications. The Reference Design represents our current choices for the Dark Survey Instrument design and construction. However, further analysis may show that better, more cost effective options are available. Estimates of the corresponding cost and schedule for the Reference Design will be discussed in Chapter 7.

References

- 1) S.E. Holland, D.E. Groom, N.P. Palaio, R. J. Stover, and M. Wei, "Fully Depleted, Back-Illuminated Charge-Coupled Devices Fabricated on High-Resistivity Silicon," IEEE Trans. Electron Dev. 50 (3), 225--238 (January 2003)
- 2) Plot take from "An Assessment of the Optical Detector Systems for the W.M. Keck Observatory," by J. Beletic, R. Stover, and K. Taylor (January 2001).
- 3) J.P. Walder, et al, "A Low-Power, Wide Dynamic Range, Multi-Gain Signal Processor for the SNAP CCD " to be published in Proceedings of the Nuclear Science Symposium, October 2003.
- 4) To be published in SPIE, H. Oluseyi et al, "LBNL 4-side Buttable CCD Package Development".
- 5) Monsoon CCD readout system developed by NOAO.

6. Data Management

The Dark Energy Survey data management component will handle the data from the moment it is written by the data acquisition system onto a disk sitting on Cerro Tololo to the time when science and public archive ready data products are available in Illinois. The goal is to develop a series of automated pipelines that produce high quality data products with minimal human intervention. The data management effort will include a significant simulation effort to verify the pipelines during the construction phase and continually test the pipelines during the survey phase. Data quality assurance through autonomous processing, human visualization, and ultimately scientific analyses by the DES collaboration will lead to robust, science-ready data for the whole community. A philosophy that underlies this data management solution is to use existing, hardened code for the bulk of the reduction pipeline. Because large CCD imagers have been around for some time and are used widely in the community, we can draw upon a wealth of existing solutions. The primary challenge will be in scaling these solutions to an order of magnitude higher data rate and creating a seamless, overarching structure that coordinates the observing, reductions, archiving, public access and science analyses. The lessons we learn will feed the solutions being designed and developed for the Large Synoptic Survey Telescope, which is a far more challenging problem.

The survey will be organized to deliver constraints on the dark energy in concert with the South Pole Telescope (SPT) cluster survey after the second observing season. Science return from the other key projects (SN survey, weak lensing and galaxy angular power spectrum evolution) will also begin after the second observing season, with analyses of the full datasets available within one year of the completion of the survey. The public data releases will be organized into two efforts: (1) raw and fully reduced, astrometrically calibrated single-pointing images with the best available photometric calibration will be released to the public 1 year after they are acquired; (2) co-added images that are being built up in four bands together with associated object catalogs with photometry and astrometry to specified accuracy will be released once at the midpoint of the survey and then again one year after the completion of the survey.

The survey data management will be a collaborative endeavor led by the University of Illinois (U Illinois) and involving chiefly Fermilab and NOAO but also with possible contributions from the University of Chicago and LBNL. U Illinois and Fermilab will provide the bulk of both the personnel and the hardware resources necessary to support the data management. Our data plan must address not only the technical issues of data handling across the sites, but also the issues of distributed software and system development. Our data plan aims to leverage efficiently the expertise and resources from the participating sites. In this chapter we describe a collaborative approach to meeting our data management goals. We also address the use of the tools developed for survey data management for non-survey observations, such as those obtained during time generally allocated by NOAO to its user community.

6.1 The Development Process

The first step toward delivering the data management system is a design phase, which is already underway. The main deliverables of this phase will be:

- Detailed requirements for a data management system necessary which meets the science requirements
- A high-level architecture design
- A set of work packages—development modules that constitute the deliverable system components.
- A software development process
- A reference software environment
- Coding guidelines

Within Chapter 7 (“Project Management Plan”), we discuss how the collaboration will deploy its personnel to deliver these design components. In this chapter, we discuss the technical side of the design as it has been developed thus far. In particular, it is worth discussing how the development process will guide design and implementation.

The software process is the set of policies that we will follow to support the distributed development of the system. The process should be lightweight enough to allow sufficiently rapid development. The development process will include a design phase for each work package containing multiple stages, each capturing increasing detail (e.g. “conceptual”, “preliminary,” and “comprehensive”); these would be reviewed by the development team across the collaboration to capture overlap and interfaces between packages early in the process.

An important part of the software process is the definition of the *reference software environment*. This is the environment necessary to develop and run the software. It includes the target hardware platform types (e.g. clusters, single-node machines), operating systems, allowed computer languages, compiler versions, and necessary libraries. All software will be required to run in this reference environment. The reference environment should not be so restrictive as to make it impractical to run the software except on a few specific computers (the exception, perhaps, being hardware interface software), nor so permissive that we support unused platforms. At a minimum it should include the platforms that we expect to use during the operation phase. If the reference environment is simple to assemble, the code—particularly the pipeline software—will be more portable to other sites.

Informing the review process should be a set of coding guidelines. Usually language-specific, these define minimum coding practices that allow for collaborative maintenance of the code and efficient integration. The documentation practices form an important part of the coding guidelines. Meeting these guidelines will be required for the code to be considered complete and accepted by the project. Another important component are any requirements for the development of associated test code for the various software components.

Finally, we will deploy a software repository, building, and testing environment. All sites will have access to the code via CVS (or some other appropriate network-aware revision control system). The build system will “check-out” the code from the repository periodically and run a battery of test suites. Thus, a testing framework will be needed to enable automatic testing which can catch inadvertent “breakage” of the code throughout the build phase.

We expect to borrow heavily from the Sloan project at Fermilab and the CARMA Computing group at NCSA to deploy the software process. In particular, it would be straight-forward to reuse many of the technologies these groups use to manage their software processes, technologies like Bugzilla for error tracking, JUnit for testing, and *make*-based build systems.

6.2 Data Products and Data Storage

In the current camera design, the focal plane is tiled with sixty-two 2048x4096 science devices, and the ADC will deliver data with 16 bits per pixel. Each detector will have 2 readout amplifiers, and a full single-pointing image will be 1.0GB. Our current plan is for a single read of the DECam to produce 128 2048x2048 FITS images. We will organize each of these reads into a directory with a naming convention and header keywords that specify the readout amplifier and detector of origin. The raw data products coming from the telescope will be images with populated header information from the CCDs in the camera after exposure; these constitute level 0 products. We will produce roughly 100 TB of raw imaging data over the course of the survey. These must be calibrated to remove instrumental response. The individual calibrated images themselves will be of value to the astronomical community as the basis for research that lies outside the scope of our science goals; thus, they can be released as a “level 1” product.

The primary product that will form the foundation for the survey science—the level 2 product—will be a set of four image collection, one for each band, formed from the co-addition/mosaicing of all the data from the survey. The data will likely be stored (and made available) as regular tiles that share a single image scale calibration, covering the entire survey region; however, access to arbitrary mosaiced cut-outs will be made available. From the co-added images, we will produce a set of higher level (level 3) catalog products. Most notable of these catalogs will be a full object catalog listing photometry and positions for all detected objects in the survey.

The highest level products—level 4—are those produced by the science teams and form the basis of scientific analysis. Among these are the photometric-redshift catalog (containing photometry and redshifts for all galaxies detected), and the galaxy cluster catalog. The practical distinction between level 3 and level 4 products is in the applicable public release policy (described in section 6.4): level 3 products will be released to the public along with the co-added images, while release of level 4 products will be released by the time of the science publication.

Experience from the SDSS shows that data processing actually expands the data collection rather than reducing it. We estimate that after the first year we will need to house roughly 100 TB of raw and reduced data products. By the end of the project, the total storage needs will approach 1 Petabyte, though much of this can reside in secondary storage (i.e. tape).

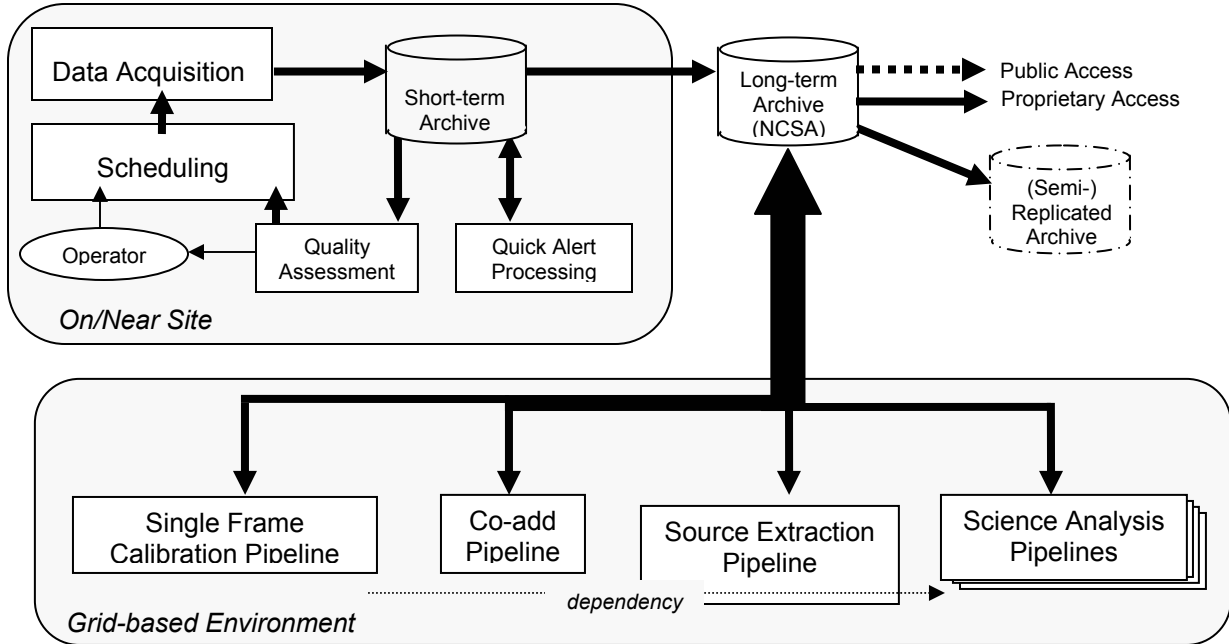


Figure 6.1 Dark Energy Survey Data Flow

6.3 System and Software Architecture

In this section, we outline the system and software architecture necessary to create and support the necessary science data products. Figure 6.1 illustrates the overall data flow. All survey data products—raw and processed—will be archived at NCSA. Our model allows some or all of the archive to be replicated at Fermilab or elsewhere in the collaboration. Similarly, while we expect that the NCSA processing resources (see section 6.5.5) will be sufficient for production processing, we adopt a grid-based architecture to allow processing to be shared with Fermilab platforms, as well as the wider grid community. This will be important when significant reprocessing is needed (we are baselining a complete reprocessing of the dataset after each observing season). Our initial requirement for grid architectures is aimed to support simulations that will be produced at Fermilab and analyzed at NCSA.

We see the pipeline as being made up of two layers. The “science” layer contains the software modules that contain the science algorithms to be applied to the data. The “data management” layer handles the execution of those modules as well as the management of the input and output data (i.e. transferring them from storage to the compute platform and back) within some execution environment. By separating data management and science software modules, the modules will be more easily adaptable to different execution environments.

In both layers, we would like to maximize the amount of software reuse. In the data management layer, we propose to build a framework from existing grid-based solutions. The major virtue of a grid-based architecture is its transparent access to computing and storage resources, regardless of the specific platforms being used. Not only will this lower the cost of developing the framework, it will be critical to leveraging the resources at both NCSA and Fermilab in a uniform way. We plan to take advantage of our previous experience with these technologies from the TeraGrid and the Open Science Grid Initiative to rapidly define our grid-based environment. In the science domain, we will draw from the existing, well-tested suites of astronomical software, only writing new software where the science demands a new implementation. This means that our software framework must support the execution environments of one—or possibly several—external packages.

6.4 Public Data Release and Pipeline Access

A public archive of the survey data will be maintained by NOAO and NCSA. This public archive will include raw and reduced (level 0 and level 1 data), single pointing images with astrometric and photometric calibration with uncertainties. The default photometric calibration will be carried out using USNO-B2 catalogs, which will provide a stable source of calibration information from the beginning of the survey. Over time we will build up directly calibrated DES imaging over the survey region; once we develop a robust calibration, we plan to transition away from USNO-B2 to an internal DES calibration. Our goal is to make this transition by the midpoint of the survey, when our first catalog and co-add data release occurs (see below). These reduced images will be made available to the public 1 year after they are acquired. Full reprocessing with improved algorithms will necessarily include some data that has already been released. These data will be replaced in the archive with updated header information to indicate the changes. In addition to these imaging-only automated releases, we expect to release the coadded images in each band and associated catalog information (astrometry, photometry, star-galaxy classification, etc) at the midpoint of the survey in 2011 and again one year after the end of the last observing season.

In addition, we plan to allow full access to the pipelines (and the pipeline software) that produce these single-pointing images and the coadded images. Cluster catalogs, shear maps, photometric redshift estimates and other derived properties will be released upon publication of the results and at the discretion of the individual science teams. These teams may choose to coordinate release of some products with the release of the level 3 products.

6.5 Overview of Data Management Operations

Following the development phase (2004-2008), the data management component will enter the operations phase (2009-2014). Naturally, the development is driven by the operational requirements of the data management component, and so we first describe the operations phase in some detail.

To estimate the nightly data production, we adopt an 8 hour observing session with an imaging cadence of 2 minutes. This corresponds to about 240 science images per night. To this we add 60 calibration images (assumed to be 10 flats in each filter, 10 bias frames and 10 dark frames)

to produce a total of 300 images or 300GB of raw data for the night. If we include a 30% data compression gain, then during the science observing, there is a sustained data rate of 0.4GB/min or 54Mbps. Add to this a 20% calibration overhead if the goal is to transfer the calibration data by the end of the night. It is likely that the raw calibration data can be transferred during the day following the observing, and only the final, reduced flats and bias frames are transferred to La Serena at the beginning of the night to facilitate the time domain reductions.

6.5.1 CTIO Operations

The DECam data acquisition system will deposit imaging data onto a disk storage system. We will install an “instrument cache” to capture all data flowing from the instrument. This will provide both a buffer for extremely rapid data quality analysis on a subset of the data and a queuing area for the data to be transported to La Serena. Nominally this would be a 4TB RAID “data brick” (\$9K today), which would provide safe storage for two weeks of observations or storage for shorter periods together with storage of calibrations and other standard files (catalogs, etc.) needed for and produced by the data quality comparisons. Data would be deleted from this mountain cache only when transfer to both La Serena and U Illinois is verified.

In general, we want to keep the mountain computing activities to a minimum, because (a) a viable link to La Serena will exist and (b) computing resources can be more easily maintained in La Serena. However, we have to expect failures in the link from time to time, and so key quality assurance processing must be carried out on the mountain. A fast workstation will be positioned on the mountain and used to process a subset of the data coming from the camera. This subset could be as few as 5 or 6 of the imaging nodes. These data would be fully reduced—including an astrometric and rough photometric calibration. This rough photometric calibration could come from either (a) the available USNO B2 stellar plate photometry, (b) the photometric solution derived from standard star observations that night, or (c) overlap with other calibrated DES imaging data. Image statistics such as the PSF and its variation, the sky brightness, the extinction, the estimated 10 sigma stellar photometric limit, and the number of bad or saturated pixels will be recorded in the survey database. A telescope pointing correction will be calculated, and the operator will be given the option of adjusting the pointing automatically. This same system will allow data visualization by the observer, and it could be used to produce the nightly calibration products to be sent to La Serena for the time domain analysis.

6.5.2 Data Transfer to La Serena

Assuming that raw calibration data will be sent post observing, the bandwidth requirements on the CTIO-La Serena link are driven by the need to transfer one science image before the next one is produced. Our minimum bandwidth needed for normal DES operations is then 1GB in 2 min = 54Mbps (assuming 30% compression). Including some contingency for overheads and other necessary network traffic (such as frequent video links between observers and survey scientists in Illinois), we should aim to have ~100Mbps available for normal survey operations.

The current CTIO-La Serena network connectivity is provided by a direct microwave link with 99.9% uptime design specifications which is shared between CTIO, SOAR, and Gemini.

The current bandwidth available to CTIO+SOAR (not including Gemini) is 155Mbps over one channel on the microwave link. Gemini operates over a separate 155Mbps channel, and the two channels provide backup/fail over for each other. Future network infrastructure could include an additional 155Mbps channel (the quantum for upgrades to the current link), which would cost ~\$50K today. If LSST is sited on Cerro Pachon, it is likely that NOAO and LSST will install a fiber link directly from La Serena to Cerro Pachon and Cerro Tololo. It may be possible to install this well before LSST's expected first light, possibly even before the commencement of DES survey operations. Such a fiber link would allow almost unlimited bandwidth for use by DECam and other high-data-rate instruments coming to Cerro Tololo and Cerro Pachon.

Although we would have room to cache two weeks of data on the mountain, in the unlikely event of a failure in the mountain to La Serena link, we would like to continue to move the data at a relatively normal cadence. This would be required to ensure full quality assurance and timely processing for time domain analysis. In the case of failure, we would use "sneakernet", shipping the data on disks down from the mountain and possibly all the way to U Illinois. This disk-based transfer (if done today) would be based on 1TB firewire/USB 2.0 drives, which could store three nights of raw data. We might plan to have three to five 1TB boxes (\$1.2K each today) on the mountain, ready for use in the event of such a failure.

6.5.3 La Serena Operations

Data processing at La Serena will focus on the SN alert processing. Roughly 10% of the survey time will be used for repeat observations of fields to find and follow SNe. Given the time sensitive nature of the data analysis and SN discovery, the main processing center for this component of the survey data will be in La Serena. DES/SN data will be analyzed for transients, and SN candidates will be automatically flagged for external followup (such as spectroscopy) and filed to a publicly accessible database. Candidates will be analyzed for color and light curve shape on the fly, which will facilitate the SN type and distance estimates, providing necessary information for prioritization of the candidates. This processing should be rapid enough that candidates are made available to the community before the next observing night. The processing infrastructure should be modular and scalable, allowing for the addition of processing modules. An existing solution to process the SN survey data, the SuperMACHO/ESSENCE projects' SM/SN pipeline, is currently in operation at CTIO. This pipeline handles 20 GB of raw CTIO 4m MOSAIC data (this camera is 7.5times smaller than DECam) in a night. The DES/SN component will deliver data at a rate of ~30GB/night, not far beyond the current data rate handled by the SM/SN computing cluster (20 1Ghz class CPUs). Thus, we expect the natural increase in CPU speeds between now and 2009 will enable a cluster of moderate scale to carry out these reductions.

6.5.4 Data Transfer to Illinois

We plan to use international network connectivity to automatically transfer the data from La Serena to the NCSA archive at U Illinois. Our goal is to completely transfer each night of data in under 24 hours. One night of data is about 300GB, so we need a sustained transfer rate of at least 21Mbps for the DES, assuming that we transfer only raw data and achieve 30% compression. Note that this assumes we do not bother transferring anything besides the raw data. To allow for contingency and overheads in the transfer, we require a bandwidth of

50Mbps for DES operations. Currently there is a 10 Mbps link directly from La Serena to Miami, where we access Internet2. This 10 Mbps is broken up “4/6/10”, where NOAO is guaranteed 4 Mbps, Gemini 6 Mbps, but either can burst up to the full 10Mbps. This link will definitely need to be upgraded in order to provide effective data transfer of DES data to NCSA. NOAO is currently actively pursuing a variety of avenues to provide a significant upgrade to its current international bandwidth. These efforts are being undertaken in collaboration with Gemini and other Chilean-based astronomical facilities. It is likely that the bandwidth will grow by 2009, the first year of observing for DES, and we will work with NOAO to make sure this happens.

This international connectivity will almost certainly not be as reliable as the connection from telescope down to La Serena, and therefore a backup data transfer strategy is an even higher priority. Although the transport time is significantly longer, the same “sneakernet” solution described above, regularly shipping TB disks, will be used in the case of extended network outages and/or when the network transfer gets significantly behind the real time data flow. Given that the NCSA data processing is not as time critical, the delay of approximately one week for international shipping should not pose a significant problem for the survey. It is however necessary to scale the NCSA (and/or grid) processing capability to be able to “catch up” with any significant delay by processing more than one night’s data per day.

6.5.5 U Illinois Operations

U Illinois operations will largely rely on NCSA computing resources for archiving and processing the DES data. The goals are to (a) produce calibrated single pointing images, (b) produce coadded images in each of the four bands, (c) produce object catalogs that will feed the science analysis, (d) provide for seamless collaboration and public access to the data, and (e) process the data at a rate faster than it is being produced. In addition, we expect to reprocess all the data from time to time as improvements in the algorithms and better calibration products become available. These goals require a large data storage facility approaching 500TB, modest real-time processing capabilities, and the development of grid-based processing algorithms to speed the reprocessing of the data. Below we describe each of these components in more detail.

NCSA has large amounts of storage available today, and there are plans to increase this capacity by more than an order of magnitude on the timescale of the DES. The NCSA director will provide 100TB of spinning disk storage together with mass tape storage of 400TB to support the DES reductions and archiving (see attached letter of support). All raw data will be stored, and processed data products like single-pointing images, coadded images and object catalogs will also be stored.

The single image processing pipeline will be the same as the one deployed for the SN alert processing in La Serena. The single pointing image will consist of 128 individual FITS images (one for each amplifier). Images will be bias and dark subtracted, flat fielded, fringe corrected, cross-talk corrected and pupil ghost corrected. An astrometric solution will be determined and WCS parameters will be stored in the header. Photometric calibration will be performed using calibration data from the night of observation, indirect calibration data from previously obtained directly calibrated DES data, or indirect calibration data from existing plate

photometry catalogs like USNO B2. The photometric zeropoint and uncertainty will be stored in the image header. As noted previously, the modules required for this analysis exist in a variety of packages currently being used to reduce similar data on a smaller scale.

The full dataset will be probed for time domain purposes during the processing at NCSA. Varying sources of value to the community will be flagged and released to the community through the system set up to support the DES/SN time domain science at CTIO.

The fully reduced single-pointing images will be combined or co-added into deeper images. This process will enhance the uniformity of the data (removing blank spots caused by chip gaps, reducing PSF variations) and will allow us to push to the depths required to obtain cluster photometric redshifts out to $z \sim 1.3$. There are existing solutions for this pipeline as well, and we will be examining these to see how they perform under seeing variations and image depth variations. We will construct a pipeline that will deliver accurate star galaxy separation and galaxy photometry based on the DES data.

Cataloging will be carried out at many points in the data management. Object lists will be needed for the astrometric and photometric calibration of the single-pointing images. Time domain astronomy requires comparison of photometry in multi-epoch single frame images. Science-focused catalogues will be derived primarily from the co-added images (except for time domain science), because faint object detection, object characterization and corruption caused by edge effects will be less of a problem in these data.

There are many available cataloging programs, and some have seen extensive use. We plan to explore a range of cataloguers, but our strawman application is SExtractor, written by Emanuel Bertin. This cataloguer is very fast, produces simple ASCII object lists, and we have experience using it to do science.

Data reprocessing is inevitable. We will plan to reprocess all the data during the periods March-August, between every observing season. This may not be necessary, but we will adopt this processing in our strawman design. We will develop and apply grid based processing algorithms for this reprocessing, which will significantly speed the process. Single-pointing processing can be data-parallelized at the level of one night's data trivially, and further partitioning of the data is also possible. The DES will serve as a challenging test application for the computer science community at NCSA, Fermilab and elsewhere as they develop the next generation tools.

6.5.6 Fermilab Operations

Computing facilities at Fermilab, managed on behalf of the DES project by the Experimental Astrophysics Group and the Computing Division, will be configured as processing node in our deployed pipeline framework. Part or all of the archive will be replicated there as well, allowing us to leverage resources there for processing as needed. While we expect that much of the day-to-day processing will be carried out using NCSA facilities, we expect to make heavy use of Fermilab resources during bulk reprocessing. We also expect to use Fermilab facilities in part to support the generation of some level 4 products and the science analysis of those products.

6.5.7 Science Operations

Science operations will be underway at all five collaboration sites. In addition to the primary data processing, time domain and simulation pipelines described above, there will be a series of special purpose, science focused pipelines developed to facilitate the key science program, a study of the dark energy using (a) cluster surveys, (b) weak lensing studies, (c) galaxy angular power spectrum evolution and (d) SNe Ia distance estimates. The DES science operations and data management are separate components of the project, but close coordination and broad avenues for feedback are required for the efforts to succeed. The data management will facilitate the science operations, and the science operations will be a key data quality verification tool for the DES.

6.6 General User DECam Data Management

While we have focused on the data management for the Dark Energy Survey in the previous sections, we recognize that the DECam instrument will also be commonly used as a facility instrument for observers granted time through the normal NOAO time allocation process. Indeed, as we outline in Chapter 9, there are many exciting science cases for use of this wide-field instrument on the Blanco 4m which lie well outside the DES science case. Given the size of DECam images, pursuit of those and other observations by NOAO users will require significant resources to transform the raw data into data products ready for scientific analysis.

Fortunately, the data reduction requirements for almost any scientific project using the DECam instrument will share the general requirements of most of the DES processing steps described above, at least through production of level 2 and possibly level 3 products (stacked combined images and catalogs, respectively). Thus, while the DES collaboration itself cannot take responsibility for actually delivering such reduced data products to all users, the collaboration will work closely with the NOAO Data Products Program to ensure that the software can be run on general user data to provide level 1, 2, and 3 data products for NOAO users and the NOAO Science Archive.

Indeed, a significant portion of the DES pipeline and infrastructure will be installed and run on-site at the La Serena facilities in support of the DES/SN program. Working with the DES, the NOAO Data Products Program can build upon this foundation of both hardware and software to provide general users of the DECam with reduced data products on timescales similar to those required for the SN analysis, usually within less than 24 hours, if not in near-real time. The rapid availability of such high quality data products would not only make use of the DECam feasible for general users, it could also open new opportunities for exciting scientific programs which require rapid analysis for the planning of observations on subsequent nights, either on the DECam or other followup telescope facilities.

The archiving both raw and reduced data products from general DECam use will be the responsibility of the NOAO Data Products Program. However, it should be noted that NOAO and NCSA are currently developing a close data management collaboration covering the transport, storage, reduction, and retrieval of current and future NOAO data products through advanced archives, portals, and the VO. It is therefore highly likely that the final processing

and archiving of the data obtained by general NOAO users will be done in collaboration with NCSA, using much of the same infrastructure (both hardware and software) used in support of the DES.

6.7 Work Packages

As will be described in Chapter 7, we will manage our software development through a well planned work breakdown structure (WBS)—a hierarchical organization of tasks necessary to complete and operate the data management system. Work packages, which form the second level of our WBS, represent a logical component of the system that should be designed and implemented as an integrated unit. In this section, we summarize each of the work packages necessary to enable the operations described in the previous section. These packages are numbered according to the project WBS outlined and displayed in Ch. 7. While the focus of this section is on the purpose of each package and the expected approach to design, estimated person-power costs are also given (in units of FTE-months). We revisit these packages and cost in the next chapter where we discuss costs and schedule.

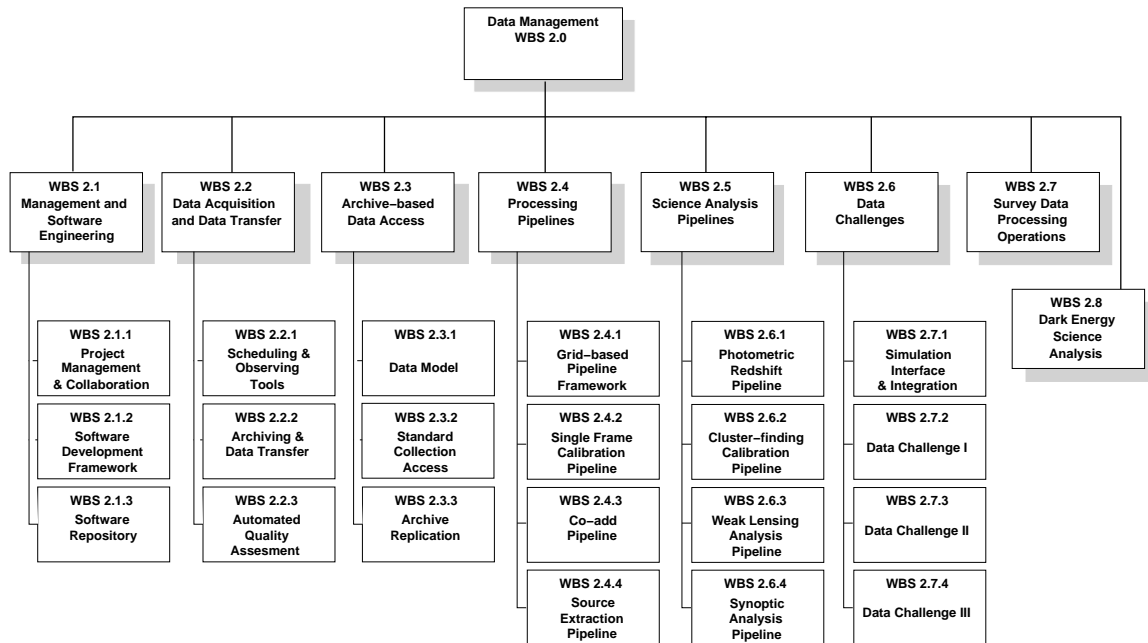


Figure 6.1. Dark Energy Survey Data Management Work Breakdown Structure

WBS 2.1 Management and Software Engineering (20 total FTE-months)

WBS 2.1.1. Project Management and Collaboration (FTE-months: 12.0*)

This package covers time and effort by the Project Manager necessary to manage and track the development of the software. Each developer will spend time participating in design reviews and regular telecons.

WBS 2.1.2 Software Development Framework: (FTE-months: 6)

This package covers the software that supports our data management development. It includes an automated system for building and testing the software (apart from the simulation testbed). It also includes work that might come with managing code review activities. It may also include software for packaging our software and delivering to the processing platforms. This package will depend critically on the high-level choices to be made by the DMSC, including the definition of a software design and review process and the design reference platform, discussed in section 6.1.

The build system can be built on GNU make or Apache Ant, drawing on the experience within our group developing and using build systems that operate in an distributed environment. Tinderbox (used by CARMA) can be used to monitor and test automated builds.

WBS 2.1.3 Software Repository: (FTE-months: 1 months)

This package concerns the setting up and maintenance of a shared repository for software. This repository will have two parts to it. The tools half will house third party software, imported for reuse in the DES DM system. The other half will come in the form of a CVS archive maintained at NCSA with remote access enabled; this archive will hold all software that is written specifically for this project. This package includes the initial design and setup as well as on-going maintenance.

WBS 2.2 Data Acquisition and Transfer (20 total FTE-months)

WBS 2.2.1 Scheduling and Observing Tools: (FTE-months: 12)

This program will include a GUI that serves as the observer's primary interface with the camera and the telescope. The tool will be an expert system of sorts to remove the vagaries of observing and observers from the long term survey. Interaction with the survey database will be critical, as this program determines the observing sequence and allows inputs from the observer on any changes to that program. For example, on a typical night this program will select an observing strategy given the seeing, transparency, lunar phase, and date. This interface will drive the transition from filter to filter at a single pointing (using either the dark time set g/r or the bright time set i/z) or send commands to the telescope for short slew to the next pointing. The tool will send readout commands to the camera guider devices, using expected positions of guide stars of interest to select subchip regions. In addition, the tool will trigger data quality calculations on each frame that comes off the camera, and use the results to adjust the observing plan.

A variety of observing modes will have to be supported, such as: (a) main survey mode, (b) SNe time domain sequences, (c) dither patterns for deep exposures in a single field, (d) dome

* this estimate assumes 8 hours per week for the Project Member and 2 hours a week for each additional developer. The number of developers, of course, depends on the cost of the estimated cost of the other packages. We assumed two additional programmers and a four year development period.

flats, (e) sky flats, (f) dark and bias frames, (g) photometric calibration sequences, and (g) simple point and shoot. This range of modes should provide for efficient observing both for survey operations and for non-survey, visiting astronomer use.

This program will automatically display some components of each frame coming from DECam as well as a range of image statistics. As part of the data quality assessment carried out on each frame, an astrometric solution will be calculated. This will enable automated updating of the telescope pointing, and over time these updates can be tracked and folded into an improved pointing model for the telescope.

There will have to be a monitoring component of this program that keeps watch on a wide range of important camera, telescope, data and weather issues that together specify the observing environment for the night and impact the data quality. For example, detector temperatures and LN2 levels within the dewar should be monitored. Seeing from the seeing monitor, seeing from direct measurements on the DECam frames and transparency should be monitored. Disk space on the data acquisition computer and the progress of data transfer to La Serena and NCSA should be monitored. The observer will be alerted when any monitored quantity begins to fall outside a predefined allowed range or begins to trend toward one of these boundaries. We will draw upon experience at Fermilab with a similar system used in the SDSS.

Tools with much of the functionality described above already exist at CTIO and other observatories. The freshest component of this tool is its expert capability in planning a night of survey observing, given the state of the data already taken and the observing conditions. Efficient interaction with a survey database, where data quality for each image is stored, will be critical. Development of this tool must involve CTIO telescope experts led by Tim Abbott, the data acquisition team led by Jon Thaler, the survey strategy team led by Jim Annis as well as the data management team.

WBS 2.2.2 Archiving and Data Transfer: (FTE-months: 4)

The goal of this package is to accept the raw data from the data acquisition (DA) system, deliver it to the time-critical processing center in La Serena, and from there deliver it to the long-term archive at NCSA. This package may include some facilities that aid the DA in producing proper level 0 data products; for example, it may provide an interface that allows the DA to include scheduling related metadata in the output FITS files. It may also include software for managing the on-site and La Serena data caches. An automated system for data mirroring will continually transfer data from the telescope site through La Serena to NCSA. At NCSA, a data ingest module will be necessary for “ingesting” new data products into the archive: this includes extracting metadata from the datasets for loading into an observation database as well as organizing and packaging the data files for long term storage.

The raw data—i.e. the level 0 products—will be stored in the archive as FITS files, ensuring they will be readable well beyond the supported life of the project. To avoid any data transformations—and thus opportunity for data corruption—before the raw data is archived, the DA system should write the data directly into FITS files. Standard community code (FITSIO) will be used to read and write this data. Data cache management and data mirroring

will leverage a general purpose system being developed jointly by NOAO and NCSA; this work in turn is leveraging existing software currently in use by these partners (including the Storage Resource Broker, SRB; the queue-based image caching system used at NOAO, STB; the open source mirroring tool, rsync; the rsync-based data transfer system for the BIMA telescope, the data cache management system used by the BIMA Data Archive, and Fermilab/Jefferson Lab/LBNL Storage Resource Management SRM). Data ingest operations tend to be highly project-specific; thus, there is less opportunity for reusing software for this task.

WBS 2.2.3 Automated Quality Assessment: (FTE-months: 4)

Tools to automatically evaluate the data quality will be critical to the success of the Dark Energy Survey. We will deploy these tools at the telescope to assess a fraction of the imaging data (~10%) from each exposure. We could deploy these tools in La Serena to fully characterize the data coming from the mountain, and we will deploy the same tools at NCSA and elsewhere, where full scale data processing is carried out. Specific characteristics of interest include: (a) PSF statistics and variations over the field, (b) sky brightness and variations, (c) transparency and photometric zeropoint estimates, (d) number of bad pixels or saturated pixels, (e) bias levels and their variations, (f) number of detected stars and galaxies, and (g) perhaps even object by object comparisons within some magnitude range to previously obtained DES frames (or the USNO-B2 catalog when no DES data are available). Object by object comparisons could examine the scatter in the photometry as well as the star/galaxy classification.

The tools required for automated quality assurance largely hinge on a robust cataloguer (i.e. SExtractor), automated astrometric solutions (required as a standard part of the processing) and efficient correlation of catalogs. As our experience with the DECam improves, we will undoubtedly want to build in new data quality tests.

WBS 2.3 Archive-based Data Access: (12 total FTE-months)

WBS 2.3.1 Data Model (FTE-months: 2)

The data model is a description of all the data entities and their logical relationships managed by the system. Access to the data typically reflects this data model as it is used to organize the data. In this package, we inventory the data streams and products to ensure we can capture all of the information necessary to meet our goals. We will define all of the catalogs and forms of the image data products to ensure efficient and correct processing. We must also ensure that our exported metadata is sufficient to make the data useful to the community, particularly within the Virtual Observatory. In addition to establishing an overall abstract model, we will also identify the technologies we will use to instantiate the model (e.g. XML, RDBMS, etc.), store data on disc, and track information through the processing pipelines. We expect that our model will evolve during the development phase as we better understand the processing techniques.

WBS 2.3.2 Standard Collection Access: (FTE-months: 7)

The goal of this package is to provide uniform access to both proprietary data (by scientists and pipelines within the project) and public data (by outside users). Logical access typically

reflects the data model used to organize the data. This package must incorporate the two main types of data products we manage, namely, files (primarily images) and catalog data (stored in databases). It must also incorporate the different product levels and the access rights associated with each of them. The data model will be used then to organize the data products both in physical storage and in the logical views presented by access interfaces. There will be a variety of access interfaces: programmatic access locally differs from programmatic access across the grid using the techniques of the Virtual Data Toolkit (VDT), and both are different from public access to the data via the protocols of the Virtual Observatory (VO). Interactive access is also important: web browser based methods are crucial for efficient community scientist access to the data and often scientists within the collaboration will find this useful to download proprietary data. To the practicing scientist `wget` and `rsync` are often the data transport mechanisms of choice. In all of these forms of access, access rights must be handled transparently, or at least in simple clear ways. Access to file data will be based on logical identifiers as this allows mapping to the closest (in terms of the network) physical copy of the file from any one of the replicated archives or data caches at any of the sites.

This package may also be able to leverage the emerging data management collaboration between NOAO and NCSA; however, we should plan to handle the development within this work package. Since data models are ultimately project specific, there is limited opportunity for reusing an existing design; however, we will leverage the considerable experience among the partner institutions in this area. We will use an off-the-shelf database that can be easily deployed at all sites; it will be used to store the observation catalog and the various science catalogs. We will employ a grid community tool like SRB or the replica location services in the VDT to track replicas of files and databases across our sites. SSL and the Globus Security Infrastructure (GSI) will be employed to honor access rights. Interactive, browser-based access to data also tends to be project specific (as it reflects the data model); thus, a fair amount of implementation (albeit, based on access patterns typical of many data archives) will be needed here. This will include catalog search and browsing pages. We plan to use existing software to enable the cut-out service. Strategic use of VO standards (like VOTable for exporting catalog data) will allow us to leverage existing data browsing tools. The other component of interactive access is support for downloading data in bulk; here we can leverage the Data Retrieval Tool (DaRT), currently employed by users of the BIMA Data Archive. There is some activity within the Grid community to provide tools and standards for database access; we will consider any such tools that might exist and are sufficiently mature.

WBS 2.3.3 Archive Replication: (FTE-months: 3)

The purpose of this package is to allow transparent replication of portions (or, in principle, all) of the DES archive. The replication framework will be based on the organizing principles of the project data model. This package will define an interface that compliant archive mirrors may use to request bulk replication of file-based data via whole collection identifiers. A separate interface will be needed for database replication. Data replicas will be managed by a replica management system deployed via package 4.2.2.1. The actual data copying will also be handled by the same data transfer system as described by the “Archiving” package.

WBS 2.4 Processing Pipelines: (51 total FTE-months)

WBS 2.4.1 Grid-based Pipeline Framework: (FTE-months: 9)

The goal of this package is to provide a common data retrieval and execution environment for pipelines to run at any of the processing sites in our system. This grid-base environment will feature a set of common services that provide:

- **Access to data through logical identifiers.** This allows any platform at any site to retrieve any data in a location-independent way.
- **Authentication and Authorization Services.** These will be used to honor access rights to data and computing resources.
- **Pipeline job execution.** The framework will provide a common method for executing applications that hides platform-specific details.
- **Workflow management and execution.** This allows a complex chain of pipelines to be executed and monitored.
- **Process monitoring, error detection, and error recovery.** We will have an automated way of capturing and monitoring output messages from processes and detecting problems. This facility is key to enabling recovery from common environment-related errors (e.g. network is down).
- **Automated archiving of processing products.** When a pipeline has finished the processing for a set of data, the products will be automatically ingested into the archive.

The existing Virtual Data Toolkit provides a convenient package that implements these services. In addition to these services, the framework will adopt a programming model that hides details about the data and execution management from the software modules containing the science algorithms. This will ultimately make the modules more portable and applicable beyond the automated DES pipeline processing (e.g. application to guest observer use of the DES camera).

These services will be “grid-based” in the sense that we will employ existing, off-the-shelf tools from the grid community that are designed for flexible, distributed computing. Among the existing grid solutions that are relevant to our system are:

- **Data Access:** SRB, Globus Replica Location Service (RLS), gridftp
- **Security:** Globus Security Infrastructure (GSI), ssh
- **Job execution and workflow management:** Globus GRAM, Condor, Chimera/Pegasus, OGSE OGRE.
- **Process monitoring:** Globus GRAM

We will benefit from the considerable experience at NCSA and Fermilab in grid computing.

WBS 2.4.2 Single-Frame Calibration Pipeline: (FTE-months: 12)

This pipeline will take raw level 0 data and reduce them to level 1 data. We expect the level 0 data to be in the form of 128 FITS files, one for each readout amplifier in operation (2 per chip). Much of the reduction of a single pointing will essentially be the independent reduction of 128 4Kx1K CCD images. Reduction will include bias subtraction, flat fielding, fringe correction, cross-talk correction (if needed), pupil ghost correction, and masking of bad pixels.

Astrometric solutions will be recorded using WCS parameters within the image headers. A photometric zeropoint, associated uncertainty and source will be recorded in each header, using either the photometric solution obtained from standard star observations that night, crude calibration using the plate photometry of the USNO-B2 catalog, or previously calibrated DES data taken over the same portion of the sky. These level 1 data will be the primary inputs to produce the co-added imaging, and all level 1 and level 0 imaging data will be archived and released to the public 1 year after acquisition. It is important that the single-frame calibration pipeline be relatively fast; a goal will be to produce the level 1 products from the level 0 products during the time it takes to obtain the next set of level 0 products. While at the primary processing station at NCSA this is not absolutely necessary (because full nights can be processed in parallel), having a fast pipeline will allow a more complete data quality assessment to be run on the data flowing from the camera each night, and this will enable more rapid feedback to the survey operator.

There are many tools available in the community that can be drawn upon to build this pipeline. Tools of special relevance are those currently in use in the SM/SN MOSAIC survey pipeline at CTIO and the MOSAIC imaging pipeline under development at NOAO. Using these and other existing pipelines, we will produce a pipeline tuned to the data from the DECam, with emphasis on parallelization and fully automated execution.

Issues that will require special effort will be the astrometric solution for the field. We will obtain imaging data of open clusters and other relatively dense stellar fields to characterize the field distortions. This together with the relative positions of the 62 DECam devices, should in principle allow an accurate astrometric solution over the full field to be calculated with only a few free parameters: (a) the field center in Right Ascension and Declination and (b) the amplitude of atmospheric dispersion variation over the field (which will depend on air mass, filter, and pointing direction). While in principle there should be more than enough stars ($\sim 10^3$) to calculate an astrometric solution directly in each field, fully characterizing the field distortions and then using that mapping in deriving the astrometric solution could offer several advantages: (a) stellar positions from only a few of the chips would be needed, reducing the computation required to calculate the solution (especially important on the mountain), (b) using a well characterized distortion map should lead to more accurate astrometry assuming the chips do not wander with time, and (c) bringing together all catalogued astrometric standards from the full field for an astrometric solution places limits on the parallelization of the single pointing calibration pipeline.

Lastly, we will have to consider whether production of masks are necessary at this stage. The user, whether they be pipelines downstream or community scientists, often want to know which pixels in the image are saturated, which pixels are affected by bleed trails, which pixels are on or adjacent to bad columns, which pixels are affected by cosmic rays, and even which pixels are affected by satellites and meteor trails.

WBS 2.4.3 Co-add Pipeline: (FTE-months: 12 months)

The level 1 products in each band will be combined into images of greater depth, uniformity and photometric accuracy. We refer to these co-added images as the level 2 data, and we expect that the bulk of DES science (excepting time domain science) will be carried out on

catalogues created from an analysis of these level 2 images. The structure of the level 2 images will be FITS files containing square tilings of the full survey region. The solid angle of these square tilings could range from 1 deg^2 to 10 deg^2 , and the sampling should be approximately a factor of two finer than the intrinsic sampling of the detectors (i.e. 0.125 arcsec pixels in the level 2 data). This implies a library of 500 to 5000 level 2 images for each of the four bands. Characteristic sizes of these images would range from 3GB to 30GB, depending on the solid angle and the adopted pixel size.

The process of combining multiple images of the same part of the sky is complex, because in general the image quality and depths vary from exposure to exposure. Nearby objects can even move from epoch to epoch, complicating the co-adding procedure. There are several existing techniques and software modules used to combine multiple images of the same part of the sky. In general, the surface brightness within a single pixel in a level 2 image will be estimated from pixels or sets of pixels within multiple level 1 images by a mapping that conserves flux. The co-adding process requires combining these multiple constraints in a manner that accounts for variations in seeing, zeropoint and image noise, and thus we will have to track both the number of images that went into each pixel and the error associated with each pixel, for every pixel within a level 2 image. We will test some of these schemes with emphasis on the returned photometric accuracy and combined image quality. Ultimately, we will likely deploy a tool based on several packaged that will produce the images that make up the map of the level 2 on the available level 1 products for a variety of criteria: best seeing, deepest photometry, smoothest PSF. These different filterings of the level 1 products are driven by different science goals; ; for example, the weak lensing science may benefit from a more stringent seeing limit that will sacrifice depth, whereas the galaxy and galaxy cluster studies will benefit primary from depth as long as star-galaxy classification isn't compromised.

Level 2 processing will generally be carried out multiple times, and it is this processing which will benefit most from the grid-based computing model. In principle, each level 2 image is independent of the others (although in the end we will want to stitch together the photometric zeropoints to yield seamless transitions from one image to the next and to maintain photometric uniformity across the full survey). Thus, the level 2 processing is easily parallelized, and so tasks can be carried out in parallel on hundreds to even tens of thousands of processing nodes.

In addition to the actual co-add pipeline, we will require tools that can extract images of a particular size, sampling, and location from this archive. There are several image extraction tools available, and we will adopt one of those for this purpose.

WBS 2.4.4 Source Extraction Pipeline: (FTE-months: 12)

Cataloging will be carried out for each image in the creation of the level 1 data and in quality assessment. In addition, the science cataloging will be carried out primarily on the level 2 data. For this discussion, we consider the source extraction pipeline to be the cataloging of objects detected in the level 2 data. These catalogs will be considered the level 3 data, and they will be released to the community with the level 2 data.

There are many available cataloging programs. A current favorite in the astronomy community is SExtractor, a program written by Emanuel Bertin. We will adopt SExtractor as our standard cataloging program, but it is likely that special purpose software will be required to support our science goals. For example, weak lensing analysis requires the characterization of galaxy and stellar shapes, and so we will likely require more than the functionality offered by SExtractor. Furthermore, SExtractor does not handle varying seeing in a natural way: we will need to measure PSF magnitudes for the stars for a variety of purposes, including photometric calibration. It will likely be important to have not only galaxy colors calculated from each band independently, but also colors over the same physical portion of each galaxy; the latter requires adopting the galaxy region definition from one band in the photometric calculations in all the bands, and this will likely require functionality beyond that offered in SExtractor. In general, we could simply run SExtractor to characterize objects, their positions and their photometric properties, and then use these initial catalogs to guide additional image calculations by other tools.

We note that the SDSS Photometric Pipeline could in principal be used. Given our experience with using it on non-SDSS data, we are much more likely to use the toolkit photo, which the Photometric Pipeline is built out of, to take advantage of some of the sophisticated algorithms developed and tested by the SDSS. Since it is modular and easily extendable, we can without much development use the tools on the positions found by SExtractor.

WBS 2.5 Science Analysis Pipelines: (3 total FTE-months)

As is described below, much of the work associated with the science analysis will not be considered a contribution to the data management part of the project, but rather will be charged against the science time of the participating astronomers. Nevertheless, for the purposes of tracking integration with the rest of data management, we list these activities below.

WBS 2.5.1 Photometric Redshift Pipeline: (FTE-months: 3 months)

This pipeline will take the photometry in four colors for all extended objects and estimate photometric redshifts and associated uncertainties. Huan Lin has existing tools, but they will need to be folded into the grid based processing framework. This is central to essentially all the science, and so folding this pipeline into the project data framework should be considered a part of the data management effort.

WBS 2.5.2 Cluster-finding Pipeline: (FTE-months: 0)

The goal of this pipeline is to create a multi-frequency catalog of galaxy clusters. Cluster finding in the optical and multiwavelength cluster finding pipelines will be written as part of the science analysis of the survey. This effort lies outside the DM domain, but pipelines should be structured to operate within a common framework, and data products will be available to the collaboration.

WBS 2.5.3 Weak Lensing Analysis Pipeline: (FTE-months: 0)

The goal of this pipeline is in part the creation of cosmic shear maps. Weak lensing pipelines will be written as part of the science analysis of the survey. It is also likely that additional, co-added datasets to optimize PSF quality will be produced and archived. This effort also lies outside the DM domain, but pipelines should be structured within a common framework, and data products will be available to the collaboration.

WBS 2.5.4 Synoptic Analysis Pipeline: (FTE-months: 0)

General synoptic analysis pipelines will be written as part of the science analysis of the survey. These pipelines will include SN detection and light curve measurement tools similar to those already being used to analyze the SM/SN data from the CTIO 4m. A quick alert system will be put in place to facilitate spectroscopic and photometric followup by the larger community. In addition, the main survey data will enable a study of variable objects over longer timescales with much cruder sampling. These existing pipelines will have to be brought within the common framework, and data products should be available to the collaboration.

WBS 2.6 Data Challenge (7 total FTE-months)

A critical part of the preparation for first light will be the verification of our processing system to ensure the scientific integrity of our data products. Verification will be accomplished through a series of “data challenges” in which we create simulated data based on a model of the universe, pass it through our processing system, and attempt to recover the model through analysis of the resulting products. In addition to scientific integrity, we will also test the technical robustness of the system, ensuring it can handle the required data rates and expected modes of failure.

Significant portions of this work will be centered at Fermilab, including the creation of simulated data and analysis of results; consequently, this particular part of the work will be tracked through a separate WBS (1.3). The portions of the work tracked under the Data Management part of the project cover the integration of the simulator with the processing system and execution of the actual challenges; these are enumerated below.

WBS 2.6.1 Simulation Interface and Integration: (FTE-months: 3)

This package defines the interface that allows simulated data to be injected into the processing system. This may in fact be designed as several interfaces that allow data to be inserted at several places in the chain. We allow most of the time in this package to be focused on general integration issues and testing prior to use by an actual data challenge.

WBS 2.6.2 Data Challenge I: (2 FTE-month)

In this challenge, our simulated data will be adapted from actual data from similar scientific instruments (e.g. the NOAO Mosaic Camera). The purpose is to assess existing software and conduct preliminary tests of techniques we expect to use in our processing. The processing will be done largely “by hand,” by which we run software interactively. Our goal is to capture all of the processing chain from calibration to object catalog generation (which, given existing software in the community, should be easily accomplished). We will use the results to refine our design and further discern the development and integration costs.

WBS 6.2.3 Data Challenge II: (1 FTE-month)

The purpose of this challenge is to test the archive and pipeline framework. The input data will likely be a combination of simulated data and real data adapted for this challenge. We will ingest the data into the archive as if it is part of the raw data stream and automatically initiate single-frame calibration.

WBS 2.6.4 Data Challenge III: (1 FTE-month)

The purpose of this challenge is to provide a full stress test of the entire data management system from data ingest to co-addition. The input will be a full year's worth of simulated raw data (provided via WBS 1.3.4; see Chapter 7). The challenge will include simulations of selected failure modes (e.g. network failures, machines going down during processing). When the processing is complete, the data challenge analysis team (WBS 1.3.5) will analyze the data to verify sufficient recovery of the input imaging model.

WBS 2.7 Survey Data Processing Operations (216 total FTE-months)

After the build phase of the project, the survey will begin and the data processing engine will begin operations. The survey data acquisition lasts 5 years; we adopt a 6 year timescale for the survey data processing. Survey data processing operations will involve maintenance of the processing platforms and pipelines at CTIO, in La Serena, at NCSA and at Fermilab. In addition, quality assessment of the data will be an ongoing, hands-on process that we expect will be driven by the science progress in the dark energy studies. A person will have to be available to respond to inquiries from the public regarding the publicly released data. Feedback from the data quality assessment will naturally provide input for pipeline improvements. We estimate that this task will require approximately 3 FTE, and this effort will be shared between U Illinois and Fermilab. Over the six years of the survey data processing, this corresponds to 18 FTE years. Funding for this portion of the project will be requested as the DES build phase nears an end.

WBS 2.8 Dark Energy Science Analysis

During the survey operations phase the science effort will begin. The science analysis will be a critical data quality feedback tool, and the science results are the underlying motivation for this project. We will request funding for this portion of the project as the DES build phase nears an end.

7. Project Management Plan

We will manage the DES as two projects, the Survey Instrument and the Data Management, during the construction and commissioning phases of the Survey. Each project has separate well-defined deliverables that will mark the end of the construction and commissioning phases. The primary Survey Instrument project deliverable is a working instrument that has been fully integrated and commissioned on the Blanco telescope. The Data Management project has two deliverables software and hardware systems; one that can process the data from the Survey Instrument and the second that can archive and then distribute the processed data to the DES collaboration and after a period of quality validation, distribute the DES Archive to the astronomical community. The delivery of mock data and survey quality commissioning data by the Survey Instrument team to the Data Management team and the subsequent processing of the mock data and the commissioning data by the Data Management team are the important deliverables that tie the two projects together. The processing of survey quality commissioning data and its subsequent delivery to the archive marks the end of the commissioning phase of the Survey and the start of Survey Operations.

We anticipate that once observations begin the Survey Instrument team will be responsible for the maintenance of the Survey Instrument and the Data Management Team will be responsible for production data processing and distribution of the data and catalogs, including data quality assurance of the data products. Both teams in partnership with CTIO operations will contribute to survey operations on the mountain required to acquire the survey data. The primary and most important Survey deliverable is the Dark Energy Survey Archive since it will enable both collaboration and community to obtain scientific results from the data. While we discuss some of the strategic elements of a survey operations management plan in this chapter we are still developing this part of the Project Management Plan.

Each project has its own project management team, Work Breakdown Structure, budget, schedule, and project management plan, including a change control process. This choice recognizes that the nature of the work in each project is very different and that schedules for the two projects become strongly coupled only near the end of the construction phase. Thus the two projects will proceed more efficiently if each is delegated adequate authority and if the project teams are allowed to manage their work somewhat independently. Because an appropriate level of active management of the two projects is needed, we have created a Management Committee to coordinate and oversee the efforts of the two projects throughout the life of the two projects. Moreover, we anticipate that the Management Committee will continue to coordinate the work of the Survey Instrument Team and the Data Management Team during the five-year operations period. The Management Committee will also be responsible for obtaining the financial and personnel resources that are needed to carry out the two projects.

The remainder of this chapter describes the management structure outlined above in more detail starting with the Management Committee.

7.1 Management Committee

7.1.1 Management Committee Responsibilities and Authority

The Management Committee (MC) is responsible for broadly defining the hardware and software interfaces between the two projects. The Project Managers will develop an implementation plan for these interfaces that is consistent with the broad definitions and the MC will approve the plan. It is also responsible for preparing agreements between the Dark Energy Survey and the participating institutions, CTIO operations and NOAO Data Products Division. The current list of the responsibilities of the Management committee is as follows:

1. Develop and approve fund raising strategies.
2. Organize preparation of proposals for funding.
3. Organize presentations to the funding agencies (DOE, NSF & private) and federal agencies that set funding policy (OMB, OSTP).
4. Coordination of the work and the schedules of the two projects and their interfaces with CTIO and the NOAO Data Products Division.
5. Preparation of documents for NOAO and AURA committees that oversee Blanco operations.
6. Preparation and approval for the DES agreements between the participating institutions and the DES.
7. Preparation of an annual budget for the Survey sponsors.
8. Serve as the highest-level change control board for the Survey. This will include any necessary changes to the management of the projects, the primary science requirements, significant changes in cost and schedule.
9. Schedule collaboration meetings and approve their agendas. The host institution is responsible for the meeting.

7.1.2 Management Committee Membership

MC has at least one representative from each of the participating institutions. The current membership of the MC is as follows:

Chair	John Peoples (alternate B. Flaugher)
Instrument Project Leader	Brenna Flaugher
Data Management Leader	Joe Mohr
Fermilab rep	Jim Annis (alternate B. Flaugher)
Chicago rep	Josh Frieman
CTIO/NOAO rep	Alistair Walker (alternate T. Abbott)
U of I rep	Jon Thaler (alternate J. Mohr)
LBNL rep	M. Levi (alternate S. Perlmutter)

7.1.3 The Change Control Process

A formal change control process will be used to coordinate and oversee the work of the two projects. The Science and Technical requirements, presented in Chapter 3, flow from the Survey Science Program, described in Chapter 2. The Science and Technical requirements, the total baseline cost of each project, and the major project milestones constitute the level 1

requirements. The Management Committee is responsible for defining the level 1 requirements and for assuring the DES sponsors that the level 1 requirements will be met. The level 2 requirements will flow from the level 1 requirements and will be defined by the technical specification of level 2 elements in the WBS, the schedule for the level 2 elements and their cost. While the project managers are responsible for meeting the level 2 requirements, changes to level 2 requirements will be proposed by the project managers and approved by the Management Committee. Prior to baselining the Survey the level 2 and level 3 technical specifications, costs, budgets, and schedule milestones for each project will be proposed by the respective Project Managers and then approved by the Management Committee. We anticipate that the Survey Baseline, which will consist of the level 1 requirements, will be established by the sponsoring agencies following the Baseline Review.

Each project manager will have the authority to make changes to the level 3 technical specifications, cost, and schedule provided that they do not change the level 1 or level 2 requirements. The Project managers will be responsible for managing changes to the level 3 requirements, which are defined by the technical specifications, costs, and schedule at level 3 in the WBS. The change control board for each project will process level 3 changes and decisions and the background for the decisions will be reported to the Management Committee in writing for information. Each project manager will be allocated a fraction of the annual allocation of contingency funds to manage problems appropriate to level 3.

7.1.4 Science Working Group

The Science Working Group developed the science program contained in Chapter 2. It continues to be responsible for the further development of the scientific program and the refinement of the DES science goals. While the Science team is open to all collaboration members, Frieman, Mohr and Annis have led the development of the proposal science with significant contributions from Aldering, Hu, Lin, Kent, Perlmutter, Sheldon, Smith, Suntzeff, Thaler, and Wechsler. The Science Working Group reports to the Management Committee. When it is time to prepare a new proposal or revise an old proposal for funding, the Management committee will ask the Science Working Group to review the science material, particularly the relationship of the DES to other projects.

7.1.5 Project Advisory Board

Prior to baselining the projects, the DES will recruit a committee of technical and management experts to review each project. The Project Advisory Board (PAB) will advise the DES Management Committee on the status of the project. It is intended that the committee will meet at least once a year to review the project status and provide advice to the Management Committee until the commissioning phase is complete. The PAB will submit a report describing its findings and advice to the URA/DES oversight board.

7.1.6 Collaboration Policies

The Collaboration will be organized so that the key science projects, described in chapter 2, can be executed and published by the participants. At the appropriate time the Management Committee will authorize the creation of a Collaboration Council that will define policies for data access and publications and that will guide the science effort of the Collaboration. The policies will be subject to approval by the Management Committee.

7.2 Survey Instrument (WBS 1.0)

Fermilab is the lead institution with contributions from all the participating institutions. Brenna Flaughner (Fermilab) is the Survey Instrument Project Manager and Tim Abbott (CTIO) is the Deputy Project Manager. Jim Annis serves as the Instrument Project Scientist.

7.2.1 Survey Instrument project Work Breakdown Structure

The Dark Energy Survey Instrument project is divided into seven level 2 projects as shown in Figure 7.1.

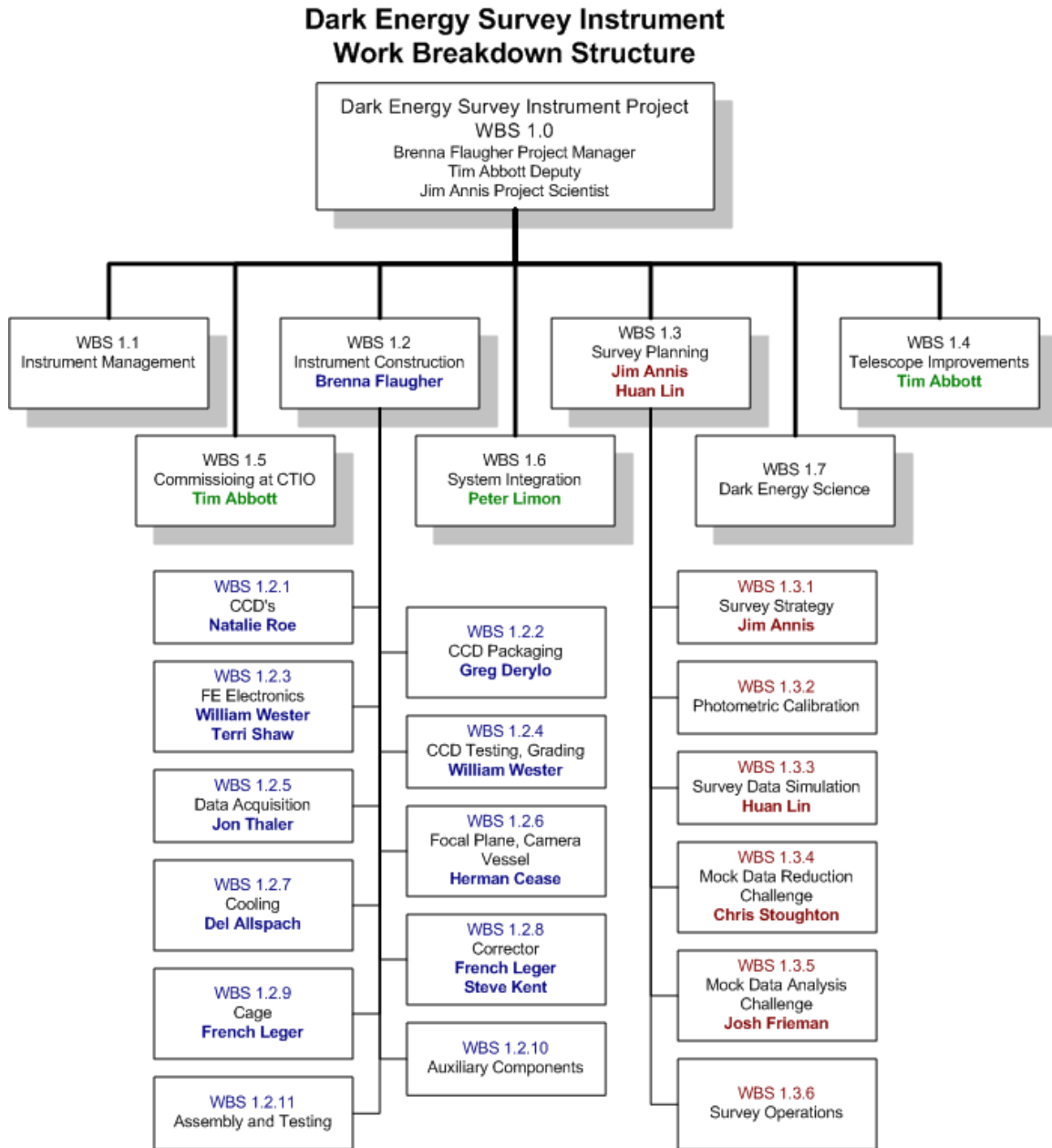


Figure 7.1 Survey Instrument project WBS elements.

Management, WBS 1.1, captures all the costs associated with the Survey Instrument construction project management. It covers preparation of schedule and costs, management and specification of technical requirements, active tracking of progress of the project through periodic reports and reviews.

As shown in the Figure 7.1, the Instrument, WBS 1.2, and the Survey Planning, WBS 1.3, elements are further divided into Level 3 elements. These were described in detail in chapters 5 and 4 respectively. WBS elements 1.4, telescope improvements and 1.5, commissioning at CTIO, are both activities that will occur at CTIO and Tim Abbott is leading those efforts. System Integration is led by Peter Limon (FNAL). He is responsible for defining a system for assuring that all the components of the instrument project can be successfully integrated. WBS 1.7 supports the scientific effort of the Survey Instrument team and miscellaneous costs that it needs to carry out the science analysis of the archived data and to prepare scientific papers.

7.2.2 Survey Instrument Project Organization

A description the Survey Instrument construction and commissioning tasks by WBS element at (Level 3) is presented in this section and will form the basis for the Survey Instrument project management plan. The level 3 leaders will work with the Project Manager to develop cost and schedule and provide monthly updates, in addition, to the specific tasks listed below.

- 1.2.1 CCDs covers the procurement of the CCDs, including the preparation of a QA plan for wafer fabrication and processing, managing the procurement, as well as the thinning and dicing. Natalie Roe (LBNL) is the L3 task manager.
- 1.2.2 CCD packaging covers the design and implementation of the CCD packaging in conjunction with the Front End electronics group, development of a QA system, and oversight of the packaging assembly process. Greg Derylo (FNAL) is the L3 task manager.
- 1.2.3 Front End Electronics covers the design and implementation of the electrical system from the CCDs to the DAQ system (WBS 1.2.5) working with the CCD packaging group (WBS 1.2.2) on the AIN board and with the UIUC group on the interface to the DAQ. This also includes development of appropriate QA measures for the various components and oversight of the testing and construction of the FE system. William Wester and Terri Shaw are the L3 task managers.
- 1.2.4 CCD testing and grading covers development of a testing plan, designing and developing adequate testing facilities, developing testing documentation (e.g. paper travelers and a web based tracking system), over site of the testing and grading efforts, developing a plan for testing the CCDs after they are installed in the focal plane, and developing a testing plan for the fully assembled focal plane. William Wester is the L3 task manager.
- 1.2.5 Data Acquisition (DAQ) covers the design and implementation of the electrical system starting from the connection to the front-end electronics to the output of an assembled image on disk. This also includes providing advice and support for the DAQ at the CCD testing facility at Fermilab, working with the Front End group to define the connections between the DAQ and the front end electronics, working with the data management group to define the output format of the images and the transmittal of data into the data management system. Jon Thaler is the L3 task manager.

- 1.2.6 Camera Vessel and Focal plane covers design of the camera vessel and focal plane in conjunction with the cooling, packaging and front end electronics groups, developing an assembly plane for the camera including installation of CCDs into the focal plane, cable routing, connections from cooling system to the focal plane, working with the FE, DAQ and cooling groups to develop and implement a testing plan for the fully populated focal plane. Herman Cease is the L3 task manager.
- 1.2.7 Cooling covers the design and implementation of a system capable of setting and maintaining the CCDs at a constant and well-known temp, developing a cooling system for any additional heat sources in the primary cage, documenting and developing thermal management plans for everything in the cage, developing a testing plan for the cooling system on the full focal plane, and providing support for cooling systems in the CCD test stations. Del Allspach is the L3 task manger.
- 1.2.8 Corrector includes optical design, contracting and working with a professional optical engineer, procurement and testing of the optical components, and developing an assembly and testing plan for the completed corrector. Steve Kent and French Leger are the L3 task mangers.
- 1.2.9 Prime focus cage covers the design and construction of the primary cage and all of the systems external to the camera and corrector. This also includes handling of the F/8 secondary, alignment to the primary, the shutter and the connection between the camera and the corrector, and providing support if needed for an in situ full system calibration system. French Leger is the L3 task manger.
- 1.2.10 Assembly and testing covers the final assembly of the completed and fully tested main systems (e.g. camera, corrector, prime focus cage). This will evolve from the testing and QA procedures of the individual components.

7.2.3 Manpower and Coordination Activities

This section outlines the contributions of the DES collaboration institutions to the DES Instrument project. Both Fermilab and UIUC will contribute technical labor to the DES instrument project and these contributions will be outlined in the next section.

7.2.3.1 Fermilab

Fermilab is the lead institution on the DES Instrument project. The Project Manager, Brenna Flaughner, coordinates the efforts of the Fermilab staff on the Instrument project and directs the lead scientists and engineers who are responsible for the Level 2 and 3 projects. Typically one videoconference meeting per week is devoted to the Instrument design and nearly all of the people working on the Instrument participate.

Within the Fermilab Particle Physics Division (PPD), William Wester coordinates the Electrical Engineering Department participation in the area of the front-end electronics and the CCD testing efforts and Brenna Flaughner coordinates the mechanical Engineering Department support in the areas of CCD packaging, the camera vessel, the cooling system and the prime focus cage. To supplement our experience with silicon detectors, we are exploring a partnership with Richard Stover at Lick Observatory since he has experience packaging the LBNL CCDs, with the goal of establishing a technology transfer program during the development phases of the CCD work (Phases A, B, and C).

Jim Annis and Huan Lin, members of the Computing Division Experimental Astrophysics Group, lead the survey planning effort and will concentrate on designing a survey which can achieve our science goals with particular focus on the photometric calibration. This task will expand to include the simulations that are relevant to observing strategy and the mock data challenge. The planning for the mock data challenge will begin in September 2004, and it will be done jointly with the Data Management team. The Survey Strategy team will include liaisons from the Data Management team, the Science team, and the Dark Energy Instrument team, who will serve as the points of contact.

7.2.3.2 LBNL

Natalie Roe is the L3 project leader for the CCD procurement project and Mike Levi is the LBNL representative on the DES management committee. They, and other members of the LBNL groups, have given the Instrument Team considerable guidance on how to plan the acquisition of the CCDs. LBNL will manage the procurement of the CCDs from the wafer vendor, their subsequent thinning, processing and dicing of the devices. LBNL will test the devices on a cold probe station and deliver them to FNAL with the testing results.

7.2.3.3 CTIO

Tim Abbott is the project deputy project manager and the primary contact with CTIO. He is also the L3 project leader for the activities that will occur at CTIO such as telescope improvements and commissioning of the instrument. He provides critical information on the Blanco performance and the Cerro Tololo infrastructure. The DAQ working group (WBS 1.2.3 and WBS1.2.5) is also working with the developers of the Monsoon system at CTIO and Tucson to understand and adapt the current system to our needs. We are investigating additional partnership arrangements with CTIO including assistance with the fabrication of the prime focus cage, development of a Sol-Gel coating facility that could handle the large optical elements of our corrector and development of the infrastructure to accommodate the large cooling facility needed for our instrument among others.

7.2.3.4 University of Chicago

University of Chicago will take the lead in the design, acquisition and testing of the optics. Steve Kent (Chicago and Fermilab) will lead the effort with contributions from French Leger (FNAL) and Mike Gladders (Carnegie Obs.). They have significant experience in the design, construction and procurement of optical systems. An optical designer will supplement their efforts when funds become available. The optical designer will be charged with exploring cost savings, the preparation of the procurement documents and the specifications for acceptance testing at the vendors, and the design of an optics test facility at Fermilab suitable for testing the individual lenses and the complete corrector. We anticipate extending the contract to cover oversight of the work at the vendors.

7.2.3.5 UIUC

John Thaler of U Illinois leads the design of the Data Acquisition System and its integration with the front-end electronics and CTIO infrastructure. He will be responsible for ensuring the system meets the scientific requirements. Todd Moore, the DAQ project manager, will lead the day-to-day operations of the DAQ design and implementation. A Data Acquisition working group will assist these two. The working group will consist of those members of the collaboration who are working on the various parts of the DAQ as well as others from the teams working on front end electronics, telescope monitor and control system, and data processing that have interfaces with the DAQ.

7.2.4 Survey Instrument Project Cost Estimate

The cost estimate for the Dark Energy Survey Instrument is given in Table 7.1 in then year \$ without institutional overhead. The costs are rolled up to level 2 except for the Instrument construction where the details are provided at Level 3. We have followed the Fermilab/DOE practice for preparing cost estimates by including only the cost of technical labor (technicians, engineers and computing professionals). We have not included the cost of salaries of senior scientists and faculty in view of their commitments to service work on other projects and teaching respectively. Fermilab plans to provide technical labor with a value of \$ 6,503 k and UIUC plans to contribute technical labor with a value of \$ 450 k to the DAQ system. The labor column in Table 7.1 is the sum of the Fermilab and UIUC technical labor.

The Fermilab labor costs were estimated using the average salary information in FY04 dollars (SWF) without overhead for mid range salaries in each category and based on the number of hours estimated for each task. The UIUC technical labor costs are similarly included in the total for the DAQ labor. The labor costs are roughly equal to the M&S costs with for two notable exceptions, the optics and the CCDs. Both are very large procurements with little labor needed from the Fermilab technical staff. The optics will be purchased as blanks from a glass vendor (\$665k) and will then be ground to the correct shape by another vendor (~\$1,000k). In addition, the filters and the coatings will be purchased from outside companies. We also will contract with an optical engineer for the design of the corrector and to oversee the procurement and testing of the corrector elements. This is costed as M&S because it will be a contract for services with a non Fermilab engineer. The CCD M&S cost was based on the Reference Design that includes processing and testing the wafers after they are received from the wafer vendor.

Table 7.1 Cost Estimate for the Dark Energy Survey Instrument in then-year \$ and excluding overhead

		M&S (\$K)	Labor (\$K)	Total (\$K)
1	Dark Energy Survey Instrument	8,368	4,635	13,003
1.1	Management	235	189	423
1.2	Dark Energy Instrument Construction	7,734	3,692	11,426
1.2.1	CCDs	2,155	25	2,180
1.2.2	CCD Packaging	287	607	895
1.2.3	Front End Electronics	595	640	1,235
1.2.4	CCD Testing	579	364	942
1.2.5	Data Acquisition	167	299	466
1.2.6	Focal Plane, Camera Vessel	163	366	529
1.2.7	Cooling	427	160	587
1.2.8	Optical Corrector	2,463	121	2,584
1.2.9	Prime Focus Cage	618	779	1,397
1.2.10	Auxiliary Components	146	164	309
1.2.11	Final Assembly and Testing	135	167	302
1.3	Survey Strategy	399	539	938
1.4	Telescope Improvements*	0	0	0
1.5	Commissioning (at CTIO)	0	134	134
1.6	System Integration	0	82	82
1.7	Dark Energy Science+	0	0	0
	Contingency	3,080	2,318	5,397
	Total cost (w/o overhead)	11,447	6,953	18,400

- * CTIO will support the costs of the telescope improvements that were anticipated in the AO. The DES collaboration will support the cost of other upgrades only if they significantly benefit the DES project. At this time, none are planned but we are discussing possibilities for reducing the slew time from 35 sec to ~ 17 sec, the anticipated time to read out the CCDs.
- + Dark Energy Science will be carried out by the scientific staff university faculty. It will be treated as a contribution from the scientists' and/or faculty members' institution. This WBS element will capture the additional costs for scientific investigations.

In estimating total project costs for the DOE, it is standard to separate the total project cost into a base cost estimate plus a contingency. The base cost estimate covers the current best estimate of the cost of the project. The total contingency is derived by separately assigning a contingency factor on each task based on the confidence in the base cost estimate. Typically at such an early stage of a project a contingency of ~40-50% is expected. History has shown that, this contingency money has always been needed to complete the project. As a result DOE, considers the total project cost as the sum of the base estimate and the contingency based on the expectation that this represents the best and realistic estimate of total cost.

We have followed the Fermilab/DOE practice in estimating and assigning the contingency for the DES instrument as follows. A contingency factor was assigned at the task level. A general factor of 40% was taken for everything unless a quote from a vendor had been obtained. In these cases (corrector blanks, DAQ equipment) 10% was taken. For the CCDs, the contingency has two components. First is a 20% contingency on the detailed estimate from LBNL on the costs for procuring the CCD wafers and processing them at the LBNL Microsystems Laboratory. In addition, the cost of an extra 24 wafer run has been included, bringing the total contingency on the CCDs to 43%. The resulting contingency on the M&S cost is 36% for a total M&S cost of \$11,447 K. For contingency on the labor costs we assume 50% at this time for all tasks. This results in a total labor cost of \$6,953 K and a total project cost of \$18,400 K in then-year \$, exclusive of institutional overhead. When that overhead is included the total project cost of the Survey Instrument (WBS 1.0) is \$22.5M.

We show UIUC DAQ personnel in Table 7.2. The people listed are all members of the UIUC high energy physics group. There are sufficient personnel to complete the telescope DAQ on schedule. The costs are included to show the contribution of the UIUC group supported by the UIUC HEPG grant from DOE to the DES instrument project. Only the technical labor costs in this table are included in the total in Table 7.1.

Table 7.2. UIUC DAQ Personnel

Name	Role	Effort (6/2004 → 6/2009)	Cost (with overhead)
Jon Thaler	Physicist, DAQ project scientist	50%	\$125 k
Todd Moore	Engineer, DAQ project manager	75% → 100%	\$623 k
Inga Karliner	Physicist	50% → 80%	\$538 k
Mats Selen	Physicist	20% → 50%	\$79 k
Allison Sibert	Technician	As needed	\$105 k
TBD	Physicist (post-doc)	0% → 100%	\$360 k
TBD	Physicists (1-2 graduate students)	0% → 100%	\$271 k
Total cost			\$2101 k

Cost includes summer salary (at level of effort) for faculty, and fully loaded salaries for personnel supported by the UIUC HEPG grant from DOE.

7.2.5 Funding Model for Survey Instrument M&S costs

The estimated cost of the materials and services for the Survey Instrument project, after including a contingency of 36% and excluding overhead, is \$11.4 million. We propose that DOE provide ~65% of the required M&S funds and that we obtain other funds for the remaining ~35% of the M&S cost. Table 7.3 presents the funding profile that is required to meet the proposed schedule that allows commissioning to be completed in May 2009. We

believe that we could complete commissioning by October 2008 if the funding profile did not constrain the placement of orders. The placement of some of the corrector optics cannot be made until the beginning of FY07 thereby introducing a delay of 7 months relative to the schedule that is not constrained by the funding profile. However, it reduces the peak request for M&S funds from Fermilab to \$2.5 million (excluding overhead) in FY06 relative to the funding unconstrained profile which required \$4.5M for M&S funds (excluding overhead) from Fermilab in FY05. We also shift the start of CCD production by 1 month into FY06 in order to flatten the funding profile. This funding profile put the optics procurement on the critical path.

Table 7.3. M&S Costs in then-year \$K without overhead

	FY05	FY06	FY07	FY08	FY09	Total
M&S base	1,097	3,321	3,362	520	68	8,368
M&S Contingency	0	379	338	1580	782	3080
Total M&S	1097	3321	3362	520	68	11448
DOE - Fermilab	500	2500	2500	1100	800	7400
Other Funding	600	1200	1200	1000	50	4050
Total Funding	1100	3700	3700	2100	850	11450
DOE Fraction	0.45	0.68	0.68	0.52	0.94	0.65

The M&S Contingency is distributed to match the difference between the funding and the M&S base needs.

The UIUC HEP group has provided the funds to purchase the DAQ hardware for the first CCD test station (~\$30K) from its FY04 DOE and those costs are included in the FY05 costs in Table 7.3. The other funds for the survey instrument in FY05 will be used to initiate the CCD preproduction order and to initiate the final optical design.

We propose that Fermilab account for its overhead costs on all M&S purchases made through Fermilab as an in-kind contribution from the Fermilab base budget.

7.2.5 Survey Instrument Schedule

The schedule for the Survey Instrument is funding limited. It begins in 2004 with the design work already underway and continues through the instrument commissioning on the Blanco. The critical path milestones are shown in Table 7.4. The procurement of the largest optic is the critical path item. The down selection of the CCD source is very close to the critical path.

Table 7.4 Critical Path Milestones for Instrument Construction.

ID	Task Name	Start	2004		2005		2006		2007		2008		20
			Qtr 3	Qtr 1	Qtr 3								
10	Funds available (Fermilab R&D, external)	Fri 10/29/04	■										
38	Ready to submit masks to Dalsa	Thu 12/2/04	■										
40	Order 24 wafers of devices	Thu 12/30/04	■										
43	1st fully processed CCDs (8) in hand	Thu 10/6/05			■								
46	Submit order for final processing of remainig 1st batch wafers	Thu 10/13/05			■								
58	First production CCDs in hand	Thu 7/6/06				■							
17	FY07 funding available	Tue 10/31/06					■						
363	Order Corrector elements	Tue 10/31/06					■						
146	CCDs Ready for mounting on focal plane	Tue 1/15/08						■					
368	Lenses and filters complete	Mon 1/21/08						■					
335	Dewar closed, ready for testing	Tue 3/11/08						■					
265	Camera testing complete - ready for corrector	Tue 8/26/08							■				
423	corrector, filters and cage ready for camera	Mon 9/1/08							■				
453	Prime focus cage complete	Mon 10/27/08							■				
455	Testing complete	Mon 1/5/09								■			
457	Ready to Ship to Chile	Mon 1/19/09								■			
489	Ready to Mount on Blanco	Mon 3/16/09									■		
491	1st light	Mon 4/27/09										■	
493	1st useful data	Mon 5/25/09											■

7.2.6 Survey Instrument Reviews

We anticipate having a series of meetings and reviews throughout the course of the project. These will be motivated by the desire to determine if significant milestones have been met and to authorize major procurements. Each Level 3 task in the Instrument project will undergo the following reviews

- 1) Conceptual Design (ready to proceed with development and prototyping)
- 2) Preliminary Design (ready to proceed to preproduction)
- 3) Production Readiness
- 4) Annual Production updates

These will occur as appropriate to the status of the task, but will roughly correspond to annual review, beginning in the fall of 2004.

We anticipate a full baseline review in the spring of 2005 by DOE and Fermilab (and perhaps other sponsors). If we successfully pass the review, we expect to receive authorization to proceed with spending money on the optics. After this point in time changes in the design at level 2 and level 1 will require the sponsors approval. The Project Advisory Board will participate in this process by holding a pre-baseline review.

We will review the Phase B test results in August 05 prior to authorizing the production order and the processing of the rest of the Phase B wafers.

7.3 Data Management Project Plan (WBS 2.0)

In Chapter 6, Data Management, we describe the technical approach of the data management plan. This includes technical summaries of the various work packages that make up WBS 2.0. In this section, we discuss our plan for managing resources to deliver the data management system and process the data over the course of the survey.

7.3.1 Data Management Project Organization

The University of Illinois Astronomy Department will lead the data management and archiving effort. Their efforts will be supported by the National Center for Supercomputing Applications (NCSA) and the Fermilab Experimental Astrophysics Group. This will allow the Collaboration to take advantage of the experience that NCSA and Fermilab have gained in processing, archiving and distributing astronomical data. The Management Committee has delegated the definition of the computing framework, within which the Collaboration will develop software, including the simulations, to the Data Management Steering Group (DMSG). The DMSG is described in 7.3.3. The University of Chicago group also plans to contribute to the software systems through a major contribution to the simulations. Already several Chicago students and post docs are contributing to the simulations. Fermilab scientists and University of Illinois faculty and students are also making similar contributions.

Joe Mohr at U Illinois leads the Data Management project with C. Smith (NOAO/CTIO) as a co-leader and R. Plante (U Illinois/NCSA) as the Data Management Project Manager. The University of Illinois at Urban-Champaign is the lead institution, with key involvement of the Department of Astronomy, Department of Physics and NCSA. Fermilab, the NOAO Data Products Division and the University of Chicago will make supporting contributions. The technical plan for this project is presented in Chapter 6.

7.3.2 Data Management project Work Breakdown Structure

The Dark Energy Survey Data Management project is broken down into eight level 2 projects as shown in Figure 7.2. The University of Illinois is the lead institution with contributions from all other collaborating institutions.

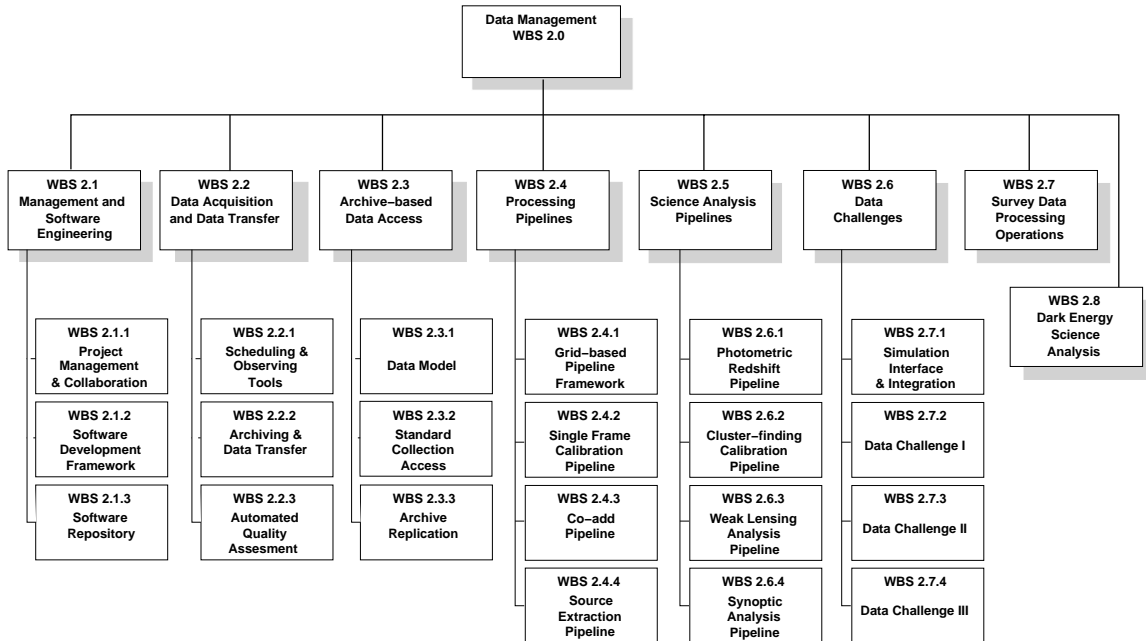


Figure 7.2. Dark Energy Survey Data Management Work Breakdown Structure

Below we provide a brief description of each of the work packages.

- 2.1.1 Project Management and Collaboration (12 FTE-months) - this covers the management of the project.
- 2.1.2 Software Development Framework (6 FTE-months) - system and policies for developing and testing the software.
- 2.1.3 Software Repository (1 FTE-month)- software revision control system.
- 2.2.1 Scheduling and Observing Tools (12 FTE-months) - graphical user interface that is primary user interface with camera (and telescope). Includes interface with survey database to help in scheduling observations and includes monitors of a range of camera, telescope and data quality characteristics.
- 2.2.2 Archiving and Data Transfer (4 FTE-months) - deploy tools to enable internet (and backup option) data transfer from the mountain to the collaboration sites.
- 2.2.3 Automated Quality Assessment (4 FTE-months) - tools to automatically assess data quality. These tools will be deployed on the mountain and also at the primary data processing station at NCSA.
- 2.3.1 Data Model (2 FTE-months) - definition of data products, metadata, and catalog tables.
- 2.3.2 Standard Collection Access (7 FTE-months) - deploy tools to enable data access for the collaboration and the public.
- 2.3.3 Archive Replication (3 FTE-months) - tools to replicate (portions of) the archive at partner sites.
- 2.4.1 Pipeline Processing Framework (9 FTE-months) - grid based framework for the automated management and execution of processing pipelines.
- 2.4.2 Single Frame Calibration Pipeline (12 FTE-months) - tool for basic reductions and astrometric and photometric calibration of single pointing images
- 2.4.3 Co-add Pipeline (12 FTE-months) - tool to take calibrated single pointing images and combine to build deeper, coadded images from which much of the Dark Energy Survey science will be done. Images and variance images will be produced.
- 2.4.4 Source Extraction Pipeline (12 FTE-months) - tool that will create catalogs and characterize objects found in the co-added survey data.
- 2.5.1 Simulation Interface and Integration (3 FTE-months) - Creation of insert interface for mock data used for data challenges, in collaboration with simulation team (WBS 1.3.3 and WBS 1.3.4).
- 2.5.2 Data Challenge I (2 FTE-month) - Interactive survey and testing of existing software.
- 2.5.3 Data Challenge II (1 FTE-month) - Test of archive and pipeline framework.
- 2.5.4 Data Challenge III (1 FTE-month) - Full challenge of data reduction using up to a year's worth of data.
- 2.6 Science Analysis Pipelines (3 FTE-months) - effort tracked within the Data Management WBS for integrating science analysis pipelines (e.g. photometric redshift catalog pipeline) into the pipeline infrastructure.
- 2.7 Survey Operations (216 FTE-months) - data management operations during the survey observing phase.
- 2.8 Dark Energy Science Analysis (0 FTE-months) - scientific staff effort to analyze and publish the results of the survey.

7.3.3 Data Management Coordination

A Data Management Steering Group (DMSG) has been formed to drive high-level design activities for Data Management. Membership will include software and science representatives from each partner institution. (Currently, it includes Plante, Mohr, Annis, Smith, and Chris Stoughton.) The DMSG is responsible for setting the overall roadmap for data management, defining system requirements and the development process, and working out the high-level design.

In contrast to the DMSG, the Computing Working Group (CWG) will be formed later once the project is up and running. It will be made up primarily of the software developers and system specialists. (It is likely the two groups will share membership.) Once the CWG is formed, much of the design activity will shift to this group as they flesh out the data management work package designs. They will also handle design and code reviews as necessary.

7.3.4 Data Management Project Cost Estimate

The total estimated manpower requirements for the data management portion of the project—excluding WBS 2.7 (which covers survey operations at 216 FTE-months) and WBS 2.8 (covering science analysis) is 112 FTE-months. Our labor model has 0.25 FTE/yr covered by the Project Manager for Data Management (primarily covering management tasks), 0.25 FTE/yr covered by the Project Scientist, and 3 FTE/yr of programming and postdoctoral support. Over four years, this level of effort sums to 168 FTE/months, providing 50% contingency on the work package labor estimates during the build phase of the data management project. In addition, we will request \$100k to support hardware upgrades (drives) at NCSA to partially support the requirements for the data processing and archiving. As shown

Table 7.5 Cost Estimate for the Dark Energy Survey Data Management

	Labor (FTE-Mths)	Cost (K\$)	Matching (K\$)	NSF Costs (K\$)
Dark Energy Survey Data Management		\$1,769.21	\$570.98	\$1,198.23
Labor	168	\$1,669.21	\$570.98	\$1,098.23
Project Manager	12	\$146.88	\$0.00	\$146.88
Project Scientist	12	\$221.95	\$147.97	\$73.98
Programmers	96	\$908.70	\$227.17	\$681.52
Astronomer	48	\$391.68	\$195.84	\$195.84
Hardware		\$100.00	\$0.00	\$100.00

in Table 7.4, the total estimated cost of the data management project build phase (not including survey operations) is \$1.77 million. Of this amount, \$0.57 million is available as an institutional match through the provision of 1 FTE over the four year extent of the build phase and 2 FTE-months/yr of salary for the project scientist. (Note that the cost of maintaining the equipment at NCSA is an in-kind contribution, estimated to be 0.5 FTE/yr for an additional \$0.2 million institutional contribution to the project.) The remainder, \$1.2 million, will be funded through a proposal to NSF.

7.3.5 Data Management Project Schedule

The data management project schedule has the full data management system tested and in operation at the beginning of 2009, when the camera is being shipped to the mountain for commissioning. A conceptual timeline for the major work packages appears in Figure 7.3. The data management project will begin in earnest in fall 2004 with the hiring of one person (using U Illinois institutional support) to help Mohr and Plante further refine the data management design and begin the build phase. In 2009 the transition to operations will take place, and in fall 2009 the survey operations at CTIO will trigger full scale data management operations. These operations will continue for the five year survey and extend one year beyond the end of the survey. Funding to support these activities will be requested as the operations phase approaches. At the end of survey operations there will still be an archive to support. We currently envision this archive remaining at NCSA indefinitely, perhaps as part of a new partnership to archive a wide range of NOAO data. Support for these activities, which we expect to be minimal, will be sought as the survey operations phase nears an end.

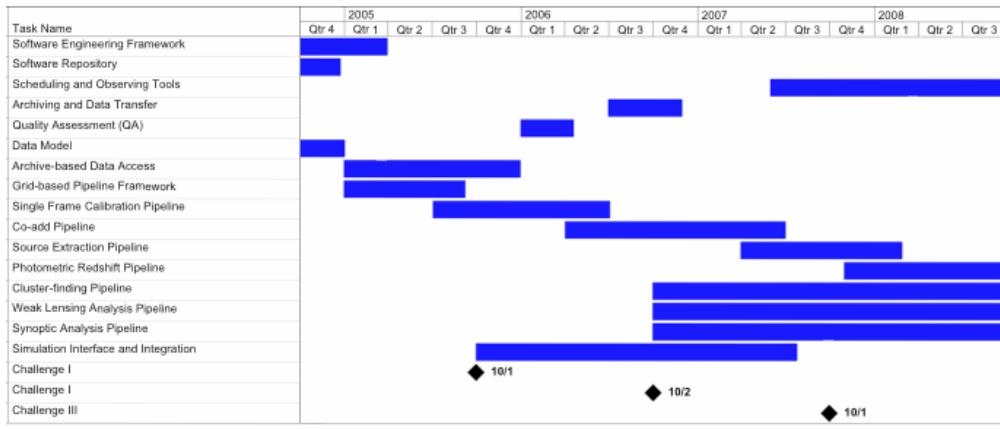


Figure 7.3 Data Management Schedule

7.3.5 Data Management Reviews

We are planning three levels of review of the data management effort: the design and code review process, the data challenges, and a general review by the Project Advisory Board.

The first two levels occur internal to the Data Management portion of the project and are overseen by the project manager. The internal design and code review is the process defined by the Data Management Steering Group (see sections 6.1 and 7.3.3). The purpose of this process is to make the design and implementation transparent to the entire collaboration and to ensure efficient integration of the various components. The data challenges (sections 6.6 WBS 2.5) are designed to verify that the system is capable of extracting the target science and meets the requirements imposed by the expected data rate.

In addition to the internal reviews, we will coordinate with the Instrument project a series of reviews by the Project Advisory Board, or by a panel of outside experts invited by the Board, to evaluate our progress toward a working system.

7.4 Funding and Resource Model

The funding and resource model that is presented here addresses the construction and commissioning phases of the project and the initial operations. We propose that DOE provide the primary funding for the Survey Instrument project, because Fermilab is the lead institution and that the NSF provide the primary funding for the Data Management project, because NCSA is the lead institution. Since all institutions plan to participate in both projects we plan to request funds from both agencies for each project. At this time we plan to submit one large proposal to the NSF for funds for the Survey Instrument and Data Management projects. We also plan to submit smaller proposals to the NSF and private foundations for FY2005 funding in order to keep the development program on track.

We plan to request ~\$5M for the construction and commissioning phases of the Survey through proposals to the NSF Astronomy and Physics Division. The purpose of these proposals would be to obtain \$3.4 M (~35%) for the M&S costs of the Survey Instrument as well as \$1.2 M for the Data Management Project. We also plan to make requests to private foundations for \$1.5 million in order to provide a cushion in the event our proposals to the NSF fall short of the mark. Should we be successful in obtaining private funds they would be used to advance the schedule. Fermilab has recently given us stage one approval (July 2004). Until NOAO has also approved our proposal, it will be difficult to engage the NSF in a discussion of the specific details of our proposals to the NSF. Moreover, we cannot approach private foundations in earnest until we have received this approval.

We first present the funding model for the Survey Instrument project in section 7.4.1 and then the funding model for the Data Management project in section 7.4.2. In each instance, we present the funding model for the institutional labor costs separately from the funding model for the materials and services costs.

7.4.1 Survey Instrument Funding Model

7.4.1.1 Model for Survey Instrument Labor Costs

The collaborating institutions have provided the scientific and engineering support for the preparation of the Reference Design of the Dark Energy Survey Instrument from their institutional funding and existing grants. Our model assumes that these institutions will continue this support through the construction and commissioning phases of the project. In particular, it assumes that Fermilab will provide the scientific, engineering and technical labor for the instrument project as described in section 7.2.4. The model requires a modest increase in the Fermilab scientific, engineering, and technical support from within the laboratory. The estimated Fermilab labor cost of \$7 M is shown in Table 7.1. Our model assumes that the UIUC HEP group will provide the scientific, engineering and technical labor for the data acquisition system. It further assumes that CTIO will contribute to scientific, engineering and technical effort to the survey instrument project as part of the partnership arrangement that is mentioned in the Announcement of Opportunity. This will include the effort to upgrade the telescope and its controls and to install and integrate the instrument on the Blanco. The model assumes that the University of Chicago will continue to support their faculty, graduate students and post-docs through institutional funds and existing and future grants. It further assumes that

the University of Illinois Astronomy Department will continue to support its faculty when they work on the Survey Instrument project.

We will actively seek additional scientists and technical staff from within the collaborating institutions as well as from new institutions. We are open to admitting additional groups provided they will bring additional resources to the construction and commissioning of the Instrument without increasing the costs of the current participants.

7.4.1.2 Model for Funding Materials and Service Costs

The estimated cost of the materials and services for the Survey Instrument project, after including a contingency of 36% and excluding overhead, is \$11.45 million. We propose that DOE provide ~65% of the required M&S funds and that we obtain other funds for the remaining ~35% of the M&S funds. Table 7.3 presented the funding profile in our model for obtaining the funds for the base M&S costs. This profile will allow commissioning to be completed in March 2009, whereas we believe that we could complete commissioning in October 2008 if the funding profile did not constrain the placement of orders. The cost profiles for both M&S and labor (excluding institutional overhead) are shown in Table 7.6.

Table 7.6: Instrument costs (then year \$K) based on the funding profile in Table 1.

	FY04	FY05	FY06	FY07	FY08	FY09	Total
M&S	0	1,097	3,321	3,362	520	68	8,368
M&S Contingency	0	0	379	338	1,580	782	3,079
Total M&S	0	1,097	3,700	3,700	2,100	850	11,447
Labor	609	1062	955	1150	560	299	4,635
Labor Contingency	304	531	478	575	280	150	2,318
Total Labor	913	1593	1433	1724	839	449	6,953
Total (M&S + Labor)	913	2,690	5,133	5,424	2,939	1,299	18,400
DOE (UIUC+Fermilab)	913	2,090	3,933	4,224	1,939	1,249	14,350

The DOE cost to UIUC and Fermilab is the fully total minus the other contributions shown in table. When overhead is included the total project cost for the DES instrument is \$22.5M.

7.4.2 Data Management Funding Model

The NCSA has agreed to provide the Dark Energy Survey Data Management operation with 100 TB of disk storage, 400 TB of fast tape storage, and the CPU hardware platform to process the data. The estimated CPU needs can be met with a range of machines that can provide a minimal guaranteed allocation of 10,000 SU/year. Additional CPU needs will be met through a formal proposal process at NCSA. These resources and their maintenance will be provided by NCSA at no cost to the project. The proposed hardware platform should be adequate for routine (normal) processing and distribution of the data. We expect that Fermilab will provide the computing equipment that the Fermilab participants will need to carry out their work

related to simulations and archival research, including sufficient disk and tape storage to contain copies of the various data products as needed. Compute farms at Fermilab will be employed as necessary for processing, particularly during full data reprocessing. We will also leverage the expertise in the Fermilab Experimental Astrophysics Group (EAG) that is currently dedicated to the SDSS.

The major new funding need for the Data Management project will be for additional staff support from NCSA and post docs and graduate students from the University of Illinois Astronomy Department dedicated to building the processing system and then processing and distributing the data to the collaboration and the astronomy community. The University of Illinois has committed 1.0 FTE (comprised of a 0.5 FTE commitment from the NCSA director and 0.5 FTE from the Associate Dean of LAS and the Astronomy Department Chair). During this phase, we estimate that we will need the support of another 1.5 FTEs plus partial support for the Data Management Project Manager at the University of Illinois. In addition, funds at the level of \$100K will be needed for additional disk purchases at NCSA. Funds are also needed for travel and archival research. When the support of a post doc and student at the University of Illinois Astronomy Department is included we estimate that the total funding need for the period 2005 through 2009 is \$1.2 M (FY04\$). As noted earlier we will submit a proposal to the NSF that will include a request for this support in the amount of \$1.2 M as part of a larger proposal. This part of the request will be submitted to the NSF through the University of Illinois Astronomy Department.

7.5 Outreach

The Collaboration will contribute to outreach by connecting with the established, highly developed education and public outreach activities at the participating institutions. Fermilab, LBNL, NCSA, and NOAO have developed extensive programs with teachers and K-12 that present natural opportunities. In addition, the Collaboration will build a website that will serve the Collaboration for communication and documentation during the construction phase and then as the operation phase draws near the website will have substantial content for the general public as well as the astronomy community. This website will also be a portal for both the collaboration and public access to the data and the catalogs. This approach was used successfully with the Sloan Digital Sky Survey. See <http://www.sdss.org> .

7.5.1 Websites

The NOAO website will be a natural way to present the capabilities of the Survey Instrument and the plans and status of the DES to the NOAO community. Indeed this is already being done. We envision a partnership with NOAO through their office of public outreach in all aspects of public outreach and education. The DES Collaboration could contribute material for the pages dedicated to the DES on this website as well as to other appropriate pages. We propose that the dedicated DES pages will have content that describes the DES Survey Instrument and the DES Science Goals in a way that is appropriate for the NOAO communities (both astronomers and the general public) and it will have links to the DES website, the NCSA website and websites of the other participating groups. Once commissioning begins the NOAO website will be the place to show schedules for operations and links to the portals for the data and catalogs.

We propose that the collaboration create special DES pages for the NCSA website that will contain the status of data processing operations and software development as well as descriptive material that describes the DES and the NCSA role in the DES. Since the primary location of the data and the catalogs will be at NCSA this website will provide information on how to access the data and catalogs and it will provide the primary access to the data and the catalogs. These web pages will have content that describes the DES is appropriate for the general public and the special communities that use NCSA.

The DES collaboration plans to develop a website at Fermilab for its internal needs in the very near future. While this website will be initially for collaboration documentation and communications, we will add content of interest to the general public and the scientific community. This content will have a particular emphasis on the connections among particle physics, astrophysics and cosmology. The website will be accessible to the public although the portions of the website that will contain documents that describe collaboration work that is in progress will only be accessible to the collaboration through passwords. The public portion of this website will present the status of the construction of the Survey Instrument and after data taking begins it will provide the same information on the data and catalogs as will be on the NCSA DES web pages. Since Fermilab will be a mirror site for the data and catalogs this website will also be a portal to the data and catalogs. This approach was used very successfully with the SDSS website, which is currently maintained by Fermilab. We quote from a brief description of the SDSS website here.

“The SDSS collaboration is engaged in a broad outreach effort that reflects the extended geographic distribution of the participating institutions and the participants. The project team at Fermilab maintains two publicly accessible, closely related websites, <http://www.sdss.org/> and <http://skyserver.fnal.gov/en/>. One of the objectives of these websites is the communication of the exciting discoveries in astronomy, astrophysics, and cosmology that are being made with the SDSS Archive to the public. They serve readily understandable, popular materials about the SDSS that are designed to appeal to people of all ages interested in the Universe. Both also provide access to the public SDSS Archive, a rich resource that the astronomical community uses for research. The SkyServer specializes in presenting written and graphical material to K-12 and college students and their teachers on current developments in astronomy, astrophysics, and cosmology. The SDSS website provides popular descriptions of the SDSS telescope and instruments, the goals of the survey, and the Apache Point Observatory, the home of the SDSS telescopes, for the layperson. It also displays the recent press releases and news articles describing research results obtained by the SDSS Collaboration. The SDSS web site displays the image of the week taken from SDSS observation and it provides the status of the survey, information on research topics submitted for publication, and access to the Archive, thus enabling the public to follow the progress of the survey.”

We propose to build a DES website that is very similar to the SDSS.org website for the collaboration and we will request funds to partially support the development of the educational content for a website that is similar to the Skyserver. At this time we have not decided on whether to host the Skyserver like website at NCSA, NOAO or Fermilab, although we believe

that this development work could be best done if it were done through one of the education efforts at NOAO, NCSA, or Fermilab. We anticipate that the request for funds will be made through a separate proposal jointly submitted by the interested education offices.

7.5.2 Education

All of the participating institutions are engaged in educational activities and we propose to contribute to their existing activities with material that is specific to the DES. Fermilab, LBNL, NCSA, and NOAO have educational outreach activities that focus on K-12 students and teachers. Except as noted in the websites above we propose that each DES group contribute to the activities associated with its institution. Thus the Fermilab groups would contribute to the K-12 educational activities at Fermilab, the University of Illinois groups and the NOAO groups would contribute to similar activities at the NCSA and CTIO and Tucson respectively. It may be appropriate for these offices to submit a joint proposal for a program that ties astrophysics, cosmology and particle physics together for K-12 students and their teachers. Alternatively they could make a significant addition to a program such as Quarknet that introduces the connections between the early universe and particle physics. In any event such efforts would require additional funding and this funding is best managed by the education offices working together with help from the DES collaboration. Once the DES is approved and secure funding profile has been obtained the DES collaboration will work with the education offices to determine whether these possibilities can be developed.

7.5.3 Public Information

When it is necessary to prepare press releases and other formal statements to announce important accomplishments we propose to do this through institutional contact persons with the offices of public affairs at each institution. Initially a lead public affairs officer will be designated to coordinate such public information activities among the participating institutions, the funding agency representatives, and the media. This arrangement worked quite well for the SDSS, although once operations became routine and science publications being routinely released a public affairs consultant was hired to manage the day-to-day work.

7.5.4 Existing Outreach Activities

Some members of the DES Collaboration are already involved in public outreach as noted in the following:

- The U Illinois Physics Department runs a Saturday Physics program for the local community. It is aimed at HS students, but everyone is welcome. See <http://www.physics.uiuc.edu/outreach/Honors/> .
- Mats Selen, University of Illinois Physics Department, has a weekly TV show on the local CBS station, and the videos are available on the web. See <http://www.hep.uiuc.edu/home/mats/whysguy.html> .
- Tom Droege is the creator of The Amateur Sky Survey which is described on: <http://www.tass-survey.org/>. One of the outreach programs was a science fair project. A technical description is at: <http://www.tass-survey.org/tass/tass.shtml> And a recent write up on TASS can be found at <http://www.tass-survey.org/tass/showtell/st0010.html>

The Amateur Sky Survey is a unique feature of the DES and we would like to use the DES website and perhaps the NOAO website to make it more readily available to the amateur astronomy community.

7.6 Relevant, Prior Experience of the Dark Energy Survey Collaboration

7.6.1 Instrument Construction

While the construction of a wide-field camera will be a new challenge for Fermilab, the Dark Energy Camera team includes scientists and engineers who have built state of the art silicon vertex detectors. Vertex detectors use many of the technologies and technical skills that are directly relevant for the construction of wide-field cameras. The accurate placement of sensors in a silicon vertex detector has important similarities with the accurate placement of CCDs on a focal plane and SiDet has superb facilities to build a focal plane. The Fermilab group at SiDet, which has extensive experience in wire bonding. These techniques can be adapted to bonding the camera front-end electronics onto the CCDs. In addition, CCD sensors share a common technology base with the silicon vertex detectors sensors. As noted earlier, the Fermilab and LBNL groups are exploring the use of the thick, high resistivity CCDs in the Dark Energy Camera. The LBNL groups have developed state of the art CCDs of this type, including their front-end electronics, for applications in astronomy over the past five years. Devices very similar to the devices specified in the Camera Reference Design have already been successfully deployed in telescopes at Kitt Peak. However, the use of the 2K x 4K LBNL CCDs in our proposed camera will require the creation and evaluation of a new mask for the production vendors. The Fermilab and LBNL members of the Instrument team have developed a preliminary plan to do this. In the past, Fermilab and LBNL have worked closely to develop several generations of the SVX chips and silicon strip vertex detectors for the current CDF and DZero experiments and thus it is natural for the Fermilab and LBNL participants to explore a similar partnership for the Dark Energy Survey.

7.6.2 Data Management

The University of Illinois Astronomy group has extensive experience in analyzing and archiving large optical and radio astronomy datasets. NCSA provides basic data management for all users of NCSA computing facilities across a variety of fields of science and engineering. Plante, as part of the NCSA Radio Astronomy Imaging group, has led the development and operation of the NCSA Astronomy Digital Image Library, the BIMA Data Archive and Image Pipeline. The astronomy group also has extensive experience in distributed (cross-institution) software development. In the early 1990s, NCSA was a partner in the development of the Miriad software system for radio interferometers. It was a founding member of the AIPS++ consortium, and it is currently a collaborator in the CARMA (Combined Array for Research in Millimeter Astronomy) Software Development project. Along with Fermilab, it is a collaborating institution in the National Virtual Observatory (NVO).

The Fermilab participants from the Experimental Astrophysics Group (EAG) have gained extensive experience with data management of large surveys through their fourteen-year participation in the SDSS. In particular, they contributed to coding and debugging the

pipelines for the SDSS, they operate the data processing and public data distribution center for the SDSS, and they are responsible for a major part of performing data quality assurance on the processed SDSS data. The EAG was very active in the creation of the SDSS archive and it manages and operates it.

It is from this extensive experience in data management and distributed software development that our data management plan has been drawn and gives us confidence that we can meet the DES requirements for data management and place this archive in the NVO.

7.6.3 Data Analysis and Interpretation

The members of the Fermilab Theoretical Astrophysics Group and the University of Chicago participants have made important contributions to the interpretation of the data from large surveys in the framework of the standard model of cosmology. The Fermilab Theoretical Astrophysics group was the first group at a DOE National Laboratory to specifically set out to explore the connection between the early universe and particle physics. Both groups have made important contributions to the interpretation of large-scale structure (galaxy), cluster counts, and weak lensing, and all of the analysis techniques that will be used to achieve the scientific goals of the Dark Energy Survey. Moreover, with members of the EAG, they have been active in applying these techniques to the analysis of SDSS data. The EAG participants also have experience in the analysis of wide-field multi-color surveys such as SDSS and CNO2. The Fermilab particle physicists plan to contribute to the science analyses.

University of Illinois scientists have focused on cosmology, structure formation, quasars and galaxy formation using data from X-ray satellites, optical observations, interferometric SZE observations and large scale, near-infrared surveys carried out by 2MASS and at Kitt Peak National Observatory using the FLAMINGOS camera. These analyses have led to important contributions to our concordance model of cosmology through precise constraints on the matter density from cluster baryon fraction measurements. Scientists at U Illinois and their collaborators have introduced and further developed the use of galaxy cluster surveys for the study of dark energy. In addition, one Illinois scientist is involved in the data analysis and interpretation of the DPOSS optical plate survey and the QUEST2 time domain CCD survey.

The LBNL Cosmology Group established a strong reputation for developing the successful observing strategies that allowed them to discover large numbers of supernova and follow their light curves. Their subsequent analysis of this data helped to establish some of the basic parameters of the concordance model of cosmology. The CTIO Dark Energy Survey participants are members of an independent group that developed similar observation strategies and analysis techniques for discovering and understanding supernovae. That group has achieved similar results of great importance. The two competing teams independently discovered the accelerating universe, perhaps the most profound discovery in cosmology in the past two decades and have joined forces in the DES Collaboration.

8. The Relationship of the Dark Energy Survey to other Astrophysics Projects

In the course of preparing this proposal we gave considerable thought to the place that the DES has in relationship to ongoing projects and the more ambitious future projects with a longer time scale such as JDEM and LSST. We prepared section 8.1, a roadmap for a U.S. Dark Energy Program in order to place the DES in the context of the extended program that we believe must be carried in order to understand dark and dark matter. We consulted the leaders of the more ambitious projects while we prepared the roadmap, and there is agreement that it would give the U.S. a superb program. However the dates that we used for each project are our estimates of how long it will take to secure the funds. We did this to make the assumptions for approval similar. Section 8.2 describes the current commitments of the collaboration members to other astrophysics projects and their temporal relationship to the Dark Energy Survey.

8.1 A roadmap for A U.S. Dark Energy Program

What is the nature of the Dark Energy? The National Research Council Report, *Connecting Quarks With the Cosmos (2002)*, identified the dark energy as one of the most profound questions about the Universe that are ripe for critical progress in the coming years. The OSTP interagency Physics of the Universe report pegged dark energy as the highest priority area for research. More recently, the Director of the Office of Science and the Assistant Director for Mathematical Sciences of the NSF requested that HEPAP identify the key questions now faced by high energy physics, particle astrophysics and cosmology. Their response, *The Quantum Universe*, stated that the answer to the question “How can we solve the mystery of dark energy?” is crucial for progress in these fields.

Dark Energy became a central issue, in 1998, when two independent groups studying distant supernovae discovered that the expansion of the Universe is accelerating. Subsequent observations of the cosmic microwave background radiation and of the large-scale distribution of galaxies confirmed and amplified this finding. According to Einstein's General Relativity, if the Universe is filled with ordinary matter, gravity should be slowing down the expansion. Since the expansion is speeding up, we are faced with two possibilities, either of which would have profound implications for our understanding of the cosmos and of the fundamental laws of physics: either two thirds of the energy density of the Universe is in a bizarre new form called Dark Energy, or General Relativity breaks down on cosmological scales and must be replaced with a new theory of gravity, perhaps associated with extra spatial dimensions. In both cases, the first-order effects on the expansion of the Universe can be described by an effective fluid with negative pressure, $w = p/\rho c^2 < -1/3$; we will therefore follow common practice and subsume both possibilities under the general rubric of Dark Energy. For example, the dark energy could be the energy of the quantum vacuum, that is, Einstein's cosmological constant (in which case $w = -1$), or it could signal the existence of a new ultra-light particle with mass of order 10^{-33} GeV/ c^2 or less. In either case, particle physics theory currently provides no understanding of why the dark energy density should have the value that would explain the present acceleration of the Universe.

In order to pin down the nature of the dark energy and decide between the theoretical alternatives, we must probe the dark energy (and measure the parameter w) with greater precision and determine whether and how it evolves with cosmic time. Here we briefly lay out our vision for the elements of a coherent Dark Energy Program aimed at achieving those goals over the next decade. It consists of a sequence of logical, incremental steps of increasing scale, technical complexity, and scientific reach, culminating in what should be definitive measurements and, as we expect, a breakthrough to a new paradigm. Successful execution of the program will rely upon interagency cooperation, upon collaboration among national laboratories, agency-supported centers, and universities, and upon public-private partnerships. *Connecting Quarks with the Cosmos* offered a bold vision for addressing the mystery of the dark energy; the program described herein describes a plan for implementing that vision. Key elements of this vision have been endorsed and amplified in the Physics of the Universe report, the *Beyond Einstein* program at NASA, the HEPAP subpanel report, the *Quantum Universe*, the DOE Office of Science Facility Plan, and the Astronomy & Astrophysics Decadal Report.

From supernovae (Supernova Cosmology Project and High- z Supernova Search), the CMB (most recently WMAP), and large-scale galaxy clustering (the Sloan Digital Sky Survey (SDSS) and the 2 Degree Field Survey (2dF)), the dark energy parameter w is currently determined with approximately 15% uncertainty (1-sigma), and we have essentially no constraints on its time evolution. Note that this level of uncertainty is currently only achieved when combining these different probes together and when strong priors are assumed on other cosmological parameters: currently, any single method delivers at best 30% constraints on w . The Dark Energy Program is aimed at sequentially increasing the precision of w measurements to the few percent level and constraining its time evolution at the $\sim 25\%$ level, with little or no prior constraints on other parameters. It is important to emphasize that the level of uncertainty described here and below does not yet include full accounting for systematic errors in all cases. Moreover, forecast constraints for dark energy parameters generally depend on input assumptions about the time evolution of the dark energy (the numbers here and below assume constant w) and about how well the values of other cosmological parameters are determined. As a result, extreme caution must be exercised in comparing the projected dark energy sensitivity of different experiments and methods.

Experimentally, we probe dark energy by studying the impact it has had on the history of the expansion rate of the Universe. Through the expansion rate, the dark energy affects observables such as the apparent brightnesses of standard candles (such as supernovae), the apparent sizes of standard rulers, the volume of space containing 'standard structures' such as galaxies and clusters of galaxies, and the rate at which those structures form. In recent years, a number of very promising new methods for probing dark energy have been developed. Since each of them measures different combinations of these observables, with different systematic errors and with different dependences on the cosmological parameters, they are doubly complementary. Because the nature of the dark energy is such an important question, and the measurements technically challenging, the most promising complementary dark energy probes must be pursued in order to form a robust program.

Four techniques hold great promise to us as probes of dark energy: (i) the luminosity distance (apparent brightness) of Type Ia supernovae, (ii) weak gravitational lensing of distant galaxies and its dependence on redshift, (iii) the redshift distribution and clustering evolution of galaxy clusters, and (iv) the evolution of the spatial clustering of galaxies, using features in the galaxy power spectrum as standard rulers. While this list does not exhaust the potentially powerful probes of dark energy (which include, e.g., the integrated Sachs-Wolfe effect, lensing of the cosmic microwave background, the Lyman-alpha forest cross-power spectrum, and strong gravitational lensing statistics), given our current knowledge it constitutes the minimal set that together has the best opportunity to achieve the aims of the program. Of the four techniques, supernovae are the furthest advanced as a dark energy probe and the method for which systematic errors have been most thoroughly characterized. All these techniques benefit from complementarity with cosmic microwave background (CMB) measurements: while the CMB anisotropy itself does not strongly probe the nature of the dark energy, it provides important constraints on other cosmological parameters that enhance the dark energy reach of these methods. The strongest CMB constraints currently come from the WMAP satellite; later in this decade, the Planck Surveyor and ground-based CMB polarization experiments will provide even more powerful complementary constraints.

A number of surveys are underway with the aim of determining w with 10-15% statistical uncertainty (when combined with the CMB) by about 2008. The ESSENCE survey at Cerro Tololo Inter American Observatory (CTIO) in Chile and the CFHT Legacy Survey on Mauna Kea, both on-going 5-year projects, will measure distances to many hundreds of Type Ia supernovae to redshifts $z \sim 0.8$, vastly increasing the dataset over this range. The Hubble Space Telescope, using a small number of supernovae found at $z > 1$, is providing a first glimpse of the transition from an early decelerating phase of expansion to the present accelerating phase. The Nearby Supernova Factory, starting in 2004, will provide multi-epoch spectrophotometry for a few hundred low-redshift supernovae, increasing the cosmological precision of these high-redshift supernova measurements and probing systematics. The proposed extension of the SDSS will augment these surveys by measuring 200 supernovae in the redshift desert from $z = 0.1$ to 0.3. Using weak lensing measurements covering on the order of 100 square degrees, the on-going DeepLens and CFHT Legacy Surveys, among others, will provide the first constraints on dark energy from this technique.

While these projects are exploiting the supernova and weak lensing methods in the near term, these methods will be further developed in the intermediate term and augmented with the cluster counting approach to dark energy. Several projects, including APEX, the Atacama Cosmology Telescope, and the South Pole Telescope (SPT), will carry out increasingly large cluster surveys using the Sunyaev Zel'dovich effect. This effect is powerful because it can be used to find clusters at all redshifts and provides a robust estimate of the mass of each cluster. The South Pole Telescope, slated to begin operations in 2007, will find and measure $\sim 30,000$ galaxy clusters in a survey covering 4000 square degrees. The Dark Energy Survey (DES), a proposed five-year survey that could begin in 2009, will use a new wide-field camera to be built for the existing Blanco 4-meter

telescope to cover the SPT survey area in four optical passbands, providing the needed photometric redshifts for these clusters. Together, SPT+DES will aim to deliver $\sim 5\text{-}10\%$ statistical accuracy on w using the cluster counting method (and no priors) and will develop this method as a precision cosmological probe. The Dark Energy Survey will also constrain the dark energy with similar statistical accuracy via weak lensing, the evolution of galaxy clustering, and supernovae. On a similar timescale, the DUO survey, a proposed NASA MIDEX mission, if approved, would carry out an X-ray census of clusters with substantial dark energy reach. These intermediate-term projects will take the next major step in probing dark energy and will begin to seriously constrain its time evolution. They will also help explore the limitations of the different techniques. This knowledge will be useful for and help ensure the success of the more ambitious and more challenging projects to follow.

For the longer term, *Connecting Quarks with the Cosmos* and *Physics of the Universe* recommended that ground- and space-based wide-field telescopes with Gigapixel-scale cameras be pursued to address the dark energy question. They highlighted two major complementary projects that have been proposed with primary goals that include probing the dark energy. The Large Synoptic Survey Telescope (LSST) is a proposed large ground-based telescope with a wide-field imager that will carry out multiple scans over roughly half of the sky; it will study a variety of transient astronomical phenomena and will probe dark energy via weak lensing cosmic shear, lensing cluster counts, and galaxy clustering. The Supernova/ Acceleration Probe (SNAP) is a satellite concept for the NASA-DOE Joint Dark Energy Mission that will include a large survey of ~ 3000 supernovae that reaches redshifts $z \sim 1.7$ and a wide-area survey to measure weak lensing, optical cluster counts, and galaxy clustering. LSST is designed to make optimum use of the cosmological information that can be gleaned from ground-based imaging, while SNAP will be uniquely suited to measure high-redshift supernovae with optical and near-infrared detectors on a stable platform above the atmosphere. These projects aim to achieve exquisite precision on cosmological parameters using these complementary techniques, with statistical error of a few percent on w . Moreover, they have sufficient reach to offer the real possibility of determining the time evolution of the dark energy. Since they are being optimally designed *ab initio* to achieve these goals, these projects should have unprecedented control of systematic errors. Given the complementarities of the dark energy probes they will pursue and the systematic uncertainties associated particularly with the newer dark energy methods, both projects are required in order to achieve the goals of a robust dark energy program. These projects aim to begin science operations about a decade from now. In addition, a deep, wide-area spectroscopic survey, using a Wide Field Fiber-fed Multi Object Spectrograph, similar to the KAOS concept that was recently proposed for one of the Gemini telescopes, or a space-based instrument, could further exploit the galaxy clustering dark energy probe during this time period.

In sum, the Dark Energy program outlined above encompasses a coherent, graded approach to one of the great unsolved mysteries of science. The timeline of the program proceeds sequentially from the current surveys (covering roughly the period 2004-2008), aiming at 10-15% precision on the dark energy equation of state w , through the intermediate term (2009-2014), when SPT+DES should deliver 5-10% precision on w and begin to constrain its time evolution through SZ cluster counts and other probes, to the long term (after 2013),

when LSST and SNAP begin to make the definitive measurements, reaching few percent precision on w and determining its time evolution. Proceeding along the timeline, the scientific goals of the program become increasingly ambitious, requiring an increasing scale of effort that builds upon the steps taken before. The ultimate aim of the program is to fully exploit these complementary dark energy probes and thereby unravel one of the great scientific mysteries of our time.

8.2 The Relationship of the DES to other projects of the DES participants

Section 8.2 describes the current commitments of the collaboration members to other astrophysics projects and their temporal relationship to the Dark Energy Survey.

8.2.1 Fermilab Projects

The Fermilab EAG has had a major involvement in the SDSS over the past fourteen years. While the approved five-year observation phase of the SDSS will end July 1, 2005, the SDSS consortium has developed a plan for SDSS II, a three-year extension and is actively seeking funds for the extension. The Fermilab Director has approved Fermilab's continued participation in SDSS II at a reduced level of effort. Since the SDSS has been in operation for five years its operation is mature, and the demands on the Fermilab staff can be reduced without hurting SDSS or SDSS II. The Fermilab astrophysicists in the EAG who plan to participate in the DES have already reduced the level of their contributions to the SDSS infrastructure. Several Fermilab particle physicists have joined the SDSS supernova campaign, the element of SDSS II that is focused searching for type Ia SN in the red shift range between .10 and .30, a range in which the SDSS is uniquely qualified. They are already active participants in planning the campaign, which will begin in the fall of 2004. They will also share the load of infrastructure work with the EAG astronomers who plan to continue to work actively on the SDSS extension. Fermilab will support the data processing and archiving of the SDSS imaging and spectroscopic data, and it will continue to manage distribution of the full SDSS archive during the extension. The Fermilab participation in the SDSS will end in July 2008 if all of the funding for the extension is secured, and if the funding is not secured it will end earlier. Whenever that happens, the computer professionals and the astrophysicists in the EAG will be in a position to contribute to the operations phase of the Dark Energy Survey as well as to carry out research with the DES archive. After SDSS II ends the Fermilab scientists working on SDSS II plan to contribute to DES. The EAG computer professionals have the experience to support simulations, observations, data processing, data analysis and archiving for the DES. The DES does not plan to make large demands on the EAG support team, because the data management and data distribution effort will be led by and primarily supported by the University of Illinois.

The EAG astrophysicists and several Fermilab particle physicists have formed the Fermilab SNAP group. All are engaged in contributing to the SNAP collaboration development of the science case for JDEM/SNAP. The wide area survey part of SNAP, which includes both weak lensing, and cluster counts, is of particular interest to the Fermilab DES participants, who are also engaged in SNAP. They believe that this effort will speed the development of DES simulations and refine the DES observing strategy. Since the Joint

Dark Energy Mission (SNAP) will probably not be launched until after 2014, the Dark Energy Survey will fit nicely in the temporal gap between the end of the SDSS and the start of JDEM.

8.2.2 University of Illinois Projects

One of the University of Illinois astronomers (J. Mohr) is a member of the South Pole Telescope (SPT) Collaboration. Mohr's responsibilities in SPT are to secure the optical followup of the SPT cluster survey region and to improve cluster finding and characterization methods in the SZE and optical. These responsibilities are obviously well aligned with the DES. In addition, Mohr is co-I on the Dark Universe Observable (DUO), a NASA Small Explorer mission in Phase A study. If approved, that mission will carry out a large X-ray cluster survey to study the nature of the dark energy. A portion of the DUO survey will overlap the SPT/DES region near the south galactic cap, and this overlap will enable additional science such as SZE+X-ray distances and more robust determination of the evolution of cluster mass-observable relations. DUO will launch in 2008, if selected. Mohr's responsibilities include refining X-ray and optical cluster finding techniques, which is an activity that is complementary to his DES and SPT work. In addition, Mohr will continue to work on refining techniques for studying the dark energy with galaxy clusters and the clustering of galaxies. Mohr and collaborators introduced this technique, writing the first paper on how one can use large cluster surveys to study the dark energy, and he has continued to develop these ideas—introducing the concept of self-calibration into cluster surveys. This work has led directly to cluster survey work with the Sunyaev-Zel'dovich effect Array (SZA, PI Carlstrom/U Chicago), the SPT (PI Carlstrom/U Chicago), DUO (PI Griffiths/CMU) and now the DES.

NCSA is supporting a series of astronomical archive and pipeline processing projects intended to develop the necessary infrastructure to handle the largest telescopes of the next decade, including LSST. DES data management project manager Ray Plante (NCSA) continues his work on archiving and data management with the expansion of the Berkeley-Illinois-Maryland Array (BIMA; mm-wave astronomy array) into the Combined Array for Mm-wave Astronomy (CARMA). The DES Data Management plan leverages off of the existing work done on BIMA/CARMA project, particularly in the area of grid processing. Plante also leads the NCSA team in an emerging collaboration with NOAO to address distributed archiving and processing for NOAO data streams. Plante is also currently leading the project planning for the NCSA LSST effort in advance of a new NCSA LSST lead to arrive by Fall 2004. In addition to their participation in the LSST project, NCSA is also a collaborating institution in the Square Kilometer Array, a radio telescope on a similar data and time scale as LSST.

All of the University of Illinois DES members plan to participate in LSST. In particular, the University of Illinois, in partnership with the NCSA, plans to be a major data processing and archiving center for LSST. In addition, the software for the LSST data acquisition will be developed by Thaler's group in the Physics Department. As noted earlier, this relationship will strengthen the Dark Energy Survey Collaboration. The needs of the two projects and their schedules nicely match the availability and interests of the scientists and technical staff at the University of Illinois.

8.2.3 University of Chicago Projects

The University of Chicago members of the Dark Energy Collaboration are active in several astrophysical projects. Josh Frieman, who is the DES liaison with the University of Chicago Astronomy and Astrophysics Department, is a member of the SDSS, and coordinated the development of its spectroscopic pipeline software. He is co-chair of the SDSS Large Scale Structure Working Group and is active in the analysis of large-scale structure and weak lensing data. In addition, he serves on the SDSS Collaboration Council and is the Fermilab representative on the SNAP Institutional Board. He has also been engaged in unrelated observation projects at CTIO in the past. John Carlstrom is the PI of the South Pole Telescope Project and the leader of the SPT collaboration, which includes the UC Berkeley /LBNL Cosmic Microwave Background Group. He will be the primary contact between the SPT Collaboration and the Dark Energy Collaboration. In this capacity, he will help to define the procedures for analyzing the relevant data sets created by the two surveys.

8.2.4 CTIO Projects

The CTIO participants are actively engaged in the ESSENCE Project, which will detect and follow up on ~200 supernovae that will be observed with the Blanco telescope. The ESSENCE Project is expected to be complete in the next 3 years. They are also pursuing the observation of nearby supernovae, because these observations will tie down the Hubble diagram at zero redshift. They are also engaged in the use of the Monsoon system with the NEWFIRM Camera. These efforts will help the Dark Energy Survey.

8.2.5 LBNL Projects

The LBNL Cosmology Group is engaged in three projects: the Supernova Cosmology Project (SCP), the Nearby Supernova Factory (SNF), and SNAP. The Supernova teams are working with the CFHT Supernova Legacy Survey using Megacam. The goals of this observing campaign are similar to the ESSENCE Project. The Nearby Supernova Factory will discover ~300 nearby supernovae with the NEAT telescopes and follow them up with new instruments on the Hawaii 2.2-meter telescope. Both the SNF and the CFHT Supernova Legacy Survey are expected to be completed in the next 4 years. LBNL is the lead institution for the proposed SNAP mission.

9. Community Science with the DECam and the DES Legacy Archive

The Mosaic Cameras installed at the NOAO 4m telescopes, north and south, are the most popular facility instruments at NOAO. Over the last two years, the CTIO 4m imager has been assigned 42% of the total nights available. The present Mosaic imagers cover a 0.36 sq-degree field at prime focus in an 8Kx8K format, with a 100s read time. These optical imagers are the largest field imagers routinely available to US astronomers, and they support a wide range of highly-ranked science, such as planet searches, trans-Neptunian object surveys, maps of emission line regions in the Milky Way, searches for tidal streams in the Galactic Halo, microlensing in the LMC, inter-galaxian populations in nearby galaxy clusters, QSO statistics, weak lensing studies, galaxy counts at redshifts out to $z=2$, searches for galaxy clusters, and cosmology with supernovae, to name a few projects.

The assigned time to the present Mosaic projects range from very large 5 year survey projects to much smaller 1-2 night pointed surveys, and we expect that DECam will be used in the same manner. The light grasping power of a 4m telescope is ideal for finding objects to be followed up on 8m telescopes either spectroscopically or in the near-infrared. These Mosaic imagers are often the first step in any scientific project requiring Gemini or Keck time. Because the suite of 4m and 8m class telescopes will not change significantly in the next 10 years, data products provided by 4m optical mosaic surveys will continue to be extremely important for the support of the largest aperture telescopes, as well as for stand-alone photometric projects.

The DECam, with a field 8 times the size of the present Mosaic cameras, and with a read time of only 17 seconds, will provide a much wider field and more efficient use of observing time. The initial filter suite will be the SDSS "griz" filters. Any present Mosaic filter can be put into the filter bolt (during the day) so that all present Mosaic projects can be continued with these filters. We imagine, however, that a number of other filters that use the full field will be constructed for important survey projects, funded outside of the present proposal. We anticipate that the user community will want to use the interference filters DDO51, an H α set, [OIII], [SII], and Y (1 micron). Less expensive filters that users may need are the glass versions of the broadband BVR filters. However, we expect that the popularity of Johnson/Kron-Cousins filters will steadily decline over the next decade as more programs make use of SDSS databases.

In the following sections, we give a flavor of the wide range of science projects that will use the larger field and reduced read time of the DECam. As a regularly scheduled NOAO instrument, we expect that time on DECam will be assigned to projects in a similar fashion to the present Mosaic imagers - serving large surveys allotted time through the NOAO Survey TAC, as well as the traditional few night runs.

9.1 Stellar Science Cases

With DECam, CCD imaging moves further into the field of view regime previously accessible only through Schmidt cameras and photographic plates. For example, the CTIO 0.9-m Schmidt, now retired, has a field of view of 5 degrees by 5 degrees. Such cameras

have provided the basis for many directions of astronomical research, not least the exploration of populations and distributions of stars in our own and nearby galaxies. Such stellar astronomy is an obvious field in which DECam will find considerable use among the community.

-- Kuiper Belt searches

The Kuiper Belt is a region beyond Neptune containing tens of thousands of small bodies in orbit around the Sun. The KBOs allow us to study how dust grains in the early solar nebula coagulate into the planetesimals of the present epoch. The KBOs are fossil remnants of the chemical and dynamical processes that occurred in the outer solar disk at the time the Solar System formed. Their physical characteristics should tell us much about the formation of the circumstellar dust disks we see in external stars and directly tell us about the conditions of planet formation. A deep survey of the ecliptic will allow us to catalog a population of thousands of KBOs in terms of their dimensions, content, and dynamical characteristics. The statistics of such a survey will allow us to better understand the physical conditions at the time of the formation of the Solar System. A large number of KBOs will be available for spectroscopic follow-up at 8m class telescopes. Their thermal and bolometric properties can be followed up with SIRTf and ground-based mid-infrared imagers.

-- Proper motion surveys of galactic open clusters

Recent years have seen considerable progress in the identification of very low mass stars and brown dwarfs, particularly in open clusters. These systems contain stars of known distance, age and metallicity and make excellent laboratories for the study of stellar structure over the full mass range of stable, hydrogen burning stars. It is now possible to study the physics of coeval objects having masses that range over three orders of magnitude. Particularly interesting are the newly identified very low mass stars providing important insight into the study of lithium evolution, angular momentum evolution, spotting, variability, coronal activity, binary fraction and mass function. If one assumes that all disk stars originate in open clusters, then open cluster studies are relevant to the general field population

Since open clusters subtend generally large angles on the sky, the majority of work done on them has historically been via Schmidt plates. Membership is established through a number of means, but proper motion studies are prominent. DECam will be an ideal tool with which to pursue future studies, providing faster, more precise and deeper results than a photographic plate. Of course, this requires that DECam be an astrometrically stable instrument.

In this field and other explorations of low mass objects, DECam will be complemented by future wide-field IR instruments, which will permit confirmation of cluster members. DECam's significant red sensitivity will be particularly useful for observations of the redder, lower-mass cluster members.

-- Cool white dwarfs

The low-luminosity fall-off and the general form of the luminosity function of white dwarfs is an important new tool for dating and exploring the history of star formation in the Galaxy. The coolest white dwarfs represent the graveyard of the very first stars to have formed in the Milky Way, now slowly fading into thermal oblivion. It is believed that these objects are significant contributors to Galactic dark matter, being found in microlensing surveys such as MACHO+EROS. Finding these objects is a job for large surveys and DECam is ideally suited.

Such a project may require investment in additional filters beyond those planned for the Dark Energy Survey, e.g. DDO51 which separates the white dwarfs which are essentially featureless at 515nm, whereas other stars generally show significant absorption.

-- Globular cluster tidal streams

Recent years have seen the discovery of streams of stellar debris emanating from Galactic globular clusters and nearby dwarf galaxies as a result of the tidal stresses they have experienced in passage through the three dimensional gravitational potential field of the Milky Way. Clearly such tails provide invaluable probes of this potential field and details of its interaction with the source clusters and galaxies. Because these streams extend over several degrees of arc, or more, DECam will inevitably see use in their study.

-- Variable stars

Stellar variability in all its forms is an important phenomenon in the study of stellar astrophysics. From simple binaries, through pulsating and flare stars, to interacting systems, all aspects of the physics of stars are open to study, indeed many can only be studied through photometric variability. DECam, with its fast readout gives it great potential as the world's largest time series photometer. Volume-limited variability surveys on time-scales of a few minutes is still a relatively untouched region of the parameter space of ground-based astronomy and should offer a rich mine for our understanding of the space densities of numerous types of variable stars and through this, of stellar evolution in general.

To select a quick example, a single pointing of DECam near the Galactic plane might be expected to contain as many as several hundred cataclysmic variables (depending on which estimate of the poorly known space density one believes) which amounts to a significant fraction of the number of such systems currently known. A series of short exposures of such a field will generate a vast number of light curves from which the cataclysmic variable systems can be identified through their flickering -- a stochastic variation on time scales of seconds to tens of minutes resulting from the interaction of the material accreted from the late-type star in the system with the accretion disk surrounding the white dwarf component. It goes almost without saying that the same kinds of variable survey data will also expose planetary transits and permit the discovery of new extrasolar planets.

-- Space astronomy follow-ups

Finally, ground-based optical surveys have always been vital in the identification of the sources discovered during space-based surveys in other regions of the electromagnetic spectrum. In particular, X-ray surveys provide large numbers of objects which require optical follow-up. Currently, the Blanco telescope and Mosaic II are seeing use for following up on the Chandra Observatory surveys, such as the ChamPlane campaign to identify serendipitous sources in the Galactic plane, concentrating particularly on X-ray binaries and cataclysmic variables. Future missions, such as Constellation-X, will have similar needs, which will be adroitly addressed with DECam.

This is another use of DECam which could benefit greatly from the availability of filters besides those of the DES. Specifically, X-ray follow-up and variable star surveys will likely offer some demand for an H- α filter. Preliminary examination of the current corrector design implies it is sufficiently telecentric to allow the use of reasonably narrow filters. Presumably, any filters for DECam use other than for DES will have to be purchased through third parties and sources such as NSF proposals, but this is not an unusual method of facilitating a specific observing program at NOAO.

9.2 Extragalactic Science Cases

-- External stellar populations.

The DECam will be an excellent imager for studies of the stellar populations of the Magellanic Clouds. With a field of view 2.2 degrees in diameter, the DECam will cover the main body of each galaxy in a few pointings. Two science cases can be addressed with the DECam: the stellar population of the LMC/SMC region and the search for microlensing in the halo of our Galaxy.

The recent LMC Stellar Catalog by Zaritsky and collaborators done with the LCO 1m Swope telescope covered 64 sq-degree to a completeness level of $V=20$. The DECam can cover the same area in 21 pointings. We anticipate a community survey project targeting both galaxies and the extended regions around each galaxy including the bridge between the galaxies. In uncrowded regions, the photometry can reach $m=26$ to allow for searches of faint tidal streams that should be associated with the multiple passages of both galaxies around the Milky Way. A very deep search into the possible halos of these galaxies would extend to 10 degrees from the galaxy center. The whole halo of each galaxy could be covered in 100 pointings with the DECam. Such a survey would be prohibitive with the present Mosaic imagers.

The SuperMacho program for microlensing of Galactic halo stars on the screen of LMC stars covers 18 sq-degrees. The SuperMacho program has a 5 year survey mission to find lensing events with 30 half-nights each year. Each field is revisited every second night in a single color. The present microlensing search is limited by the field size and read time of the CCD. The DECam would much more efficiently cover the LMC to greater depths. The present SuperMacho search expects to find 10-20 events per year with coverage every 2

days using half nights. The same search could be done in less than 1 hour per night with DECam in two colors instead of one. With two colors, microlensing (which is achromatic) can easily be separated from other transients. With coverage every night for one hour, one could increase the chance of finding cusping events, which would indicate binary or planetary companions.

As with the Macho and SuperMacho projects, the database for the microlensing survey provides a rich hunting ground for other projects, especially those interested in time-varying phenomena.

-- Microlensing toward the Fornax Dwarf Galaxy

The DECam can cover the Fornax Dwarf in a single pointing. A routine survey of Fornax every few nights over a few months per year with single pointings will determine the Galactic halo lensing rate toward this object. With microlensing rates toward Fornax, M31, the LMC, and the SMC, a spatial distribution of dark compact objects in the Galactic halo can be determined. Present estimates are that up to 20% of the dark matter Halo is composed of compact objects, but whether this population conforms to the flattened spheroid potential of the Halo has not been determined.

-- Dwarf galaxy searches in nearby galaxy groups

While much attention has been focused on large clusters of galaxies, most galaxies in the Universe exist in the field or in loose groups, such as the nearby Sculptor, Cen A, NGC 2997, M66, and M96 groups. Hierarchical clustering predicts large number of dwarf galaxies of unknown luminosities in these groups. The number of dwarfs should be factors of 10 to 100 times the number of brighter galaxies. The search for these dwarfs requires extremely deep and wide field searches for very faint red galaxies with spheroidal structure, analogous to the Milky Way and Andromeda satellite Sph galaxies.

-- Intra-cluster light (ICL)

DECam would be able to image intra-cluster light in nearby galaxy clusters. This is the very low surface brightness signature of stars that seem to be associated with the clusters themselves, as opposed to any one galaxy, though the origin of the stars is an open question: were they formed along with the cD galaxy or in the intracluster medium, or are they the remnants of other stripped/disrupted galaxies? Studies of the spatial distribution and color of the intra-cluster light helps to pin down the origins. The distribution of the light can also be used as a tracer of the halo potential and mass to light ratio.

The DECam would also be an excellent imager for finding PNe in nearby clusters. These surveys need large apertures and large fields to go very deep in a [OIII]5007 filter, but also cover as much of the nearest clusters as possible. These tracers could probe even further

from the cluster center than diffuse light to trace the spatial distribution of the intra-cluster population. The KAOS instrument at Gemini south could be used to get spectra for the kinematics of the population to compare with the ICL. In particular, is the ICL population relaxed compared to the galaxy distribution?

In both projects, the large simultaneous area allows for deep studies of nearby (and consequently angularly large) galaxy clusters. For the diffuse light, the simultaneous coverage helps reduce the systematics in the measurements, which dominate at these low surface brightness levels. In addition, it is critical to image the cluster with a field significantly larger than the cluster so that the cluster light can be measured relative to blank sky

-- Photometric surveys of the high redshift universe

The DECam would be well suited for intermediate depth, smaller solid angle extragalactic surveys as a complement to the DES. These surveys could complement ongoing surveys by pushing to larger solid angle than is possible with current generation cameras. This is especially important if one wishes to study the clustering of galaxies and its redshift evolution, and large solid angle, deep photometry is also critical for any program that seeks rare, faint objects, such as quasars beyond a redshift $z \sim 6$.

9.3 DES Legacy Archive Science

Besides the results from the key science programs proposed by the Dark Energy Survey team, the data archive will be the rich resource for the community. The DES Legacy archive and the user community science image archive will become a major digital sky survey, the most extensive in the Southern Hemisphere until LSST is built, assuming it goes in the south. The DES data, with uniform depth and coverage, will be well suited for fundamental astronomical studies - parallaxes, Hess diagram analysis, and the like. Even in the era of the LSST, the DES data will be useful for proper motion studies and other time domain studies. We realize that the utility of the archive to the community will depend on its accessibility and the robustness of its calibration; we have designed a survey strategy to meet the calibration requirements for the data (see Chapter 3 for requirements and Chapter 4 for the survey plan), and we have developed a data management and archiving plan with the goal of rapid community data release and ease of community access (see Chapter 6).

Some of the topics listed in the previous section would benefit from the DES archive, but in addition, there are additional projects. Here we describe in detail two specific examples of doing science using the DES Legacy archive: cluster strong lensing and wide ranging quasar science

-- Strong lensing in galaxy clusters

The incidence of arc formation due to extreme strong-lensing by galaxy clusters has long been suggested as a cosmological probe. Extensive research in the 1990's, exploiting primarily the X-ray selected EMSS cluster sample, demonstrated modest consistency

between observations and theoretical predictions for open low- Ω_M cosmologies. Since this work, which culminated in the analysis of Bartelmann et al. (1998), there has been a growing realization that the predicated arc statistics are in rather gross disagreement with the flat, Λ -dominated cosmology indicated by many other probes.

The formation of arcs is dependent on essentially three things: 1) the cosmology, 2) the source population, and 3) the properties of the lenses (clusters). The cosmology will be well determined by the DES itself, and the source population is now relatively well known with further progress to be expected from follow-up of surveys such as the Hubble Ultra-Deep Field. A large sample of clusters with arcs could then be used to understand the (dark) mass structure of galaxy clusters independent of the luminous component of the cluster.

How many arcs might we expect to see in the DES? Statistics are scarce, but the most comparable dataset is the ~ 90 square degrees of RCS data, which yielded 7 arcs around 5 clusters. The DES data are in more and bluer bands (and hence likely to pick up more arcs, because arcs tend to be blue) and typically about 0.5 mags deeper than the RCS. One can thus readily expect several factors of two gain in finding arcs in the DES over the RCS. The DES has similar redshift grasp to the RCS, and is about 55 times larger in area. It is thus reasonable to expect to find something like 1000 strong-lensing clusters in the DES! Such a sample would completely revolutionize our understanding of cluster structure and could present a very powerful cosmological test in its own right.

Finally, it is worth noting that most of the strong lensing by clusters does not result in arcs, but multiple images which may not be morphologically recognizable despite being highly magnified. A particularly striking case of this is the object cB58 (Yee et al. 1996) which is a 20th magnitude galaxy at $z=2.6$. The multi-filter observations of the DES will allow us to recognize such objects as extreme outliers in magnitude-redshift space, which are on lines-of-sight behind massive clusters. Given the area of the DES we expect to find perhaps hundreds of such objects, which will be a profoundly important sample for studying the very distant universe and the formation of galaxies.

-- QSO catalogs

Wide, multi-band imaging surveys provide incredible resources for improving our understanding of the Universe. The Palomar All-Sky survey, 2MASS, and the Sloan Digital Sky Survey enabled advances in optical astronomy, as radio, X-ray, and gamma-ray surveys have done in other wavelengths, by taking advantage of unique qualities that large quantities of data offer: ability to find rare, exotic sources and reduction of uncertainties in statistical distributions due to reduced Poisson fluctuations.

Other "large" statistical samples of QSOs have been compiled by:

- SDSS -- 8,000 square degrees to a limiting magnitude of 20.1 for 80,000 spectroscopically-confirmed QSOs when SDSS is completed. From the imaging SDSS data alone, a catalog of photometrically-identified quasars to a limiting magnitude of 21

has 100,000 QSOs in 2099 square degrees (Richards et al. 2004). The highest-redshift QSOs ever discovered (up to $z=6.4$) are also from the SDSS, with spectroscopic follow-up from other instruments.

- 2dFQ -- 750 square degrees to a limiting magnitude of 21 for 49,425 spectroscopically-confirmed QSOS.
- COSMOS -- 2 square degrees, with 600 QSOs to 24th magnitude and multi-wavelength observations
- COMBO-17 -- 1/4 square degrees, with 100 QSOs to 24th magnitude, but with precision photometric redshifts (good to 0.015 in z) from narrow-band filters. (Wolf et al. 2004)
- GDDS -- 0.1 square degrees, to 26th magnitude (but with extensive coverage in many wavelengths)

In comparison, the DES will carry out a quasar survey -- during the course of normal operations -- covering 5,000 square degrees, to 24th magnitude, including 1.6 million photometrically-identified QSOs.

Clearly, this unprecedented data sample opens up new vistas:

1. The highest redshift quasars: covering an area comparable to the SDSS, but 4 to 5 magnitudes fainter satisfies the criteria of Fan et al. (2004 ASP Conference Series v311): "A deep quasar survey at $z \sim 6$ is needed to understand the complete picture of high-redshift quasar evolution and its relation to reionization history." The SDSS has tentatively found evidence of reionization at $z \sim 6$ (Becker et al. 2001) and the DES should image many more high-redshift quasar candidates than the SDSS, testing this reionization claim and potentially mapping the surface of reionization, and probing coevolution of AGN, black holes, and QSOs.
2. The catalog of quasar candidates identified in the 4-filter photometry will have photometric redshifts determined to ~ 0.15 , and a probability vs. redshift distribution to quantify ambiguities. Cross-correlation of this catalog with X-ray and radio surveys, and spectroscopic follow-up with multi-fiber spectrographs, are fertile research programs. The large numbers allow us to study the evolution of the luminosity function with redshift and absolute magnitude.
3. We estimate the number of quasars in the DES by assuming a faint-end slope of the QSO luminosity function of around 0.3. However, the distribution of quasars is itself rather uncertain, especially at fainter magnitudes and higher redshift. At around $g \sim 21$ the redshift distribution flattens; the DES could unambiguously determine whether this is due to survey incompleteness or intrinsic to the population of faint quasars.

4. The clustering of quasars alone provides a wealth of cosmological information (see, e.g., Outram et al. 2003). Relationships between the clustering of quasars along and perpendicular to the line-of-sight provide a strong constraint on the Dark Energy (the Alcock-Paczynski effect), while the relative angular correlation of the quasar and galaxy populations can provide a constraint on the matter density via the skewness statistic, without the need to measure accurate population redshifts (Menard, Bartelmann, & Mellier 2003). While many of these tests may be augmented with spectroscopic redshifts, photometric redshifts often provide sufficient information, especially in conjunction with ancillary data in other passbands (such as might be obtained in conjunction with VISTA).

5. Lensed quasars offer a unique view of the distant Universe. Knowing the number of faint quasars is critical to understanding the effects of lensing magnification bias. Assuming typical cosmological models, the DES should identify around 50 strongly lensed QSO pairs (as well as quadruples, sextuplets, etc.) with separations less than 10 arcseconds (see, e.g., figures 7-15 of Lopes & Miller 2004). The actual number of lenses found can by itself constrain cosmological models, subject to uncertainties in halo modeling, in addition to the constraints on the Hubble parameter that arise from measuring image delays between lensed pairs.

6. The general DES dataset also provides important information on the variability of quasars, via the repeated observations over the course of the survey used to build up the entire 5000 square degrees. The smaller, supernova-focused area, however, would prove even more useful in this regard due to the large number of epochs sampled over a number of years to faint magnitude limits. Variability is proving to be a powerful method for selecting quasars, at a range of redshifts (see, e.g., Rengstorf et al. 2004). The SN component of the DES should provide highly-sampled light curves (as short as 1 day in the observed frame) for around 20,000 quasars. This information can be used to constrain the mean lifetime of quasars (e.g., Martini & Schneider 2003) as well as the power spectrum of accretion that constrain models of accretion disk instabilities (Vanden Berk et al. 2004).

In addition to the strides that will be made with this QSO sample, we expect that the astronomical community could request that imaging be taken with narrow-band filters.

9.4 Community Workshop

The limited sample of science cases listed above is based on the scientific range of interests of the writers of this proposal. The US astronomical community, however, can tell us much better what is the true range of science that the DECam instrument can support. As part of the Dark Energy Survey proposal, we will call for a workshop to be held for prospective users of DECam and the DES Legacy archive. This workshop will be held in 2004 or in early 2005, preferably near the Chicago area so that most of the DES team can attend. It would be preferable to hold the workshop before the end of the year 2004.

The goals of the workshop are twofold. We want to hear from the community about their ideas for the science that can be done with this instrument. In addition, the DECam project and NOAO need to anticipate instrumental functions and data products not covered in this

proposal. For instance, what should the form of the archive be? What data products are crucial to include in the archive? What are the most important filters that need to be acquired? What should be the role of large surveys versus smaller pointed surveys? We imagine that users will suggest novel ways to use the instrument in a manner we have not anticipated. Can these novel techniques be incorporated into the user program as run by NOAO without impacting the cost, operation, and science of the Dark Energy Survey? What will be the preferred community access to the telescope and instrument during the time of year the DES is running?

We can expect the unexpected from a community of astronomers presented with a world class instrument on a mature telescope.

References

- Bartelmann, M., et al. 1998, *A&A*, 330, 1
- Becker, R.H., et al. 2001, *AJ*, 122, 2850
- Lopes, A.M., & Miller, L. 2004, *MNRAS*, 348, 519
- Martini, P., & Schneider, D.P. 2003, *ApJ*, 597, 109
- Menard, B., Bartelmann, M., & Mellier, Y. 2003, *A&A*, 409, 411
- Outram, P.J., et al. 2003, *MNRAS*, 342, 483
- Rengstorf, A.W., et al. 2004, *ApJ*, 606, 741
- Richards, G., et al. 2004, in preparation
- Vanden Berk, D.E., et al. 2004, *ApJ*, 601, 692
- Wolf, C., et al. 2004, *A&A*, 421, 913
- Yee, H.K.C., et al. 1996, *AJ*, 111, 1783

10. Conclusions

We propose to make the most precise measurement of dark energy through four independent, complementary measurements of: (i) the redshift distribution and spatial clustering of galaxy clusters using both the SZE (in cooperation with the South-Pole Telescope project) and optical methods; (ii) weak gravitational lensing of distant galaxies; (iii) the evolution of the spatial distribution of galaxies; and (iv) the distances to type Ia supernovae. Our program will yield a determination of w , the equation of state parameter of the dark energy, to a precision of 5%. While our focus is on dark energy and dark matter, the survey data will also be valuable to the community for a broad range of other science programs.

Our program is the next logical step in the precise determination of the fundamental parameters of cosmology. The giant leaps in precision of the next generation experiments require correspondingly long lead times. In contrast, the Dark Energy Survey can be completed within a decade, and it fits nicely between the current experiments and the more ambitious programs that will be reaching the observation stage in the next decade. Active members of our collaboration are participants in these programs, and wish to insure their success by taking this step.

We have assembled a strong, experienced team to reach our scientific and technical goals. We have come a long way since our first collaboration meeting at Fermilab in early December. At that time our collaboration had fewer participating institutions and there were gaps in our technical capabilities that would have hampered our ability to mount this program. Our new collaborators bring technical capabilities that more than fill those gaps and their participation will enrich our scientific program. However we are open to adding institutions that can reduce the cost of the Dark Energy Survey to the U.S. sponsors, The Department of Energy and the National Science Foundation. By today's standards for dark energy explorations this project requires a modest cash outlay. On the basis of our proposed funding profile, we plan to begin regular observations in the summer of 2009 with both the fully commissioned instrument and the validated data processing and archiving systems. We request 30% of the observing time on the Blanco between the summer of 2009 and the summer of 2014, concentrated during the period from September to February when the area of sky we are interested is visible, in exchange for creating the instrument and data management systems.

We realize that this is a significant request, but if we are to succeed we must take significant steps. The science opportunities of the Dark Energy Survey are important, timely and directly relevant to astrophysics, cosmology, and particle physics. Our collaboration has the capabilities needed to successfully execute the project.